Vanadium Phosphorus Oxide Catalyst with Novel Structure Derived from Lamellar Compounds

Yuichi Kamiya

Vanadium Phosphorus Oxide Catalyst with Novel Structure Derived from Lamellar Compounds

Yuichi Kamiya

Research & Development Center
Tonen Chemical Corporation

Under the Supervision of
Prof. Tadashi Hattori

2003

Preface

Heterogeneous catalysts play a major role in modern chemical industry. Maleic anhydride is a raw material for some useful chemicals. At present, most of maleic anhydride is produced by a selective oxidation of *n*-butane using $(VO)_2P_2O_7$ catalyst. Although numerous studies have been devoted over the past 30 years, this reaction system has a serious problem that the yield of maleic anhydride is low. It is thus strongly desired to improve the yield by improving the catalytic performance.

So far, almost all developments of the $(VO)_2P_2O_7$ catalyst have been performed by a trial-and-error method, however, now this method must be at the edge of its capabilities for improving the catalytic performance. It is well known that the catalytic performance is sensitive to structure and composition of the $(VO)_2P_2O_7$ catalyst. In this thesis, the author thus presents another strategy for developing the catalyst that design of the $(VO)_2P_2O_7$ catalyst on the basis of controlling the structure and composition. Controlling these factors makes properties of the active sites improved, consequently, the catalytic performance must be improved. However, there are two critical problems to realize this: (1) It can not be imaged that what-like structure and composition are required to improve the catalytic performance. (2) The present level of catalyst preparation of $(VO)_2P_2O_7$ is far from "designing" the structure and composition, even if one knows what-like structure and composition are required.

The aim of this thesis is to design the vanadium phosphorus oxide catalysts with novel structure on the basis of controlling the structure and composition. The first subject is to establish the concept that how the properties of the active sites should be controlled to improve the catalytic performance. The second subject is to develop the vanadium phosphorus oxide catalysts with novel structures on the basis of controlling the structure and composition.

The present thesis has been carried out during 1994-1997 at Department of Applied Chemistry, Graduate School of Engineering, Nagoya University under supervision of Professor Tadashi Hattori, and subsequently, 1997-2002 at Research and Development Center, Tonen Chemical Corporation under supervision of Dr. Eiichiro Nishikawa and Dr. Satoshi Ueki. A period of this work (1997-2002) was supported by NEDO and Japan Chemical Industry Association (JCIA) for the project on "Novel Catalysts and Chemical Reaction Processes for Selective Oxidation of Light Alkanes" under supervision of the leader of this project, Professor Tadashi Hattori.

I would like to express my sincere appreciation for kind encouragement, fruitful discussion and

philosophical suggestion given by Professor Tadashi Hattori. I am also deeply grateful to Professor Shinichi Hirano, Professor Katsuhiko Takagi, and Assistant Professor Koichi Kikuta for reviewing this thesis and making a number of helpful discussions.

I wish to express my deep gratitude to Professor Toshio Okuhara of Hokkaido University for his valuable discussions, philosophical suggestion and careful reviewing of the manuscripts. This thesis could never be completed without his continuous encouragement. I am also deeply grateful to Assistant Professor Atsushi Satusma for his heartwarming advice, fruitful discussion, philosophical suggestion and careful reviewing of the manuscripts. I wish to express my sincere gratitude to Dr. Eiichiro Nishikawa for kind encouragement, meaningful discussions and teaching me beneficial concepts for scientific research. I would like to express my deep gratitude to Dr. Satoshi Ueki for his helpful comments and discussions. I would like to express my appreciation to Dr. Syunji Matsuo for his cordial encouragement and supporting the project. I wish to express my gratitude to Professor Noritaka Mizuno of the University of Tokyo for his valuable discussions and careful reviewing of the manuscript.

I wish to thank Dr. Masahide Murata, a head of Research and Development Center, Mr. Tatsumi Ichiki, a group reader of basic chemicals and intermediates research group, and my colleagues in Tonen Chemical Corporation for their support, encouragement and valuable discussions. Also, special thanks should be given to the board members of Tonen Chemical Corporation giving me the opportunity of this work. I wish to thank the members in Laboratory of Catalysts Design led by Professor Tadashi Hattori, especially to Mr. Shin-ichi Komai, Ms. Yenni Westi, Yuki Kijima, Miki Yashiro and Mr. Takuya Ookura for the collaboration, and the members in Laboratory of Advanced Material Chemistry led by Professor Toshio Okuhara, especially to Ms. Miki Yoshimune, Dr. Norihito Hiyoshi and Dr. Naoki Yamamoto for the collaboration. Hearty thanks are made to Dr. Koji Nishi, Dr. Ken-ichi Shimizu, Dr. Yoshitaka Inaki and Mr. Naruaki Sugiyama for valuable discussions. I would like to express my appreciation to my friend, Mr. Nobuyuki Takagi, Kenji Suzuki, Masatoshi Kato and Mikio Takamatsu for their hospitality and comfortable time.

Finally, I wish to thank sincerely my wife, Yuka, my children, Moe, my brother, Noriyuki, my sister mitsuko, my parents, Hisashi and Tomoko, and my parents-in-law, Syu-ichi and Teruko Okada for their support, understanding, patience and continuous encouragement.

Yuichi Kamiya

Kawasaki

December, 2002

Contents

Chapter 1

General Introduction

1.1 Selective oxidation of n-butane

Maleic anhydride (MA) is an intermediate for some useful chemicals such as unsaturated polyester resins, succinic anhydride, γ-butyrolactone, 1,4-butanediol, tetrahydrofuran, fumaric acid and so on (Scheme 1) [1]. At present, about one million tons/year of MA is produced in the world and 140 thousand tons/year in Japan [2]. Most of MA is now produced by selective oxidation of *n*-butane using a crystalline $(VO)_2P_2O_7$ catalyst (eq. 1). Although numerous studies including preparation methods, preparation conditions, activation processes of the $(VO)_2P_2O_7$ catalyst and addition of various promoters have been performed over the past 30 years, this reaction system still has a serious problem that is low yield of MA, *ca.* 55 mol%. It is thus strongly desired to improve the yield by improving the catalytic performance.

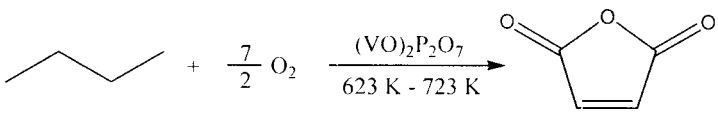

(eq. 1)

Besides industrial viewpoint, this reaction system is attractive form scientific aspect. The selective oxidation of *n*-butane to MA is a complex reaction, which proceeds through 14-electrons oxidation involving the abstraction of 8-hydrogen atoms and insertion of 3-oxygen atoms. This complex reaction proceeds on the $(VO)_2P_2O_7$ catalyst without by-product except for CO_x. In addition, more reactive product (MA) is formed from less reactive reactant (*n*-butane). Furthermore, since the $(VO)_2P_2O_7$ catalyst is a crystalline mixed oxide, this reaction system has been expected to be intriguing subject for elucidating a relationship between microstructure of the catalyst and catalytic property.

1.2 History of maleic anhydride production

Before 1960's, most of MA was produced by selective oxidation of benzene over V_2O_5-MoO_3 catalyst (eq. 2) [3-5].

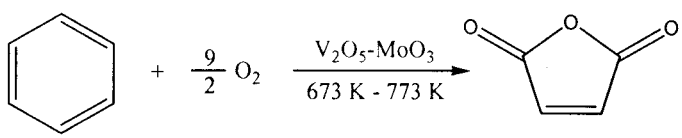

(eq.2)

In the 1970's, however, two important incidents for the benzene oxidation process occurred and would trigger to switch the production from benzene oxidation process to C_4-hydrocarbon one [5]: (1) the price of a benzene jumped up, caused by its increasing use in lead-free automobile fuel. (2) a strict regulation on benzene emission from MA production plants was introduced in the USA. In the benzene oxidation, two

carbon atoms are essentially consumed to form CO_x, so C_4-hydrocarbons are also suitable feedstock for the MA production in terms of CO_x emission.

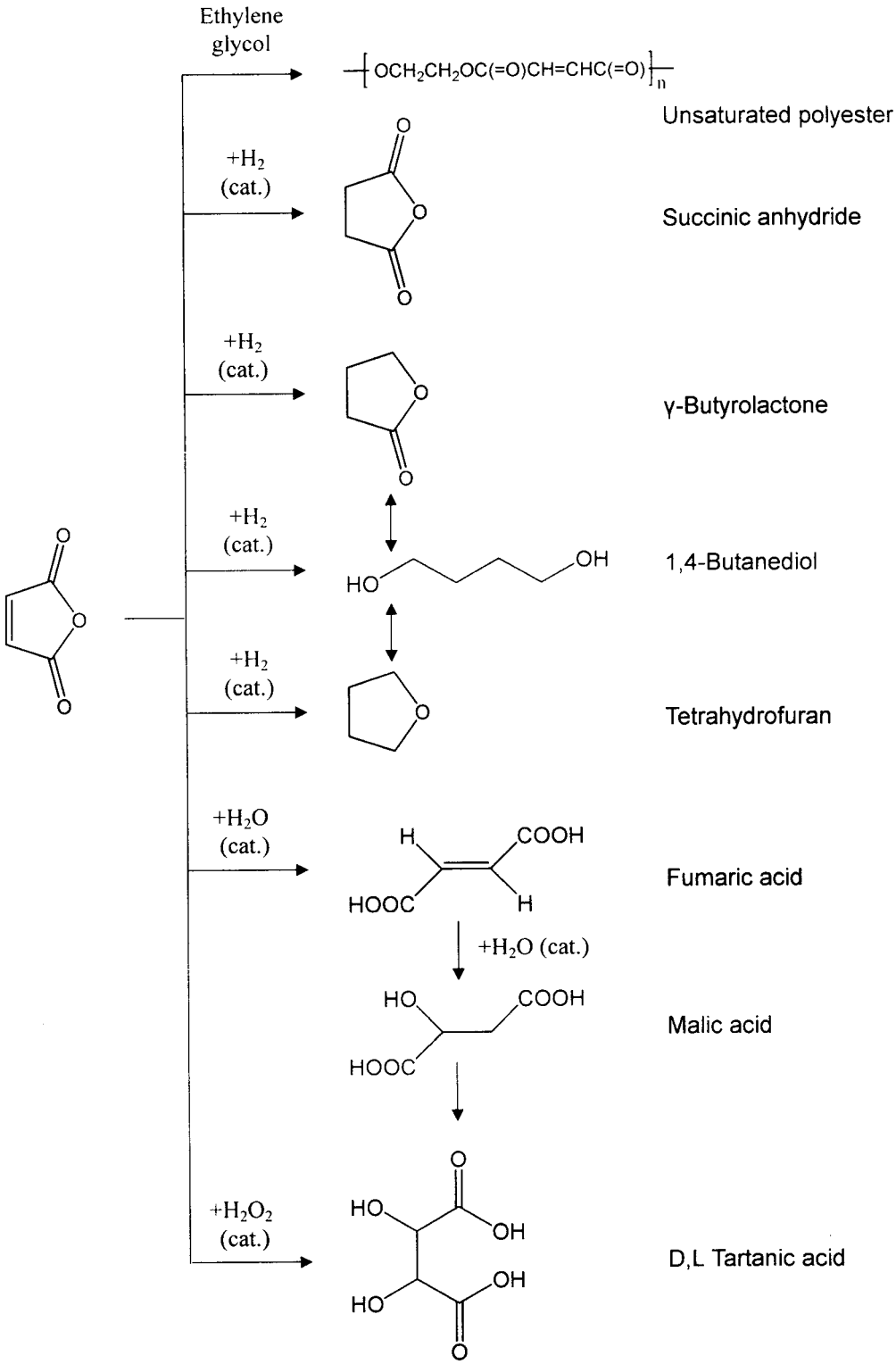

Scheme 1 Derivatives made from maleic anhydride

At first, the catalyst catalyzing butenes and butadiene to MA selectively was found out [6-8]. This catalyst was V_2O_5-P_2O_5 supported on Al_2O_3 or TiO_2, in which P/V atomic ratio was around 1.6 and valence of V was 5+ [5]. By using this catalyst, Mitsubishi Chemical, BASF, and Bayer began to produce MA in early 1970's [4]. However, this catalyst was non-selective for *n*-butane oxidation [5].

In parallel with this, many researches on the development of catalyst for selective oxidation of *n*-butane strenuously carried out. Du Pont published that $CoMoO_4$ catalyzed the reaction of *n*-butane to MA in 1954 [9], but the catalytic activity and selectivity was very low. In 1966, Bergman and Frisch found out that the oxidation of *n*-butane to MA was catalyzed selectively by vanadium phosphorus mixed oxide (VP oxide) [10]. At that time, however, the process was not economically viable in comparison with the contemporary benzene oxidation process, because catalytic activity and selectivity to MA was still insufficient [11]. As a result of considerable investigations, in 1971, researchers of Chevron Research Co. discovered that crystalline VP oxide with P/V ratio of 1.0-1.2 and vanadium of V^{4+} showed high catalytic performance for the *n*-butane oxidation to MA [12]. This catalyst opened up the use of *n*-butane as feedstock for commercial production of MA. Right after that (in 1974), Monsanto Company began the commercial production of MA from *n*-butane. Now, over 70 % of MA are produced from *n*-butane [2].

1.3 Active phase for the selective oxidation of n-butane

Table 1 lists VP oxides relating with the *n*-butane oxidation, in which P/V ratios are 1.0 or 2.0, and valences of V are 4+ or 5+. Fig. 1 illustrates the structures of these VP oxides [13]. $(VO)_2P_2O_7$, $VOHPO_4{\cdot}0.5H_2O$, and $VO(PO_3)_2$ are the VP oxides of V^{4+}. $(VO)_2P_2O_7$ consists of edge-shared VO_6 octahedra connected with P_2O_7 unit (Fig. 1a-1, a-2), while $VOHPO_4{\cdot}0.5H_2O$ consists of face-shared VO_6 octahedra connected with HPO_4 unit (Fig. 1b). In the edge- and face-shared VO_6 octahedra, two V^{4+} ions adjoin through oxygen as shown by V^{4+}-O-V^{4+}. This part is usually called as "V-O-V pair sites". On the contrary, PO_4 units surround VO_6 octahedras in $VO(PO_3)_2$ (Fig. 1c). For the VP oxides of V^{5+}, isolated VO_6 octahedras are connected by PO_4 units in α-$VOPO_4$ and β-$VOPO_4$ (Fig. 1e,f). $VOPO_4{\cdot}2H_2O$ consists of alternating V-O-P layers and H_2O ones (Fig. 1d). The V-O-P layer is made up with isolated VO_6 octahedra linked with PO_4 tetrahedra as well as α-$VOPO_4$, and H_2O is weakly held in the interlayer. The structure of γ-, δ-$VOPO_4$ and X_1 phase are not fully solved. Electron diffractions of γ- and δ-$VOPO_4$ suggested that these compounds had the edge-share VO_6 octahedras as $(VO)_2P_2O_7$ [14]. X_1 phase gives similar XRD pattern [15] and Raman spectrum to δ-$VOPO_4$ [16,17]. X_1 phase was confirmed to have the V-O-V pair

sites by EXAFS [17]

Table 1 Phases of vanadium phosphorus oxides

P/V ratio	V^{n+}	
1	5	α-$VOPO_4$, β-$VOPO_4$, γ-$VOPO_4$, δ-$VOPO_4$, $VOPO_4 \cdot 2H_2O$, X_1 phase
	4	$(VO)_2P_2O_7$, $VOHPO_4 \cdot 0.5H_2O$ (precursor)
2	4	$VO(PO_3)_2$

Table 2 Catalytic performance of vanadium phosphorus oxides in the oxidation of *n*-butane

	Conversion/%	Selectivity to MA/%	Ref.
$(VO)_2P_2O_7$	80	72	18
α-$VOPO_4$	53	18	15
β-$VOPO_4$	62	18	15
X_1 phase	59	40	15
$VO(PO_3)_2$	1	100	19,20
	20	47	21

It has been discussed which one is the active phase for this reaction. Table 2 lists the catalytic data reported in the literature [15,18-20] and that of the author [21]. The catalytic activities and selectivities remarkably depend on the VP oxides. Among them, $(VO)_2P_2O_7$ gave high selectivity and activity. In the case of α-$VOPO_4$ and β-$VOPO_4$, the selectivity is very low, and that of X_1 phase is not high. Hutchings et al. [19,20] reported that $VO(PO_3)_2$ shows ultra high selectivity (100 %), but the data reported was only at a very low conversion of *n*-butane (about 1 %), so it is suspected that the data include an large experimental errors. Actually, the author tested $VO(PO_3)_2$ under the practical conversion of *n*-butane and confirmed that the selectivity was not high (47 % at 20 % conversion). These results indicates $(VP)_2P_2O_7$ is the active phase for the selective oxidation of *n*-butane. In addition, $(VO)_2P_2O_7$ is the main component of all commercial catalysts. Considering the relationship between the structures and catalytic performances, the primal characteristics of bulk structure of the catalyst for MA formation are V-O-V pair sites, valence state of V^{4+}, and P/V ratio of 1.0.

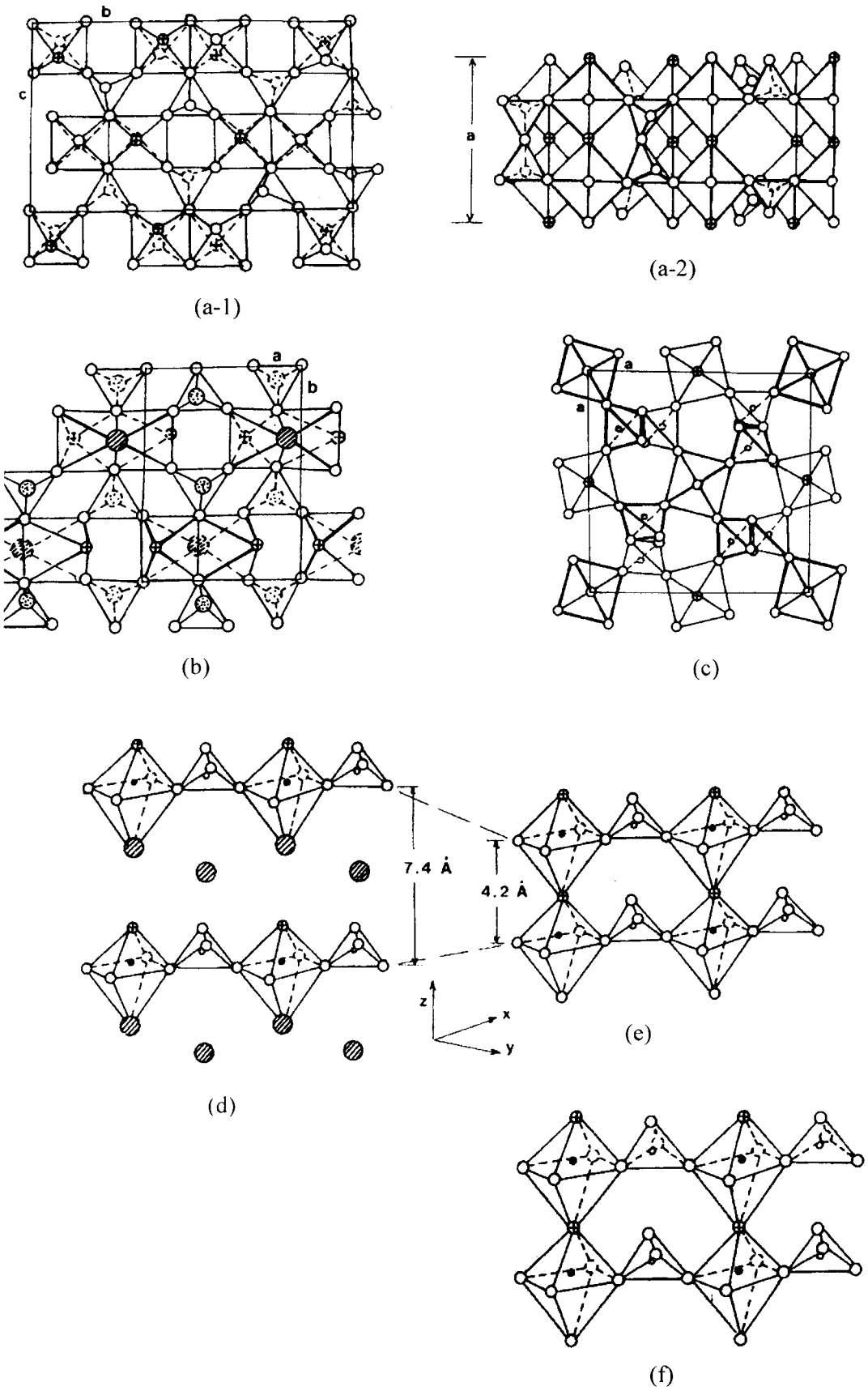

Fig.1 Structures of the VP oxides. (a) $(VO)_2P_2O_7$, (b) $VOHPO_4 \cdot 0.5H_2O$, (c) $VO(PO_3)_2$ (d) $VOPO_4 \cdot 2H_2O$, (e) α-$VOPO_4$, (f) β-$VOPO_4$. [13]

1.4 Preparation methods of conventional $(VO)_2P_2O_7$ catalyst

The $(VO)_2P_2O_7$ catalyst is usually obtained by dehydration of vanadyl hydrogen phosphate hemi-hydrate, $VOHPO_4 \cdot 0.5H_2O$. The transformation from $VOHPO_4 \cdot 0.5H_2O$ to $(VO)_2P_2O_7$ proceeds topotactically with elimination of H_2O and condensation of two P-OH [22,23]. Morphology and structural characteristic of $VOHPO_4 \cdot 0.5H_2O$ are basically retained during this transformation [22,23]. That is to say, those of the $(VO)_2P_2O_7$ catalyst are already directed at the time of preparing $VOHPO_4 \cdot 0.5H_2O$.

So far, many preparation methods for $VOHPO_4 \cdot 0.5H_2O$ are claimed in patents and research papers [1,24-26], and these are classified into three types as follows: the precursor is prepared (1) in aqueous medium, (2) in organic solvent which is called as "organic solvent method", and (3) by reduction of $VOPO_4 \cdot 2H_2O$ with alcohol. At the beginning, the precursor was prepared in the aqueous medium. In this method, V_2O_5 is reduced with HCl or oxalic acid in water, followed by reaction with H_3PO_4. Nowadays, most of the industrial catalysts are prepared by the organic solvent method [5,11,24]. H_3PO_4 is allowed to react with partially reduced V_2O_5 in alcohol such as benzyl alcohol and isobutyl alcohol to form precipitate of $VOHPO_4 \cdot 0.5H_2O$. In the method by use of $VOPO_4 \cdot 2H_2O$ as starting material, $VOPO_4 \cdot 2H_2O$ is reduced with alcohol to form $VOHPO_4 \cdot 0.5H_2O$. The main differences in these preparation methods are morphology and structural characteristics of $VOHPO_4 \cdot 0.5H_2O$ crystallites. The $VOHPO_4 \cdot 0.5H_2O$ crystallites obtained in organic solvent, aqueous medium and by reduction of $VOPO_4 \cdot 2H_2O$ have rose petal-like, block-like and plate-like morphologies, respectively [18]. In the organic solvent method, $VOHPO_4 \cdot 0.5H_2O$ crystallites with structural disorder in the layer stacking are formed [27-29]. This structural disorder is induced by the alcohol trapped between the layers [28]. On the contrary, well-crystallized $VOHPO_4 \cdot 0.5H_2O$ crystallites are formed in aqueous medium [15].

For improvement in the catalytic performance, numerous trials on preparation of the $(VO)_2P_2O_7$ catalyst have been performed so far. These trials have been mostly carried out by a conventional trial-and-error method, and almost all imaginable factors such as kinds of solvents and starting materials, reactant P/V ratios, temperature, time of preparation and addition of various promoters and so on have been already covered [5,11,24]. The trial-and-error method attained some positive results in its own way. However, the yield of MA is still low. Besides that, now there is very little room in the trial-and-error method to improve the catalytic performance.

1.5 Structure sensitivity of catalytic performance

It is well known that the preparation method greatly affects the catalytic performance [5,11,24]. The catalyst obtained by the organic solvent method shows high activity [29]. On the other hand, the $(VO)_2P_2O_7$ having block-like and plate-like shapes exhibits high selectivity to MA even at high conversions, because the consecutive oxidation of MA is suppressed over these catalysts [18]. The difference of the catalytic performance have been considered to relate with that of the microstructure of $(VO)_2P_2O_7$ crystallites [18,29].

One of the factors controlling the catalytic performance is morphology, that is, crystal plane exposed on the surface. It is generally accepted that the active sites for MA formation are located on the (100) plane. Horowitz et al. [30] investigated the relationship between morphology and catalytic performance. They prepared the catalysts with different morphology by changing the preparation conditions, and demonstrated that the catalysts, in which the (100) plane is preferentially exposed, showed higher selectivity. Okuhara et al. [31,32] performed that the $(VO)_2P_2O_7$ catalysts of plate-like morphology was first deactivated completely by deposition of SiO_2 thin layer, and then fractured to create new side faces such as the (001) and (021) planes. Since only CO and CO_2 were formed by this catalyst, they concluded that the active sites for MA formation exist on the (100) plane, on which the V-O-V pair sites are located. Koyano et al. [33,34] elucidated using Raman spectroscopy that the (100) plane is oxidized to X_1 phase, while the side planes are oxidized to β-$VOPO_4$ which is non-selective phase for MA formation. These results support the hypothesis that catalytic function is dependent on the crystal planes. Furthermore, Ziolkowski et al. [35] claimed that the (100) plane is effective for MA formation from computational simulation by use of crystallochemical model of the (100) plane.

Another factor is bulk structure of the catalyst. As mentioned in the former section (1.4), there is the structural disorder along the (100) cleavage plane of the catalyst prepared in organic solvent (VPO-org). VPO-org gave higher catalytic activity per surface area for MA formation than the catalyst prepared in aqueous medium (VPO-aq) [29]. This suggests that the structural disorder influences the specific activity for MA formation. In addition, it is known that catalytic activity and selectivity increase during the first several hundred hours under the reaction conditions [36-38]. At beginning, the catalyst consists of low crystalline $(VO)_2P_2O_7$ and amorphous VP oxides, and then the crystallinity of $(VO)_2P_2O_7$ rises as the increasing in catalytic performance. This supports the hypothesis that the bulk structure of the catalyst affects its catalytic performance. Since the catalytic reaction over the $(VO)_2P_2O_7$ catalyst certainly proceeds on its surface, the bulk structure must affect surface one.

1.6 Surface functional groups controlling the catalytic performance of $(VO)_2P_2O_7$ catalyst

Table 3 summarizes the type of functional groups thought to be present on the surface of $(VO)_2P_2O_7$ [1]. Lewis and Brønsted acid sites, one-electron redox couples, terminal oxygens of $V=O^{3+}$ and $V=O^{2+}$, and adsorbed molecular oxygen species exist on the surface. These are roughly classified to (1) oxygen species (redox sites) and (2) acid sites. It is known that these two functional groups are involved in the MA formation.

Table 3 Surface functional groups hypothesized to be present on $(VO)_2P_2O_7$

Type of functional groups
Lewis and Brønsted acid sited
One-electron redox couple: V^{5+}/V^{4+}
Bridge oxygen in V-O-V, V-O-P groups or triply bridged oxygen in VO(P)V
Terminal oxygen in $(V=O)^{3+}$, $(V=O)^{2+}$
Adsorbed oxygen species as η^2-superoxo and η^1-peroxo species

The selective oxidation of *n*-butane over the $(VO)_2P_2O_7$ catalyst has been considered to proceed via a redox mechanism between V^{4+} and V^{5+} at the top few surface layers [39-41]. Thus, the catalytic performance must depend upon the reduction and re-oxidation properties of the catalyst directly. The change of the structure of the surface on reduction and re-oxidation was investigated [40]. The surface of $(VO)_2P_2O_7$ transforms to X_1 phase (V^{5+}) on the re-oxidation, and then, the formed X_1 phase is reduced to $(VO)_2P_2O_7$, reversibly. Satsuma and co-workers [42-44] investigated reactivity of active oxygen species on the $(VO)_2P_2O_7$ catalyst. The amount of the active oxygen species was estimated using NARP (nitric oxide-ammonia rectangular plus) technique, and they demonstrated that VPO-org had the oxygen species with higher specific activity than VPO-aq by the estimations of the formation rate of MA per active oxygen species [42,43]. In order to elucidate a relationship between the redox property and catalytic performance, each rate of re-oxidation and reduction has been measured. Busca et al. [27] measured the rate of re-oxidation with air, and suggested the structural disorder enhances that rate. Hodnett et al. reported [45,46] that the rate of both re-oxidation and reduction decreased as the bulk P/V ratios increased. However, they measured the rates on not the surface but the bulk reduced or oxidized. Since the oxidation of *n*-butane proceeds via a redox of the top few surface layers, the author conceives that the rates at the top

few surface layers need to be evaluated for elucidation of those relationships.

Acid sites as well as redox sites are considered to play significant role for selective oxidation of paraffin over solid catalysts [47]. In addition, Lewis and Brønsted acid sites play different roles in the selective oxidation, and the strength of respective acid sites strongly affects the catalytic performance [48]. For $(VO)_2P_2O_7$, so far, determination of acid sites was reported and their role in the selective oxidation of *n*-butane was suggested. Centi et al. [49] demonstrated that the acid sites are necessary for this reaction, since co-feed ammonia in the reaction feed and doping of potassium to the catalyst make the activity for MA formation lowered. The presence of both Brønsted and Lewis acids on $(VO)_2P_2O_7$ was confirmed from IR spectra of basic molecule adsorbed on the catalyst [50,51]. Lewis acid sites are presumed to be a coordinatively unsaturated vanadium ions on the (100) plane, while Brønsted acid sites are P-OH group of truncated P-O bonds in terminal phosphorus tetrahedra [50]. Trifirò et al. [52] suggested that *n*-butane is activated on Lewis acid sites with basic lattice oxygen through abstraction of hydrogen, and Brønsted acid sites facilitate desorption of water and MA. Busca et al. [50] detected the presence of greater amount of the very strong Lewis acid sites on VPO-org as compared with VPO-aq, and suggested the higher specific rate of *n*-butane activation in VPO-org due to the presence of these Lewis acid sites. However, even now quantitative understanding the relationship between acidic property and catalytic performance are not reached. The cause of this should be lack of analytical method for quantitative determinations of Brønsted and Lewis acid sites separately.

1.7 Concept and strategy for developing the advanced catalyst

The conventional trial-and-error method is the strategy to seek good catalyst by repeating preparations of the catalyst and evaluating the catalytic performance time after time. For the $(VO)_2P_2O_7$ catalyst, this strategy has already been ineffective to improve the catalytic performance any more. Another strategy for developing the catalyst is to design the catalyst systematically, that is, first one pays much attention to the causal relationships between the catalytic performance and catalyst preparation, and investigates those in detail, and then designs the catalysts based upon the knowledge obtained. However, so far, development in the $(VO)_2P_2O_7$ catalysts by such strategy has been scarcely performed.

The author presents the relationships between the catalytic performance and catalyst preparation of the $(VO)_2P_2O_7$ catalyst as Scheme 2. Items existing between the catalytic performance and catalyst preparation are structure/composition and properties of the active sites. The properties of the active sites are divided

into two elements, that is, chemical and physical properties. As mentioned in the former section (1.6), two important chemical properties of the active sites on the $(VO)_2P_2O_7$ catalyst are reduction and re-oxidation property, and acidic property. On the other hand, the physical property means number of the active sites.

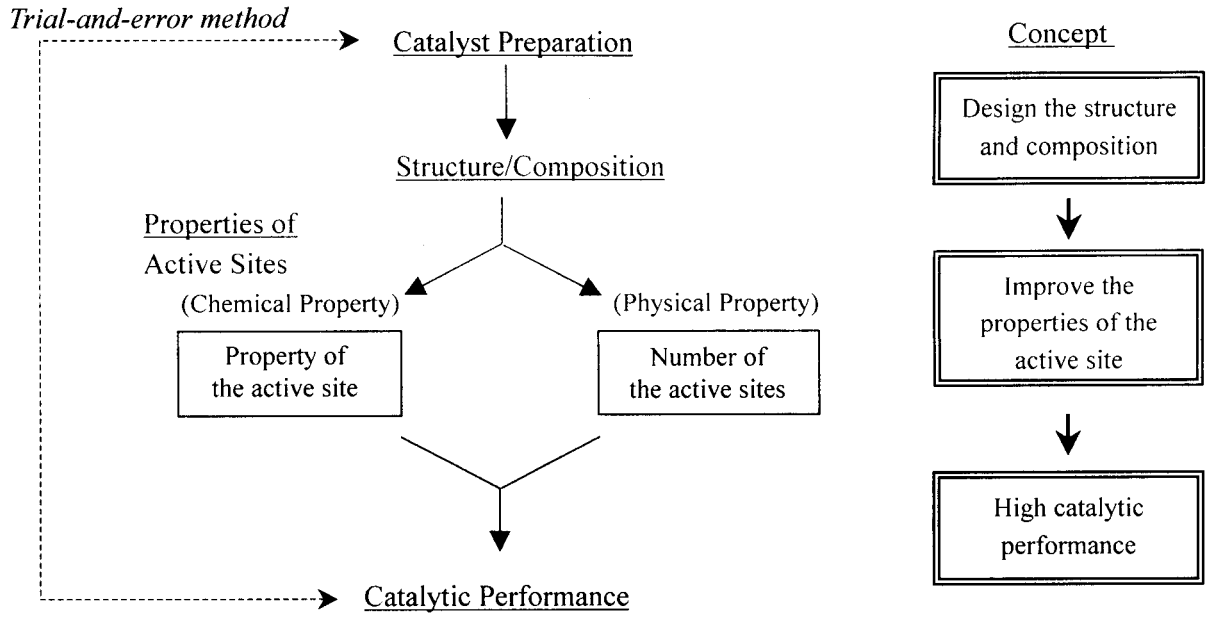

Scheme 2 The relationships between catalytic performance and catalyst preparation, and the concept for developing the catalyst of high performance.

The structure and composition of the $(VO)_2P_2O_7$ catalyst greatly affects the catalytic performance. This can be interpreted that the structure and composition influence the chemical and/or physical properties of the active sites, consequently difference of those must cause that of the catalytic performance. On the basis of these ideas, the author proposes the concept for developing the catalyst of high performance that adequate design of the structure/composition makes the properties of the active sites improved, consequently, catalytic performance must be improved. The author believes that executing the development of the catalyst according to this concept brings the catalyst of high performance. However, there are two critical problems to realize this. First is that present understanding of the relationship between the chemical properties and catalytic performance is insufficient to understand how the chemical properties should be controlled to improve the catalytic performance. In consequence, it can not be imaged that what-like structure and composition are suitable to improve the chemical property of the active sites. Second is that the present level of catalyst preparation of $(VO)_2P_2O_7$ is far from "designing" the structure and composition, even if one can know what-like structure and composition are required.

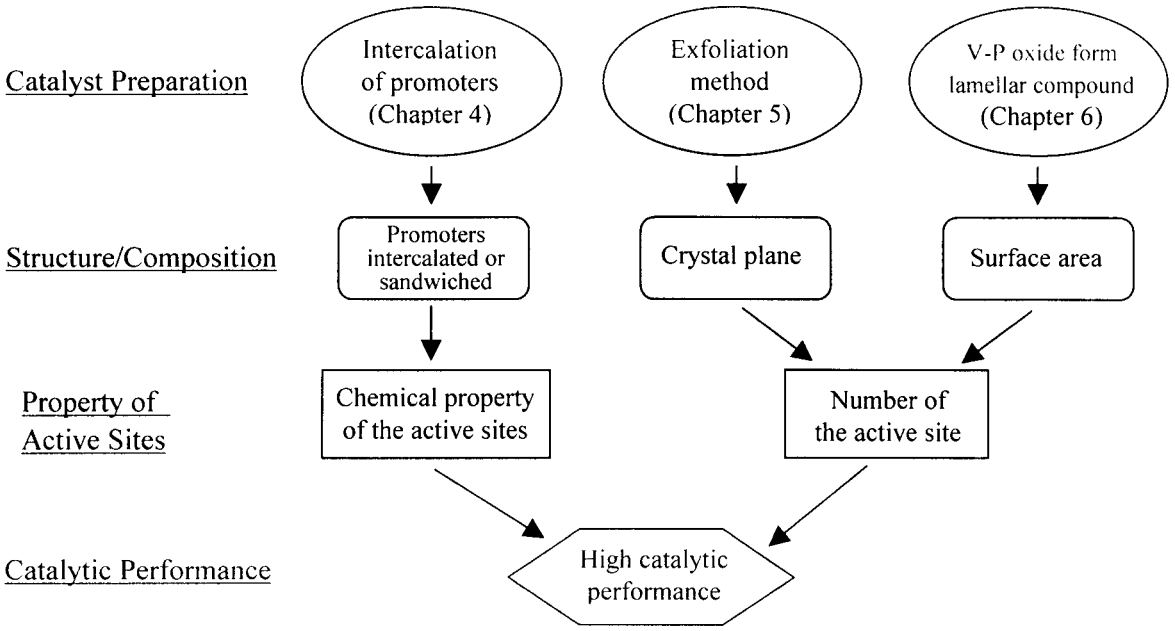

Scheme 3 Strategy for developing the catalyst in this thesis.

Scheme 3 shows the strategy for developing the catalysts with high performance according to the concept above mentioned. As will be elucidated in Chapter 2, the re-oxidation property should be improved to improve the catalytic activity per active site. One of the ways for the improvement is addition of promoters. However, retaining the characteristic structure of $(VO)_2P_2O_7$ must be required, when promoter is added to the catalyst. Besides that, the promoters added on the catalyst may form undesirable site such as aggregated metal oxides, on which combustion of *n*-butane proceeds. "*Intercalation*" is a reaction that hetero-atoms, molecules, and ions are inserted into the interlayer space of layered compound [53]. The intercalation is characterized to proceed topotactically with retaining the two-dimensional structure of host material. $VOHPO_4 \cdot 0.5H_2O$ is a layered compound, so the author came up with the method that $VOHPO_4 \cdot 0.5H_2O$ is modified by intercalation of promoters followed by calcination. By this method, the promoter can be expected to be introduced to $(VO)_2P_2O_7$ catalyst uniformly or sandwiched between their layers with the characteristic structure remaining (Fig. 2). These catalysts are hopeful to show higher specific activity for MA formation. In addition, it can be expected that the acidic property also changes by this method. However, since each V-O-P layers of $VOHPO_4 \cdot 0.5H_2O$ are held tightly by strong hydrogen bonding [22], it is difficult to modify by intercalation at present [54]. Consequently, new precursors are

required to realize the idea of this preparation method.

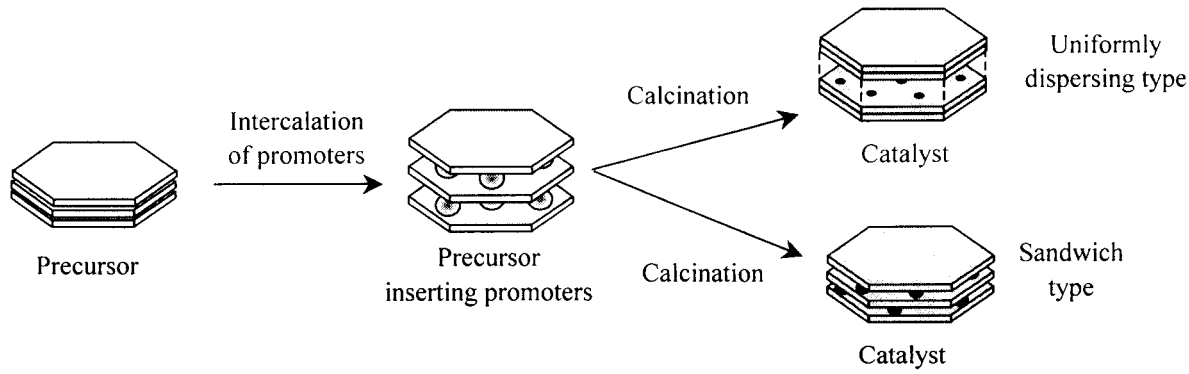

Fig. 2 Image of preparation method using intercalation of promoter

Concerning the physical property, i.e. number, of the active sites, two manners to increase the number of the active sites can be thought. The author considers that preferential expose of the (100) plane of the $(VO)_2P_2O_7$ catalyst, that is, high exposure of the active surface area, is effective in developing the catalyst of high performance, because the active sites for MA formation are located on the (100) plane. Another manner for improving the number of the active sites is to increase the total surface area of the catalyst.

Recently, "*exfoliation*" is reported in some layered compounds such as clay [55], zirconium phosphate [56], niobate [57], and titanate [58]. Exfoliation has been developed from extending the concept of intercalation and is a technique of delaminating stacked inorganic sheets in solvent by infinite swelling of their interlayer space. As mentioned above, preferential expose of the (100) plane can be effective in developing the catalyst with high performance. To realize this, the author devised a method using exfoliation of $VOPO_4 \cdot 2H_2O$ as shown in Fig. 3. $VOPO_4 \cdot 2H_2O$ possesses high intercalating capability [59]. Lamellar compound formed by intercalation of alcohols into $VOPO_4 \cdot 2H_2O$ is exfoliated, and then the thin-layers of $VOPO_4$ are reduced to from catalyst precursor. This method has the potential to obtain $(VO)_2P_2O_7$ crystallites of thin-sheet exposing preferentially the (100) plane.

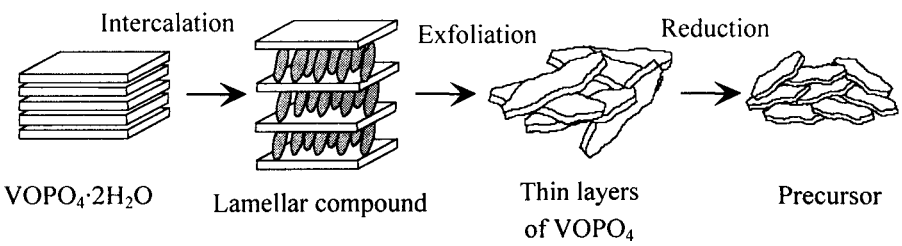

Fig. 3 Image of preparation method using exfoliation of $VOPO_4 \cdot 2H_2O$

Micro- and mesoporous materials generally have high surface area. For applications of these materials to the selective oxidation catalysts, it is considered that mesoporous materials are rather suitable, because the products may be strongly adsorbed in the micropores causing the consecutive oxidation of the products. The author expects that the mesoporous V-P oxides with card house structure are obtained from lamellar V-P compounds (Fig. 4). This structure is probably formed by peculiar elimination of the organic groups causing formation of the mesopores.

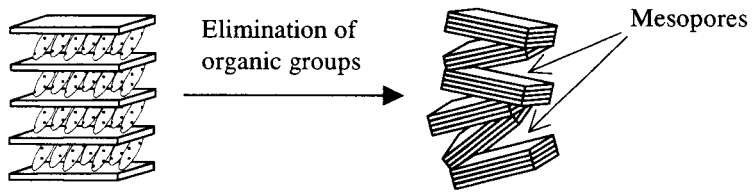

Fig. 4 Image of forming the mesoporous V-P oxide with card house structure from lamellar compound.

1.8 Objective and outline of the thesis

On the basis of these backgrounds, the aim of this thesis is to design the vanadium phosphorus oxide catalyst with novel structure on the basis of controlling the structure and composition. The first subject of this thesis (Part I) is to establish the concepts that how the reduction and re-oxidation properties (Chapter 2) and acidic property (Chapter 3) should be controlled to improve the catalytic performance. The second subject of this thesis (Part II) is to develop the vanadium phosphorus oxide catalysts with novel structures on the basis of controlling the structure and composition (Chapter 4,5,6). The outline of the thesis is as follows.

Chapter 2 intends to investigate the relationship between the reduction and re-oxidation properties and catalytic performance. The reduction and re-oxidation properties of the catalysts are evaluated from kinetic analysis and measuring the rate of reduction with *n*-butane and re-oxidation with air. The relationship are discussed by comparing with three types of the $(VO)_2P_2O_7$ catalyst with different microstructures.

In Chapter 3, the relationship between acidic properties and catalytic performance is investigated. Chapter 3.1 establishes as a new characterization method for quantitative determination of both amount and strength of Brønsted and Lewis acid sites separately using two kinds of dimethylpyridine as probes for TPD. In Chapter 3.2, the acidic properties of the $(VO)_2P_2O_7$ catalysts are evaluated by this method, and the relationship is elucidated.

In Chapter 4, iron-doped vanadyl pyrophosphate catalysts are developed by intercalation of iron-complex. Chapter 4.1 develops lamellar vanadyl alkylphosphates, which is a new precursor, and characterizes these compounds. Since the vanadyl alkylphosphates possess weakly held alcohol in their interlayer spaces, these materials can accommodate guest molecules. Furthermore, catalytic properties of V-P oxides obtained by calcination of the non-modified vanadyl alkylphosphates are investigated in order to demonstrate a prospect of these materials as a catalyst precursor. In Chapter 4.2, intercalation of iron-complex is investigated and the materials obtained are characterized systematically. Vanadyl benzylphosphate is used as a host and $Fe(acac)_3$ and ferrocene as guests. In Chapter 4.3, the method investigated in Chapter 4.2 is applied to modification of vanadyl *n*-hexylphosphate. The microstructure of the catalyst obtained by calcination of this material is investigated. The catalytic performance for *n*-butane oxidation is examined and a role of the iron incorporated will be discussed in relation to the reduction and re-oxidation properties. Furthermore, the author suggests appropriate reaction conditions for the iron-doped catalysts.

In Chapter 5, the author presents another potential method for the $(VO)_2P_2O_7$ catalyst preferentially exposing the (100) plane by using intercalation, exfoliation and reduction of $VOPO_4 \cdot 2H_2O$ in alcohols. The difference in the catalytic property and structures between this catalyst and conventional one is discussed.

In Chapter 6, highly porous vanadium phosphorus oxides of high surface area are synthesized by thermal treatment of vanadyl alkylphosphates. Micropore and mesopore size distributions are characterized from adsorption isotherm of argon and adsorption-desorption isotherm of nitrogen, respectively.

Chapter 7 includes the summary, conclusion, and future prospects.

References

[1] F. Cavani, F. Trifirò, *CHEMTECH*, **25**, (1994) 18.

[2] S. Uchida, in "*Sekiyukagaku purosesu*" E. Kikuchi Eds, Kodansha, (2001) p.159.

[3] N. Yamazoe, in "*Syokubai kouza, 14, kogyosyokubai han-nou I*" Y. Murakami Eds, (1985) p. 145.

[4] I. Matsuura, *Hyomen*, **20** (1982) 605.

[5] B.K. Hodnett, *Catal. Rev. –Sci. Eng.*, **27** (1985) 373.

[6] Mitsubishi Kasei Kogyo, Japan Kokai 7889 (1965).

[7] BASF, GP 1443452 (1968).

[8] Petro-Tex, USP 3366648 (1968).

[9] Du Pont, USP 2691660 (1954).

[10] Princeton Chemical Research, USP 3293268 (1966).

[11] G.J. Hutchings, *Appl. Catal.*, **72** (1991) 1.

[12] Chevron Research Co., USP 3864289 (1972).

[13] E. Bordes, *Catal. Today*, **1** (1987) 499.

[14] Z.G. Li, R.L. Harlow, N. Herron, N.S. Horowitz, and E.M. MaCarron, *J. Catal.*, **171** (1997) 506.

[15] T. Shimoda, T. Okuhara, and M. Misono, *Bull. Chem. Soc. Jpn.*, **58** (1985) 2163.

[16] F. Banabdelouahab, R. Olier, N. Guilhaume, F. Lefebvre, and J.C. Volta, *J. Catal.*, **134** (1992) 151.

[17] G. Koyano, T. Okuhara, and M. Misono, *J. Am. Chem. Soc.*, **120** (1998) 767.

[18] H. Igarashi, K. Tsuji, T. Okuhara, and M. Misono, *J. Phys. Chem.*, **97** (1993) 7065.

[19] M.T. Sananes, G.J. Hutchings, and J.C.Volta, *J. Chem. Soc., Chem. Commun.*, (1995) 243.

[20] M.T. Sananes, G.J. Hutchings, and J.C. Volta, *J. Catal.*, **154** (1995) 253.

[21] Private data.

[22] J.W. Johnson, D.C. Johnston, A.J. Jacobson, and J.F. Brody, *J. Am. Chem. Soc.*, **106** (1984) 8123.

[23] E. Bordes and P. Courtine, *J. Solid State Chem.*, **55** (1984) 270.

[24] G. Centi, F. Trifirò, J.R. Ebner, and V.M. Franchetti, *Chem. Rev.*, **88** (1988) 55.

[25] F. Cavani and F. Trifirò, in "*Catalysis Volume 11*", Royal Society of Chemistry, Cambridge, (1994) p. 246.

[26] F. Trifirò, F. Cavani, J.A. Horsley, and S.R. Vatcha, "*Selective Partial Oxidation of Hydrocarbons and Related Oxidations*", Catalytica Studies Division 4193 So, Mountain View, CA (1994).

[27] M.L. Granados, J.C. Conesa, and M. Fernàndez-García, *J. Catal.*, **141** (1993) 671.

[28] G. Busca, F. Cavani, G. Centi, and F. Trifirò, *J. Catal.*, **99** (1986) 400.

[29] F. Cavani, G. Centi, and F. Trifirò, *J. Chem. Soc., Chem. Commun.*, (1985) 492.

[30] H.S. Horowitz, C.M. Blackstone, A.W. Sleight, and G. Teufer, *Appl. Catal.*, **38** (1988) 193.

[31] T. Okuhara, K. Inumaru, and M. Misono, *Chem. Lett.*, (1992) 1955.

[32] T. Okuhara, K. Inumaru, and M. Misono, in "*Catalytic Selective Oxidation*", ACS Symposium Series 523, (1993) p.156.

[33] G. Koyano, T. Saito, and M. Misono, *Chem. Lett.*, (1997) 415.

[34] G. Koyano, T. Saito, and M. Misono, *J. Mol. Catal. A*, **155** (2000) 31.

[35] J. Ziolkowski, E. Bordes, and P. Courtine, *J. Catal.*, **122** (1990) 126.

[36] A.F. Ben, R. Olier, N. Guilhaume, F. Lefevre, and .J.C. Volta, *J. Catal.*, **134** (1992) 151.

[37] R.A. Overbeek, M. Versluijs-Helder, P.A. Warringa, E.J. Bosna, and J.W. Geus, *Stud. Surf. Sci. Catal.*, **82** (1994) 183.

[38] M. Abon, K.E. Bere, A. Tuel, and P. Delichere, *J. Catal.*, **156** (1995) 28.

[39] M. Pepera, J.L. Callahan, M.J. Desmond, E.C. Milberger, P.R. Blum, and N.J. Bremer, *J. Am. Chem. Soc.*, **107** (1985) 4883.

[40] G. Koyano, T. Okuhara, and M. Misono, *J. Am. Chem. Soc.*, **120** (1998) 767.

[41] T. Okuhara and M. Misono, *Catal. Today*, **16** (1993) 61.

[42] A. Satsuma, Y. Tanaka, T. Hattori, and Y. Murakami, *Appl. Surf. Sci.* **121/122** (1997) 496.

[43] A. Satusma, Y. Tanaka, T. Hattori, and Y. Murakami, in "*Science and Technology in Catalysis 1994*", Kodansha, (1995) 281.

[44] D. Ye, A. Satsuma, A. Hattori, T. Hattori, and Y. Murakami, *Catal. Today*, **16** (1993) 113.

[45] B.K. Hodnett and B. Delmon, *Appl. Catal.*, **15** (1985) 141.

[46] B.K. Hodnett and B. Delmon, *J. Catal.*, **88** (1984) 43.

[47] K. Tanabe, M. Misono, Y. Ono, and H. Hattori, in "*New Solid Acid and Bases*" Kodansha-Elsevier, Tokyo (1989) p.320.

[48] A. Corma, *Chem. Rev.*, **95** (1995) 559.

[49] G. Centi, G. Golinelli, and F. Trifirò, *Appl. Catal.*, **48** (1989) 13.

[50] G. Busca, G. Centi, F. Trifirò, and V. Lorenzelli, *J. Phys. Chem.*, **90** (1986) 1337.

[51] L.M.Cornaglia, E.A. Lombardo, J.A. Anderson, andG. Fierro, *Appl. Catal. A*, **100** (1993) 37.

[52] G. Busca, G. Centi, and F. Trifirò, *Appl. Catal.*, **25** (1986) 265.

[53] M. Ogawa and K. Kuroda, *Hyomen*, **32** (1994) 696.

[54] T. Nakato, Y. Furumi, N. Terao, and T. Okuhara, *J. Mater. Chem.*, **10** (2000) 737.

[55] E.R. Kleinfeld and G.S. Furgson, *Science*, **265** (1994) 370.

[56] S.W. Kelle, H.-N. Kim, and T.E. Mallouk, *J. Am. Chem. Soc.*, **116** (1994) 8817.

[57] R. Abe, K. Shinohara, A. Tanaka, M. Hara, J.N. Kondo, and K. Domen, *Chem. Mater.*, **9** (1997) 2179.

[58] T. Sasaki, S. Nakato, S. Yamauchi, and M. Watanabe, *Chem. Mater.*, **9** (1997) 602.

[59] G. Ladwig, *Z. Anorg. Allg. Chem.*, **338** (1965) 266.

Part I

Properties of Active Sites Controlling Catalytic Performance in the Selective Oxidation of *n*-Butane

Chapter 2

Reduction and Re-oxidation Properties as a Factor Controlling Catalytic Performance in the Selective Oxidation of *n*-Butane

Abstract

Relationship between the reduction and re-oxidation properties, and catalytic performances was investigated by using three types of the $(VO)_2P_2O_7$ catalysts with different microstructures. The catalysts were prepared in organic solvent (VPO-org), by reduction of $VOPO_4 \cdot 2H_2O$ (VPO-redu), and in aqueous medium (VPO-aq). The rates of MA formation per surface area greatly depended on the catalysts; VPO-org was much active, especially at the high partial pressure of *n*-butane. Reaction kinetics suggested that VPO-org had higher re-oxidation ability, by which the surface of VPO-org was retained as a higher oxidation state during the reaction. Actually, it was confirmed that the V^{5+} density of VPO-org during the reaction was about twice those of the other catalysts, and VPO-org showed higher rates of re-oxidation estimated by measurement of re-oxidation with air. It was concluded that the high catalytic activity of VPO-org is due to this high ability of re-oxidation. This would be caused from enhancement of the migration of the oxygen ions near the surface induced by the structural disorder of the catalyst. These results established the concept that the re-oxidation ability should be improved for improving the catalytic activity.

Introduction

Maleic anhydride (abbreviated as MA) is a useful feedstock for unsaturated polyester resins, agricultural chemicals, and food additives and has recently been utilized as a raw material for 1,4-butanediol, tetrahydrofuran, and γ-butyrolactone. In industry at present, MA is mainly produced by selective oxidation of *n*-butane with vanadium-phosphorous mixed oxide catalyst. Vanadyl pyrophosphate ($(VO)_2P_2O_7$) has been claimed to be a main component of the commercial catalyst for the MA production [1-4].

It is well known that the microstructure of $(VO)_2P_2O_7$ crystallites greatly influences their catalytic performances for *n*-butane oxidation [1,5-8]. The $(VO)_2P_2O_7$ crystallites having a block-like and a plate-like shape exhibited high selectivities to MA even at high conversions, because the consecutive oxidation of MA was suppressed over these catalysts [6]. On the other hand, $(VO)_2P_2O_7$ having a rose-petal shape, which was prepared by the so-called organic solvent method, showed the high activity [6].

In this chapter, a relationship between reduction and re-oxidation properties, and catalytic performance of $(VO)_2P_2O_7$ catalysts was investigated. Three types of $(VO)_2P_2O_7$ with different microstructures were used. The redox property of the catalysts were evaluated from kinetic analysis,

and measurement of rates in re-oxidation with O_2 and reduction with *n*-butane. The difference of the catalytic properties in these $(VO)_2P_2O_7$ catalysts will be discussed in relation to the reduction and re-oxidation properties. On the basis of these investigations, the concept concerning the reduction and re-oxidation properties to develop the catalyst of high catalytic activity will be established.

Experimental

Preparation of catalysts

Three types of precursors, vanadium hydrogen phosphate-hemihydrate ($VOHPO_4 \cdot 0.5H_2O$), were prepared according to the literature [6].

Prec-org: This precursor was obtained by the so-called organic solvent method [5]. V_2O_5 (0.08 mol; Koso Chemical Co., Ltd.) was added to a mixture of 90 cm^3 of isobutyl alcohol (Koso Chemical Co., Ltd.) and 60 cm^3 of benzyl alcohol (Koso Chemical Co., Ltd.). This suspension was refluxed at 378 K for 3 h, and was cooled to room temperature. Then, 99 % H_3PO_4 (0.16 mol; MERCK Ltd.) was added to the suspension and the mixture was again refluxed at 378 K for 3 h. The resulting light blue solid was filtered, washed with acetone and dried at room temperature for 16 h.

Prec-redu: This precursor was prepared by reducing $VOPO_4 \cdot 2H_2O$ with 2-butanol (Koso Chemical Co., Ltd.), as follows. V_2O_5 (0.14 mol) was added to an aqueous solution of 85 % H_3PO_4 (600 cm^3; 1.9 mol of H_3PO_4). This mixture was stirred under reflux for 16 h at 378 K. The resulting yellow solid was filtered, washed with acetone and dried at room temperature for 16 h. The obtained solid was confirmed to be $VOPO_4 \cdot 2H_2O$ by XRD [9]. The powder of $VOPO_4 \cdot 2H_2O$ (14 g) was reduced with 2-butanol (150 cm^3) for 18 h at 353 K. The resulting light blue solid was filtered, washed with acetone, and dried at room temperature for 16 h.

Prec-aq: This precursor was prepared by reducing V_2O_5 with $NH_2OH \cdot HCl$ in aqueous solution. V_2O_5 (0.1 mol) was added to an aqueous solution (200 cm^3) of $NH_2OH \cdot HCl$ (0.2 mol, Wako Pure Chem. Ltd.) and 85% H_3PO_4 (0.2 mol) at 353 K, and then stirred for 1 h at 353 K. This solution was evaporated at 403 K overnight. Water (20 cm^3) was added to the solid and the mixture was boiled for 10 min. The resulting light blue solid was filtered, washed with acetone and dried at room temperature for 16 h.

These precursors were pretreated at 823 K for 2 h in N_2 flow (300 cm^3 min^{-1}). The catalysts obtained from Prec-org, Prec-redu, and Prec-aq are denoted as VPO-org, VPO-redu, and VPO-aq, respectively.

Characterization

XRD patterns of the catalysts were measured by using an X-ray diffractometer (Rigaku RINT-1400) with Cu K_α radiation (λ = 0.154 nm). Infrared spectra of the catalysts were measured with an IR spectrometer (Perkin Elmer model 1600). The mixture of the catalyst powder and KBr was pressed into a disk. SEM images of the catalysts were taken with a scanning electron microscope (SEM; HITACHI S-2100B). X-ray photoelectron spectra (XPS) were obtained with a Physical Electronics Model 5600ci spectrometer with Mg K_α radiation. The P/V ratios of catalyst bulk were determined by an inductively coupled plasma atomic emission spectrometer (ICP-AES; Shimadzu ICPS-8000). The catalyst powder was dissolved into hot H_2SO_4, and the solution was diluted with water to about 30 ppm of V or P. The surface area of the catalyst was measured by the BET method using N_2 with a Carlo Erba Sorptomatic Model-1800 after the sample was evacuated at 473 K for 2 h.

Time-profiles of reduction and re-oxidation

Time-profiles of reduction of the catalyst with *n*-butane and re-oxidation with air were measured by using a TG/DTA apparatus (Seiko Instruments, TG/DTA 200). The degrees of reduction and re-oxidation of the catalysts were monitored by the weight decrease in a flow of 10 % *n*-butane (N_2 balance, 50 cm^3 min^{-1} of total flow rate) and the weight increase in air (50 cm^3 min^{-1} of total flow rate), respectively. Prior to the measurements, the catalyst was aged in a flow of 5.0 % *n*-butane in air (total flow rate: 20 cm^3 min^{-1}) at 723 K for 20 h. After the catalyst was cooled to room temperature in a N_2 flow, a part of the catalyst ($\sim$10 mg) was set on an Al pan in the apparatus. Temperature of the sample was then raised in a N_2 flow (50 cm^3 min^{-1}) to 663 K at 10 K min^{-1} and was kept there. After no further decrease in weight was detected at 663 K, the feed gas was changed to 10 % *n*-butane (N_2 balance, 50 cm^3 min^{-1}) to obtain the time-profile of reduction at 663 K. After the catalyst weight become constant, the system was purged with a N_2 flow (50 cm^3 min^{-1}) for 2 h, and again the feed gas was changed to dry air (50 cm^3 min^{-1}) at 663 K to obtain the time-profile of re-oxidation.

Catalytic oxidation of n-butane

Catalytic oxidation of *n*-butane was carried out in a conventional fixed-bed reactor of stainless tubing (inside diameter: 10 mm) under atmospheric pressure. A mixture of *n*-butane and O_2 (N_2 balance) at the total flow rate of 20 cm^3 min^{-1} was fed over the catalyst bed at 663 K. The

concentrations were varied from 0.75 % to 5.0 % for *n*-butane and from 10 % to 30 % for O_2, respectively. The conversion of *n*-butane was controlled by the weight of the catalyst under a constant total flow rate (20 cm^3 min^{-1}), where the flow rates were precisely controlled by thermal mass flow controllers (STEC SEC-310). The products were analyzed with on-line gas chromatographs (FID (Shimadzu 14A or Shimadzu 9A) and TCD (Shimadzu 9A)) equipped with a Porapak QS column (inside diameter 2.2 mm, length 1 m) for *n*-butane and MA, and a Porapak N column (inside diameter 2.2 mm, length 2 m) for CO_2. A Molecular Sieve 13X column (inside diameter 2.2mm, length 4 m) was also used to separate O_2, N_2 and CO. CO and CO_2 were converted to methane by using a Methanizer (Shimadzu MTN-1) to be detected more sensitively by the FID-GC.

Prior to the reaction, the catalysts were aged in the reaction mixture at 723 K for 20 h, and then the temperature was lowered to 663 K in the presence of the reaction mixture.

Results

Microstructure of catalysts

The XRD patterns of catalysts are shown in Fig. 1. The XRD peak positions of these catalysts were same as those reported [6]. On the other hand, the relative intensities and the line-widths were greatly different depending on the catalysts. The diffraction line of the (100) plane on VPO-org was very weak and broad, while those on VPO-redu and VPO-aq were strong and sharp.

Fig. 2 shows the infrared spectra of the catalysts. These catalysts gave peaks at 635 cm^{-1} ($\delta(PO_3)$), 743 cm^{-1} (ν(P-O-P)), 799 cm^{-1} (ν(V-O=V)), 968 cm^{-1} (ν(V=O)) and those at 1081, 1142, 1218, and 1244 cm^{-1} ($\nu(PO_3)$) [5,10]. In the cases of VPO-redu and VPO-aq, the peaks at 1218 cm^{-1}($\nu(PO_3)$) were well separated, whereas the peak of VPO-org appeared as a shoulder. The peak of 799 cm^{-1}(ν(V-O=V)) for VPO-org was very weak and broad [5,10].

The SEM images are shown in Fig. 3. VPO-org was rose-like, VPO-redu was plate-like, and VPO-aq was block-like; such results are consistent with the literature [6].

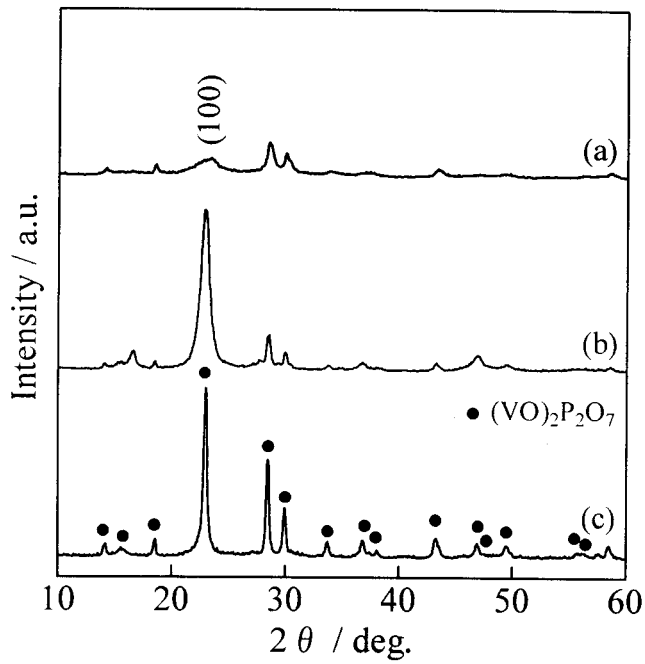

Fig. 1 XRD patterns of (a) VPO-org, (b) VPO-redu, and (c) VPO-aq.

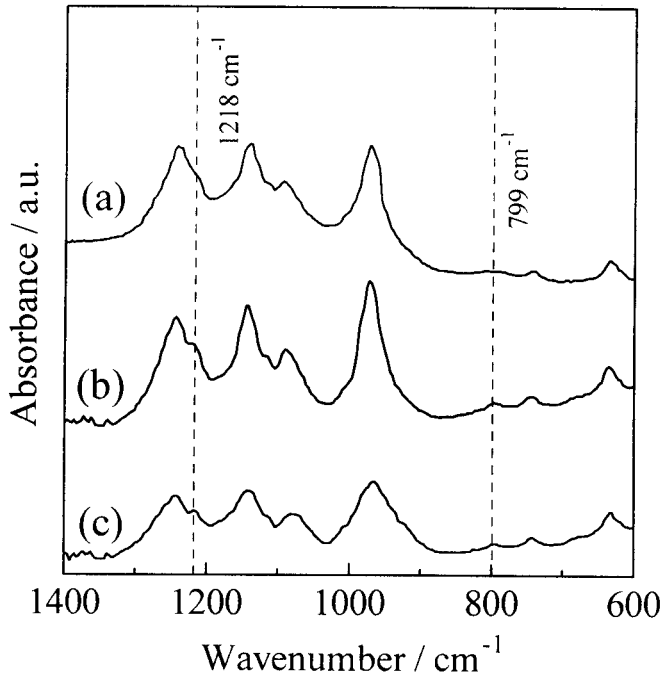

Fig. 2 IR spectra of (a) VPO-org, (b) VPO-redu, and (c) VPO-aq.

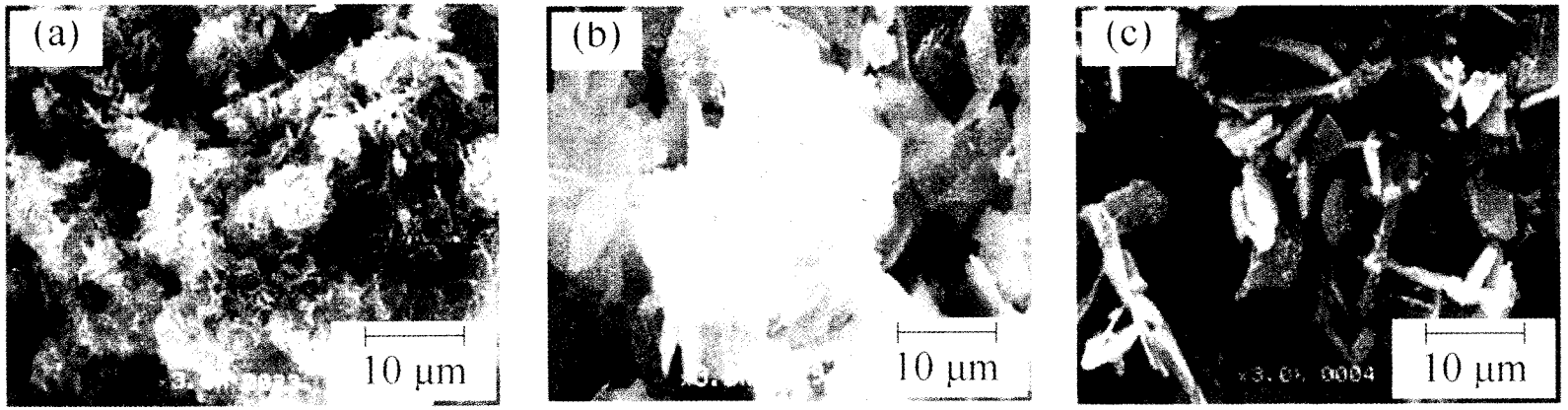

Fig. 3 SEM images of (a) VPO-org, (b) VPO-redu, and (c) VPO-aq.

Table 1 Composition and surface area of $(VO)_2P_2O_7$ catalysts.

	P/V ratio		Surface area
	bulk[a]	surface[b]	$m^2\ g^{-1}$
VPO-org	1.04	1.2	33.0
VPO-redu	1.06	1.2	24.0
VPO-aq	1.07	1.5	5.4

[a]Determined by ICP-AES.

[b]Determined by XPS. These ratios were calculated as 2.75 × I(P) / I(V) [11].

The bulk and surface P/V ratios and the BET surface areas are summarized in Table 1. Here the surface P/V ratios were determined by multiplying the XPS peak intensity (I(P)/I(V)) by a correction factor (2.75) [11]. As shown in Table 1, the bulk P/V ratios of the catalysts, which were analyzed by ICP, were close to 1. In addition, it was found that the surface P/V ratios of VPO-org and VPO-redu were 1.2, while that of VPO-aq was 1.5. There were no difference in the XPS peak positions and shapes of V (517.2 eV) and P (133.9 eV). The BET surface areas were determined to be 33.0, 24.0 and 5.4 $m^2 g^{-1}$ for VPO-org, VPO-redu, and VPO-aq, respectively.

Rates of reduction and re-oxidation

Figure 4 provides the time-profile of reduction with 10 % *n*-butane at 663 K. It is generally accepted that the selective oxidation of *n*-butane over $(VO)_2P_2O_7$ proceeds via a redox cycle between V^{4+} and V^{5+} [12,13], and that *n*-butane reacts with the oxidized surface of $(VO)_2P_2O_7$ [12-14]. Thus the author assumes that the valence of V of the catalyst is 4+, when the decrease of catalyst weight from the reduction with *n*-butane becomes negligible. The reaction is expressed by eq. (1):

$$V^{5+}PO_5 \rightarrow V^{4+}PO_{4.5} + 1/2O \qquad (1)$$

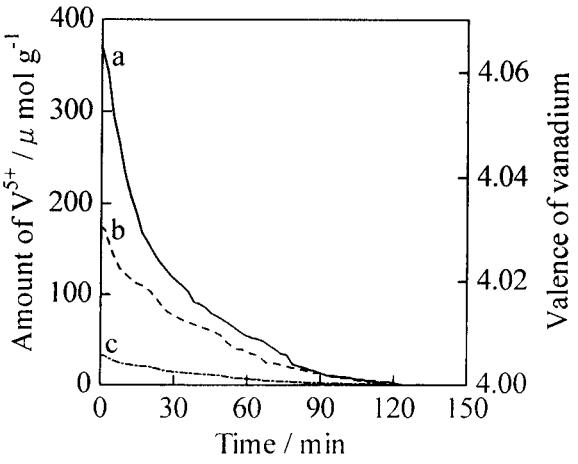

Fig. 4 Time-profiles of reduction with 10 % *n*-butane (N_2 balance) at 663 K. Prior to the reduction, the catalysts were pretreated under 5.0 % *n*-butane in air at 723 K for 20 h. (a) VPO-org, (b) VPO-redu, and (c) VPO-aq.

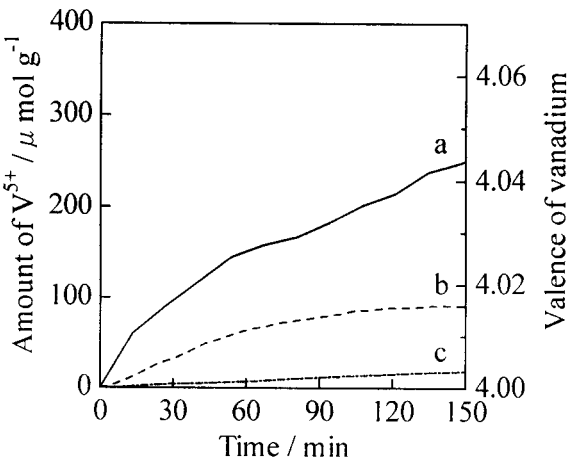

Fig. 5 Time-profiles of re-oxidation with air at 663 K. The catalysts were reduced by 10 % *n*-butane (N_2 balance) at 663 K for 150 min prior to measurement. (a) VPO-org, (b) VPO-redu, and (c) VPO-aq.

The author can estimate the amount of V^{5+} of the catalyst during the reduction process from eq. (2).

$$\text{Amount of } V^{5+} \text{ (mol g}^{-1}) = \frac{W_t \cdot W_{end}}{8 \times W_{end}} \qquad (2)$$

Here W_t (g) and W_{end} (g) represent the catalyst weight at a reduction time and the end of reduction, respectively.

Pepera et al. reported that the number of surface layers involved in the redox processes during the oxidation of *n*-butane is about unity [12]. In addition, Okuhara et al. showed that the diffusion of oxygen atoms is limited to a few surface layers of $(VO)_2P_2O_7$ during the oxidation of *n*-butane from the isotopic study [15]. Furthermore, Koyano et al. also revealed that $(VO)_2P_2O_7$ was oxidized at a top few surface layers with O_2 at 733 K [13]. Therefore, it is considered that Figs. 4 and 5 show the time-profiles of reduction and re-oxidation at a top few surface layers of catalyst, respectively.

The amounts of V^{5+} at the initial state were in the order VPO-org (372 μ mol g^{-1}) > VPO-redu (176 μ mol g^{-1}) > VPO-aq (32 μ mol g^{-1}). These amounts of V^{5+} correspond to 6.4 %, 3.0 %, and 0.4 % of total amounts of V in VPO-org, VPO-redu, and VPO-aq, respectively. The amount of V^{5+} per unit surface area (as listed in Table 1) was estimated to be 11.2 μ mol m^{-2} for VPO-org, which is higher than those for VPO-redu (7.4 μ mol m^{-2}) and VPO-aq (6.0 μ mol m^{-2}). At the initial stage, rapid decreases in catalyst weight were observed over VPO-org and VPO-redu.

Figure 5 shows the time-profiles of re-oxidation with air at 663 K. The initial rate of re-oxidation (estimated from the slope of the curve) was in the order: VPO-org > VPO-redu > VPO-aq. In the case of VPO-org, about 3.2 % of V in the catalyst was oxidized after 120 min.

The initial rates of re-oxidation of the catalysts are summarized in Table 2. The order of the initial rates of re-oxidation was VPO-org (264 μ mol g^{-1} h^{-1}) > VPO-redu (104 μ mol g^{-1} h^{-1}) > VPO-aq (28 μ mol g^{-1} h^{-1}). The re-oxidation rate per unit surface area were 8.0 μ mol m^{-2} h^{-1} for VPO-org and 4.4 – 5.2 μ mol m^{-2} h^{-1} for VPO-redu and VPO-aq.

Table 2 Initial rates of re-oxidation of $(VO)_2P_2O_7$ catalysts.

	Initial rate of re-oxidation[a]	
	μ mol g^{-1} h^{-1}	μ mol m^{-2} h^{-1}
VPO-org	264	8.0
VPO-redu	104	4.4
VPO-aq	28	5.2

[a]The initial rate was estimated by the weight increase in air at 663 K.

Catalytic oxidation of n-butane

Typical time courses of the conversion and selectivity during the aging process at 723 K over VPO-org are given in Fig. 6, where the concentration of *n*-butane was 1.5 % (Fig. 6 (a)) or 5.0 % (Fig. 6 (b)). The carbon balance was confirmed to be 98 - 100 %. At the initial stage of the reaction, the conversion of *n*-butane and selectivity to MA increased slightly with time for both reaction conditions. After 15 h, both the conversion and the selectivity reached nearly stationary values for both reaction conditions. Since VPO-redu and VPO-aq gave similar time courses to VPO-org, the catalysts were aged in each reaction mixture at 723 K for 20 h.

Figure 7 shows the dependence of conversion on *W/F* with 5.0 % *n*-butane and 20 % O_2 at 663 K, where *W* is the catalyst weight and *F* is the flow rate of *n*-butane. While the conversion increased as *W/F* increased for all catalysts, the slope of the curve became smaller at high values of *W/F*. The reaction rates were calculated from the slope of the linear portions of the curves at conversions less than 15 %.

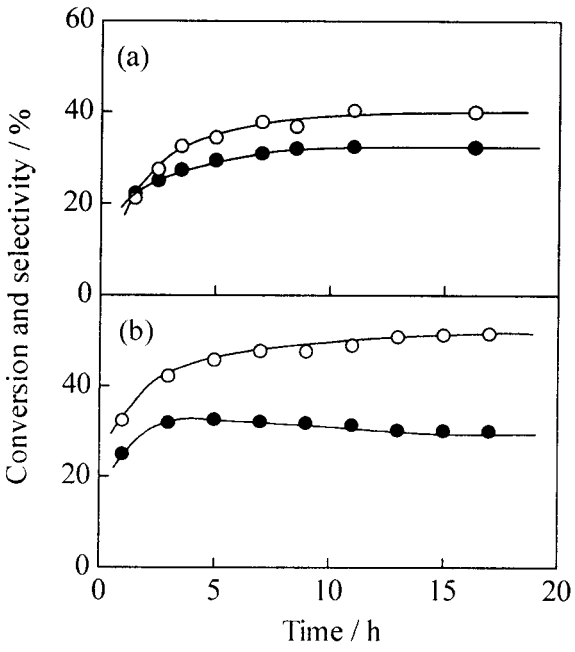

Fig. 6 Time courses of catalytic oxidation of *n*-butane over VPO-org at 723 K with 20 % O_2. Concentrations of *n*-butane were (a) 1.5 %, or (b) 5.0 %. *W/F* (catalyst weight / flow rate) were 97 and 100 g h (mol of *n*-butane)$^{-1}$ for 1.5 % and 5.0 % *n*-butane, respectively: (●) conversion of *n*-butane and (○) selectivity to maleic anhydride.

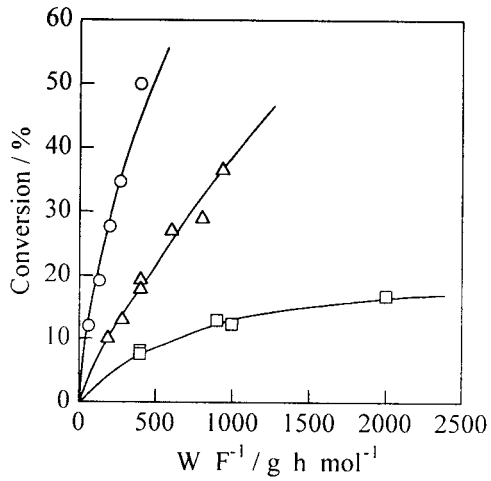

Fig. 7 Dependencies of conversion of *n*-butane on *W/F* at 663 K. Reaction was carried out with 5.0 % *n*-butane and 20 % O_2: (○) VPO-org, (△) VPO-redu, and (□) VPO-aq.

The dependence for the rate of MA or COx (CO + CO_2) formation on the concentration of *n*-butane is given in Fig. 8, where the concentration of *n*-butane was varied from 0.75 % to 5.0 %, being the concentration of O_2 (20 %) being constant. The rates are expressed for unit surface area. Since the conversions were less than 15 %, the consecutive oxidation of MA would be negligible [6,16-19]. The rates of MA formation increased as the *n*-butane concentration increased. It should be emphasized that the rates of MA formation on VPO-org increased by 3.5 times as the *n*-butane concentration increased from 0.75 % to 5.0 %, while those on VPO-redu and VPO-aq increased by only 2.0 times. The reaction orders for MA formations estimated from the slopes in the rights of Fig. 8 were about 0.6, 0.3 and 0.3 on VPO-org, VPO-redu, and VPO-aq, respectively. The reaction orders for COx formation were nearly zero on VPO-org and 0.1 for VPO-redu, and VPO-aq, the rates of COx formation were in this order: VPO-redu < VPO-aq < VPO-org.

The influence of *n*-butane concentration on the selectivity to MA is summarized in Table 3, where the data were collected at the conversions less than 15 %. The selectivity to MA was in the order: VPO-org (45 %) < VPO-aq (54 %) < VPO-redu (63 %) with 0.75 % *n*-butane. The selectivity increased from 45 % to 74 % on VPO-org as the concentration of *n*-butane increased from 0.75 % to 5.0 %. Those on VPO-redu and VPO-aq increased slightly: from 63 % to 67 % on VPO-redu and from 54 % to 61 % on VPO-aq.

Figure 9 shows the dependence of rates on the O_2 concentration; here the concentration of *n*-butane was adjusted to 5.0 %. The reaction order for MA formation on the O_2 concentration was close to 0.4 on all catalysts. On the other hand, the reaction orders on COx formation were about 0.4 on VPO-org and 0.6 on VPO-redu and VPO-aq.

Table 3 Influence of concentration of *n*-butane on selectivity to maleic anhydride in *n*-butane oxidation over $(VO)_2P_2O_7$ catalysts[a].

Catalyst	Selectivity to maleic anhydride[b]			
	0.75 %[c]	1.5 %[c]	3.0 %[c]	5.0 %[c]
VPO-org	45	57	63	74
VPO-redu	63	67	68	67
VPO-aq	54	58	67	61

[a]The reaction was carried out with 20 % O_2 at 663 K.
[b]Selectivity to maleic anhydride at conversions less than 15 %.
[c]Concentration of *n*-butane.

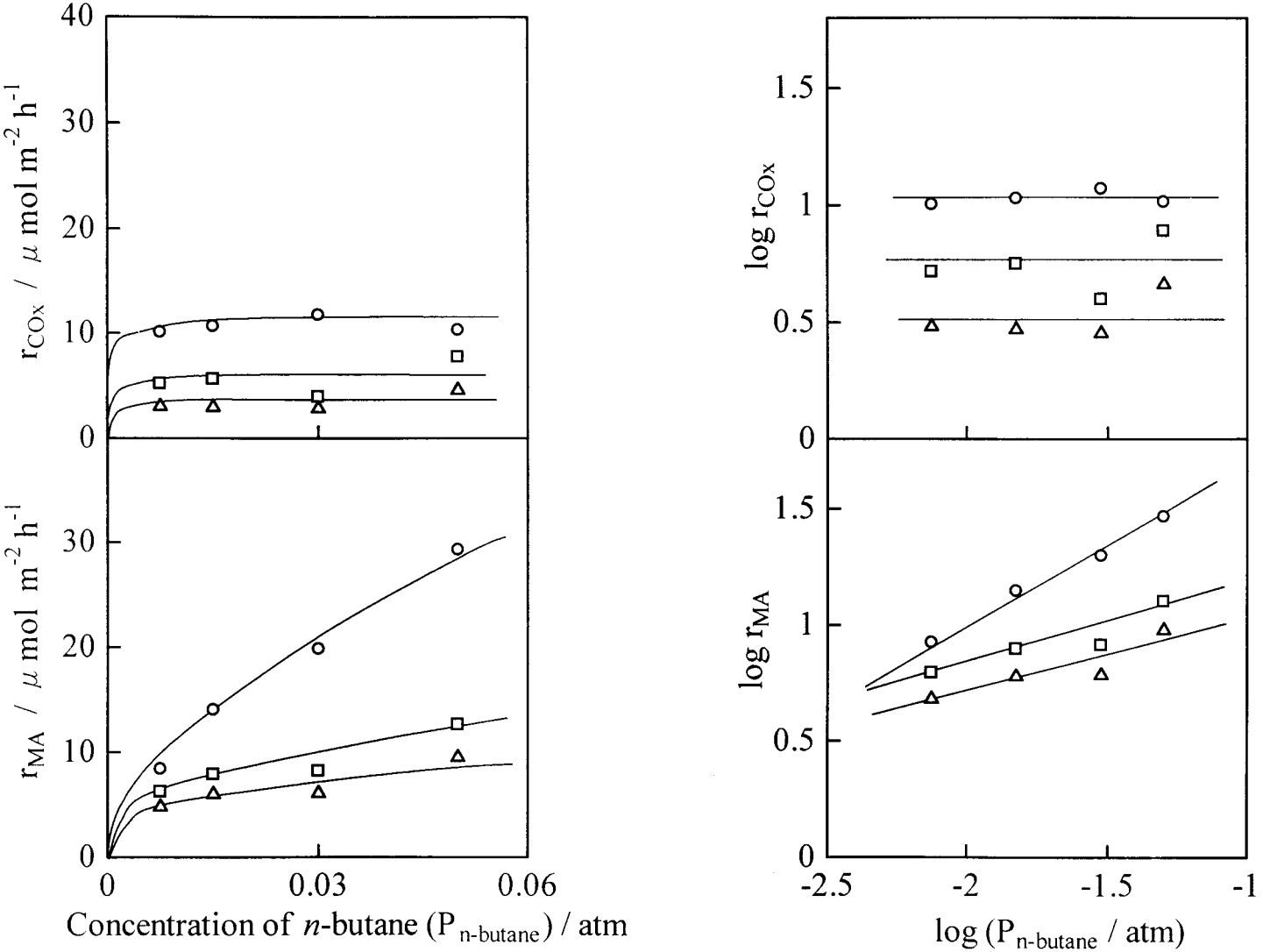

Fig. 8 Dependencies of rates for maleic anhydride and COx formation on the concentration of *n*-butane. The concentration of O_2 is 20 % and the reaction temperature is 663 K. r_{MA}, r_{COx} and $P_{n\text{-butane}}$ represent rate for maleic anhydride, COx formation and concentration of *n*-butane, respectively: (○) VPO-org, (△) VPO-redu, and (□) VPO-aq.

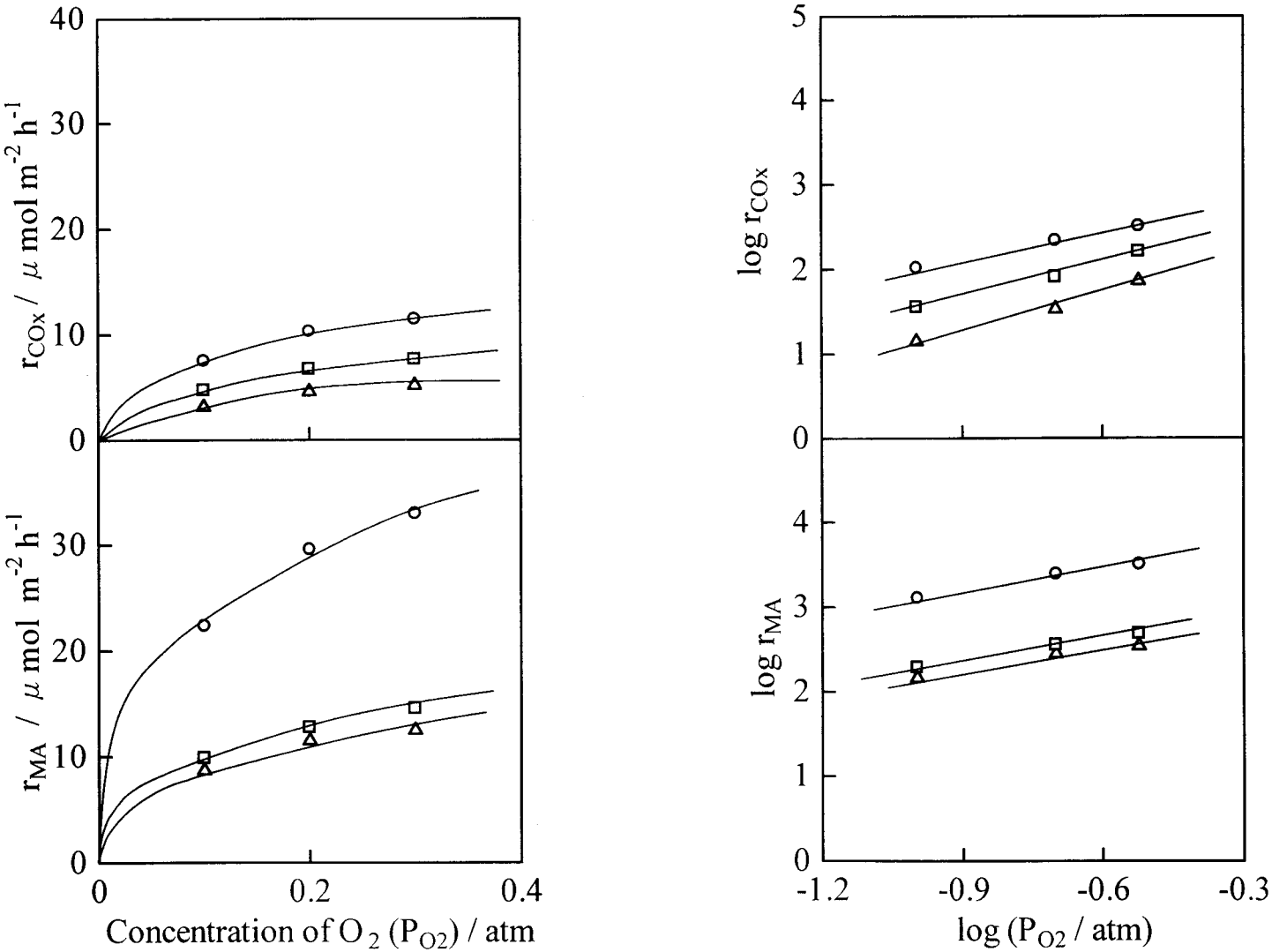

Fig. 9 Dependencies of rates for maleic anhydride and COx formation on the concentration of O_2. The concentration of *n*-butane is 5.0 % and the reaction temperature is 663 K. r_{MA}, r_{COx} and $P_{n\text{-butane}}$ represent rate for maleic anhydride, COx formation and concentration of *n*-butane, respectively: (○) VPO-org, (△) VPO-redu, and (□) VPO-aq.

Discussion

Kinetics and surface oxidation state

From Figs. 8 and 9, the kinetics for MA formation are shown by eqs. (3) and (4), where r_{MA} and r'_{MA} are rates of MA formation. $P_{n\text{-butane}}$ and P_{O2} are concentrations of *n*-butane and O_2, respectively, and k and k' represent the rate constants.

$$r_{MA} = kP_{n\text{-butane}}^{0.6}P_{O2}^{0.4} \qquad \text{(VPO-org)} \qquad (3)$$

$$r'_{MA} = k'P_{n\text{-butane}}^{0.3}P_{O2}^{0.4} \qquad \text{(VPO-redu and VPO-aq)} \qquad (4)$$

The higher reaction order of *n*-butane concentration on VPO-org gives rise to the higher catalytic performance at the high *n*-butane concentration.

The selective oxidation of *n*-butane over $(VO)_2P_2O_7$ has been considered to proceed via a redox mechanism at the surface layers [12,13,16,20]. On the basis of this mechanism, the MA formation can simply be described in the following two steps [12,17], where [ ] and [O] represent the amount of reduced sites and the amount of oxidized site of catalyst, respectively. O_2, Bu and MA represent oxygen, *n*-butane and MA in a gas phase, and k_{ox} and k_{re} are reaction constants of re-oxidation and reduction of catalyst surface, respectively.

$$[\ ] + O_2 \xrightarrow{k_{ox}} [O] \qquad (5)$$

$$[O] + Bu \xrightarrow{k_{re}} MA + [\ ] \qquad (6)$$

When the reaction reached the stationary state, the rate of re-oxidation is equal to that of reduction, and the stationary oxidation state of the surface is proportional to k_{ox} / k_{re}. The general expression for the rate of MA formation is expressed in eq. (7) from this process [12].

$$r_{MA} = \frac{1}{\dfrac{1}{k_{re}P_{n\text{-butane}}} + \dfrac{\alpha}{k_{ox}P_{O2}}} \qquad (7)$$

Here α indicates the stoichiometric number of moles of O_2 required for this reaction (α=3.5). In the expression, if the rate of reduction is much lower than that of re-oxidation ($k_{ox}>>k_{re}$), the

expression reduces to $k_{re}P_{n\text{-butane}}^{1.0}P_{O2}^{0.0}$. On the contrary, if the rate of reduction much higher than that of re-oxidation ($k_{re}>>k_{ox}$), the expression becomes $k_{ox}\alpha^{-1}P_{n\text{-butane}}^{0.0}P_{O2}^{1.0}$. The ratio of the reaction order on *n*-butane concentration (*n*) to that of O_2 concentration (*m*) is thus related to the ratio of the rate of re-oxidation to that of reduction, i.e., k_{ox}/k_{re}. As the k_{ox}/k_{re} becomes higher, *n*/*m* will become larger. It is suggested that k_{ox}/k_{re} on VPO-org is higher than those on VPO-redu and VPO-aq from the ratio of *n*/*m*; 1.5 on VPO-org and 0.75 on VPO-redu and VPO-aq. This indicates that the surface of VPO-org is in a higher oxidation state during the reaction. As shown in Fig. 4, the estimated amounts of V^{5+} at the stationary state differed greatly from one catalyst to another. The density of V^{5+} was 11.2, 7.4, and 6.0 μ mol m^{-2} on VPO-org, VPO-redu, and VPO-aq, respectively; that is, the V^{5+} density of VPO-org was about twice those of VPO-redu and VPO-aq, which indicates that VPO-org is more readily oxidized with O_2, and in the higher oxidation state during the catalytic oxidation of *n*-butane. As a matter of fact, the specific rate of re-oxidation of VPO-org was higher than those of VPO-redu and VPO-aq (Fig. 5 and Table 2). The high catalytic performance of VPO-org at the high *n*-butane concentration is due to the high re-oxidizability. By this, the catalyst surface is retained to be an appropriate oxidation state under the highly reducing reaction conditions.

The next question is why the surface of VPO-org is more readily oxidized compared to that of VPO-redu and VPO-aq. Two possible reasons should be considered. The first is the influence of the P/V ratios. Hodnett et al. reported [21] that the rate of the re-oxidation of $(VO)_2P_2O_7$ decreased as the bulk P/V ratios increased. However, as shown in Table 1, both the bulk and surface P/V ratios of VPO-org were almost the same as those of VPO-redu. Therefore it is difficult to explain the different kinetics between VPO-org and VPO-redu in terms of a difference in the P/V ratios.

The second is the influence of the structural disorder of the catalyst. Busca et al. suggested [5] that the structural disorder affected the redox property of $(VO)_2P_2O_7$. Satsuma et al. also reported [22] that the activity of the surface V=O species depended on the structural disorder of the catalyst. It is generally accepted that the reflection peak of the (100) plane of $(VO)_2P_2O_7$ prepared by the organic solvent method is broad due to the disorder of the $(VO)_2P_2O_7$ crystallites along the vertical direction against the (100) plane [5,10]. As shown in Fig. 1, the diffraction from the (100) plane of VPO-org was broader than those of the VPO-redu and VPO-aq. Furthermore, as

shown in Fig. 2, the peaks of 799 cm^{-1} (ν (V-O=V)) and 1218 cm^{-1} (ν (PO_3)) of VPO-org were weaker than those of VPO-redu and VPO-aq. These results also suggest the existence of structural disorder in VPO-org [5,6,10]. Therefore, it is concluded that the structural disorder of VPO-org is responsible for the high re-oxidizability of VPO-org.

An isotopic study revealed that the rate-determining step is a hydrogen abstraction from *n*-butane [12]. The surface oxygen atoms supplied from gas-phase O_2 are probably active oxygen species, because *n*-butane was oxidized only after the $(VO)_2P_2O_7$ was oxidized with O_2 in the pulse study [12-14]. For this key step, the abstraction of hydrogen from *n*-butane, it is likely that the specific reaction rate (per active site) is proportional to the pressure of *n*-butane under a certain oxidation state of the surface, since the adsorption of *n*-butane at the sites is weak. The overall reaction rate is considered to the product of the specific reaction rate (per active site) and the amount of active oxygen atoms. The amount of active oxygen atoms corresponds to that of V^{5+}. It is reasonably deduced that the amount of V^{5+} during the reaction is negatively dependent on the concentration of *n*-butane. By combination of the specific reaction rate ($\propto P_{n\text{-butane}}^{1.0}$) and the amount of V^{5+} ($\propto P_{n\text{-butane}}^{-x}$, $0 < x < 1$), the reaction order of *n*-butane concentration might be less than unity.

On the other hand, the kinetics for COx formation are shown by eqs. (8) and (9) from Figs. 8 and 9, where r_{COx} and r'_{COx} are the rates of CO_x formation.

$$r_{COx} = k_{COx} P_{n\text{-butane}}^{0.0} P_{O2}^{0.4} \qquad \text{(VPO-org)} \qquad (8)$$

$$r'_{COx} = k'_{COx} P_{n\text{-butane}}^{0.1} P_{O2}^{0.6} \qquad \text{(VPO-redu and VPO-aq)} \qquad (9)$$

CO_x formation has been considered to take place on the different sites from those of MA formation [23]; for example, this concerns with adsorbed oxygen species [24,25]. As a matter of fact, the reaction order of *n*-butane concentration for COx formation was nearly zero, which was different from that of the MA formation.

Applications to operations at high concentrations of n-butane

From an industrial viewpoint, the operation under a higher *n*-butane concentration makes it possible to achieve a higher space-time yield of MA. To realize such a operation, we need a

catalyst exhibiting a high activity, selectivity and stability under the high *n*-butane concentration. As shown in Fig. 6, it was confirmed that the deactivation of VPO-org was little under 5.0 % *n*-butane.

As shown in Fig. 8, the rate of MA formation effectively increased over VPO-org as the *n*-butane concentration increased. On the other hand, the rate of CO_x formation was independent of *n*-butane concentration over VPO-org, while those over VPO-redu and VPO-aq slightly increased with the increase in *n*-butane concentration. As the result, the selectivity to MA on VPO-org increased greatly with the increase in *n*-butane concentration (Table 3). It was demonstrated that VPO-org is suitable for operation under the high *n*-butane concentration for both high activity and selectivity.

It is well known that the characteristic properties of an "equilibrated catalyst", which has been kept in a reaction mixture for several hundreds hours, is a good crystallinity [3,26,27] and the formation of stable V^{4+} [27]. Shima et al. [28] reported that the equilibrated catalysts exhibit a great dependence of the catalytic activity on the O_2 concentration, and also pointed out the importance of re-oxidation process over the equilibrated catalysts.

The selectivity to MA decreases at a high conversions due to the consecutive oxidation of MA [6,18,29]. In the case of the operation under a high *n*-butane concentration, the MA concentration becomes higher. Therefore the influence of these concentration for the consecutive oxidation of MA is of great importance if one operates at the high *n*-butane concentration.

Conclusion

Selective oxidation of *n*-butane to MA was investigated with a wide range partial pressures of n-butane and O_2 using three types of $(VO)_2P_2O_7$ catalysts. It was revealed that the catalysts, exhibiting the higher catalytic performance for MA formation, possessed high redox ability, especially re-oxidation. The higher ability of re-oxidation caused appropriate oxidation state of the surface for MA formation. The higher redox ability is probably brought about from the structural disorder of the catalyst. These results established that the re-oxidation ability should be improved for improving the catalytic activity.

References

[1] B. K. Hodnett, *Catal. Rev. Eng.*, **17** (1985) 373.

[2] E. Bordes, *Catal. Today*, **1** (1987) 499.

[3] G. Centi, F. Trifirò, J. R. Ebner and V. M. Franchetti, *Chem. Rev.*, **88** (1988) 55.

[4] G. J. Hutchings, *Appl. Catal.*, **72** (1991) 1.

[5] G. Busca, F. Cavani, G. Centi and F. Trifirò, *J. Catal.*, **99** (1986) 400.

[6] H. Igarashi, K. Tsuji, T. Okuhara and M. Misono, *J. Phys. Chem.*, **97** (1993) 7065.

[7] E. Bordes and P. Courtine, *J. Solid State Chem.*, **55** (1984) 270.

[8] T. Shimoda, T. Okuhara and M. Misono, *Bull. Chem. Soc. Jpn.*, **58** (1985) 2163.

[9] G. Ladwing, *Z. Anorg. Allg. Chem.*, **338** (1965) 266.

[10] M. L. Granados, J. C. Conesa and M. Fernández-García, *J. Catal.*, **141** (1993) 671.

[11] T. Okuhara, T. Nakama and M. Misono, *Chem. Lett.*, (1990) 1941.

[12] M. Pepera, J. L. Callahan, M. J. Desmond, E. C. Milberger, P. R. Blum and N. J. Bremer, *J. Am. Chem. Soc.*, **107** (1985) 4883.

[13] G. Koyano, T. Okuhara and M. Misono, *Catal. Lett.*, **32** (1995) 205.

[14] G. Koyano, T. Okuhara and M. Misono, *J. Am. Chem. Soc.*, **120** (1995) 767.

[15] T. Okuhara and M. Misono, *Catal. Today*, **16** (1993) 61.

[16] F. B. Abdelouahab, R. Olier, N. Guilhaume, F. Lefebvre and J. C. Volta, *J. Catal.*, **134** (1992) 151.

[17] S. K. Bej and M. S. Rao, *Ind. Eng. Chem. Res.*, **30** (1991) 1824.

[18] G. Centi, G. Fornasari and F. Trifirò, *Ind. Eng. Chem. Prod. Res. Dev.*, **24** (1985) 32.

[19] F. Cavani, G. Centi and F. Trifirò, *Appl. Catal.*, **15** (1985) 151.

[20] G. H. Hutchings, A. D. Chomel, R. Olier and J. C. Volta, *Nature*, **368** (1994) 41.

[21] B. K. Hodnett and B. Delmon, *Appl. Catal.*, **15** (1985) 141.

[22] A. Satsuma, Y. Tanaka, T. Hattori and Y. Murakami, *Appl. Surf. Sci.*, **121/122** (1997) 496.

[23] K. Inumaru, T. Okuhara and M. Misono, *Chem. Lett.*, (1992) 947.

[24] U. Rodemerck, B. Kubis, H.-W. Zanthoff and M. Baerns, *Appl. Catal. A*, **153** (1997) 203.

[25] J. T. Gleaves, J. R. Ebner and T. C. Kuechler, *Catal. Rev.-Sci. Eng.*, **30** (1988) 49.

[26] F. Cavani and F. Trifirò, *Chemtech*, **18** (1994).

[27] F. Trifirò, *Catal. Today*, **16** (1993) 91.

[28] K. Shima and M. Hatano, *Appl. Surf. Sci.*, **121/122** (1997) 452.

[29] T. P. Moser, R. W. Wenig and G. L. Schrader, *Appl. Catal.*, **34** (1987) 39.

Chapter 3

Acidic Property as a Factor Controlling Catalytic Performance in the Selective Oxidation of *n*-Butane

3.1 Dimethylpyridine-temperature programmed desorption method for quantitative determination of Brønsted and Lewis acid sites on solid acid catalysts

Abstract

Temperature-programmed desorption of dimethylpyridine (DMP-TPD) was established for quantitative measurement of strengths and amounts of Brønsted acid and Lewis acid sites on metal oxide catalysts. Alumina, alumina-boria, silica-magnesia, and silica-alumina were employed as typical samples. From IR spectra of adsorbed pyridine and ammonia, it was confirmed that Lewis acid sites were abundant on alumina, Brønsted acid sites were abundant on alumina-boria, and both were present on silica-magnesia and silica-alumina surfaces. TPD spectra of 2,6-DMP on alumina depended on purging temperatures. The amount of desorbed 2,6-DMP decreased with the increase in the purging temperature, and only negligible amount of 2,6-DMP was detected with the purging of 523 K. These results suggested the selective adsorption of 2,6-DMP on the Brønsted acid sites. Selective adsorption of 2,6-DMP on Brønsted acid sites was also confirmed from in-situ IR spectra. The steric hindrance of the methyl groups would be due to the selective adsorption on the Brønsted acid sites. On the other hand, 3,5-DMP was adsorbed on Lewis acid sites of alumina. In the case of alumina-boria on which Brønsted acid sites are abundant, both 2,6-DMP-TPD and 3,5-DMP-TPD spectra showed similar desorption profiles. Profiles of acid strength determined from DMP-TPD were agreed well with those determined from IR spectra of 3,5-DMP adsorbed on silica-magnesia. From these results, it was elucidated that 3,5-DMP-TPD, 2,6-DMP-TPD and the differential spectra indicate the total, Brønsted and Lewis acid sites, respectively.

Introduction

Temperature-programmed desorption of basic molecules is a popular method for determination of acid amount of solid catalysts as well as acid strength, because this is an easy and reproducible method [1-5]. Ammonia is frequently used as a probe molecule because of its small molecular size, stability and strong basicity (pKa=9.2). Theoretical analysis of NH_3-TPD spectra has also been done, thus, one can estimate the change of enthalpy and the activation energy for desorption of NH_3 on the

basis of such a theoretical analysis [6-11]. There have also been some attempts by using pyridine as a probe molecule in TPD [12,13]. Although the application of Py-TPD is not suitable for porous materials because the steric factor plays a dominant role in diffusion in zeolite channels [10], it was demonstrated that Py-TPD is applicable to superacids and binary oxide catalysts [13,14]. A good correlation can be obtained between the H_0 values of the highest acid strength (H_0,max) determined by the Hammett method and the termination temperature of pyridine desorption.

Since ammonia and pyridine adsorb on both Brønsted and Lewis acid sites, the determination of respective strength of acid sites is impossible by using only NH_3-TPD and Py-TPD. Brønsted and Lewis acid sites play different roles in various types of catalytic reactions, and the strength of respective acid sites strongly affects the catalytic performance [4]. Therefore, there is a significant motivation to develop an easy and reproducible method for the quantitative measurement of both strength and amount of Brønsted and Lewis acid sites, separately. It has been reported that dimethylpyridine (DMP) is useful probe for the selective determination of the Brønsted acid sites. Benesi [15] suggested that 2,6-dimethylpyridine (2,6-DMP) can be used as a proton specific probe. Several researchers also applied 2,6-DMP as a probe for Brønsted acid sites in static IR measurements [16-19]. Jacobs et al. [16] reported that 2,6-DMP was strongly adsorbed on Brønsted acid sites of Y-zeolite, but it also formed weaker bonds with Lewis acid sites. The formation of weak bonds between 2,6-DMP and Lewis acid sites was also reported in the cases of alumina and boron phosphate as well as Y-zeolite [17-19]. According to their reports, suitable adsorption temperature must be required in order to apply 2,6-DMP as a selective probe for detection of the Brønsted acid sites. Although Sato et al. [20] suggested the possibility of use of 2,6-DMP for the determination of Brønsted acid sites, the selective adsorption of 2,6-DMP was not verified and the scope of this method is still unclear.

In this section, the possibility of use of 2,6-DMP and 3,5-DMP as probe molecules for the determination of the acid strength of Brønsted and Lewis acid sites was investigated. For the verification of use of DMP-TPD, the adsorption state of DMP molecules are studied by in-situ IR spectra.

Experimental

Catalysts

Solid acid catalysts used in this study are listed in Table 1. Alumina, silica-magnesia, silica-alumina and H-mordenite were supplied from the Committee on Reference Catalysts of the Catalyst Society of Japan. Alumina-boria catalyst was prepared by impregnation of alumina (JRC-ALO-1A) with an aqueous solution of H_3BO_4 followed by evaporation at 353 K for 5 h [21]. The content of supported boria was 30 wt%. The obtained solid was dried at 403 K for 3 h in air and then calcined at 673 K for 5 h in air.

Table 1 List of solid acid catalysts examined in this study.

catalyst	source	BET surface area /m^2g^{-1}
alumina	JRC-ALO-1A (Sumitomo Chemical)	160
silica-magnesia	JRC-SM-1 (Mizusawa Industrial Chemicals)	353
silica-alumina	JRC-SAH-1 (Catalysts & Chemicals)	513
alumina-boria	Prepared (70wt% alumina- 30wt% boria)	86
H-mordenite	JRC-Z-HM10 (Tosoh Corp.)	-

Temperature Programmed Desorption (TPD)

TPD measurement was performed by using the same apparatus reported in the literature [14]. Pyridine (Py), 2,6-dimethylpyridine (2,6-DMP) and 3,5-dimethylpyridine (3,5-DMP) were used as probe molecules. A U-shaped tube made of quartz was used as the sample cell. A catalyst of 100 mg was placed in a sample cell and pretreated at 673 K for 2 h in flowing dehydrated helium at 150 cm^3 min^{-1}. After cooling to prescribed temperature, the catalyst was exposed to a stream of the probe molecule diluted in helium for 30 min. The probe molecule was saturated in helium at 300-330 K. The equilibrium adsorption was confirmed by the concentration of the probe molecule passed through the catalyst. Then, the sample was left in flowing helium at the same temperature for 120 min in order to purge any excess and/or weakly adsorbed probe molecule. This temperature was termed "purging temperature" hereafter. Finally, the TPD measurement was performed from the purging temperature to 1073 K at 5 K min^{-1}. The desorbed probes were detected with a flame-ionization detector (FID) because of its high sensitivity to organic molecules and no influence by water vapor. The line between the sample cell and the FID detector was heated at 400 K.

In-situ Infrared Spectra

The infrared spectra were measured with JASCO FT/IR-300 equipped with a quartz cell and a flow system similar to that used in the TPD measurement [14]. A self-supported catalyst disk (ca. 40 mg) was placed in a quartz cell. The sample was pretreated at 673 K for 120 min in helium at 150 cm^3 min^{-1}. A background spectrum was measured in flowing helium after cooling to the prescribed temperature, and then 20 mm^3 of probe molecule or 20 cm^3 of ammonia was injected into a stream of helium with heating. After purging in flowing helium for 120 min, infrared spectra were measured in the following conditions: scan, 100 times; resolution, 2 cm^{-1}; detector, TGS.

Results and discussion

IR spectra of adsorbed pyridine

Table 2 summarized the absorption bands of pyridine adsorbed on the metal oxide catalysts at 473 K. In the case of alumina, the adsorption bands were observed at 1620, 1614, 1575, 1492 and 1450 cm^{-1}. These bands were assigned to coordinately held pyridine [22]. No band was observed in OH stretching region, 3700-3800 cm^{-1}. These results indicate that Lewis acid sites are abundant on alumina surface, being in agreement with the general knowledge that alumina is a typical solid Lewis acid [18]. On silica-magnesia and silica-alumina, the bands for pyridine adsorbed on both Brønsted and Lewis acid sites were observed. Negative bands were also observed at 3730-3740 cm^{-1} after the adsorption of pyridine, indicating the adsorption of pyridine on surface OH group. With increasing in the purging temperature, the absorption bands of pyridine almost disappeared on silica-magnesia at 773 K, while the small bands due to pyridine adsorbed on Lewis acid sites remained on silica-alumina.

In the case of alumina-boria, although the bands around 1640-1428cm^{-1} and negative band around 3702-3686 cm^{-1} were observed, absorbance below 1600cm^{-1} was near to zero because of strong absorption of alumina-boria itself. The negative bands around OH stretching region indicates the presence of Brønsted acid sites, however, the presence or absence of Lewis acid sites cannot be determined. Then, the presence of Lewis acid sites on alumina-bolia was examined with IR spectra of adsorbed ammonia at 423 K. At the boria content of 3wt%, a small absorption band was observed at 1620 cm^{-1}, which is attributable to ammonia adsorbed on Lewis acid sites [22]. At the boria content of 30%, the band at 1620 cm^{-1} was not observed and the negative bands at 3671-3705 cm^{-1}

were observed, indicating the increase in Brønsted acid sites at the sacrifice of disappearance of Lewis acid sites. This result agreed well with the report that the boria content of 30 wt% is enough amount for the covering all the surface of alumina with boria [21].

Consequently, the solid acid catalysts examined in this study were classified into three categories: (1) Alumina having Lewis acid sites in abundance, (2) 30wt% alumina-boria having Brønsted acid sites in abundance, and (3) silica-magnesia and silica-alumina having both Brønsted acid and Lewis acid sites, and the Lewis acid sites of the silica-alumina were very strong.

Table 2 Wavenumber of absorption bands on IR spectra of adsorbed pyridine at 473 K.

mode	assignment [a)]	wavenumber / cm^{-1}		
		alumina	silica-magnesia	silica-alumina
8a	B		1637	1636
8a	L	1620, 1614	1607	1620
8b	B and/or L	1575	1573	1575
19b	B		1543	1542
19a	B and/or L	1492	1490	1491
19b	L	1450	1446	1454

[a)] B, pyridinium ion on Brønsted acid site; L, coordinately held pyridine on Lewis acid site

Alumina: Selectivity in adsorption of dimethylpyridines on Lewis acid sites

In order to examine the selectivity in adsorption of dimethylpyridines on Lewis acid sites, alumina was employed as a model for Lewis acid catalyst. Fig. 1 shows the TPD spectra for 2,6-DMP adsorbed on alumina after purging at various temperatures. The spectrum after purging at 423 K showed a sharp desorption peak having a maximum at ca. 500 K and a broad peak at 650-900 K. The integrated amount of desorbed 2,6-DMP was 1.59×10^{-4} mmol m^{-2}. As the purging temperature increased, the amount of desorbed 2,6-DMP significantly decreased. When 2,6-DMP was purged at 523 K, only a negligible amount of 2,6-DMP (2.33×10^{-6} mmol m^{-2}) desorbed at 520 – 1073 K.

Figs. 2a and 2b show 3,5-DMP-TPD spectra of alumina. When the TPD run started from 423 K, the spectrum showed a broad peak having a small shoulder above 600 K. Starting from 523 K, the single peak having a maximum at 640 K was observed. The desorbed amount of 3,5-DMP started form 523 K was 2.33×10^{-4} mmol m^{-2}, which was larger enough than that of 2,6-DMP (Fig. 2c).

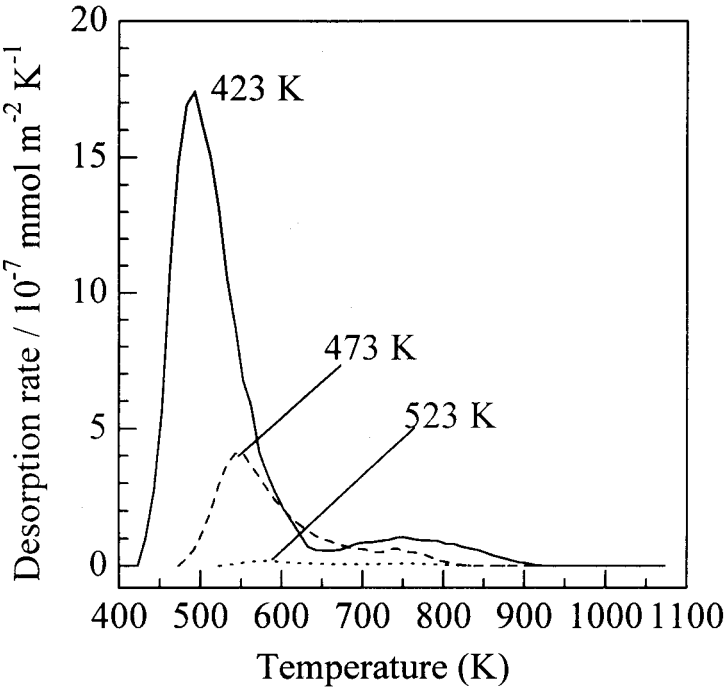

Fig. 1 TPD spectra for 2,6-DMP adsorbed on alumina after purging at various temperatures.

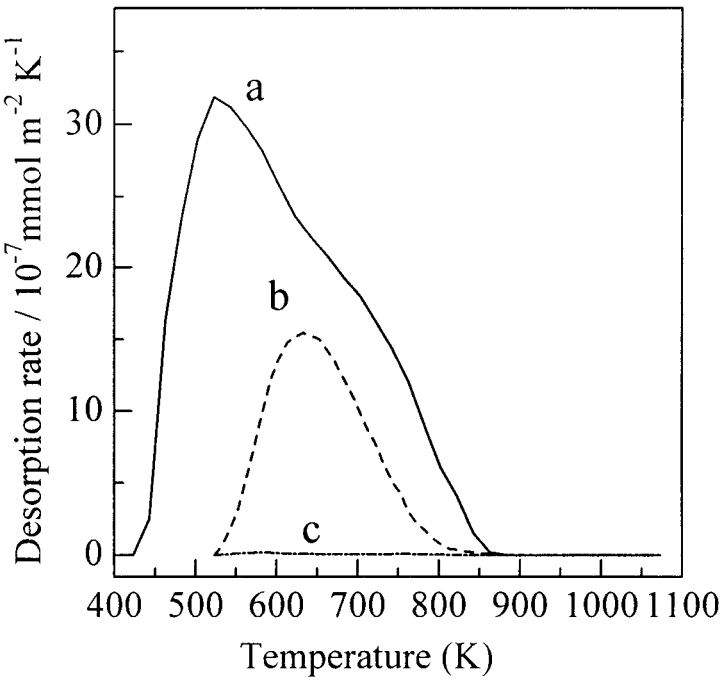

Fig. 2 TPD spectra for dimethylpyridines adsorbed on alumina. 3,5-DMP after purging at (a) 423 K and (b) 523 K, and (c) 2,6-DMP after purging at 523 K.

Figure 3 shows the IR spectra of 2,6-DMP adsorbed on alumina at various temperatures. The absorption bands were observed at 1618, 1574, 1462, and 1387 cm^{-1} in IR spectra of adsorbed 2,6-DMP at 423 K. According to the assignment in literature [16-19], the bands at 1618 and 1574 cm^{-1} was attributed to 8a mode of the 2,6-DMP adsorbed on the Lewis acid sites, and those at 1462 and 1387 cm^{-1} to $\delta_{as}CH_3$ stretching and δ_sCH_3 stretching mode, respectively. These absorption bands gradually decreased with the purging temperature. The weak bands at 1648 and 1633 cm^{-1} may be due to 8a and 8b mode of dimethylpyridinium ion adsorbed on Brønsted acid sites, and the intensities of these bands steeply decreased at 473 K. The detection of Brønsted acid sites by 2,6-DMP may be due to the stronger basicity, i.e., higher pKa value, of 2,6-DMP than pyridine, however, the Brønsted acid sites are very weak because adsorbed 2,6-DMP molecules were purged at 523 K. Thus, the results indicate that there is no contribution of Brønsted acid on 2,6-DMP adsorption after purging above 523 K. The band at 1490 cm^{-1} was attributed to the 19a mode of 2,6-DMP on both Brønsted and Lewis acid sites. Because of the disappearance of the bands at 1633 and 1648 cm^{-1} at 523 K, the band at 1490 cm^{-1} was assigned to 2,6-DMP on Lewis acid sites. After purging at 523 K, the intensities of all bands finally became very small, indicating that the purging at 523 K is practically sufficient for eliminating adsorbed 2,6-DMP on Lewis acid sites of alumina.

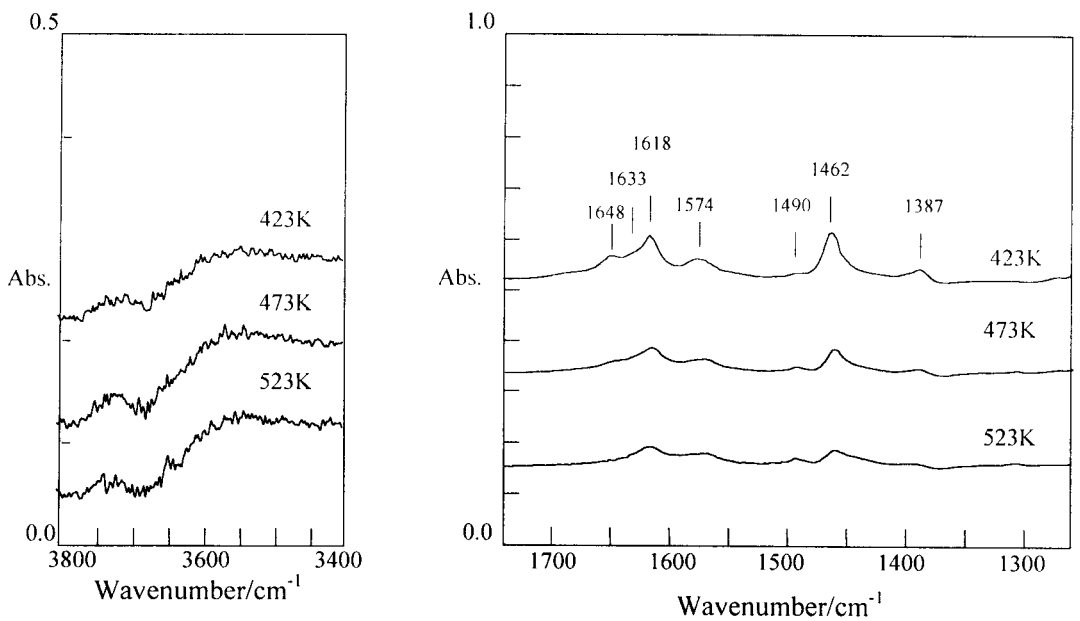

Fig. 3 IR spectra of 2,6-DMP adsorbed on alumia at various temperatures.

From the IR spectra, it was clarified that 2,6-DMP was coordinately held on Lewis acid sites at lower temperature. This may be due to rather weak effect of the steric hindrance caused from the two methyl groups neighboring basic site of pyridine. The weak bond between 2,6-DMP and Lewis acid sites at low temperature was also reported previously [16-19]. The amount of 2,6-DMP adsorption was strongly dependent on the purging temperature, and it was found that the coordinately adsorbed 2,6-DMP on Lewis acid sites can be eliminated by purging at appropriate temperature, i.e., above 573 K. Therefore, for the selective adsorption of 2,6-DMP on Brønsted acid sites, the importance of purging temperature in TPD experiment was indicated. As a result of comparison between 2,6- and 3,5-DMP-TPD, the amount of desorbed 2,6-DMP was less than 1% of that of 3,5-DMP, which is a practically negligible amount for the measurement of respective amount of Brønsted and Lewis acid sites using these probe molecules.

Consequently, by employing the appropriate purging temperature, 2,6-DMP is selectively eliminated from Lewis acid sites, and, on the other hand, 3,5-DMP adsorbs both Brønsted and Lewis acid sites. Thus, in order to obtain the selective adsorption of 2,6-DMP on Brønsted acid sites, the purging temperature of DMP-TPD was fixed at 573 K, hereafter.

Alumina-Boria: Comparison of TPD profiles of 2,6-DMP and 3,5-DMP

Fig. 4 shows the IR spectra of 2,6-DMP adsorbed on alumina-boria. The absorption band was observed at 1630, 1642 and 1685 cm^{-1}. Below 1600cm^{-1}, no signal was observed because of strong absorption band of B-O vibration [21]. The bands at 1630 and 1642 cm^{-1} were attributed to the dimethylpyridinium ion adsorbed on alumina-boria [16-19]. This assignment was also supported from the changes in the spectra at OH stretching band region, i.e., the negative absorption bands were observed at 3686, 3702 and 3785 cm^{-1}, those should be due to a bond between 2,6-DMP and Brønsted acid site on alumina-boria. The intensities of these bands were monotonously decreased and the negative bands above 3600 cm^{-1} recovered with increasing temperature. These results indicate that 2,6-DMP was adsorbed on the Brønsted acid sites of the alumina-boria.

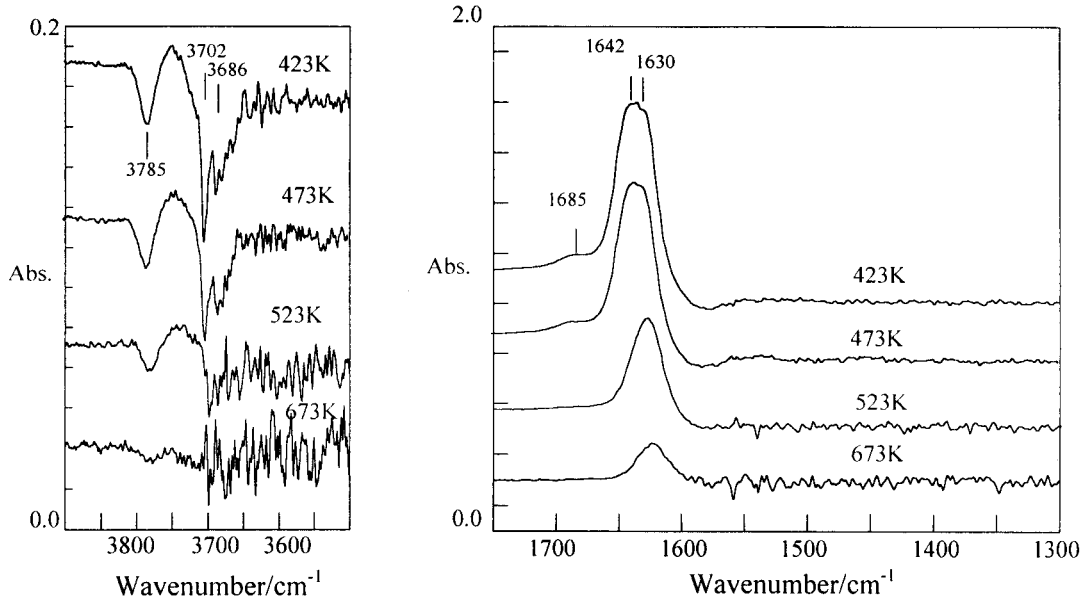

Fig. 4 IR spectra of 2,6-DMP adsorbed on alumina-boria at various temperatures.

By using alumina-boria having Brønsted acid as abundant acid sites, difference of the adsorption temperatures for 2,6-DMP and 3,5-DMP was compared. Fig. 5 shows the TPD spectra of pyridine, 2,6-DMP and 3,5-DMP from alumina-boria catalyst. The TPD measurements were started from 523 K, as described in previous section. On the contrary to the DMP-TPD of alumina, the 2,6-DMP and 3,5-DMP-TPD spectra of alumina-boria showed similar desorption profiles, i.e., the maximum rate was observed at ca. 620 K, and the desorption of DMP terminated at 850 K. 2,6-DMP desorbed at slightly higher temperatures than 3,5-DMP. The integrated amount of desorbed DMP was 7.40 x 10^{-4} mmol m^{-2} for 3,5-DMP and 7.52 x 10^{-4} mmol m^{-2} for 2,6-DMP, respectively. The Py-TPD spectrum of the same catalyst gave a sharper profile than the DMP-TPD spectra. The termination temperature in Py-TPD spectrum was 25 K lower than those of DMP-TPD.

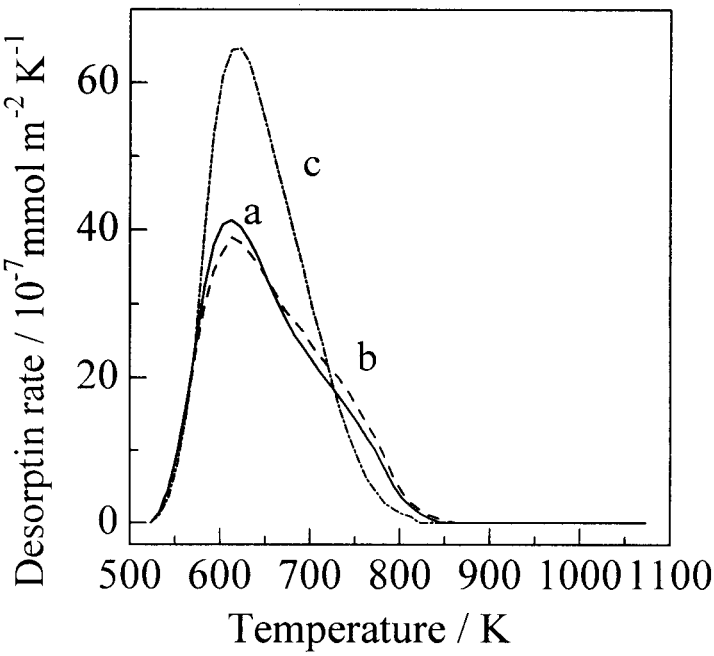

Fig. 5 TPD spectra of (a) 3,5-DMP, (b) 2,6-DMP, and (c) pyridine adsorbed on alumina-boria.

On Brønsted acid sites, 3,5-DMP and 2,6-DMP gave similar TPD profiles. As confirmed in the previous section, 3,5-DMP adsorbs on Lewis acid sites, while the adsorption of 2,6-DMP on Lewis acid sites is negligible. These results suggest that it is possible to distinguish the profile of acid strength of Brønsted and Lewis acid sites by using DMP-TPD. The Py-TPD spectrum was, however, different from those of 2,6- and 3,5-DMP-TPD, due to the difference in the basic strength. The basic strength of the probe molecules, pKa, is 5.25 for pyridine, 6.15 for 2,6-DMP, and 6.77 for 2,5-DMP [18]. Since pyridine is weaker base than DMPs, the Py-TPD spectrum was observed at a lower temperature as a sharper peak. On the other hand, the integrated amounts of desorbed 2,6-DMP and 3,5-DMP were almost the same, indicating both 2,6-DMP and 3,5-DMP adsorbed on the same acid sites. Because of the abundance of Brønsted acid sites on alumina-boria and selective adsorption of 2,6-DMP on Brønsted sites in the conditions employed, both 2,6-DMP and 3,5-DMP should desorb from Brønsted acid sites. Furthermore, these DMP-TPD spectra gave the similar profile. Therefore, small difference in the values of pKa can be neglected in the DMP-TPD spectra, and thus, the differential spectrum of 2,6-DMP and 3,5-DMP may be an indicator of relative strength of Lewis acid sites.

Silica-Magnesia: DMP-TPD for Determination of Brønsted and Lewis Acid Sites

Fig. 6 shows the TPD spectra for 2,6-DMP and 3,5-DMP adsorbed on silica-magnesia. Although both probes exhibited a single peak, the profiles of desorption and integrated amounts were different. The desorption of 2,6-DMP terminated at 853 K, while that of 3,5-DMP terminated at 80 K higher than 2,6-DMP, i.e., 933 K. The amounts of desorbed DMPs were 3.20 x 10^{-4} mmol m^{-2} for 3,5-DMP and 1.70 x 10^{-4} mmol m^{-2} for 2,6-DMP, respectively. Fig. 6c shows the differential spectrum of 3,5-DMP-TPD (6a) and 2,6-DMP-TPD (6b). Since it was confirmed in the previous section that effect of basic strength of 2,6-DMP and 3,5-DMP on desorption temperature is negligible, the differential spectrum of Fig. 6c and spectrum of 2,6-DMP may indicate the relative strength of Lewis acid sites and Brønsted acid sites on silica-magnesia.

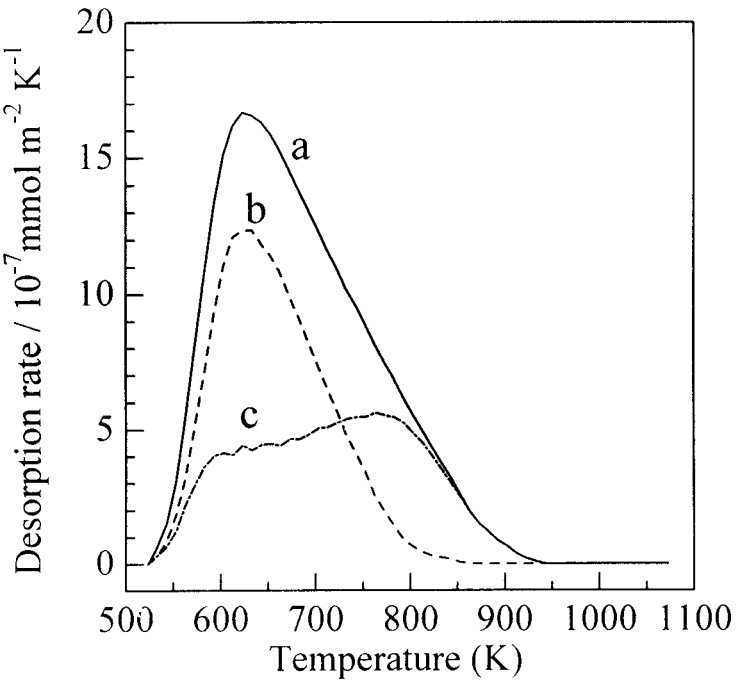

Fig. 6 TPD spectra of (a) 3,5-DMP and (b) 2,6-DMP adsorbed on silica-magnesia and (c) a differential spectrum of (a)-(b).

Fig. 7 shows IR spectra of 3,5-DMP adsorbed on silica-magnesia. The absorption bands were observed at 1624, 1600, 1564, 1465, 1434, 1389 and 1330 cm^{-1}. Since the assignment of absorption bands of 3,5-DMP has not been well examined so far, the IR spectra of 3,5-DMP adsorbed on H-mordenite (HM) and alumina were also examined, as shown in Table 3. The absorption bands of

3,5-DMP on HM calcined at 673 K were observed at 1624, 1567, 1465, 1390 cm^{-1}. After calcination at 873 K, the bands at 1600 and 1444 cm^{-1} appeared, and the intensities of the bands at 1567 and 1465 cm^{-1} reduced. It is well known that calcination of zeolites at higher temperature results in the increase in Lewis acid sites [24]. In the case of alumina, absorption bands were observed at 1611, 1601, 1440 and 1388 cm^{-1}. Thus, the bands at 1600 and 1444 cm^{-1} can be attributed to 3,5-DMP coordinately held on Lewis acid sites, while the bands at 1567 and 1465 cm^{-1} to dimethylpyridinium ion on Brønsted acid sites. As for silica-magnesia, bands attributed to 3,5-DMP on both Brønsted acid and Lewis acid sites were observed. As shown in Fig. 7, these bands monotonously decreased with increasing purging temperature. At 723 K, both the bands at 1600 and 1564 cm^{-1} remained. A negative band at 3736 cm^{-1} in OH stretching region was also observed at 723 K. The trend in the IR bands suggests that the strength of Brønsted and Lewis acid sites on silica-magnesia are comparable.

For a detail analysis of the desorption of 3,5-DMP, the IR bands at 1600 cm^{-1} and 1564 cm^{-1} were deconvoluted using Gaussian curve, as shown in Fig.8. The integrated intensity of the IR bands and the amount of adsorbed dimethylpyridine determined from the DMP-TPD were compared in Fig. 9. The depletion of the band at 1564 cm^{-1} was agreed very well with that of the integrated 2,6-DMP-TPD spectrum. The intensity of the band at 1600 cm^{-1} decreased along with the integrated amount of the differential spectrum of 3,5-DMP and 2,6-DMP. These results clearly demonstrates that the combination of 2,6- and 3,5-DMP-TPD is applicable for the separation of the profiles of acid strength of Brønsted and Lewis acid sites on metal oxide catalysts.

Table 3 Wavenumber of absorption bands on IR spectra of 3,5-DMP adsorbed on catalysts at 423 K.

tentative assignment [a)]	wavenumber / cm^{-1}			
	HM calcined at 673 K	HM calcined at 873 K	alumina	silica-magnesia
B and/or L	1624	1620	1611	1624
L		1600	1601	1600
B	1567	1567		1564
B	1465	1465		1465
L		1444	1440	1434
B and/or L	1390	1390	1388	1389

[a)] B, dimethylpyridinium ion on Brønsted acid site; L, coordinately held dimethylpyridine on Lewis acid site

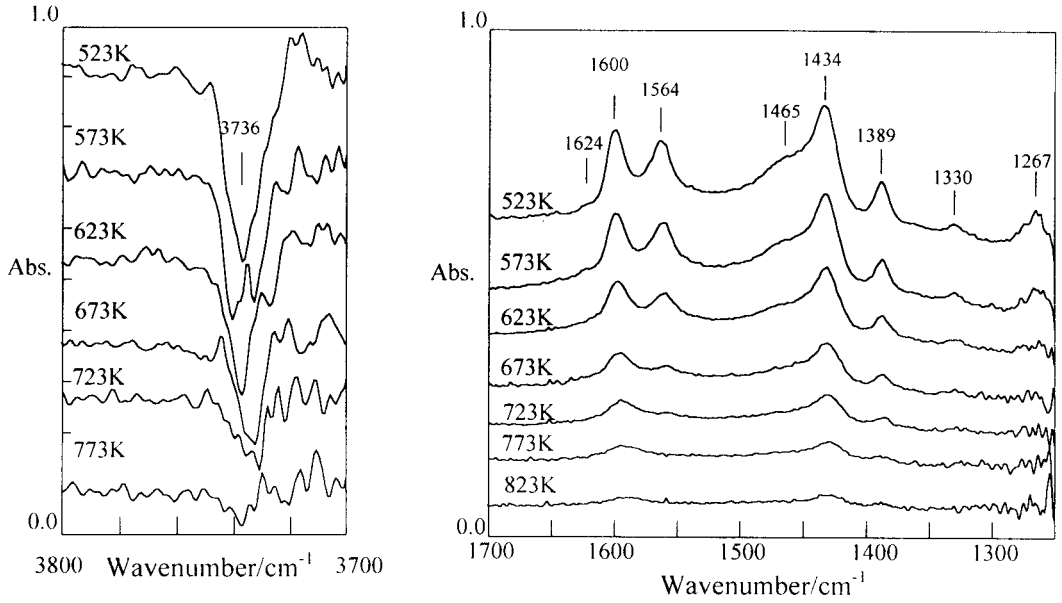

Fig. 7 IR spectra of 3,5-DMP adsorbed on silica-magnesia at various temperatures.

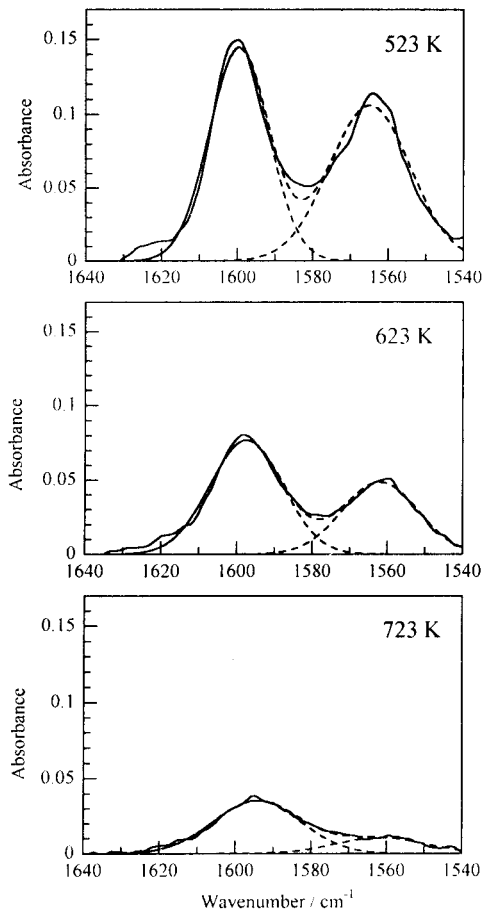

Fig. 8 Deconvolution of IR band of 3,5-DMP adsorbed on silica-magnesia at 523 K, 673 K and 723 K.

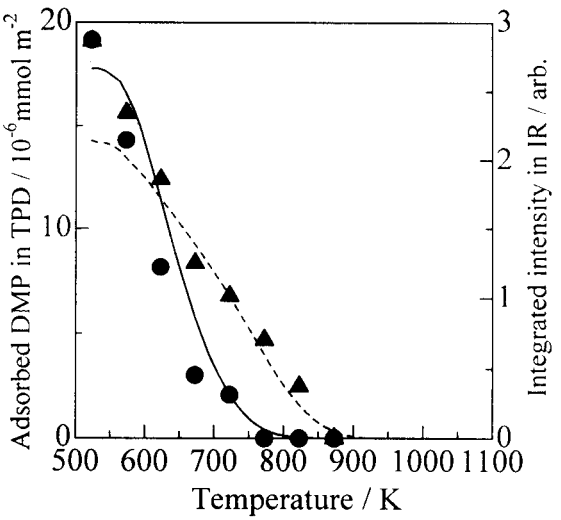

Fig. 9 Comparison of integrated amount of adsorbed dimethylpyridines on silica-magnesia detected by DMP-TPD and in-situ IR. Lines represent the amount of Brønsted acid (solid line) and Lewis acid (broken line) determined from DMP-TPD. Symbols represent the integrated intensity of IR bands of 3,5-DMP at 1564cm^{-1}(●) and 1600cm^{-1}(▲).

Silica-Alumina: Scope of application of DMP-TPD

Fig. 10 shows the TPD spectra for DMP adsorbed on silica-alumina. As for the 3,5-DMP-TPD spectra, two desorption peaks were observed at 620 K and 900 K, respectively. The desorption temperature was about 100 K higher that that of 3,5-DMP-TPD spectrum of silica-magnesia. This is reasonable that $H_{0,max}$ of these metal oxides is –11.99 for silica-alumina and –8.2 for silica-magnesia, respectively [14]. 2,6-DMP-TPD showed a broad peak at 620 K, and terminated at 900 K.

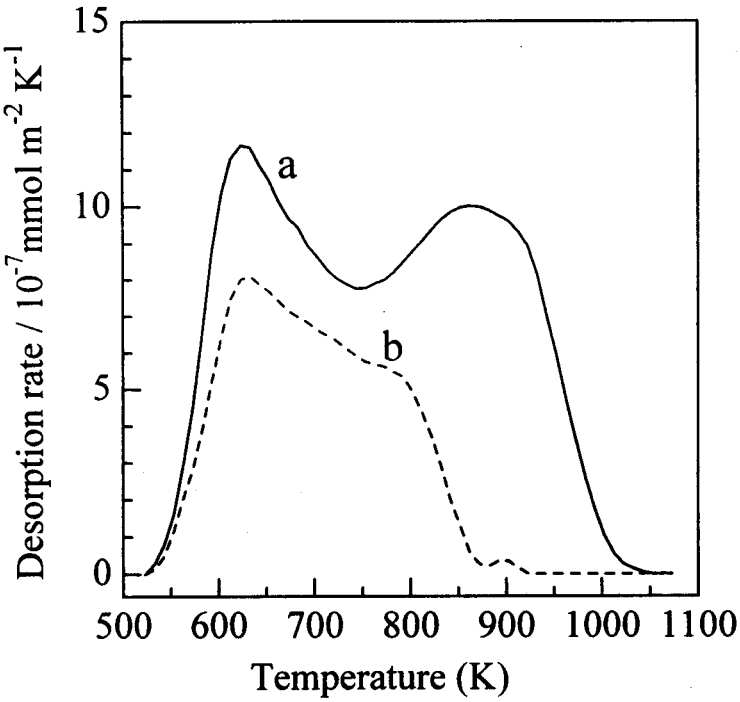

Fig. 10 TPD spectra of (a) 3,5-DMP and (b) 2,6-DMP adsorbed on silica-alumina.

Fig. 11 shows the IR spectra of 2,6-DMP adsorbed on silica-alumina. The band at 1638, 1618, and 1582 cm^{-1} were deconvoluted in the same manner as shown in Fig. 8. The intensity of the band at 1638 cm^{-1}, due to 2,6-DMP on Brønsted acid sites, decreased with increasing temperature. On the other hand, the intensities of the band at 1618 cm^{-1}, due to 2,6-DMP on Lewis acid sites, was almost unchanged. Furthermore, 2,6-DMP on Lewis acid sites remained after purging at 573 K which is 50 K higher than the purging temperature used in this study. The strong adsorption of 2,6-DMP on silica-alumina suggests that DMP-TPD is not effective for catalysts having very strong Lewis acid sites, such as silica-alumina. Good performance of DMP-TPD can be obtained in the measurement of solid acid catalysts having moderate acid sites such as silica-magnesia.

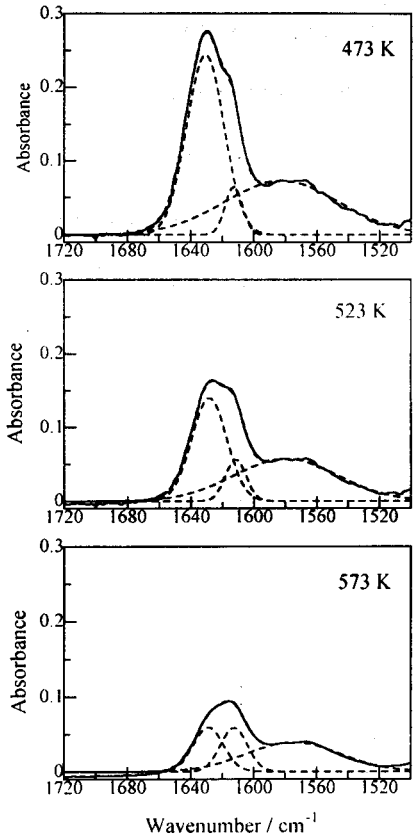

Fig. 11 Deconvolution of IR band of 2,6-DMP adsorbed on silica-alumina at 523 K, 673 K and 723 K.

Table 4 summarized the amount of adsorbed dimethylpyridines determined by DMP-TPD. The total acid amount determined from 3,5-DMP-TPD was in the range of 2.3-7.4 x 10^{-4} mmol m^{-2} for the catalysts examined. In the case of alumina, the amount of desorbed 3,5-DMP (2.33 x 10^{-7} mol m^{-2} = 0.14 nm^{-2}) was only about 1 % of surface Al^{3+} site on (111) plane of γ-Al_2O_3 (14.5 Al^{3+} nm^{-2}) [24]. DMP-TPD can detect only a part of surface acid sites. The high purging temperature, i.e., 523 K, may be one of the reasons for the small amount of detectable acid sites. Large molecular diameter of dimethylpyridines is also the possible reason. However, the advantage in the use of the combination of DMP-TPD is the applicability to determination of Brønsted acid and Lewis acid strength of metal oxide catalysts having moderate acid strength.

Table 4 Amount of dimethylpyridines adsorbed on metal oxide catalysts.

probe	desorbed amount / 10^{-4}mmol m^{-2}			
	alumina	boria-alumia	silica-magnesia	silica-alumina
3,5-DMP[a)]	2.33	7.40	3.20	3.73
2,6-DMP[b)]	0.02	7.52	1.77	1.70
(3,5-DMP) - (2,6-DMP)	2.31	-	1.43	2.03

[a)] 3,5-dimethylpyridine, [b)] 2,6-dimethylpyridine

Conclusion

The potential of DMP-TPD for the quantitative determination of both acid strength and amount of Brønsted acid and Lewis acid sites on solid acid catalysts were examined, and the scope of this method was clarified. The verification of the use of DMP was examined by using alumina and

alumina-boria, on which Lewis acid sites and Brønsted acid sites are abundant on the surface, respectively. The purging temperature should be more than 523 K, to obtain the selective adsorption of 2,6-DMP on Brønsted acid sites. From the examination of DMP-TPD spectra of alumina-boria catalyst of which the Brønsted acid sites are abundant, it was demonstrated that the small difference in pKa of 2,6-DMP and 3,5-DMP is negligible in the desorption temperature of TPD profiles. It was also demonstrated that the profiles of acid strength of Brønsted and Lewis acid sites on solid catalysts can be measured by using both 2,6- and 3,5-DMP-TPD. The scope of the DMP-TPD was also indicated, i.e., solid acids having very strong Lewis acid sites, such as silica-alumina, cannot be determined with the measurement conditions used in this study.

References

[1] R. J. Cvetanovic, and Y. Amenomiya, *Adv. Catal.*, **17** (1967)103.

[2] K. Tanabe, in "*Solid Acids and Bases - Their Catalytic Properties*" Kodansha, Tokyo, Academic Press, New York, (1970).

[3] K. Tanabe, M. Misono, Y. Ono and H. Hattori, in "*New Solid Acids and Bases*" Kodansha-Elsevier, Tokyo (1989).

[4] A. Corma, *Chem. Rev.*, **95** (1995) 559.

[5] W. E. Farneth and R. J. Gorte, *Chem. Rev.*, **95** (1995) 615.

[6] M. Niwa, M. Iwamoto, and K. Segawa, *Bull. Chem. Soc. Jpn.*, **59** (1986) 3735.

[7] M. Sawa, M. Niwa and Y. Murakami, *Zeolites*, **10** (1990) 307.

[8] M. Niwa, N. Katada, M. Sawa, and Y. Murakami, *J. Phys. Chem.*, **99** (1995) 8812.

[9] N. Katada, H. Igi, J. H. Kim, and M. Niwa, *J. Phys. Chem. B*, **101** (1997) 5969.

[10] H. G. Karge, V. Dondur, and J. Weitkamp, *J. Phys. Chem.*, **95** (1991) 283.

[11] H. G. Karge and V. Dondur, *J. Phys. Chem.*, **94** (1990) 765.

[12] M. Kojima, M. W. Rautenbach and C. T. O'Connor, *J. Catal.*, **112** (1988) 495.

[13] H. Matsuhashi, H. Motoi and K. Arata, *Catal. Lett.*, **26** (1994) 325.

[14] A. Satsuma, Yenni Westi, Y. Kamiya, T. Hattori and Y. Murakami, *Bull. Chem. Soc. Jpn.*, **70** (1997) 1311.

[15] H. A. Benesi, *J. Catal.*, **28** (1973) 176.

[16] P. A. Jacobs, and C. F. Heylen, *J. Catal.*, **34** (1974) 267.

[17] H. Knözinger, H. Krietenbrink, P. Ratnasamy, *J. Catal.*, **48** (1977) 436.

[18] A. Corma, C. Rodellas, and V. Fornes, *J. Catal.*, **88** (1984) 374.

[19] H. Miyata and J. B. Moffat, *J. Catal.*, **62** (1980) 357.

[20] S. Sato, M. Tokumitsu, T. Sodesawa, and F. Nozaki, *Bull. Chem. Soc. Jpn.*, **64** (1991) 1005.

[21] Y. Izumi and T. Shiba, *Bull. Chem. Soc. Jpn.*, **37** (1964) 1797.

[22] H. Knözinger, *Adv. Catal.*, **25** (1976) 184.

[23] J. Ward, in J. A. Rabo, (Ed.), "*Zeolite Chemistry and Catalysis (ACS Monograph, 171)*" Am. Chem. Soc., Washington, D. C., (1976) p. 140.

[24] H. Knözinger and P. Ratnasamy, *Catal. Rev. Sci. Eng.*, **17** (1978) 31.

3.2 Quantitative determination of acid sites on vanadyl pyrophosphate catalysts and their function for MA formation

Abstract

Acidic properties of three types of $(VO)_2P_2O_7$ catalysts were investigated by temperature programmed desorption (TPD) using 3,5- and 2,6-dimethylpyridine as probes, and the selective oxidation of *n*-butane to maleic anhydride (MA) was performed. VPO-org was prepared in organic solvent, VPO-redu was obtained by reduction of $VOPO_4 \cdot 2H_2O$, and VPO-aq was prepared in aqueous medium. 3,5-Dimethylpyridine (3,5-DMP) is adsorbed on both Brønsted and Lewis acid sites, whereas 2,6-dimethylpyridine (2,6-DMP) is selectively adsorbed on Brønsted acid sites due to the steric hindrance of the two methyl groups, so the amounts and strengths of the Brønsted and Lewis acid sites could be determined separately. The $(VO)_2P_2O_7$ catalysts had four types of acid sites: weak and strong Brønsted acid sites, and weak and strong Lewis acid sites. The acidic properties were greatly dependent on the preparation methods as follows: VPO-org had a larger amount of the strong Brønsted acid sites and these acid sites were relatively weak. VPO-redu had a larger amount of the strong Lewis acid sites and VPO-aq had fewer acid sites. The selectivity to MA at low conversion increased with the amount of strong Lewis acid sites, indicating that the strong Lewis acid sites are important for MA formation. The strong Brønsted acid sites may promote the consecutive oxidation of MA.

Introduction

Vanadyl pyrophosphate, $(VO)_2P_2O_7$, demonstrates a characteristic activity for the selective oxidation of *n*-butane to maleic anhydride (MA), and is used as the main component of industrial catalysts for this reaction [1-4]. The catalytic performance of this catalyst greatly depends on the preparation method and conditions [2,3]. Although many investigations have focused on this reaction system, the nature of the active sites on the $(VO)_2P_2O_7$ catalyst is still controversial.

Both redox sites and acid sites may be significantly involved in the selective oxidation of paraffins over solid catalysts [5]. In addition, Brønsted and Lewis acid sites have different functions in selective oxidation, and the strength of these respective acid sites strongly affects the catalytic performance [6]. Investigation of the involvement and function of acid sites on $(VO)_2P_2O_7$ catalysts

in the selective oxidation of *n*-butane has shown that the acid sites are necessary for this reaction, since adding ammonia to the reaction feed and doping of potassium to the catalyst make the activity for MA formation lowered [7]. Both Brønsted and Lewis acids are present on $(VO)_2P_2O_7$ based on the IR spectra of basic molecules adsorbed on the catalyst [8]. The ratio of Lewis to Brønsted acid sites has been estimated from the IR spectra of pyridine adsorbed on $(VO)_2P_2O_7$ [9]. However, quantitative determinations of individual Brønsted and Lewis acid sites have not been performed.

Temperature programmed desorption (TPD) of basic molecules is a useful method for the determination of acid amount as well as acid strength of solid catalysts [10-13]. Ammonia is used frequently as the probe molecule, but the amount and strength of the Brønsted and Lewis acid sites can not be estimated separately, because of the non-selective adsorption of ammonia. Benesi [14] suggested that 2,6-dimethylpyridine (2,6-DMP) could be used as a probe to selectively detect the protonic sites due to steric hindrance of the two methyl groups near the nitrogen atom. In contrast, 3,5-dimethylpyridine (3,5-DMP) is adsorbed on both Brønsted and Lewis acid sites non-selectively. Consequently, if both dimethylpyridines are used as probe molecules for TPD measurement, both the amount and strength of Brønsted and Lewis acid sites can be determined.

The present section examined the acidic properties of $(VO)_2P_2O_7$ catalysts by the DMP-TPD method developed in former section (3.1). Further, the catalytic performance of three types of $(VO)_2P_2O_7$ catalysts were assessed for the selective oxidation of *n*-butane based on acidic properties. On the basis of these investigations, the concept concerning the acidic property of the $(VO)_2P_2O_7$ catalyst will be established to develop the catalyst of high catalytic performance.

Experimental

Preparation of catalysts

The same catalysts as the former section (Chapter 2) , that is, VPO-org, VPO-redu, and VPO-aq, were used.

Temperature programmed desorption of dimethylpyridine (DMP-TPD)

DMP-TPD was performed using the same apparatus of the former section. 2,6-DMP and 3,5-DMP were used as the probe molecules. The sample powder (100 mg) was placed in the sample cell and pretreated at 673 K for 2 h in a flow of dehydrated He at 150 cm^3 min^{-1}. After cooling to 523

K under the He flow, the sample powder was exposed to a stream of the probe molecules diluted in He for 30 min. Equilibrium adsorption was confirmed by measurement of the concentration of probe molecules passed through the sample cell. The sample was kept at 523 K for 2 h in the He flow to purge excess or weakly adsorbed probe molecules. The temperature of the sample powder was then raised from 523 K to 1073 K at 5 K min^{-1} in the He flow and the probe molecules desorbed from the sample were detected with a flame-ionization detector (FID, Shimadzu GC-9A). The line between the sample cell and the detector was heated at 400 K.

Catalytic oxidation of butane

Catalytic oxidation of *n*-butane was carried out in a flow reactor (Pyrex tube, inside diameter of 6 mm) under atmospheric pressure at 723 K. A mixture of 1.5 vol% butane, 20 vol% O_2 and N_2 (balance) at a total flow rate of 10 cm^3 min^{-1} was fed over the catalyst bed. The conversion of butane was controlled by the weight of the catalyst under the constant flow rate. The products were analyzed with on-line gas chromatographs (FID (Shimadzu 14A, Shimadzu 9A) and TCD (Shimadzu 9A)) equipped with a Porapak QS column (inside diameter 2.2 mm, length 1 m) for butane and MA, and a Porapak N column (inside diameter 2.2 mm, length 2 m) for CO_2. A Molecular Sieve 13X column (inside diameter 2.2mm, length 4 m) was also used to separate O_2, N_2 and CO. CO and CO_2 were converted to methane by using a Methanizer (Shimadzu MTN-1) for more sensitive detection by the FID-GC. Prior to the analysis, the catalysts were aged in the reaction mixture at 723 K for 10 h.

Results and discussion

Acidic property of the catalysts

Fig. 1 shows the TPD spectra of 2,6-DMP and 3,5-DMP, with the desorption rates expressed per unit surface area. The differential spectra calculated by subtracting the 2,6-DMP-TPD spectra from 3,5-DMP-TPD ones are also shown. As verified in the former section (3-1), 2,6-DMP is adsorbed on the Brønsted acid sites selectively with purging at 523 K for 2 h, unless very strong Lewis acid sites with exceptional behavior are present. 3,5-DMP is adsorbed on both Brønsted and Lewis acid sites. In the TPD spectrum of 3,5-DMP for silica-magnesia which has no very strong Lewis acid sites, desorption of 3,5-DMP continued up to 950 K, but this desorption was scarcely observed over 900 K for the $(VO)_2P_2O_7$ catalysts. These results indicate that the $(VO)_2P_2O_7$ catalysts do not have the very

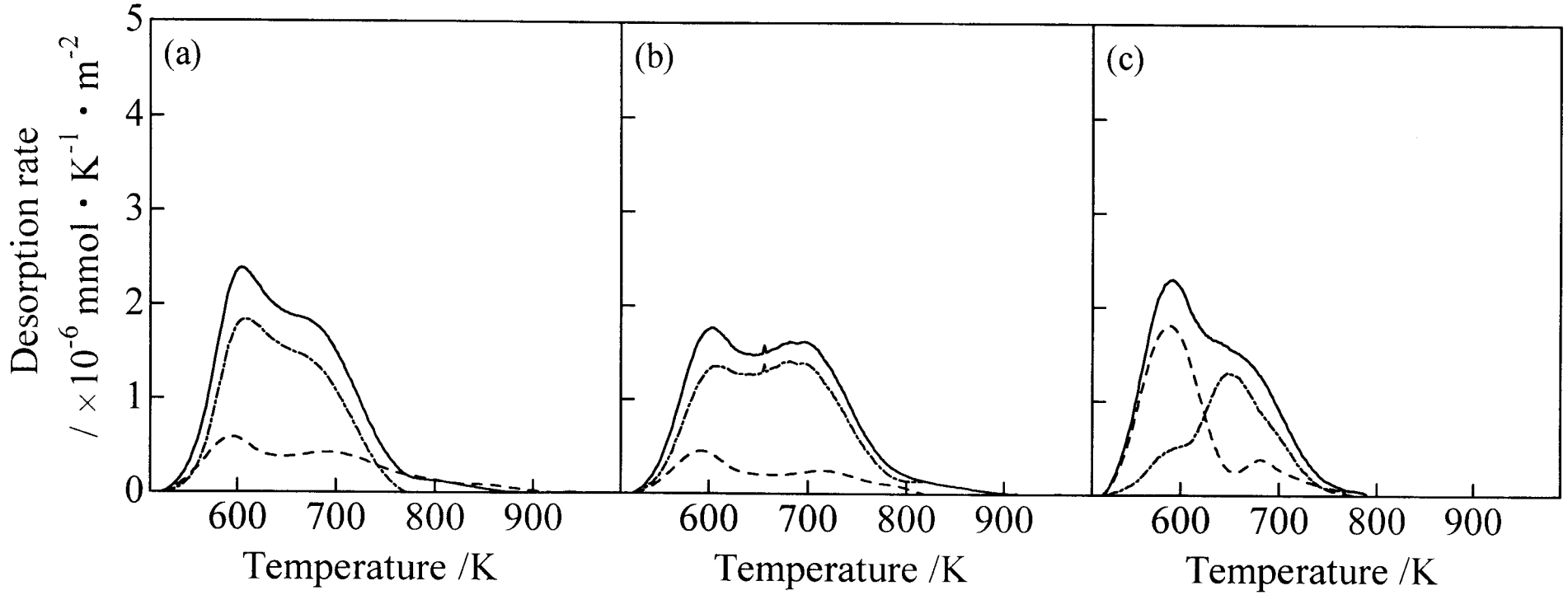

Fig. 1 TPD spectra for (————) 3,5-DMP, (- - - - - -) 2,6-DMP adsorbed on (a) VPO-org, (b) VPO-redu, and (c) VPO-aq and (- · - · - · - · -) differential spectra of (3,5-DMP) – (2,6-DMP).

strong Lewis acid sites. The desorption temperatures of 2,6-DMP and 3,5-DMP adsorbed on one material are demonstrated to be almost the same, although the chemical properties, *e.g.*, pK_b and vaporization enthalpy, of these isomers are slightly different. Therefore, 3,5-DMP-TPD, 2,6-DMP-TPD and the differential spectra indicate the total, Brønsted and Lewis acid sites, respectively.

The spectra confirmed that the $(VO)_2P_2O_7$ catalysts have both Brønsted and Lewis acid sites [8]. The spectra of Brønsted and Lewis acid sites exhibited two desorption peaks, indicating the existence of at least four types of acid sites, that is, weak and strong Brønsted acid sites, and weak and strong Lewis acid sites, which are denoted as B_{weak}, B_{strong}, L_{weak} and L_{strong}, respectively. The acidic properties of these catalysts depended on the preparation methods.

The densities of the acid sites and the temperatures of the maximum desorption rates (abbreviated as T_{max}) are summarized in Table 1. These estimates defined the weak and strong acid sites for VPO-org and VPO-redu as the acid sites below and above 650 K of the desorption temperatures, respectively, whereas this temperature was defined as 620 K for VPO-aq. VPO-aq had a higher density of B_{weak}. The density of L_{strong} on VPO-redu was higher than on the other two catalysts, in the order VPO-aq (0.081 μmol m^{-2}) < VPO-org (0.096 μmol m^{-2}) < VPO-redu (0.138 μmol m^{-2}). The density of B_{strong} was almost the same for VPO-redu and VPO-aq. On the other hand, the density of B_{strong} on VPO-org was almost twice as high as on VPO-redu and VPO-aq.

The T_{max} of L_{strong} was in the following order: VPO-aq (655 K) < VPO-org (680 K) < VPO-redu (690 K). Niwa et al. [15] demonstrated that T_{max} is shifted toward higher temperatures with the increase in acid sites in the measurement system by ammonia-TPD, which indicates that the product of the sample weight (g) and the concentration of acid sites (μmol g^{-1}). In this study, these spectra were measured with the same sample weight (100 mg), so the amount of the acid sites in the measurement system was different for each experiment. The amount of L_{storng} in the measurement system was as follows; VPO-aq (0.044 μmol) < VPO-org (0.317 μmol) < VPO-redu (0.331 μmol). This order is consistent with that of T_{max}. In addition to that, these amounts were roughly correlated with T_{max}. Therefore, it is reasonable to consider that the L_{strong} of these catalysts had similar strength.

Table 1 Densities of acid sites and temperature of maximum desorption rate[a] measured by dimethylpyridine-temperature programmed desorption.

Catalyst	Brønsted acid[b] / μmol m^{-2}		Lewis acid[c] / μmol m^{-2}		Total[d]
	Weak[e]	Strong[e]	Weak[e]	Strong[e]	(μmol m^{-2})
VPO-org	0.040 (595 K)	0.055 (695 K)	0.121 (605 K)	0.096 (680 K)	0.312
VPO-redu	0.031 (590 K)	0.025 (720 K)	0.104 (600 K)	0.138 (690 K)	0.298
VPO-aq	0.110 (590 K)	0.023 (685 K)	0.042 (595 K)	0.081 (655 K)	0.259

[a] The figures in parentheses are temperature of maximum desorption rate.

[b] Density of Brønstead acid sites was estimated from 2,6-dimethylpyridine-TPD spectra.

[c] Density of Lewis acid sites was calculated by subtracting that of Brønsted acid sites from that of total acid sites.

[d] Density of total acid sites was estimated from 3,5-dimethylpyridine-TPD spectra.

[e] For VPO-org and VPO-redu, weak and strong acids were defined as below and above 650 K of desorption temperature, respectively, and this temperature was defined as 620 K for VPO-aq.

The T_{max} of B_{strong} was in the following order: VPO-aq (685 K)<VPO-org (695 K)<VPO-redu (720 K). In contrast, amount of B_{strong} in the measurement system was as follows: VPO-aq (0.012 μmol)<VPO-redu (0.060 μmol)<VPO-org (0.176 μmol). VPO-org had almost the same T_{max} as VPO-aq, but the amount of B_{strong} in the measurement system on VPO-org was about 15-times that of VPO-aq. Furthermore, VPO-org had lower T_{max} than VPO-redu, whereas the total amount of B_{strong} in the measurement system on VPO-org was larger than that of VPO-redu. These results indicate that the B_{strong} of VPO-org was relatively weak compared to the other two catalysts.

The acidic properties of the catalysts can be summarized as follows: (1) VPO-org has a higher density of B_{strong}, but the B_{strong} are relatively weak compared to the other two catalysts. (2) VPO-redu has a higher density of L_{strong}. (3) VPO-aq has fewer acid sites except for B_{weak}.

The bulk P/V ratios of the catalysts were almost unity, that is the stoichiometric number of $(VO)_2P_2O_7$, but the surface P/V ratios were larger than unity, indicating that there is excess phosphorus on the surface. The surface P/V ratio of VPO-aq (1.5) was higher than those of VPO-org and VPO-redu (1.2) as shown in Table 1 of Chapter 2. This is consistent with the density of B_{weak} as listed in Table 1. VPO-org catalysts with various bulk P/V ratios show that the density of B_{weak} increases with the surface P/V ratio [16]. Therefore, B_{weak} can be attributed to P-OH groups, like H_3PO_4, derived from the excess phosphorus on the catalyst surface.

The DMP-TPD spectra indicate that there are at least three types of acid sites in addition to B_{weak}. The Brønsted and Lewis acid sites on $(VO)_2P_2O_7$ may be attributed to P-OH groups belonging to truncated P-O bonds in terminal phosphorus tetrahedra and coordinatively unsaturated vanadium ions on the (100) planes, respectively [8]. Although it is difficult to make reasonable assignments for these acid sites from only the data of this study, further quantitative measurement of acidic property of well-characterized $(VO)_2P_2O_7$ by the DMP-TPD method can be expected to clarify the structure of these acid sites.

Correlation between acidic properties and catalytic performance of $(VO)_2P_2O_7$ catalysts

Figure 2 shows the changes in selectivity to MA as a function of the conversion of *n*-butane. VPO-redu showed the highest selectivity among these catalysts. The selectivity decreased with increased conversion, but the trends of the catalysts were greatly different. The selectivity to MA of VPO-org fell remarkably, but that for VPO-redu scarcely decreased. This decrease of the is due to

consecutive oxidation of MA [17].

The catalytic data are summarized in Table 2, in which the data for catalytic activity were obtained at around 20 % conversion. The extent of consecutive oxidation of MA (ECO_{MA}) was defined as the difference of the selectivity between 80 % and 20 % of the conversion, and was calculated from Eq. (1).

$$ECO_{MA}\ (\%) = Selectivity_{80\ \%\ conversion} - Selectivity_{20\ \%\ conversion} \quad (1)$$

The selectivity at 20 % conversion was in the following order: VPO-aq (54 %) < VPO-org (60 %) < VPO-redu (66 %). On the other hand, ECO_{MA} was as follows: VPO-org (-9 %) < VPO-aq (-4 %) < VPO-redu (-2 %).

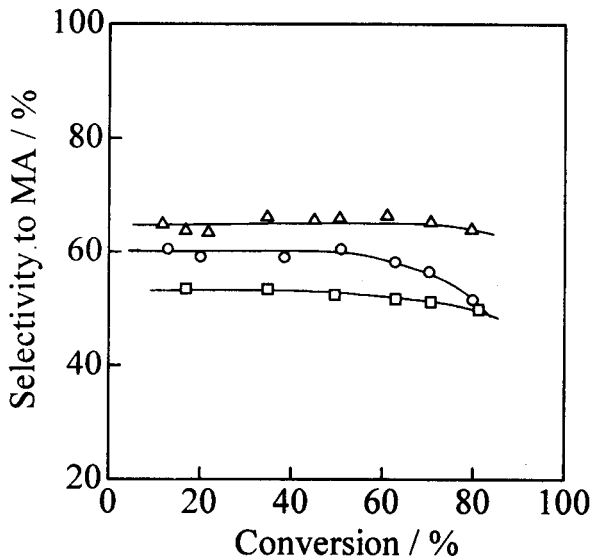

Fig. 2 Selectivity to MA as a function of the conversion of *n*-butane: (○) VPO-org, (△) VPO-redu, and (□) VPO-aq. The reaction was performed with *n*-butane (1.5 %), O_2 (20 %), and N_2 (balance) at 723 K.

Table 2 Activity and selectivity to maleic anhydride in *n*-butane oxidation over $(VO)_2P_2O_7$ catalysts[a].

Catalyst	Activity[b] ($\mu mol\ m^{-2}\ h^{-1}$)	Selectivity to maleic anhydride[c] (%)		Difference of selectivity between 80 % and 20 % of conversions[d] (%)
		20 %	80 %	
VPO-org	132	60	51	-9.2
VPO-redu	55	66	64	-1.6
VPO-aq	70	54	50	-4.4

[a] The reaction was carried out with 1.5 % *n*-butane and 20 % O_2 in N_2 (balance) at 723 K.

[b] Calculated from the data at around 20 % of the conversion.

[c] Selectivity to maleic anhydride at 20 % or 80 % of the conversions.

[d] Calculated by subtracting selectivity to MA at 80 % conversion from that at 20 % conversion.

The catalytic activity of VPO-org was greater than those of the other two catalysts, but this difference could not be explained by the acidic properties, possibly because the catalytic activity is strongly affected by the redox properties of the catalyst as investigated in Chapter 2.

Figure 3 shows the relationship between the selectivity at 20 % conversion and the density of L_{strong}. The selectivity increased with increased density of L_{strong}. *n*-Butane may be selectively activated on strong Lewis acid sites through abstraction of hydrogen atoms from butane, and then, the formed olefinic-like intermediate is quickly oxidized up to MA by neighboring oxygen atoms [4]. The trend of Fig. 3 supports this proposal, indicating that L_{strong} is important for MA formation. The higher density of L_{strong} is one of the reasons for the high selectivity of VPO-redu.

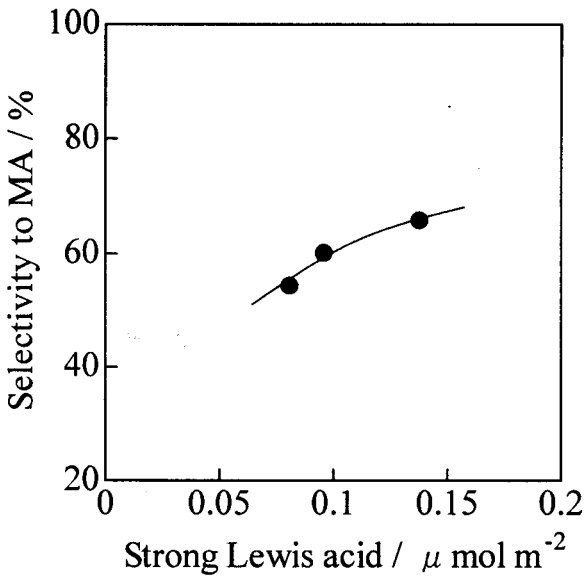

Fig. 3 Correlation between the selectivity to MA at 20 % conversion and the density of the strong Lewis acid sites.

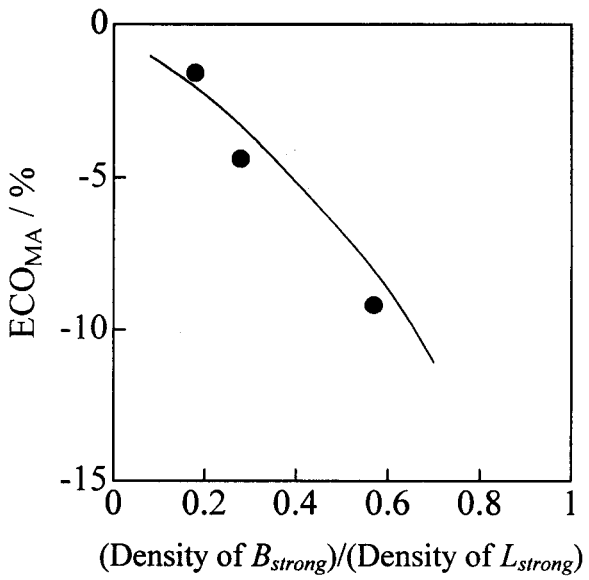

Fig. 4 Relationship between the extent of consecutive oxidation of MA and the ratio of (density of the strong Brønsted acid sites)/(density of the strong Lewis acid sites). Y axis (ECO_{MA}) was calculated by subtracting selectivity at 80 % conversion from that at 20 % conversion.

It has been considered that the V-rich sites on $(VO)_2P_2O_7$, where the surface P/V ratio is relatively low, are highly active for the consecutive oxidation of MA [17,18]. However, the surface P/V ratio of VPO-org is the same as that of VPO-redu, as shown in Table 1 of Chapter 2. In addition, the surface P/V ratio of VPO-aq is rather higher than that of VPO-org. Therefore, it is difficult to explain the difference in the consecutive oxidation of MA as suggested in the literature. As shown in Fig. 4, a correlation between ECO_{MA} and the ratio of (density of B_{strong})/(density of L_{strong}) was observed, but no correlation with only the density of Brønsted or Lewis acid sites. If MA is readily desorbed from the surface of a catalyst, MA is not subject to consecutive oxidation. It is generally accepted that acid sites are necessary for catalytic formation of anhydride or acidic molecules over solid catalysts, because these sites promote desorption of the product [19]. As shown in Fig. 4, L_{strong} is likely to have a good influence for the selectivity to MA. In contrast, B_{strong} will promote the consecutive oxidation of MA. Protons are readily added to the carbonyl group of carboxylic acid derivatives, as in the Brønsted acid-catalyzed hydrolysis of ester [20]. The strong Brønsted acid may activate the carbonyl of MA to induce subsequently oxidation into CO_x. Therefore, the consecutive oxidation of MA is probably more accelerated on catalysts with higher densities of B_{strong} such as VPO-org.

Conclusion

Acidic properties of three types of $(VO)_2P_2O_7$ catalysts were investigated by DMP-TPD. VPO-org had a higher density of B_{strong} and these B_{strong} sites were relatively weak compared with the other catalysts. VPO-redu had a higher density of L_{strong}. VPO-aq had fewer acid sites except for B_{weak}. VPO-redu had a high selectivity to MA at low conversion, and a higher density of L_{strong}. The extent of consecutive oxidation of MA is related to the ratio of (density of B_{strong})/(density of L_{strong}). B_{strong} may promote the consecutive oxidation of MA, whereas L_{strong} hinders this oxidation. These results established the concept that he density of the strong Lewis acid sites increases, and contrary that of the strong Brønsted acid sites decreases to improve the catalytic performance.

References

[1] Hodnett, B. K., *Catal. Rev. –Sci. Eng.*, **17** (1985) 373.

[2] Bordes, E., *Catal. Today*, **1** (1987) 499.

[3] Centi, G., Trifirò, F., Ebner, J. R., Franchetti, V. M., *Chem. Rev.*, **88** (1988) 55.

[4] Cavani, F., Trifirò, F., *Chemtech*, **24** (1994) 18.

[5] Tanabe, K., Misono, M., Ono, Y., Hattori, H., "*New Solid Acid and Bases*," Kodansha-Elsevier, Tokyo (1989), p.320-325.

[6] Corma, A., *Chem. Rev.*, **95** (1995) 559.

[7] Centi, G., Golinelli, G, Trifirò, F., *Appl. Catal.*, **48** (1989) 13.

[8] Busca, G., Centi, G., Trifirò, F., Lorenzelli, V., *J. Phys. Chem.*, **90** (1986) 1337.

[9] Cornaglia, L. M., Lombardo, E. A., Anderson, J. A., Fierro, G., *Appl. Catal. A*, **100** (1993) 37.

[10] Cvetanovic, R. J., Amenomia, Y., *Adv. Catal.*, **17** (1967) 103.

[11] Tanabe, K., Misono, M., Ono, Y., Hattori, H., "*New Solid Acid and Bases*," Kodansha-Elsevier, Tokyo (1989), p.5-14.

[12] Niwa, M., Iwamoto, M., Segawa. K., *Bull. Chem. Soc. Jpn.*, **59** (1986) 3735.

[13] Katada, N., Igi, H., Kim, J. H., Niwa, M., *J. Phys. Chem. B*, **101** (1997) 5969.

[14] Benesi, H. A., *J. Catal.*, **28** (1973) 176.

[15] Niwa, M., Katada, N., Sawa, M., Murakami, Y., *J. Phys. Chem.*, **99** (1995) 8812.

[16] Private data

[17] Igarashi, H., Tsuji, K., Okuhara, T., Misono, M., *J. Phys. Chem.*, **97** (1993) 7065.

[18] Moser, T. P., Wenig, R. W., Schrader, G. L., *App. Catal.*, **34** (1987) 39.

[19] Albonetti, S., Cavani, F., Trifirò, F., *Catal. Rev. –Sci. Eng.*, **38** (1996) 413.

[20] Pine S. H., Hendrickson J. B., Cram D. J., Hammond G. S., "*Organic Chemistry, 4th edition*," McGraw-Hill International Book Co., (1981) p.319-320.

Part II

Vanadium Phosphorus Oxide Catalysts with Novel Structure

Chapter 4

Iron-doped Vanadyl Pyrophosphate Catalysts by Intercalation of Iron-complex

4.1 Preparation of lamellar vanadyl alkylphosphates as precursor

Abstract

Vanadyl alkylphosphates consisting of V^{4+} and P^{5+} were synthesized by reaction of a solid mixture of V_2O_5 and V_4O_9 (2:3 in mol) with P_2O_5 in primary aliphatic (from C_1 to C_8), secondary aliphatic (C_3 and C_4), and alicyclic (C_5) alcohols, and were characterized by means of elemental analysis, thermogravimetric analysis, X-ray diffraction, IR spectroscopy, and magnetic susceptibility. The chemical formulae of the products were determined to be $VO(RO)_x(HO)_{1-x}PO_3 \cdot (ROH)_y$ (x = 0.5-0.7, y = 0.3-0.5 for primary aliphatic alcohols; x = 0.1-0.2, y = 0.4-0.9 for secondary aliphatic and alicyclic alcohols; and R = organic group). X-ray diffraction revealed that the compounds had a lamellar structure, where the organic groups existed as double layers with a tilt of about 56° against the basal plane. Magnetism and IR spectroscopy demonstrated that the construction of basal planes in the vanadyl alkylphosphates was similar to that of $VOHPO_4 \cdot 0.5H_2O$ which consists of the V^{4+} dimers linked with PO_4, except for vanadyl *sec*-butylphosphate consisting of isolated V^{4+} monomers. Calcination of vanadyl methylphosphate and vanadyl cyclopentylphosphate brought about crystallites of $(VO)_2P_2O_7$. These $(VO)_2P_2O_7$ exhibited high selectivities to maleic anhydride (65-68 %) for selective oxidation of *n*-butane under high concentration of *n*-butane (5.0 %).

Introduction

Selective oxidation of *n*-butane to maleic anhydride (abbreviated as MA) is an important commercial process, because MA is a useful raw material for agricultural chemicals, food additives, and unsaturated polymer resins. Furthermore, at present, this reaction has only a few commercialized applications in gas-solid catalytic oxidations of lower alkanes with molecular oxygen [1]. Vanadyl pyrophosphate, $(VO)_2P_2O_7$, is claimed to be a efficient phase for this reaction and is a main component of the commercial catalyst [2-4]. The $(VO)_2P_2O_7$ catalyst is usually formed by a topotactic transformation of $VOHPO_4 \cdot 0.5H_2O$ [5,6], which is a prevailing precursor. So far, preparation methods, preparation conditions, and activation processes have been extensively studied, and present yield of MA is ca. 55 % reported in patent literatures [7-9]. However, further improvement of the yield is still desired greatly.

A series of vanadium phosphorus (V-P) oxides have attracted a great deal of attentions, because of their structural diversity and unique catalytic property. So far, there are many reports on the various V-P oxides such as lamellar compounds [10-16], large crystallites [17], mesostructured materials [18-21], and thin-layer compounds [22-24]. Lamellar compounds are demonstrated by vanadyl alkylphosphonates and alkylphosphates consisting of alternating inorganic V-P-O layers and organic group ones. Vanadyl alkylphosphonates are shown by $VO(RPO_3)\cdot nH_2O$, in which the oxidation numbers of V and P are +4 and +3, respectively, and R is alkyl group. These compounds contain P-C bonds. Johnson et al. synthesized a number of vanadyl alkylphosphonates from V_2O_5 and a variety of corresponding alkylphosphonic acid, $RPO(OH)_2$ [12-14, 16]. Guliants et al. claimed that vanadyl methylphosphonate was transformed to $(VO)_2P_2O_7$ by calcination [11].

On the contrary, there are only few reports about vanadyl alkylphosphates, in which ester bonds of (O=)P-O-C are included, and V and P are 4+ and 5+, respectively. Researchers of DuPont described vanadyl alkylphosphates synthesized by the reaction of V_2O_5 with P_2O_5 in alcohol [10]. However, the alkylphosphates incorporated are limited to only those obtained from primary aliphatic alcohols. In addition, the structure has been characterized insufficiently.

In this section, in order to realized the preparation method by using intercalation of methal-complex mentioned in Chapter 1, the vanadyl alkylphosphates were develped as new precursors. In addition, these compounds were systematically characterized by means of elemental analysis, X-ray diffraction, IR spectroscopy, thermogravimetric analysis, and magnetic susceptibility. The catalytic properties of the V-P oxides obtained from these vanadyl alkylphosphates were also investigated for the selective oxidation of *n*-butane. Their catalytic performances will be discussed in relation to microstructure of the catalyst crystallites.

Experimental

Materials

Vanadyl alkylphosphates were prepared as follows. V_2O_5 (29.2 g (0.16 mol), Koso Chemical Co., Ltd.) was reduced with a mixture of isobutyl alcohol (180 cm^3, Koso Chemical Co., Ltd.), and benzyl alcohol (120 cm^3, Koso Chemical Co., Ltd.) at the refluxing temperature (387 K) for 3 h. The obtained black solid was separated by filtration. The powder XRD pattern revealed that this solid

was a mixture of V_2O_5 and V_4O_9. The average oxidation number of V was determined by a titration method[26] to be +4.73, indicating that V_2O_5 and V_4O_9 coexisted at the molar ratio of 2:3. The $V_2O_{4.73}$ (20 g) obtained was added to 300 cm^3 of each alcohol. The following alcohols were used: primary aliphatic alcohol; methanol, ethanol, 1-propanol, 1-butanol (Koso Chemical Co., Ltd.), 1-hexanol, and 1-octanol (Tokyo Kasei Kogyo Co., Ltd.), secondary aliphatic alcohol; 2-propanol and 2-butanol (Koso Chemical Co., Ltd.), and alicyclic alcohol; cyclopentanol (Tokyo Kasei Kogyo Co., Ltd.). A mixture of P_2O_5 (29.6 g (0.21 mol), Koso Chemical Co., Ltd.) and toluene (70 cm^3, Koso Chemical Co., Ltd.) was slowly added to the alcoholic suspension with stirring at room temperature. The mixture was then refluxed until color of the suspension changed to light blue, *e.g.*, methanol (80 h), ethanol (30 h), 1-propanol (18 h), 1-butanol (3 h), 1-hexanol (2 h), 1-octanol (2 h), 2-propanol (40 h), and cyclopentanol (20 h). In the case of 2-butanol, the mixture was refluxed for 100 h, and the suspension of greenish brown was obtained instead of light blue suspension. The resulting vanadyl alkylphosphates were separated by filtration, washed with acetone and dried at room temperature for 16 h. Hereafter, these vanadyl alkylphosphates will be denoted to VAP-*alcohol name, e.g.,* VAP-*methanol.*

As a reference, vanadyl hydrogen phosphate hemihydrate, $VOHPO_4 \cdot 0.5H_2O$, was prepared according to the literature [27]. V_2O_5 (14.7 g (0.08 mol)) was added to a mixture of 90 cm^3 of isobutyl alcohol and 60 cm^3 of benzyl alcohol. The suspension was refluxed at 387 K for 3 h, and was cooled to room temperature. 99 % H_3PO_4 (15.8 g (0.16 mol), MERCK Ltd.) was added to the suspension, followed by refluxing at 387 K for 3 h. The resulting solid was filtered, washed with acetone and dried at room temperature for 16 h. The XRD pattern of this material was in good agreement with that of $VOHPO_4 \cdot 0.5H_2O$ reported in the literature [27,28].

Characterization

XRD patterns were recorded on an X-ray diffractometer (Rigaku RINT-1400) with Cu K_α radiation (λ=0.154 nm) at room temperature. Infrared spectra were obtained with an IR spectrometer (Perkin Elmer model 1600) at room temperature using pressed disks of mixture of the samples and KBr. Magnetic susceptibility was collected on a SQUID magnetometer (Quantum Design MPMS-5) with magnetic field (H) of 1 kG. The sample was evacuated at 323 K for 1 h, and then the

temperature of the sample was swept from 300 K to 2 K.

Elemental analysis of the compound was performed with a Mikroanalytisches Labor Pascher (Germany) for V, P, C, and H. The content of oxygen in the sample was calculated by subtracting the sum of weights of V, P, C, and H. Prior to the analysis, the sample was evacuated at 323 K for 24 h. The average oxidation number of V was determined by a redox titration method using $KMnO_4$ and $FeSO_4(NH_4)_2SO_4 \cdot 6H_2O$ according to the literature [26]. The surface area was measured by a BET method with automatic adsorption system (BELSORP 28SA, BEL Japan Inc.). SEM images were taken with scanning electron microscope (HITACHI S-2100).

Thermogravimetric analysis (TG/DTA) was performed using a TG/DTA 200 of Seiko Instruments. The sample was pretreated in a flow of dried air (50 cm^3 min^{-1}) at 323 K for 24 h, then temperature of the sample was raised to 853 K at a rate of 5 K min^{-1} in the flow.

Temperature programmed decomposition of VAP-*methanol* was carried out using a flow system. The sample powder (10 mg) was placed in a flow reactor (Pyrex-tube, 6 mm of inside diameter) and pretreated in a flow of dried air (10 cm^3 min^{-1}) at 323 K for 24 h. The temperature was raised from 323 K to 493 K at a rate of 5 K min^{-1} and molecules desorbed from the sample were collected in a U-shaped tube at 77 K. Then the molecules trapped were analyzed by a gas chromatograph (TCD (GL science, GC-380)) equipped with Chromosorb 105 column.

Catalytic oxidation of n-butane

Catalytic oxidation of *n*-butane was carried out in a fixed bed reactor (Stainless tube, 10 mm of inside diameter) under an atmospheric pressure at 703 K. Prior to the reaction, the vanadyl alkylphosphates were calcined in a flow of a mixture of O_2 (10 %) and N_2 (90 %) for 2 h. The calcination temperatures were adjusted to 703 K for VAP-*methanol*, VAP-*2-propanol*, and VAP-*2-butanol*, and 803 K for VAP-*1-butanol*, VAP-*1-octanol*, and VAP-*cyclopentanol*. These calcination temperatures approximately correspond to the end temperatures of weight decrease on the TG profiles. The catalysts obtained are denoted to VPO(*alcohol name*). $VOHPO_4 \cdot 0.5H_2O$ was treated in a flow of N_2 at 823 K for 2 h.

The reaction mixture consisting of 5.0 % *n*-butane, 20 % O_2, and N_2 (balance) was fed to the catalyst (1.5 g) at a rate of 30 cm^3 min^{-1}, and temperature of the reactor was raised from room

temperature to 703 K at a rate of 5 K min^{-1}. Since the stationary activity and selectivity were obtained after about 25 h of the reaction at 703 K, the data were collected at 30 h of the reaction. The products were analyzed with on-line gas chromatographs (FID (Shimadzu 14A, Shimadzu 9A) and TCD (Shimadzu 9A)). For *n*-butane and MA, a Porapak QS column (inside diameter 2.2 mm, length 1 m) was used. A Molecular Sieve 13X column (inside diameter 2.2 mm, length 4 m) was utilized for O_2, N_2 and CO and a Porapak N column (inside diameter 2.2 mm, length 2 m) for CO_2. CO and CO_2 were converted to methane by using a Methanizer (Shimadzu MTN-1) for an FID analysis.

Results

Vanadyl alkylphosphates obtained from primary aliphatic alcohols

Table 1 summarizes the results of elemental chemical analysis for the vanadyl alkylphosphates from primary aliphatic alcohols (abbreviated as VAPs-*Pri*). The P/V ratios of all the compounds were 1.00 ± 0.03. Expectedly, the C/P ratio increased as the carbon number of the starting alcohol increased. The R/P ratios calculated from the C/P ratios were 1.00 ± 0.11, where R shows an alkyl group. The oxidation numbers of V in these compounds were determined to 4.00 ± 0.02.

IR spectra of VAPs-*Pri* are shown in Fig. 1. The IR bands at around 900 – 1300 cm^{-1} are due to the lattice vibration of V-P-O layers of these compounds. The bands of 1192, 1095, and 1054 cm^{-1} are assigned to $\nu(PO_3)$ and that at 981 cm^{-1} is due to $\nu(V=O)$ [29]. The vibrations of P-O-C bond were detected at around 1161 cm^{-1} as shoulder peaks [30]. The C-H vibration of alkyl groups appeared at 2850-3000 cm^{-1}, where intensities of these bands greatly depended on the kinds of alkyl groups. Furthermore, two bands at 3528 and 3581 cm^{-1} are assignable to free OH stretching [31].

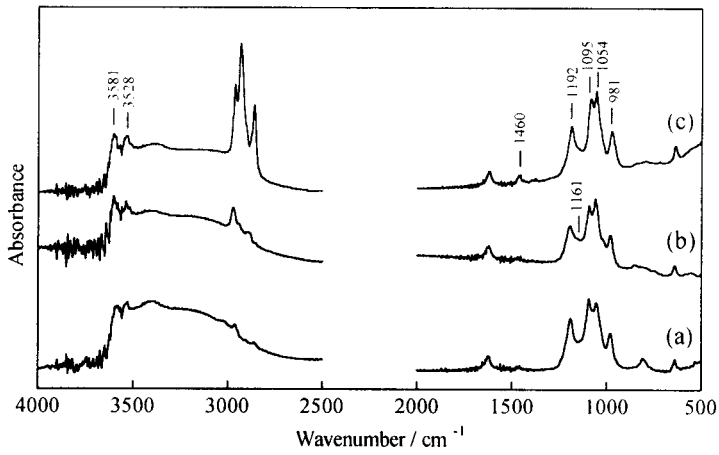

Fig. 1 Infrared spectra of vanadyl alkylphosphate obtained from (a) methanol, (b) 1-propanol, and (c) 1-octanol.

Table 1. Elemental chemical analysis for vanadyl alkylphosphates synthesized from primary aliphatic alcohols

Alcohol	Elemental analysis/wt%[a]					Atomic ratio of P/V	Atomic ratio of C/P	Formula
	V	P	C	H	O[b]			
methanol	28.1	17.4	6.5	2.0	46.1	1.02	0.96	$VO\{(CH_3)_{0.5}/H_{0.5}\}PO_4\cdot(CH_3OH)_{0.5}$
	(27.4)	(16.7)	(6.5)	(2.2)	(47.3)			
ethanol	24.8	15.1	12.8	3.1	44.2	1.00	2.19	$VO\{(C_2H_5)_{0.7}/H_{0.3}\}PO_4\cdot(C_2H_5OH)_{0.4}$
	(25.4)	(15.4)	(13.2)	(3.1)	(43.0)			
1-propanol	25.0	15.0	15.6	3.3	41.1	0.99	2.68	$VO\{(n\text{-}C_3H_7)_{0.6}/H_{0.4}\}PO_4\cdot(n\text{-}C_3H_7OH)_{0.3}$
	(24.8)	(15.1)	(15.8)	(3.2)	(41.2)			
1-butanol	23.3	14.3	21.1	4.2	37.2	1.01	3.81	$VO\{(n\text{-}C_4H_9)_{0.7}/H_{0.3}\}PO_4\cdot(n\text{-}C_4H_9OH)_{0.3}$
	(22.7)	(13.8)	(21.4)	(4.3)	(37.8)			
1-hexanol	19.3	12.0	30.5	6.0	32.2	1.02	6.56	$VO\{(n\text{-}C_6H_{13})_{0.6}/H_{0.4}\}PO_4\cdot(n\text{-}C_6H_{13}OH)_{0.5}$
	(19.3)	(11.7)	(30.0)	(5.7)	(33.3)			
1-octanol	17.3	10.2	34.4	6.8	31.3	0.97	8.71	$VO\{(n\text{-}C_8H_{17})_{0.6}/H_{0.4}\}PO_4\cdot(n\text{-}C_8H_{17}OH)_{0.5}$
	(17.3)	(10.5)	(35.8)	(6.6)	(29.8)			

a) The figures in parentheses are the values calculated from the formulae.

b) The oxygen content was estimated by subtracting the sum of weights of V, P, C, and H.

TG/DTA profiles of VAPs-*Pri* are illustrated in Fig. 2. As shown in Fig. 2a, the weight decreased in two steps for VAP-*methanol*. The first weight loss observed below 490 K with a slight endothermic and the second one above 570 K was exothermic. The molecules desorbed from VAP-*methanol* measured by the temperature programmed decomposition were mostly methanol (97 mol%) and a small amount of water. As will be discussed below, the first and second weight losses correspond to the desorption of intercalated methanol and the combustion of methyl group connected by covalent bond, respectively. The TG profiles of other VAPs-*Pri* showed loose changes (Fig. 2b-d). The sharp exothermic peaks were detected above 500 K for the all compounds and the magnitudes of the peaks increased with increase in the carbon number of the alcohol.

Figure 3 presents the XRD patterns of VAPs-*Pri*. All compounds gave intense lines at less than 10° of 2θ. The compounds from smaller alcohol such as methanol, ethanol, and 1-propanol showed similar XRD patterns (Figs. 3a-c). On the other hand, VAP-*1-butanol*, VAP-*1-hexanol* and VAP-*1-octanol* gave typical patterns due to lamellar compounds (Figs. 3d-f). For example, VAP-*1-octanol* (Fig. 3f) has the reflections at 2θ = 3.72° (2.37 nm), 7.38° (1.20 nm), 11.00° (0.80 nm), and 14.68° (0.60 nm), which were assignable to the (001), (002), (003), and (004) reflections of lamellar phase, respectively. The basal spacings (d(001)) were estimated from 2θ of the (001) reflections to be 0.91 nm (VAP-*methanol*), 1.04 nm (VAP-*ethanol*), 1.23 nm (VAP-*1-propnaol*), 1.54 nm (VAP-*1-butanol*), 1.93 nm (VAP-*1-hexanol*), and 2.37 nm (VAP-*1-octanol*), respectively. The d(001) value increased as the carbon number of the starting alcohol increased.

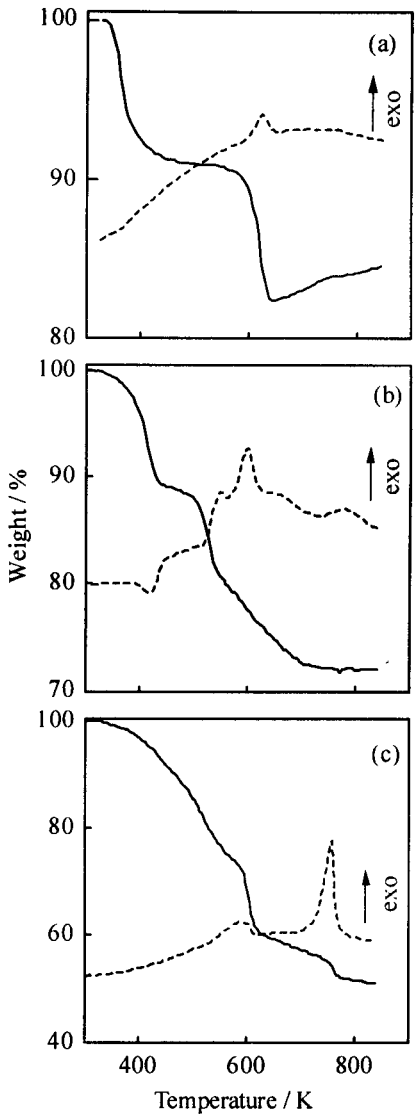

Fig. 2 TG/DTA profiles of vanadyl alkylphosphates measured in air. The vanadyl alkylphosphates were obtained from (a) methanol, (b) 1-propanol, and (c) 1-octanol.

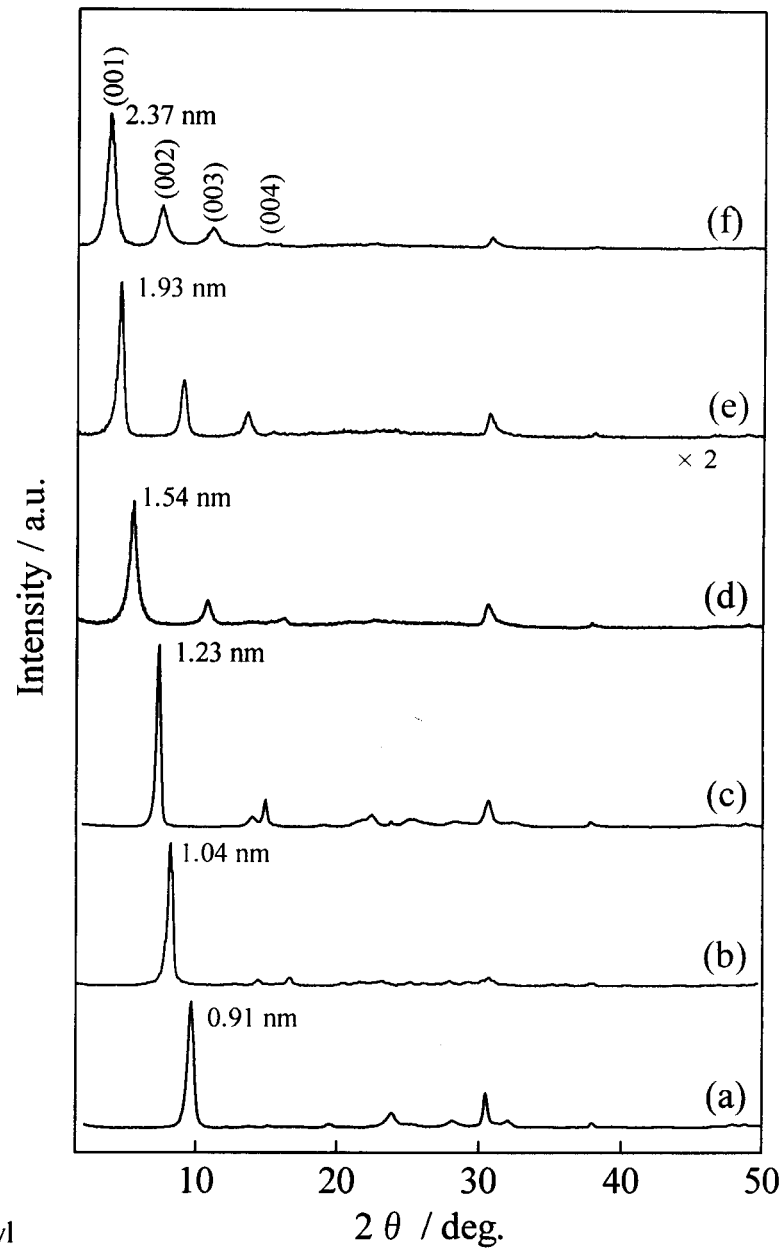

Fig. 3 XRD patterns of vanadyl alkylphosphates obtained from (a) methanol, (b) ethanol, (c) 1-propanol, (d) 1-butanol, (e) 1-hexanol, and (f) 1-octanol.

Figure 4 provides a correlation between the $d(001)$ value and molecular length of the starting alcohol, where the molecular length as the distance between H of OH (H_{-OH}) and farthest H from H_{-OH} was estimated on the basis of the covalent bond lengths with MOPAC (FUJITSU, WinMOPAC Version 1.0). It was found that the $d(001)$ values increased in proportional to the length of the alcohol.

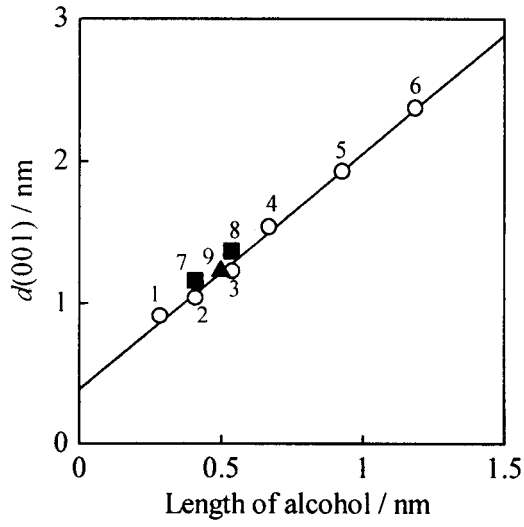

Fig. 4 Correlation between the $d(001)$ values of vanadyl alkylphosphates and length of the starting alcohol. The vanadyl alkylphosphates were obtained from primary aliphatic alcohol (○) (1) methanol, (2) ethanol, (3) 1-propanol, (4) 1-butanol, (5) 1-hexanol, (6) 1-octanol; secondary aliphatic alcohol (■) (7) 2-propanol, (8) 2-butanol; and alicyclic alcohol (▲) (9) cyclopentanol.

Figure 5 shows the dependencies of magnetic susceptibility on temperature for VAP-*methanol* (Fig. 5a) and VAP-*1-octanol* (Fig. 5b). Magnetic susceptibility is an indication of existence of exchange coupled V^{4+} dimers in various V-P oxides [5,11,32]. When the temperature decreased from 300 K, χ_g gradually increased, and then decreased through a maximum around 45 K. These changes were similar to those of $VOHPO_4 \cdot 0.5H_2O$ [5] and $VOHPO_3 \cdot 1.5H_2O$ [32] in the literatures, which have the V^{4+} dimers. These results indicate the presence of the V^{4+} dimers in the vanadyl alkylphosphates. The data can be analyzed by the Bleaney-Bowers expression (eq. 1) for isolated dimer model containing two $S = 1/2$ cations with isotopic g tensor [33]:

$$\chi = \chi_0 + C_i/(T-\theta) + 4C_d/(T(3 + \exp(-2J/k_BT))) \qquad (1)$$

where χ_0 is the temperature-independent parameter; C_i and θ, the constants associated with the magnetic impurities (*i.e.* the residual isolated paramagnetic V^{4+} monomers); T, temperature; C_d, Curie constant associated with the V^{4+} dimer; J, the coupling constant within the V^{4+} dimer; and k_B, Boltzman's constant. The results of least-squares fit in the whole temperature range are shown in Fig. 5 (solid line) and the parameters are listed in Table 2 along with the data for $VOHPO_4 \cdot 0.5H_2O$.

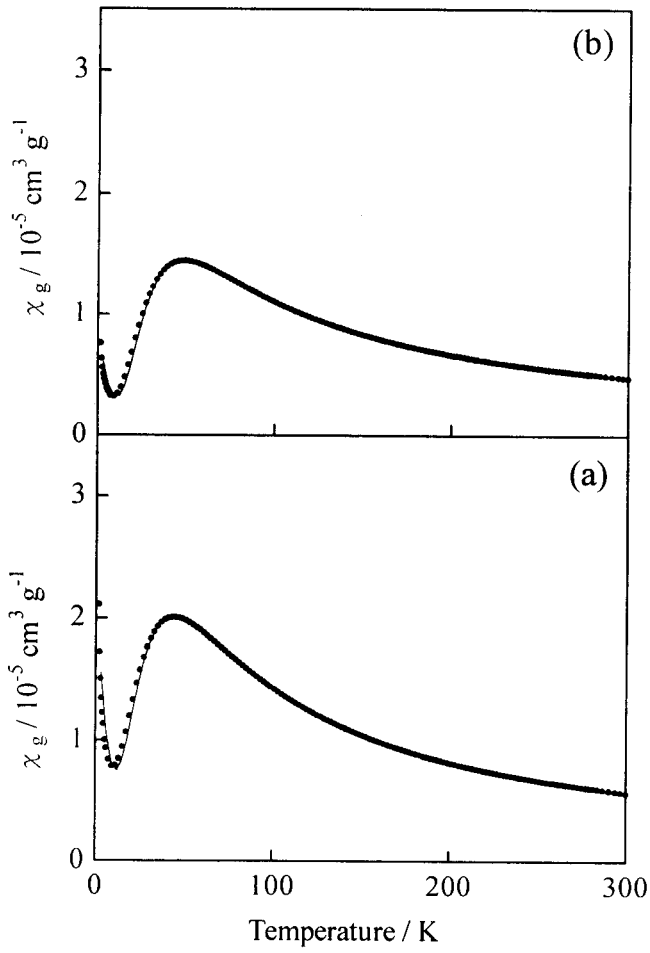

Fig. 5 Magnetic susceptibility of vanadyl alkylphosphates obtained from (a) methanol and (b) 1-octanol. Solid lines represent the result simulated by using the Bleaney-Bowers expression.

Table 2. Parameters used to fit the magnetic susceptibility of vanadyl alkylphosphates synthesized from various alcohols and $VOHPO_4 \cdot 0.5H_2O$

Alcohol	χ_0	C_I	θ	C_d	C	J	μ_{eff}
	10^{-7} cm^3 K g^{-1}	10^{-5} cm^3 K g^{-1}	deg.	10^{-3} cm^3 K g^{-1}	10^{-3} cm^3 K g^{-1}	cm^{-1}	μ_B
$VOHPO_4 \cdot 0.5H_2O$[a)]	2.5	15.3	-0.6	1.99	---	-30.6	1.72
methanol	0.8	9.9	-3.4	1.69	---	-26.1	1.63
1-octanol	5.6	3.0	-2.4	1.31	---	-27.5	1.77
2-propanol	3.2	5.6	-1.3	1.59	---	-29.5	1.66
cyclopentanol	0.5	8.1	-0.9	1.70	---	-28.8	1.69
2-butanol	-15.4	---	-9.1	---	1.86	---	1.90

a) $VOHPO_4 \cdot 0.5H_2O$ which was prepared by the so-called organic solvent method [27].

Vanadyl alkylphosphates obtained from secondary aliphatic and alicyclic alcohols.

The compositions of VAP-*2-propanol*, VAP-*2-butanol*, and VAP-*cyclopentanol* are listed in Table 3. The P/V ratios were near unity in all the compounds. The R/P ratios of VAP-*2-butanol* and VAP-*2-propanol* were 0.98 and 0.88, respectively. On the other hand, the ratio of VAP-*cyclopentanol* was 0.55. The oxidation numbers of V for these vanadyl alkylphosphates were 4.00 ± 0.04.

Figure 6 shows XRD patterns of VAP-*2-propanol*, VAP-*2-butanol*, and VAP-*cyclopentanol*. These compounds gave intense diffraction lines at less than 2θ = 10°. For VAP-*2-propanol* (Fig. 6a), a weak diffraction line (2θ = 6.7°) at a slightly lower 2θ angle of the intense one (2θ = 7.6°) was observed. Since this weak line accompaning the (200) at 13.8°, this phase is probably a contaminant lamellar phase. The *d*(001) values were 1.16 nm (VAP-*2-propanol*), 1.37 nm (VAP-*2-butanol*), and 1.23 nm (VAP-*cyclopentanol*), respectively. The correlation between the *d*(001) value and molecular length of the starting alcohol was in good accordance with that for VAPs-*Pri* (Fig. 4).

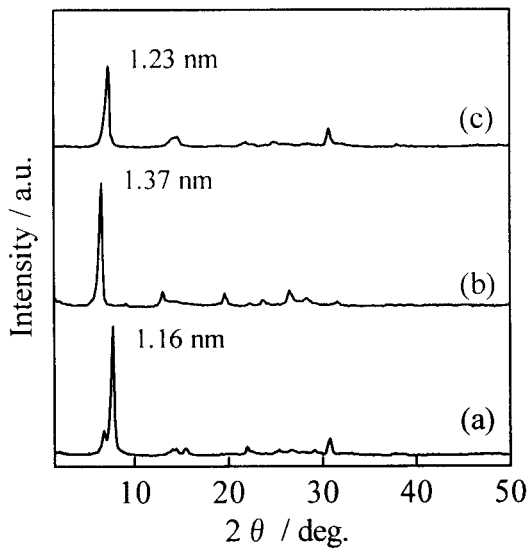

Fig. 6 XRD patterns of vanadyl alkylphosphates obtained from (a) 2-propanol, (b) 2-butanol, and (c) cyclopentanol.

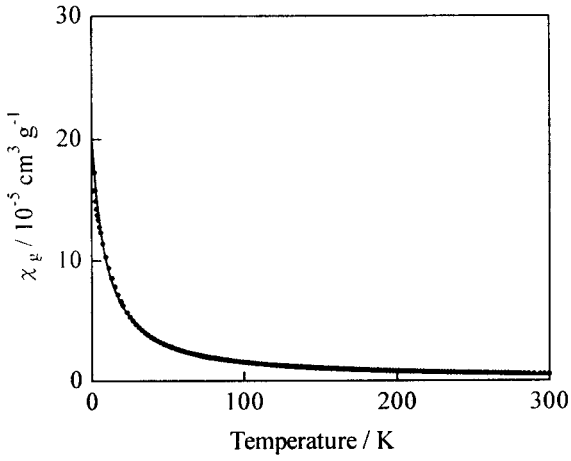

Fig. 7 Magnetic susceptibility of vanadyl alkylphosphate obtained from 2-butanol. Solid line represents the result simulated by using the Curie-Weiss expression.

Table 3. Elemental analysis for vanadyl alkylphosphates synthesized from secondary aliphatic and alicyclic alcohols

Alcohol	Elemental analysis/wt%[a]					Atomic ratio of P/V	Atomic ratio of C/P	Formula
	V	P	C	H	O[b]			
2-propanol	24.3	15.9	16.2	3.5	40.1	1.07	2.64	$VO\{(sec\text{-}C_3H_7)_{0.2}/H_{0.8}\}PO_4\cdot(sec\text{-}C_3H_7OH)_{0.7}$
	(23.9)	(14.5)	(15.2)	(3.7)	(42.7)			
2-butanol	21.0	13.7	20.7	4.8	39.8	1.07	3.90	$VO\{(sec\text{-}C_4H_9)_{0.1}/H_{0.9}\}PO_4\cdot(sec\text{-}C_4H_9OH)_{0.9}$
	(22.0)	(13.4)	(22.5)	(4.7)	(37.4)			
cyclopentanol	25.4	15.7	16.7	2.8	39.4	1.02	2.74	$VO\{(C_5H_9)_{0.2}/H_{0.8}\}PO_4\cdot(C_5H_9OH)_{0.4}$
	(24.2)	(14.7)	(17.1)	(3.1)	(40.9)			

a) The figures in parentheses are theoretical values calculated from formulae.

b) The oxygen content was estimated by subtracting the sum of weight of V, P, C, and H.

As was not shown, the magnetic susceptibility of VAP-*2-propanol* and VAP-*cyclopentanol* gave a maximum of χ_g around 45 K as well, showing the presence of the V^{4+} dimers in these compounds. The data could be well fitted by the Bleaney-Bowers expression (eq. 1). The parameters obtained are listed in Table 2. As shown in Fig. 7, VAP-*2-butanol* showed a distinctly different profile of magnetic susceptibility. When the temperature decreased from 300 K, χ_g monotonously increased. The data were well fitted to the Curie-Weiss expression (eq. 2) for whole temperature range as listed in Table 2 and Fig. 7 (solid line).

$$\chi_g = \chi_0 + C/(T-\theta) \qquad (2)$$

As will be discussed below, isolated V^{4+} monomers exist in VAP-*2-butanol*.

As shown in Fig 8, the IR spectra of VAP-*2-propanol* (Fig. 8a) and VAP-*cyclopentanol* (Fig. 8c) were similar to those of VAPs-*Pri*. On the other hand, VAP-*2-butanol* gave a broad band around 1040 cm^{-1} together with a broad band around 3380 cm^{-1} (Fig. 8b).

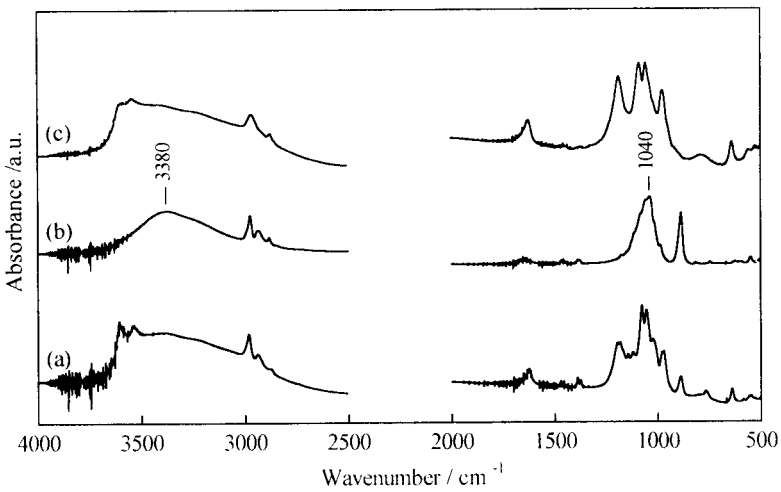

Fig. 8 Infrared spectra of vanadyl alkylphosphate obtained from (a) 2-propanol, (b) 2-butanol, and (c) cyclopentanol.

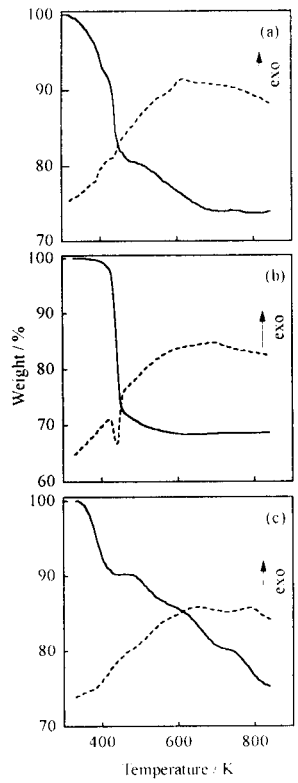

Fig. 9 TG/DTA profiles of vanadyl alkylphosphates measured in air. The vanadyl alkylphosphates were obtained from (a) 2-propanol, (b) 2-butanol, and (c) cyclopentanol.

TG/DTA profiles of VAP-*2-propanol*, VAP-*2-butanol*, and VAP-*cyclopentanol* are given in Fig. 9. VAP-*2-propanol* and VAP-*cyclopentanol* gave loose changes of weight in TG profiles (Fig. 9a and c) and indistinct exothermic peaks were observed. On the other hand, the TG profile of VAP-*2-butanol* (Fig. 9b) showed a very sharp weight loss with endothermic at 440 K.

Catalytic oxidation of n-butane

The surface area and the catalytic data are summarized in Table 4. As a reference, the data of a typical $(VO)_2P_2O_7$ catalyst (abbreviated as VPO-org) obtained from $VOHPO_4 \cdot 0.5H_2O$ are shown. The catalytic activity differed significantly depending on kinds of the precursors. VPO(*methanol*) and VPO(*cyclopentanol*) were highly active because of the high surface areas, *e.g.*, 37.6 and 21.2 $m^2\ g^{-1}$, respectively. VPO(*1-octanol*) and VPO(*2-butanol*) having a surface area less than 4 $m^2\ g^{-1}$ showed low activities for the reaction. VPO(*methanol*) and VPO(*cyclopentanol*) exhibited selectivities comparable to that of VPO-*org*. VPO(*1-butanol*), VPO(*1-octanol*), and VPO(*2-propanol*) are slightly less selective than VPO(*methanol*) and VPO(*cyclopentanol*). On the other hand, VPO(*2-butanol*) gave low selectivity (31.0 % at 16.7 % conversion).

Table 4 Activity and selectivity of VP oxide catalysts for oxidation of *n*-butane[a)]

Catalyst[b)]	SA[c)] / $m^2\ g^{-1}$	Conversion[d] / %	Selectivity[d),e)] / %		
			MA	CO_2	CO
VPO(*methanol*)	37.6	59.0	65.3	14.7	20.0
VPO(*1-butanol*)	6.4	21.7	59.3	16.2	23.5
VPO(*1-octanol*)	3.8	15.5	56.7	15.7	27.6
VPO(*2-propanol*)	11.5	34.3	61.6	13.8	24.6
VPO(*2-butanol*)	3.1	16.7	31.0	20.1	48.9
VPO(*cyclopentanol*)	21.2	58.9	68.0	13.4	18.6
VPO-org[f)]	43.5	68.9	66.0	15.8	18.3

a) The reaction was performed at 703 K with the mixture of 5.0 % *n*-butane, 20 % O_2, and N_2 (balance). *W/F* (catalyst weight / flow rate) was 373 g h (mol of *n*-butane)$^{-1}$. b) The precursors were previously calcined in a flow of a mixture of 10 % O_2 and N_2 (balance) for 2 h at 703 K (VAP-*methanol*, VAP-*2-propanol*, VAP-*2-butanol*), 803 K (VAP-*1-butanol*, VAP-*1-octanol*, VAP-*cyclopentanol*). c) Surface area after the reaction. d) Stationary values obtained after 30 h of the reaction. e) Selectivity based on butane. f) VPO-org which was prepared by the so-called organic solvent method [27].

Powder XRD patterns of the catalysts after the reactions are given in Fig. 10. These samples gave basically the patterns of $(VO)_2P_2O_7$ except for VPO(*2-butanol)* (Fig. 10e). VPO(*methanol*), VPO(*cyclopentanol*), and VPO-*org* were assigned to highly crystallized $(VO)_2P_2O_7$. Weak diffraction lines of $(VO)_2P_2O_7$ were observed for VPO(*1-butanol*) and VPO(*1-octanol*) with halo patterns around $2\theta = 20^\circ$, indicating the presence of amorphous phase. VPO(*2-propanol*) gave weak diffraction lines of γ-$VOPO_4$, besides medium intense lines of $(VO)_2P_2O_7$. On the other hand, VPO(*2-butanol)* showed only diffraction lines due to α-$VOPO_4$ and X_1 phase [34].

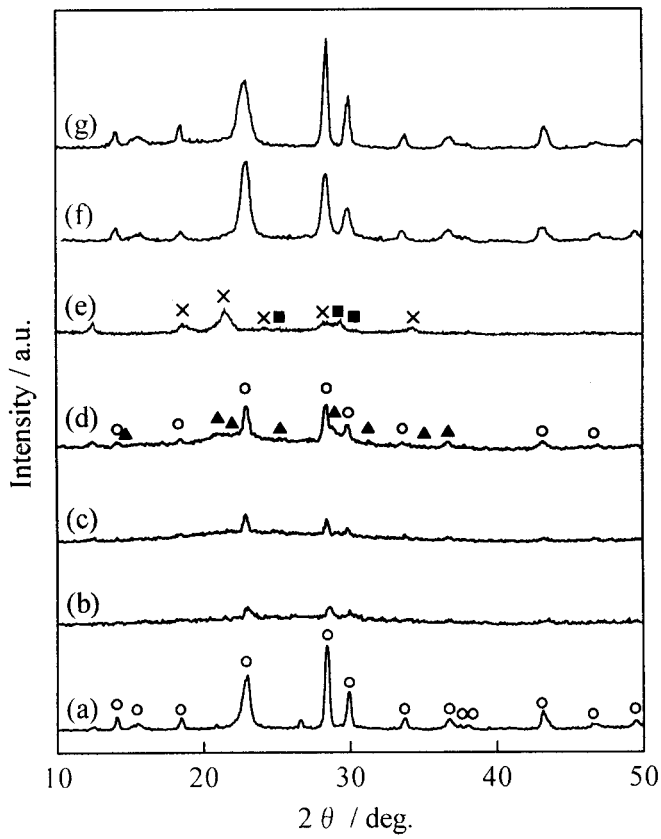

Fig. 10 XRD patterns of vanadium phosphorus oxide catalysts after the oxidation of *n*-butane. (a) VPO(*methanol*), (b) VPO(*1-butanol*), (c) VPO(*1-octanol*), (d) VPO(*2-propnaol*), (e) VPO(*2-butanol*), (f) VPO(*cyclopentanol*), and (g) VP oxide obtained from $VOHPO_4 \cdot 0.5H_2O$. (○) $(VO)_2P_2O_7$, (▲) γ-$VOPO_4$, (×) X_1 phase, and (■) α-$VOPO_4$.

SEM images of the catalysts are given in Fig. 11. It was found that the morphology of these compounds changed significantly depending on the alcohol. VPO(*methanol*) displayed sponge-like shapes which consisted of microcrystallites of thin flakes (Fig. 11a). VPO(*1-butanol*) showed bunches of grapes (Fig. 11b). VPO(*cyclopentanol*) displayed rose-petal morphology, which was shown in the catalyst prepared by the so-called organic solvent method [27].

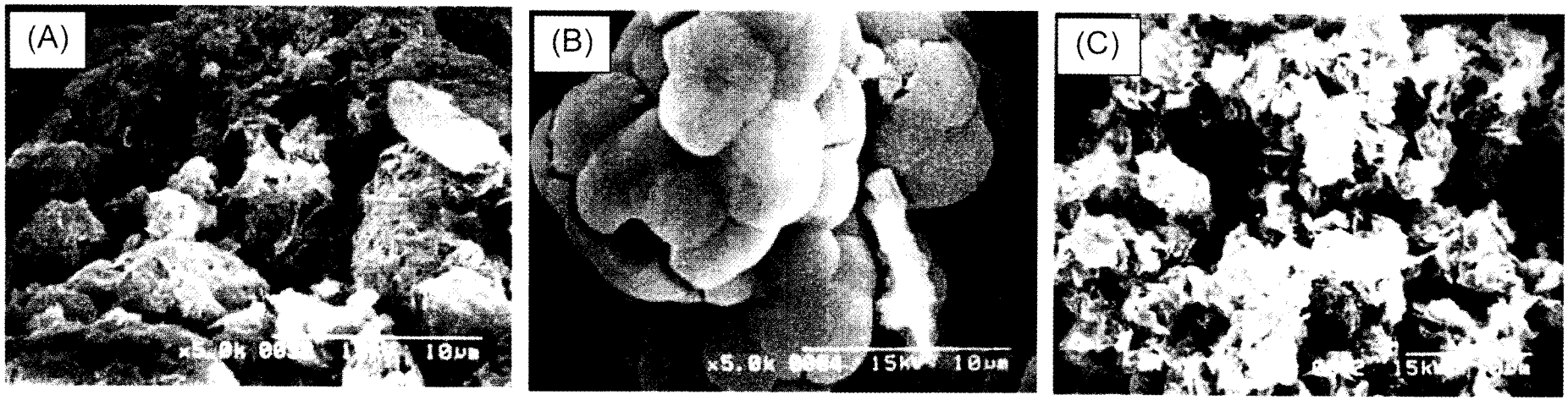

Fig. 11 SEM images of the catalysts after the oxidation of butane. (a) VPO(*methanol*), (b) VPO(*1-butanol*), and (c) VPO(*cyclopentanol*).

Discussion

Structure of vanadyl alkylphosphates synthesized from primary aliphatic alcohols

VAPs-*Pri* have a lamellar structure, because these compounds showed a typical XRD pattern of the lamellar phase as shown in Fig. 3. The linear correlation of the *d*(001) values with the molecular length of the starting alcohol (Fig. 4) indicates that these alkyl groups are present in the interlayer space of these compounds. In other words, VAPs-*Pri* consists of alternating V-P-O layers and organic group ones. In Fig. 4, the value of intercept, 0.40 nm, of vertical axis is close to that of $VOPO_4$ (0.411 nm) [35]. If the alkyl groups existed as a single or double layer perpendicularly against the V-P-O layer, the slope of the line in Fig. 4 would be 1.0 or 2.0, respectively. Since the observed slope is 1.65, it is deduced that the alkyl groups are present as a double layer with a tilt of about 56° in the interlayer space.

The P/V atomic ratios of VAPs-*Pri* were nearly unity and average oxidation numbers of V were near to +4.0. The absorption bands of $\nu(PO_3)$ and $\nu(V=O)$ were observed at almost the same positions as that for $VOHPO_4 \cdot 0.5H_2O$ [5]. The magnetic susceptibility (Fig. 5) indicates the existence of the V^{4+} dimers in these compounds. In addition, the coupling constants (*J*) of VAP-*methanol* ($-26.1 cm^{-1}$) and VAP-*1-octanol* ($-27.5 cm^{-1}$) were almost the same as that of $VOHPO_4 \cdot 0.5H_2O$ ($-30.6\ cm^{-1}$). The layered $VOHPO_4 \cdot 0.5H_2O$ consists of alternating $VOHPO_4$ layers and H_2O ones. The $VOHPO_4$ layer is made up with edge-shared VO_6 octahedras, which is the V^{4+} dimers, connected through corners by PO_4 tetrahedras [5]. These results demonstrate that the V-P-O layer of the VAPs-*Pri* are similar to that of $VOHPO_4 \cdot 0.5H_2O$.

The formula of VAP-*methanol* will be first discussed. The IR spectrum showed the vibration of P-O-C ($1161\ cm^{-1}$) for VAP-*methanol* (Fig. 1). Thus, the methyl group would exist as methyl phosphate ($P\text{-}O\text{-}CH_3$). Alkyl phosphate is known to be formed by a reaction of P_2O_5 with corresponding alcohol [36], supporting the existence of methyl phosphate in this compound. As shown in Fig. 2a, the TG profile showed two step weight decreases, 8.7 wt% and 8.9 wt%. Since the first decrease was the desorptions of methanol and small amount of water, this weight loss is due to the removal of methanol intercalated. Considering the exothermic and the relatively high temperature, the second weight loss is due to combustion of methyl group. From these results, the chemical formula of VAP-*methanol* is described as $VO(CH_3O)_x(HO)_{1-x}PO_3 \cdot (CH_3OH)_{1-x}$. Since the C/P ratio of

VAP-*methanol* was almost unity (0.96), the chemical formula of VAP-*methanol* is determined to $VO(CH_3O)_{0.5}(HO)_{0.5}PO_3 \cdot (CH_3OH)_{0.5}$. The composition calculated from this chemical formula is in good agreement with the experimental values as listed in Table 1. The two weight losses on the TG profile (8.7 wt% and 8.9 wt%) are also consistent with calculated values (8.4 wt% and 8.7 wt%).

Next, we will estimate the chemical formulae of the other VAPs-*Pri*. Similarly to the case of VAP-*methanol*, it was deduced that the exothermic weight losses were due to the combustion of alkyl group on alkyl phosphate and the other weight losses due to the intercalated alcohol. From this assumption, the chemical formulae of these VAPs-*Pri* were proposed as listed in Table 1. These formulae are well consistent with the experimental data.

On the basis of these results, the schematic structure of VAP-*methanol* as a typical sample of VAPs-*Pri* is depicted in Fig. 12. VAPs-*Pri* are lamellar compounds consisting of alternating of V-P-O layers with thickness of 0.40 nm and alkyl group layers. In this structure, the V-P-O layer is similar to $VOHPO_4 \cdot 0.5H_2O$, in which the V^{4+} dimers are connected by PO_4 tetrahedra. About half of PO_4 presents as alkyl phosphate and the others as hydrogen phosphate (H-O-P-). The alkyl groups of alcohol and alkyl phosphate exist as a double layer with a tilt of about 56°. Since the XRD pattern of the sample, which was the compound treated with an air flow at 450 K, was almost the same as that of VAP-*methanol*, methyl groups of the methyl phosphate in the adjoining layers may be located in contacted position. Two bands due to free OH vibration observed in IR spectra (Fig. 1) indicate that the interaction between alcohol and hydrogenphosphate is weak. Probably, the alcohols are apart from the hydrogen phosphates.

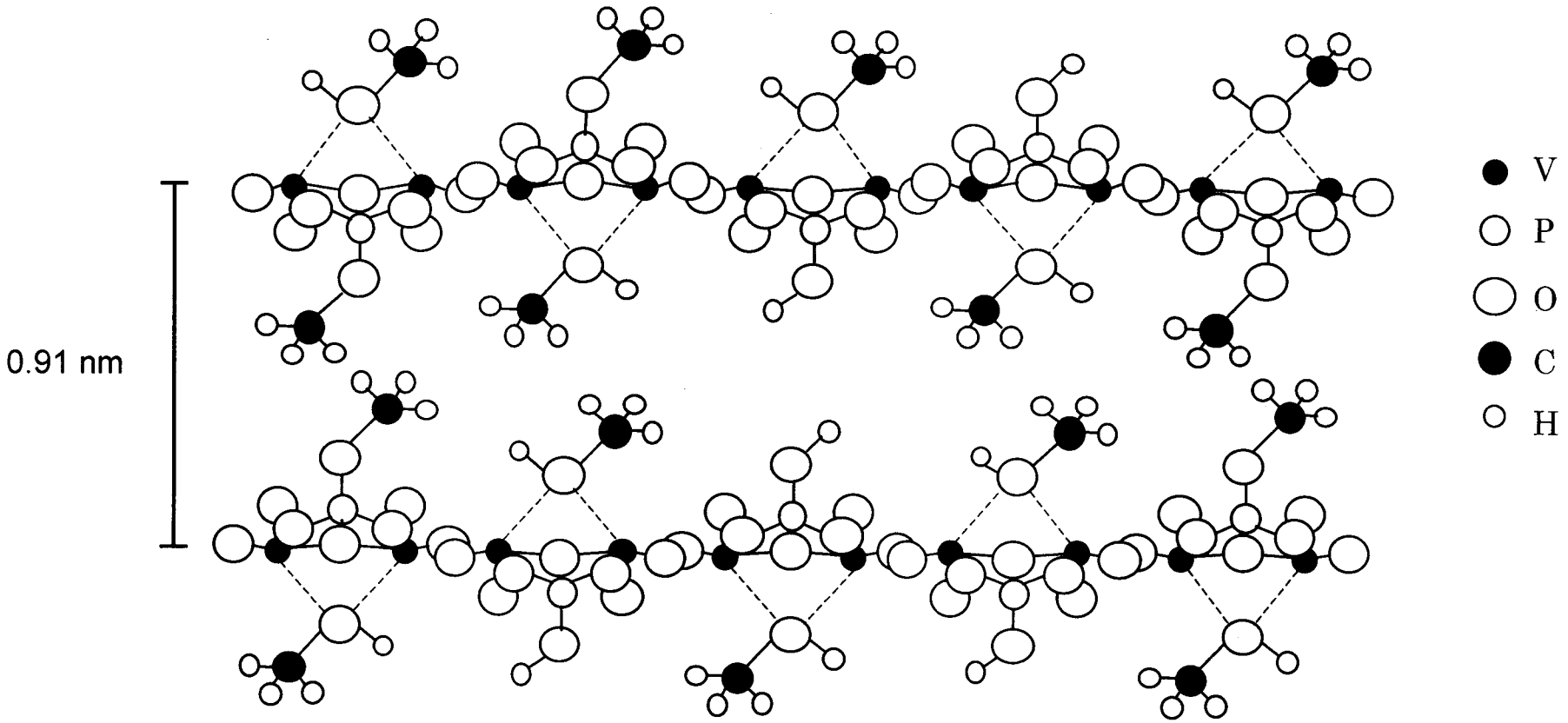

Fig. 12 Proposed model for structure of vanadyl methylphosphate as a typical sample of vanadyl alkylphosphates. The V-P-O layer consists of edge-shared VO_4 dimers connected through corners by $(HO)PO_3$ or $(CH_3O)PO_3$ tetrahedra.

Structure of vanadyl alkylphosphates synthesized from secondary aliphatic and alicyclic alcohols

The P/V ratios and oxidation numbers of V for VAP-*2-propnaol*, VAP-*2-butanol* (abbreviated as VAPs-*sec*), and VAP-*cyclopentanol* (abbreviated as VAP-*cycl*) are 1.02–1.07 and 3.99–4.04, respectively, which are very close to those of VAPs-*Pri*. The good correlation between the *d*(001) value and the length of the alcohol is also well-fitted (Fig. 4), indicating that the branched-alkyl and alicyclic groups in these vanadyl alkylphosphates exist in the same configuration as straight alkyl groups.

The IR spectra of VAP-*2-propanol* and VAP-*cyclopentanol* were similar to those of VAPs-*Pri* and the magnetic susceptibility was accordance with the presence of the V^{4+} dimers (Table 2). Thus it is considered that the structure of the V-P-O layer is analogous to those of VAPs-*Pri*. The chemical formulae of these compounds were estimated in the similar manner to VAPs-*Pri* (Table 3). Only 10 – 20 % of total phosphorus exists as alkyl phosphate (R-O-P-) in these compounds, while 50-70 % of total phosphorus was alkyl phosphate in VAPs-*Pri*. Hiyama et al. reported that secondary aliphatic alcohol was readily dehydrated under presence of P_2O_5 [38]. Since P_2O_5 reacts with H_2O to form H_3PO_4, the most of the added P_2O_5 was probably converted to H_3PO_4. Consequently, the concentrations of alkyl phosphate formed from secondary alcohols would be low. By this, it is deduced that the incorporation of these alkyl phosphates into VAPs-*sec* and VAP-*cycl* was limited.

Contrary to the above compounds, the structure of V-P-O layers for VAP-*2-butanol* was different from that of the other vanadyl alkylphosphates. As shown in Fig. 7, the magnetic susceptibility of VAP-*2-butanol* obeyed the Curie-Weiss expression (eq. 2). The magnetism like this was observed for vanadyl benzylphosphonate [12] and vanadyl *n*-pentylphosphonate [13], which have isolated V^{4+} monomers. The IR spectra of VAP-*2-butanol* having the broad band around 1040 cm^{-1} in V-P-O lattice vibration region (Fig. 8) was also different from the others compounds. These broad bands were observed in intercalated $VOPO_4$ compounds having isolated VO_6 octahedra, *e.g.*, $VOPO_4$-aniline [39], $VOPO_4$-anilinoaniline [40], and $VOPO_4$-4-butylaniline [41]. These results indicate that the isolated V^{4+} monomers exist in VAP-*2-butanol*. Furthermore, VAP-*2-butanol* gave the broad band around 3380 cm^{-1} in the IR spectra, suggesting that hydrogenphosphate (POH) of the V-P-O layer interacts with OH of intercalated 2-butanol.

In summary, the structure of VAP-*2-propanol* and VAP-*cyclopentanol* is the same as those of VAPs-*Pri*, while the $ROPO_3/HOPO_3$ ratios were smaller than those in VAPs-*Pri*. On the other hand,

VAP-*2-butanol* has the different structure from that of the above compounds, and has isolated V^{4+} monomers linked with PO_4 tetrahedra.

Selective oxidation of n-butane with the catalysts obtained from vanadyl alkylphosphates

Highly crystalline $(VO)_2P_2O_7$ phases were obtained from VAP-*methanol* and VAP-*cyclopentanol* by the calcination, followed by the activation under the reaction conditions for 30 h. These vanadyl alkylphosphates with the structure containing the V^{4+} dimers were transformed to $(VO)_2P_2O_7$. On the other hand, only VAP-*2-butanol* having isolated V^{4+} monomers changed to the mixture of α-$VOPO_4$ and X_1 phases instead of $(VO)_2P_2O_7$. The difference among these vanadyl alkylphosphates would be brought about from the difference in the structures of V-P-O layers. VAP-*1-butanol* and VAP-*1-octanol* were transformed to less crystalline $(VO)_2P_2O_7$ with amorphous V-P oxides. VAP-*1-butanol* and VAP-*1-octanol* gave large exothermic peaks over 500 K in TG/DTA as compared to that for VAP-*methanol* and VAP-*cyclopentanol* (Fig. 2). Therefore, the amorphous V-P oxides would arise from local temperature excursions resulted from exothermic combustion of these alkyl phosphates.

The concentrations of butane used for the commercial processes of selective oxidation of *n*-butane are usually about 1.5 vol.% and 4.0 vol.% for fixed-bed and fluidized-bed reactor, respectively. From an industrial viewpoint, the operation under higher concentrations of *n*-butane is preferred for higher space-time yield of MA. The catalytic performances were thus evaluated at 5.0 vol.% of *n*-butane.

VPO(*methanol*) and VPO(*cyclopentanol*) showed the high catalytic activities and selectivities to MA (Table 4). The catalytic performances of these catalysts were comparable to that of VPO-*org* (66 % of selectivity), which was reported to be selective at 5 % of *n*-butane [41]. On the other hand, the selectivities of VPO(*1-butanol*), VPO(*1-octanol*), and VPO(*2-propanol*) were not high (about 60 %) and that of VPO(*2-butanol*) was low (31 % at 16.7 % conversion).

Shimoda et al. reported that $VOPO_4$ phases of V^{5+} such as α-$VOPO_4$ and β-$VOPO_4$ as well as amorphous and X_1 phases were less selective than $(VO)_2P_2O_7$ [34]. Therefore, the low selectivity of VPO(*2-butanol)* is owing to the presence of X_1 and α-$VOPO_4$ predominantly. It is also considered that the presence of amorphous V-P oxides or γ-$VOPO_4$ is responsible for relatively low selectivities of VPO(*1-butanol*), VPO(*1-octanol*), and VPO(*2-propanol*). On the other hand, the high selectivities

of VPO(*methanol*) and VPO(*cyclopentanol*) are due to the single phase of $(VO)_2P_2O_7$.

It is known that the catalytic performance greatly depends on morphology of the catalyst as well. The catalysts consisted of the the microcrystallites of thinner plates shows higher selectivity to MA [42], because of higher exposure of the (100) plane of $(VO)_2P_2O_7$. Both VPO(*methanol*) and VPO(*cyclopentanol*) consisted of the microcrystallites of thinner plates (Fig. 11a,c). This may be another reason for higher selectivity to MA on these catalysts.

Conclusion

In the present section, the vanadyl alkylphosphates from various alcohols were developed and their structures were characterized systematically. The vanadyl alkylphosphates have lamellar structure and the alkyl groups exist as a double layers with a tilt of about 56° against the V-P-O layer. The structure of the V-P-O layers is similar to that of $VOHPO_4 \cdot 0.5H_2O$ having the V^{4+} dimers connected by PO_4 tetrahedra except for vanadyl *sec*-butylphosphate. In vanadyl *sec*-butylphosphate, isolated VO_6 monomers exists. The ratios of $(ROPO_3)$/(total P) were 0.5-0.7 for the vanadyl alkylphosphates obtained from primary aliphatic alcohols and 0.1-0.2 for that from secondary aliphatic and alicyclic alcohols. These structural characteristics indicate that the vanadyl alkylphosphates must be useful as host for intercalation of metal-complex.

The well crystallized $(VO)_2P_2O_7$ catalysts were obtained from vanadyl methylphosphate and vanadyl cyclopentylphosphate. These catalysts showed both high catalytic activity and selectivity to MA under the high concentration of *n*-butane, which was comparative to the catalysts prepared by the so-called organic solvent method.

References

[1] S. Albonetti, F. Cavani, and F. Trifirò, *Catal. Rev. –Sci, Eng.*, **38** (1996) 413.

[2] G. J. Hutchings, *Appl. Catal.*, **72** (1991) 1.

[3] B. K. Hodnett, *Catal. Rev. Eng.*, **17** (1985) 373.

[4] G. Centi, F. Trifirò, J. R. Ebner, and V. M. Franchetti, *Chem. Rev.*, **88** (1988) 55.

[5] J. W. Johnson, D. C. Johnston, A. J. Jacobson, and J. F. Brody, *J. Am. Chem. Soc.*, **106** (1984) 8123.

[6] E. Bordes and P. Courtine, *J. Solid State Chem.*, **55** (1984) 270.

[7] S. Tomita, T. Ihara, and H. Suwa, *Japan Kokai*, 5-261292 (1993) to Mitsukasei Kogyo.

[8] I. Sawa, H. Suwa, and Y. Ishii, *Japan Kokai*, 11-92973 (1999) to Mitsubishi Kagaku.

[9] T. A. Byser Jr., Japan Kokai, 58-69577 (1983) to El Du Pont de Memous and Company.

[10] S. H. Horowitz, *WO Patent* 98/15353 (1998) to El Du Pont de Memous and Company.

[11] V. V. Guliants, J. B. Benziger, S. Sundaresan, I. E. Wachs, and J.-M. Jehng, *Chem. Mater.*, 7 (1995) 1493.

[12] J. W. Johnson, A. J. Jacobson, J. F. Brody, and J. T. Lewandowski, *Inorg. Chem.*, **23** (1984) 3842.

[13] G. Huan, J. W. Johnson, J. F. Brody, D. P. Goshorn, and A. J. Jacobson, *Mater. Chem. Phys.*, **35**, (1993) 199.

[14] G. Huan, A. J. Jacobson, J. W. Johnson, and D. P. Goshorn, *Chem. Mater.*, **4** (1992) 661.

[15] E. M. Sabbar, M. E. de Roy, A. Ennaqadi, C. Gueho, and J. P. Besse, *Chem. Mater.*, **10** (1998) 3856.

[16] J. W. Johnson, J. F. Brody, and R. M. Alexander, *Chem. Mater.*, **2** (1990) 198.

[17] N. Mizuno, H. Hatayama, S. Uchida, and A. Taguchi, *Chem. Mater.*, **13** (2001) 179.

[18] T. Doi and T. Miyake, *J. Chem. Soc., Chem. Commun.*, (1996) 1635.

[19] T. Abe, A. Taguchi, and M. Iwamoto, *Chem. Mater.*, 7 (1995) 1429.

[20] M. Roca, J. E. Haskouri, S. Cabrera, A. B. Porter, J. Alamo, D. B. Porter, M. D. Marcos, and P. Amorós, *J. Chem. Soc., Chem. Commun.*, (1998) 1883.

[21] H. Hatayama, M. Misono, A. Taguchi, and N. Mizuno, *Chem. Lett.*, (2000) 884.

[22] N. Hiyoshi, N. Yamamoto, N. Terao, T. Nakato, and T. Okuhara, *Stud. Surf. Sci. Catal.*, **130** (2000) 1715.

[23] N. Hiyoshi, N. Yamamoto, and T. Okuhara, *Chem. Lett.*, (2001) 484.

[24] T. Nakato, Y. Furumi, and T. Okuhara, *Chem. Lett.*, (1998) 611.

[25] Y. Kamiya, E. Nishikawa, A. Satsuma, N. Mizuno, and T. Okuhara, *Sekiyu Gakkaishi*, **44** (2001) 265.

[26] B. K. Hodnett, P. Permanne, and B. Delmon, *Appl. Catal.*, **6** (1983) 231.

[27] H. Igarashi, K. Tsuji, T. Okuhara, and M. Misono, *J. Phys. Chem.*, **97** (1993) 7065.

[28] F. Cavani, G. Centi, and F. Trifirò, *Ind. Eng. Chem. Prod. Res. Des.*, **22** (1983) 570.

[29] G. Basca, F. Cavani, G. Centi, and F. Trifirò, *J. Catal.*, **99** (1986) 400.

[30] L. J. Bellamy, "*The Infra-red Spectra of Complex Molecules*," Chapman and Hall, London (1975), Vol. 1, pp. 354.

[31] L. J. Bellamy, "*The Infra-red Spectra of Complex Molecules*," Chapman and Hall, London (1975), Vol. 1, pp. 109.

[32] V. V. Guliants, J. B. Benziger, and S. Sundaresan, *Chem. Mater.*, **7** (1995) 1485.

[33] B. Bleaney and K. D. Bowers, *Proc. R. Soc. London, Ser. A*, **A214** (1952) 451.

[34] T. Shimoda, T. Okuhara, and M. Misono, *Bull. Chem. Soc. Jpn.*, **58** (1985) 2163.

[35] E. Bordes, P. Courtine, and G. Pannetier, *Ann. Chim. (Paris)*, **8** (1973) 105.

[36] Private data.

[37] D. F. Toy, "*Comprehensive Inorganic Chemistry*," Pergamon Press, Oxford (1968) p. 442.

[38] K. Hiyama, M. Suzuki, M. Nakamura, Y. Hatanaka, O. Kobayashi, and M. Higashihara, *Sci. Ind.*, **72** (1998) 89.

[39] H. Nakajima and G. Matsubayashi, *Chem. Lett.*, (1993) 423.

[40] H. Nakajima and G. Matsubayashi, *J. Mater. Chem.*, **5** (1995) 105.

[41] T. Nakato, Y. Furumi, N. Terao, and T. Okuhara, *J. Mater. Chem.*, **10** (2000) 737.

[42] Y. Kamiya, E. Nishikawa, T. Okuhara, and T. Hattori, *Appl. Catal. A*, **206** (2001) 103.

[43] H. S. Horowitz, C. M. Bladostone. A. W. Sleight, and G. Teufer, *Appl. Catal.*, **38** (1988) 193.

4.2 Insertion of Iron-Complex to Lamellar Vanadyl Benzylphosphate for Preparation of Well-Defined Catalyst

Abstract

A novel approach for preparation of promoted vanadium-phosphorous oxide (VPO) in well-defined structure was examined. Lamellar vanadyl benzylphosphate (LVPO) was used as a host and Fe-complex ($Fe(acac)_3$ and ferrocene) as a guest. It was found that Fe-complex was successfully inserted into LVPO by heating of LVPO and Fe-complex in toluene solution. The obtained material was characterized by means of XRD, TEM, EDX, XPS, and FT/IR. It was confirmed that Fe-complex was uniformly dispersed in the interlayer of LVPO without significant distraction of lamellar structure of parent LVPO.

Introduction

$(VO)_2P_2O_7$ for n-butane oxidation and effect of promoters

Vanadyl pyrophosphate, $(VO)_2P_2O_7$, has been widely accepted as an active and selective phase for partial oxidation of *n*-butane to maleic anhydride [1-7]. For improvement in catalytic performance, industrial $(VO)_2P_2O_7$ catalysts contain additional cations those act as promoters of different kind. Various types of elements, such as Co, Mo, Cr, Fe, Ce, Zn, Ti, Zr, Si and so on, can be found in patents, and some of scientific literatures clarified the effect of those promoters.

Haber et al. [8] clarified that the incorporation of Li, Na, K, Cs, Be, Mg, Ca, and Ba can easily donate electrons to the framework of vanadyl phosphate, leading to an increase in the negative charge of oxygen atom and in the rate of *n*-butane oxidation. They concluded that the high activity in *n*-butane oxidation and high selectivity to MA requires a fine tuning of the basicity of surface oxygen atoms to accelerate the activation of *n*-butane and of the acidity of the surface to secure the appropriate time of the reaction intermediates. Takita et al. [9] observed a linear relationship between catalytic activity for MA formation and the frequency of the V=O vibration of solids containing different promoters (Mn, Co, Fe, Zn, and Zr).

On the other hand, promoters can optimize prepration conditions and structures of $(VO)_2P_2O_7$. As reported by Horowitz et al. [10], the addition of tetraethyl orthosilicate is thought to eliminate water as a by-product in the organic solvent, leading to the formation of $(VO)_2P_2O_7$ having favorable

morphology. The structural modification of $(VO)_2P_2O_7$ is also regarded as an important effect of promoters. The structural disorder, which is related to the broadening of the (200) line in XRD patterns, is related to high activity of VPO prepared from organic media [11-14]. In the case of promoted $(VO)_2P_2O_7$, Ye et al. [13] reported that the activity per surface V=O species was found to be dependent on the disorder of VPO crystal along the (100) plane, which can be controlled by the addition of various promoters.

These various roles of promoters have been categorized. Hutchings [4] classified into two types of promoters which (1) enable the formation of the required V-P phase, and (2) form solid solutions with the active phase and that regulate the catalytic activity. Cavati and Trifiro [6] summarized that the additives can be divided into following three groups: (1) ions (Zn and Co) that interact with free phosphoric acid acting as a tool of fine tuning of the optimal surface P/V ratio and acidity, (2) ions (S and Si) that can substitute for phosphorous in the precursor controlling the morphology and defects of $(VO)_2P_2O_7$ after calcination, and (3) transition metal ions (e.g., Ti, Zr, Ce, and Mo) that substitute for vanadium acting as real modifiers directly involved in the reaction pattern. Latter two types of promoters directly interact to $(VO)_2P_2O_7$, i.e., (1) modification of structural features of $(VO)_2P_2O_7$, (2) modification of chemical properties of $(VO)_2P_2O_7$, e.g., acidity, basicity, and V=O species as redox sites.

Since preparation method for addition of promoters often strongly affects on these features of promoted VPO catalysts, a novel preparation method would result in fine control of promoted VPO structures and be a possible break-through for the enhancement of catalytic performance. Intercalation is one of the candidates for the preparation of tailored VPO catalysts, as Datta and Keller demonstrated incorporation of $Pd(NO_3)_2$ into $VOHPO_4{\cdot}0.5H_2O$ [15]. Although VPO catalysts are usually prepared from $VOHPO_4 \cdot 0.5H_2O$ as a precursor, use of other material having wide range of flexibility may result in the fine-control of the structure and chemical properties.

$(VO)_2P_2O_7$ and related VPO compounds

It has been paid much attention on a series of vanadium phosphate (VPO) chemistry, because of wide structural diversity and high dependence of catalytic performance on the crystal phase. Currently, VPO compounds having novel structures have been synthesized by means of intercalation of various organic compounds [16-25]. Benziger et al. [19, 21] demonstrated an intercalation of

n-alkylamines into $VOHPO_4 \cdot 0.5H_2O$. Formation of ordered lamellar structure of VPO compound incorporating *n*-tetradecyltrimethyl ammonium into $VOHPO_4 \cdot 0.5H_2O$ was clearly shown by Miyake et al. [22]. Okuhara et al. [24,25] successfully demonstrated "exfoliation", which is intercalation of 4-butylaniline into $VOPO_4 \cdot 2H_2O$ followed by stirring in THF, and deposition of thin lamellar sheets onto alumina support.

A series of VPO compounds with lamellar structure is the most interesting materials. Vanadyl alkylphosphonates [17,18,20,23] having the formula of $VO(RO)_x(HO)_{1-x}PO_3 \cdot (ROH)_y(H_2O)_z$ has a lamella structure with alternating inorganic and organic layers, and the intercalation property of vanadyl alkylphosphonate was greatly dependent on shape and size of the alkyl group [26]. On the other hand, DuPont's researchers recently claimed that vanadyl alkylphosphate which has P-O-C bond with a lamellar structure could be synthesized through reacting V_2O_5 with P_2O_5 in alcohol [27]. Although this method is only applicable for intercalation of primary aliphatic alcohol, Kamiya et al. developed a different method which enables to intercalate not only primary alcohol but also secondary aliphatic and alicyclic alcohols [28, 29]. This method can control the distance of interlayer in the range from 0.91 to 2.37 nm, and the distance linearly increases with molecular diameter of alcohols, indicating ordered filling of the interlayer with alcohols. It can be expected that the use of these lamellar VPO materials as a precursor may open up a novel preparation method for fine control of promoted VPO catalysts.

Possible method for preparation of well-defined VPO

Use of lamellar VPO materials as precursors for VPO catalysts would be very useful because of high potential of interlayer nano-space for catalyst design. Since the interlayer of VPO compounds is acidic, intercalation of basic amine molecules may too much stabilize the lamellar structure, and thus further modification is expected to be difficult. The lamellar VPO containing alcohols is expected to be more suitable for further modification because of weaker connection of VPO layers. After insertion of metal-complexes followed by calcination, promoter ions can be uniformly fixed in the interlayer. This nano-structural modification of VPO may results in fine-control of oxidation activity or acid-base property. Furthermore, the heteroatoms in the interlayer may cause some disorder of VPO crystal, which often play an important role in the enhancement of catalytic performance.

In this section, the author demonstrate a potential method for preparation of well-defined

promoted VPO catalysts. Lamellar VPO incorporating benzyl alcohol (lamellar vanadyl benzylphosphate, LVPO) was used as a host, because of the sufficient distance of interlayer space (ca. 1.8 nm) for various metal-complexes. The possible advantage of this material is the hydrophobic property of the inter-layer, which makes the favorable filed for coordination compounds. This section focuses on insertion of Fe-complexes into the interlayer of lamellar VPO. The obtained materials are characterized to determine the layered structure and dispersion of metal compounds.

Experimental

Preparation of catalysts

Vanadyl benzylphosphate (LVPO) was prepared by the method reported in the former section (4.1). V_2O_5 (29.2 g, Kishida, 99 %) was reduced with mixture of isobutyl alcohol (180 cm^3, Kishida, 99.5 %) and benzyl alcohol (120 cm^3, Kishida, 99.5 %) at refluxing temperature for 3 h. The resulted black solid was separated by filtration and confirmed to be a mixture of V_2O_5 and V_4O_9 by XRD. The solid was suspended in 300 cm^3 of benzyl alcohol, then a suspension of P_2O_5 in 75 cm^3 of toluene was slowly added with stirring. Then the mixture was refluxed for 6 h until valence of vanadium in obtained VPO reached +4. After cooling to room temperature, the obtained blue solid was filtered and washed with 40 cm^3 of acetone, and then dried at room temperature in air for 12 h.

For the insertion of Fe-complex, benzyl alchol or toluene (Kishida, 99.5 %) was used as a solvent, and $Fe(acac)_3$ (Kishida, 98 %) and ferrocene (Kishida, 98 %) were used as a guest molecule. LVPO and Fe-compound at a loading ratio of Fe/V = 0.5 were dissolved in 36 cm^3 of the solution and heated at 358 K with stirring for 3 h. The obtained solid was filtered, washed with 250 cm^3 of acetone, and then dried at room temperature in air for 12 h. The preparation conditions of the samples were summarized in Table 1.

Characterizations

XRD patterns were recorded with Rigaku RINT-1200 diffractometer using Cu K_α radiation. XPS spectra were measured with Shimazu ESCA-3300 using Mg K_α radiation. SEM images were taken by HITACHI S-800S. TEM and EDS images were taken by JEOL JEM-2010 coupled with Voyager III EDS analyzer, respectively. Chemical compositions of obtained materials were measured by Jarrell-Ash 975 PLASMA ATOMCOMP inductive coupled plasma spectrometer. Elemental

analysis was performed by Microanalytisch Labor Pascher, Germany.

Results and Discussion

Preparation conditions

Figure 1 shows XRD patterns of lamellar vanadyl benzylphosphate and after the insertion of Fe-complexes. Before insertion of Fe-complexes, the XRD pattern exhibited strong diffraction line attributable to the (001) at 2θ = 4.95 degree with a shoulder at 5.28 degree. Weak diffraction lines were also observed at 9.76 and 14.6 degree, which can be attributable to the (002) and the (003), representing lamellar structure of LVPO having the d(001) value of 1.78 nm [28]. Weak lines were also observed at 10.4 and 15.7 degree, representing contaminant lamella phase having the d(001) value of 1.67 nm. The previous section (4.1) showed a linear correlation between the d(001) value and molecular length of alcohol which corresponds to the distance between OH and farthest H. Molecular length of benzyl alcohol (0.709 nm) and the d(001) values (1.78 nm) also agree well with this correlation. Thus, benzyl alcohol existed in the interlayer space can be estimated as double layer tilting 56.6 degree against inorganic layer having thickness of 0.40 nm. A series of diffraction lines having the d(001) value of 1.67 nm indicates a minor phase. Since the molecular diameter of toluene (0.592 nm), which was used as a diluent of P_2O_5, is smaller than benzyl alcohol (0.709 nm), the minor phase could be lamella VPO phase incorporating toluene in the interlayer. After the insertion of Fe-complexes, the diffraction patterns of all the samples showed lamellar structure, while decrease in the interlayer distance was observed. The presence of minor lamellar phase was not significant. The d(001) values of each samples were listed in Table 1.

Table 1 also shows the Fe/V ratio of Fe-loaded LVPO. A part (17 % - 1.4 %) of Fe-complex was loaded in LVPO, though the Fe content was dependent on the preparation conditions in the sequence of A > B > C > D. The best condition for Fe-insertion was the use of $Fe(acac)_3$ as iron source and toluene as solvent. In the case of LVPO-Fe-A, the surface Fe/V ratio was only around twice as in the bulk, suggesting most of $Fe(acac)_3$ was inserted into LVPO bulk. The surface Fe/V ratio of other samples was 4 to 11 times higher than that in the bulk, suggesting higher concentration of Fe in the surface.

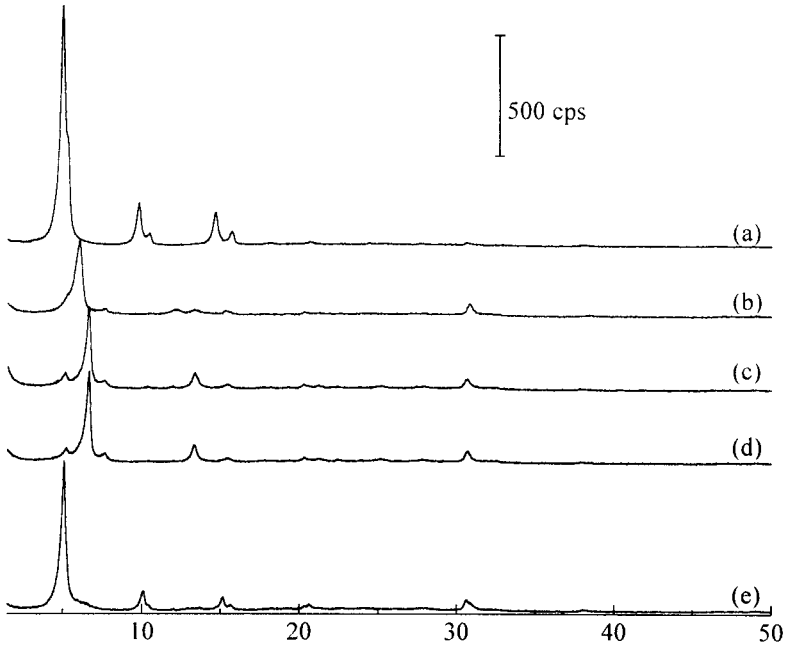

Fig. 1 XRD patterns of (a) parent LVPO, (b)LVPO-Fe-A, (c)LVPO-Fe-B, (d)LVPO-Fe-C, (e)LVPO-Fe-D

As a consequence, it was found that the insertion of Fe-complexes into lamellar VPO is possible without significant destruction of lamellar VPO structure. The use of toluene and $Fe(acac)_3$ was suggested to be the most suitable condition. In the next section, structure and Fe distribution of LVPO-Fe-A catalyst are characterized in detail.

Table 1 Preparation conditions, chemical compositions, and d(001) in parent LVPO and Fe-loaded LVPO

Sample	Prepration		Atom ratio in bulk					Fe/V	d(001) / nm
	Solvent	Fe source	P/V	C/V	O/V	H/V	Fe/V	in surface	
LVPO	-	-	0.94	8.56	5.44	10.4	< 0.001	< 0.01	1.78
LVPO-Fe-A	Toluene	$Fe(acac)_3$	1.01	5.71	5.69	7.19	0.084	0.18	1.46
LVPO-Fe-B	Toluene	ferrocene	0.99	5.34	5.46	6.73	0.023	0.09	1.33
LVPO-Fe-C	Benzyl alcohol	$Fe(acac)_3$	1.02	5.20	5.53	6.69	0.020	0.09	1.33
LVPO-Fe-D	Benzyl alcohol	ferrocene	0.98	8.40	5.74	9.77	0.007	0.08	1.74

Characterization of Fe-inserted lamellar VPO

Figure 2a shows SEM image of LVPO-Fe-A. The particles of LVPO-Fe-A were composed of plate-like crystallites. The size of crystallite was 1-3 μm in diameter and 50-100 nm in thickness. SEM images of parent LVPO and other Fe-loaded LVPO were almost the same in the shape of crystallites. Figure 2b shows TEM image of the side view of crystallites. The TEM image clearly indicates the lamellar structure of LVPO-Fe-A. From the patterns of lamella, the interlayer distance can be estimated as ca. 1.5 nm, which agrees well with the estimation from XRD patterns.

Fig 2 SEM image (left) and TEM image (right) of LVPO-Fe-A.

Figure 3 shows TEM image of LVPO-Fe-A and EDX images of V, P and Fe. The white points in the EDX images, which indicates the presence of the atoms, are agreed well with each other and TEM image. From these images, it is clear that those atoms are well dispersed, and there are no aggregates such as iron oxides.

Uniform distribution of Fe atoms was also supported by the comparison of bulk and surface composition. In the case of LVPO-Fe-A, Fe/V ratio was 0.084 in the bulk and 0.18 in the surface. If $Fe(acac)_3$ complex was only deposited on surface, the surface Fe/V ratio observed by XPS spectra was above 1.05, taking the escape depth of 3 nm and average particle size of 75 nm observed from

SEM images into account. However, the Fe/V ratio in surface was 10 times smaller (0.18) than the estimated value. This fact indicates that $Fe(acac)_3$ is mainly inserted into the interlayer of lamellar VPO. On the other samples, the surface Fe/V ratio was 4 to 11 times higher than that in bulk, suggesting Fe-complex is partly concentrated or aggregated in surface.

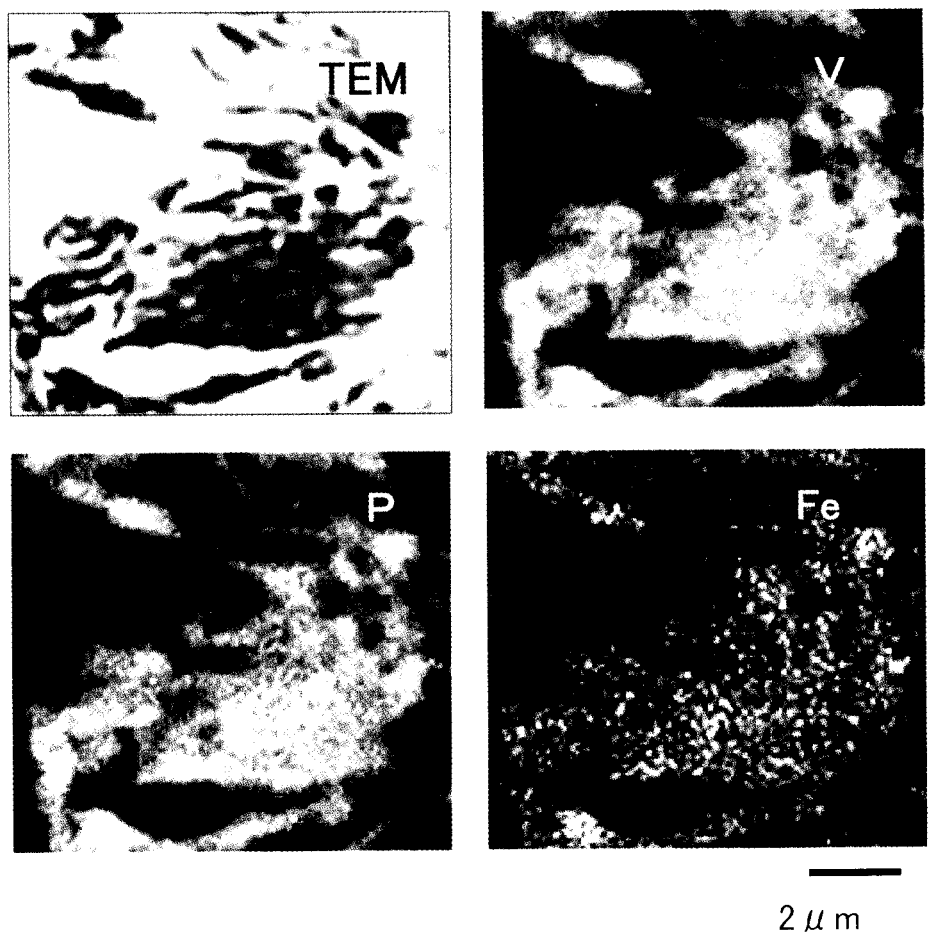

Fig. 3 TEM image of LVPO-Fe-A and EDS images of V, P and Fe.

Figure 4 shows FT/IR spectra of the parent LVPO and LVPO-Fe-A. LVPO shows the band at 695, 740, 975, 1045, 1085, 1160, 1185, 1395, 1456 and 1500 cm^{-1}. These bands can be tentatively assigned to ν(P-O-C) for 1160 cm^{-1}, ν(V=O) for 975 cm^{-1}, ν(PO_3) or Ph-O stretch for 1045, 1085, 1185 cm^{-1}, deformation mode of OH of benzyl alcohol for 1395, 1456 and 1500 cm^{-1}, respectively [30-32]. After the insertion of $Fe(acac)_3$, a small bands appeared at 1283,1368 and 1526 cm^{-1}, while the bands due to VPO layer (ν(V=O), ν(PO_3), ν(P-O-C)) was hardly affected. Spectrum c more clearly shows the difference in the spectrum a and b. The spectrum c was very close to the spectrum of $Fe(acac)_3$ and the bands newly observed at 936, 1283, 1368, 1526, and 1570 cm^{-1}. These bands were attributed to ν(C-C) + ν(C-O) for 936, 1283, 1526, and 1570 cm^{-1} and $\delta_s(CH_3)$ for 1368 cm^{-1}, respectively [33]. The presence of these bands attributable to $Fe(acac)_3$ suggests that the structure of $Fe(acac)_3$ is not significantly changed in the interlayer of LVPO.

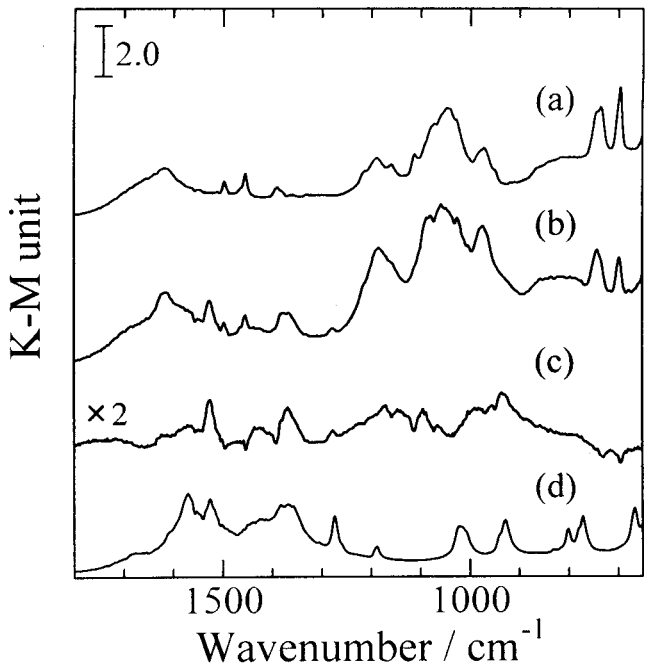

Fig. 4 FT/IR spectra of (a) parent LVPO, (b) LVPO-Fe-A, (c) (LVPO-Fe-A)/(LVPO) and (d) $Fe(acac)_3$.

From the chemical analysis shown in Table 1, P/V ratio of all the samples was around unity, and the samples are basically composed of ideal composition of V-P sheet. From the C/V ratio, 1.5 times of benzyl alcohol relative to vanadium or phosphorous are in the internal layer. It is already clarified that around a half of alcohol is settled in the layer by ester bond, and other by hydrogen bonded [28]. The TGA data of this LVPO material showed that the ratio in weak and strong bonded alcohol is around 2:1. According to these characters, the rational formula of the original LVPO-compound is $VO((C_7H_7OH)_{0.72}/H_{0.28})PO_4 \cdot 0.50C_7H_7OH$. On the other hand, the rational formula of LVPO-Fe-A is $VO((C_7H_7OH)_{0.45}/H_{0.55})PO_4 \cdot 0.18C_7H_7OH \cdot 0.08Fe(acac)_3$. After the insertion of $Fe(acac)_3$, the number of benzylalcohol reduced into a half. The fact indicates that $Fe(acac)_3$ was replaced with the internal alcohol. Actually, the loaded amount of Fe-complex was also almost equivalent to the removed alcohol in the case of LVPO-Fe-B and -C. The elimination of alcohol also can be rationalized by the decrease in the interlayer distance observed in XRD patters.

Conclusion

In the present section, a novel approach for the preparation of well-defined promoted VPO catalysts was demonstrated. It was fund that heating of lamellar vanadyl benzylphosphate in toluene with $Fe(acac)_3$ be successfully introduced the $Fe(acac)_3$ into the interlayer. Based on the results of various characterizations, the insertion of $Fe(acac)_3$ into lamellar vanadyl benzylphosphate can be depicted as shown in Figure 5, i.e., (1) internal benzyl alcohol was removed by the heating in toluene with $Fe(acac)_3$, (2) $Fe(acac)_3$ was replaced with benzyl alcohol, and (3) decrease in the internal distance occurred due to the elimination of benzyl alcohol. Further investigation on the structure of calcined VPO catalyst and catalytic profiles will be reported elsewhere.

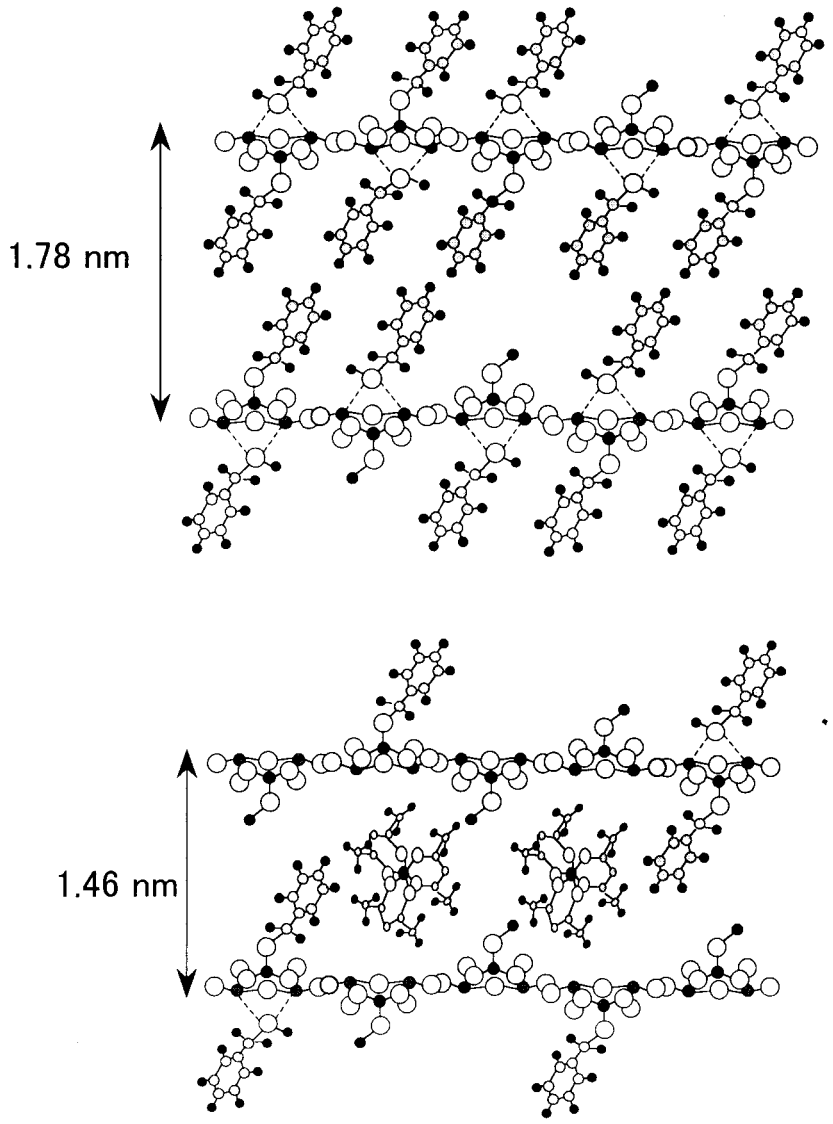

Fig. 5 Schematic model of LVPO before (a) and after (b) insertion of $Fe(acac)_3$.

References

[1] B. K. Hodnett, *Catal. Rev. Eng.*, **17** (1985) 373.

[2] E. Bordes, *Catal. Today*, **1** (1987) 499.

[3] G. Centi, F. Trifiro, J. R. Ebner, and V. M. Franchetti, *Chem. Rev.*, **88** (1988) 55.

[4] G. J. Hutchings, *Appl. Catal.*, **72** (1991) 1.

[5] F. Cavani, F. Trifiro, *Chemtech*, April (1994) 18.

[6] F. Cavani, F. Trifiro, "*Catalysis, Vol. 11*" p. 246, Royal Society of Chemistry, Cambridge (1994).

[7] B. K. Hodnett, "*Heterogeneous Catalytic Oxidation, Chapter 5*" p. 132, John Wiley & Sons, New Tork (2001).

[8] V. A. Zazhigalov, J. Haber, J. Stoch, I. V. Bacherikova, G. A. Komashko, A. I. Pyatnitskaya, *Appl. Catal. A*, **134** (1996) 225.

[9] Y. Takita, K. Tanaka, S. Ichimaru, Y. Mizuhara, Y. Abe, Y. Ishihara, *Appl. Catal. A*, **103** (1993) 281.

[10] H. S. Horowitz, C. M. Blackstone, A. W. Sleight, G. Teufer, *Appl. Catal.*, **38** (1988) 193.

[11] G. Busca, F. Cavani, G. Centi and F. Trifiro, *J. Catal.*, **99** (1986) 400.

[12] M. L. Granados, J. C. Conesa and M. F. Garcia, *J. Catal.*, **141** (1993) 671.

[13] D. Ye, A. Satsuma, A. Hattori, T. Hattori, Y. Murakami, *Catal. Today*, **16** (1993) 113.

[14] A. Satsuma, Y. Tanaka, T. Hattori, Y. Murakami, *Appl. Surf. Sci.*, **121/122** (1996) 496.

[15] A. Datta and R. Y. Kelar, *Chem. Commun.*, (1996) 89.

[16] K. Beneke and G. Lagaly, *Inorg. Chem.*, **22** (1983) 1503.

[17] G. Huan, A. J. Jacobson, J. W. Johnson, and D. P. Goshorn, *Chem. Mater.*, **4** (1992) 661.

[18] G. Huan, J. W. Johnson, J. F. Brody., D. P. Goshorn, and A. J. Jacobson, *Mater. Chem. Phys.*, **35** (1993) 199.

[19] V. V. Guliants, J. B. Benzinger, and S. Sundaresan, *Chem. Mater.*, **6** (1994) 353.

[20] V. V. Guliants, J. B. Benzinger, and S. Sundaresan, *Chem. Mater.*, 7 (1995) 1493.

[21] J. B. Benziger, V. Guliants, S. Sundaresam, *Catal. Today*, **33** (1997) 49.

[22] T. Doi, T. Miyake, *Chem. Commun.*, (1996) 1635.

[23] E. M. Sabbar, M. E. de Roy, A. Ennaqadi, C. Gueho, and J. P. Besse, *Chem. Mater.*, **10** (1998) 3856.

[24] T. Nakato, Y. Furumi, T. Okuhara, *Chem. Lett.*, (1998) 611.

[25] T. Nakato, Y. Furumi, N. Terao, T. Okuhara, *J. Mater. Cheem.*, **10** (2000) 737.

[26] J. W. Johnson, A. J. Jacobson, W. M. Butler, S.E. Rosenthatl, J. F. Brody, and J. T. Lewandowski, *J. Am. Chem. Soc.*, **111** (1989) 381.

[27] H. S. Horowitz, *WO Patent* 98/15353 (1998).

[28] Y. Kamiya, E. Nishikawa, *Japan Kokai*, 11-319860 (1999).

[29] Y. Kamiya, E. Nishikawa, A. Satsuma, and T. Okuhara, *Bull. Chem. Soc. Jpn.*, (in press).

[30] C. J. Pouchert, "*The Aldrich Library of Infrared Spectra (2nd Edition)*" Aldrich Chemical Company, Milwaukee, (1975).

[31] L. J. Bellamy, "*The Infra-red Spectra of Complex Molecules*", Chapman and Hall, London, (1975), p. 353.

[32] G. Busca, F. Cavani, G. Centi and F. Trifiro, *J. Catal.*, **99** (1986) 400.

[33] K. Nakamoto, "*Infrared and Raman Spectra of Inorganic and Coordination Compounds (4th Edition)*", Wiley Interscience, New Yoak, (1986), p. 260.

4.3 Catalytic property of iron-doped $(VO)_2P_2O_7$ catalyst prepared by intercalation of $Fe(acac)_3$

Abstract

Intercalation of $Fe(acac)_3$ into lamellar vanadyl *n*-hexylphosphate, $VO\{(n\text{-}C_6H_{13})_{0.6}/H_{0.4}\}PO_4{\cdot}(n\text{-}C_6H_{13}OH)_{0.5}$, followed by calcination, has been investigated for preparation of Fe-doped $(VO)_2P_2O_7$ catalyst and selective oxidation of *n*-butane to maleic anhydride was performed. $Fe(acac)_3$ was successfully intercalated into the vanadyl *n*-hexylphosphate by heating in toluene. The obtained precursor was transformed to single phase of $(VO)_2P_2O_7$ by a calcination at 823 K in the presence of a mixture of 5 % *n*-butane and 20 % O_2 in N_2 (balance). The doped Fe ions uniformly spread in the bulk of the catalyst and were substituted for V^{4+} in $(VO)_2P_2O_7$ crystal. The catalytic activity for maleic anhydride formation per surface area on the Fe-doped catalyst was higher than that on the Fe-free catalyst prepared by calcination of the vanadyl *n*-hexylphosphate. Rates of reduction with *n*-butane at a top few surface layers of the catalysts and re-oxidation with air were estimated from weight decrease and increase detected on TG/DAT apparatus. The Fe-dope catalysts gave high rates of both the reduction and re-oxidation, especially re-oxidation. It was confirmed from XPS that the surface of the Fe-doped catalysts is in a higher oxidation state under the steady state of the reaction. In addition, the Fe-doped catalysts showed a smaller reaction order on partial pressure of O_2. Therefore, it is concluded that the doped Fe can enhance the redox ability, especially re-oxidation of the catalyst, resulting in the high catalytic performance.

Introduction

Vanadyl pyrophosphate, $(VO)_2P_2O_7$, has been recognized as an active and selective phase for selective oxidation of *n*-butane to maleic anhydride (abbreviated as MA) [1-4]. Addition of wide variety of promoters to the catalysts, such as Co, Mo, Cr, Fe, Ce, Zn, Ti, Zr, Si and so on, has been attempted to improve catalytic performance [5-7]. Among them, Fe is known to be one of the elements enhancing the catalytic performance [8-10] and contained in many industrial $(VO)_2P_2O_7$ catalysts [9,11,12].

$(VO)_2P_2O_7$ consists of edge-shared VO_6 octahedras, which are V-O-V pair sites, linked with

pyrophosphates (P_2O_7) [13]. The specificity of $(VO)_2P_2O_7$ for the selective oxidation of *n*-butane has been claimed to be due to this characteristic structure, because some vanadyl phosphates which do not have the V-O-V pair sites, e.g., α-$VOPO_4$ and β-$VOPO_4$, are non-selective for this reaction [14]. Therefore, retaining the characteristic structure of $(VO)_2P_2O_7$ must be required, when promoter is added to the catalyst. Besides that, the promoters added on the catalyst have possibility to form undesirable site such as aggregated metal oxides, on which combustion of *n*-butane proceeds. Thus, it is desired to develop more advanced method that can finely control introductions of the promoters.

It has been paid much attention on a series of vanadium phosphorus oxides, because of their structural diversity and unique catalytic property. So far, there are many reports about synthesis of various vanadium phosphorus oxides having novel structures, such as intercalation compounds [15,16], lamellar compounds [17-20], mesostructured materials [21,22], and thin-layered compounds [23,24]. Vanadyl alkylphosphonates and vanadyl alkylphosphates are lamellar compounds consisting of alternating basal V-P-O layers and organic groups.

In Chapter 4.1, a synthetic method of vanadyl alkylphosphates, $VO(R_x/H_{1-x})PO_4 \cdot (ROH)_y$, where R is straight-, branched-alkyl, alicyclic and aliphatic groups was developed. In the series of these vanadyl alkylphosphates, an existence of the V-O-V pair sites was confirmed. The vanadyl alkylphosphates are transformed into $(VO)_2P_2O_7$ by calcination, and the obtained catalysts exhibit good selectivity for the selective oxidation of *n*-butane. Since these vanadyl alkylphosphates possess weakly held alcohols (ROH) in their interlayer, it is expected that these materials can be used as host for modification of their interlayer space by using metal-complexes. After intercalation of metal-complex followed by calcination, the promoter may be fixed in the catalyst bulk uniformly. In Chapter 4.2, the author found that iron-complex, such as $Fe(acac)_3$ and ferrocene, was successfully intercalated into interlayer of vanadyl benzylphosphate by heating in toluene.

In this Chapter, the author applied this method for intercalation of $Fe(acac)_3$ into vanadyl *n*-hexylphosphate, followed by calcination. The obtained catalysts were characterized by means of XRD, IR, XPS and elemental analysis. The catalytic performance for the selective oxidation of *n*-butane was examined with a wide range of concentrations of *n*-butane (from 1.5 to 5.0 %) and O_2 (from 10 to 30 %) and their redox properties were measured by uptake of O_2 and by reduction with *n*-butane. A role of the Fe will be discussed in relation to redox property, comparing with the Fe-free $(VO)_2P_2O_7$ catalyst obtained by calcination of the vanadyl *n*-hexylphosphate.

Experimental

Preparation of Fe-doped catalysts by intercalation of $Fe(acac)_3$

Vanadyl *n*-hexylphosphate was prepared as described in Chapter 4.1. V_2O_5 (29.2 g, Kishida Chemical Co., Ltd.) was reduced in a mixture of isobutyl alcohol (180 cm^3, Kishida Chemical Co., Ltd.) and benzyl alcohol (120 cm^3, Kishida Chemical Co., Ltd.) at refluxing temperature for 3 h. The obtained black solid was separated by filtration. The solid (about 20 g) was added to 1-hexanol (300 cm^3, Kishida Chemical Co., Ltd.), and then a mixture of P_2O_5 (29.6 g, Kishida Chemical Co., Ltd.) and toluene (75 cm^3, Kishida Chemical Co., Ltd.) was slowly added to the suspension with stirring at room temperature. The mixture was then refluxed for 3 h. The resultant light-blue solid was filtered, washed with acetone (250 cm^3, Kishida Chemical Co., Ltd.), and dried at room temperature for 12 h. Elemental analysis, IR, TG-DTA, and magnetic susceptibility reveal that the obtained solid was $VO\{(n\text{-}C_6H_{13})_{0.6}/H_{0.4}\}PO_4\cdot(n\text{-}C_6H_{13}OH)_{0.5}$ (abbreviated as VHexP).

Powder of $Fe(acac)_3$ (Kishida Chemical Co., Ltd.) was dissolved in 36 cm^3 of toluene at room temperature. $Fe(acac)_3$ was loaded as molar ratio of $Fe(acac)_3$/VHexP=0.1 or 0.5. VHexP (4.0 g) was added to the solution at room temperature and then heated with stirring at 358 K for 3 h. Then, the solid was filtered, washed with acetone (40 cm^3), and dried at room temperature for 12 h. Hereafter, these precursors obtained from the loading ration of $Fe(acac)_3$/VHexP=0.1 and 0.5 are denoted to Fe(0.1)-VHexP and Fe(0.5)-VHexP, respectively.

These precursors were calcined in a flow of a mixture of *n*-butane 5 %, O_2 20% and N_2 75% (100 cm^3 min^{-1}) at 823 K for 12 h. The catalysts obtained from VHexP, Fe(0.1)-VHexP and Fe(0.5)-VHexP are denoted to VHexP-VPO, Fe(0.1)-VPO, and Fe(0.5)-VPO, respectively.

Characterization

Powder XRD patterns were recorded on an X-ray diffractometer (Rigaku RINT-1200) with Cu K_α radiation (λ=0.154 nm). Infrared spectra were obtained with an IR spectrometer (JASCO FTIR-470/Plus) using a pressed disk made from a mixture of the sample powder and KBr. Elemental analysis of the compounds was performed with a Mikroanalytisches Labor Pascher (Germany). Surface area of the catalyst was estimated by a BET method using adsorption isotherm of N_2 at 77 K measured with BELSORP 28 SA (BEL Japan Inc.), after the sample was evacuated at 473 K for 2 h.

X-ray photoelectron spectra (XPS) were recorded using a Surface Science Instruments S-Probe

ESCA Model 2803 with Al K_α radiation. Prior to the measurements, 100 mg of the catalyst powder after the reaction was aged in a flow of a mixture of 5 % *n*-butane, 20 % O_2 and 75 % N_2 (20 cm^3 min^{-1} of total flow rate) at 723 K for 2 h. After the pretreatment, the catalyst powder was cooled to room temperature in N_2 flow (20 cm^3 min^{-1}) within 1 min. All spectra were referenced to the carbon 1s peak at a binding energy of 285.0 eV.

Time-profiles of reduction and re-oxidation

Time-profiles of reduction of the catalyst with *n*-butane and re-oxidation with air were measured by using a Seiko Instrument TG/DTA-6300. The level of the reduction and oxidation were monitored by the weight decrease in a flow of 5 % *n*-butane (N_2 balance) and the weight increase in a flow of air, respectively. The catalyst sample was pretreated in the same way of the XPS measurement. The pretreated sample (ca. 10 mg) was set on a sample holder in the TG/DTA apparatus. The temperature of the sample was then rose in a N_2 flow (50 cm^3 min^{-1}) to 723 K at a rate of 10 K min^{-1} and was held there. After further decrease in the weight was not detected at 723 K, the feed gas was changed to 5 % *n*-butane (N_2 balance, 50 cm^3 min^{-1} of total flow rate) to obtain the time-profile of reduction.

For a measurement of re-oxidation profile, another part of the pretreated sample was used. After further decrease in the weight was not detected in a N_2 flow at 723 K, the feed gas was changed to air (50 cm^3 min^{-1}) to obtain the time-profile of re-oxidation.

Catalytic oxidation of n-butane

Catalytic oxidation of *n*-butane was carried out in a conventional fixed-bed flow reactor of Pyrex tubing (inside diameter of 6 mm) under atmospheric pressure. A mixture of *n*-butane and O_2 (N_2 balance) at a total flow rate of 20 cm^3 min^{-1} was fed over the catalyst bed at 723 K. The concentrations were varied from 1.5 % to 5.0 % for *n*-butane and from 10 % to 30 % for O_2, respectively. The conversion of *n*-butane was adjusted in the range of 10 - 15 % by changing of the catalyst weight under the constant total flow rate in order to estimate the reaction rate under differential conditions. The flow rates were controlled by thermal mass flow controllers (STEC SEC-310). The products were analyzed with on-line gas chromatographs (FID (Shimadzu 14A, Shimadzu 9A) and TCD (Shimadzu 9A)) equipped with a Porapak QS column (inside diameter 2.2

mm, length 1 m) for *n*-butane and MA, and a Porapak N column (inside diameter 2.2 mm, length 2 m) for CO_2. A Molecular Sieve 13X column (inside diameter 2.2 mm, length 4 m) was also used to separate O_2, N_2 and CO. CO and CO_2 were converted to methane by using a Methanizer (Shimadzu MTN-1) to be detected more sensitively by the FID-GC. Prior to the reaction, the catalysts were aged in the reaction mixture at 723 K for 5 h.

Results

Intercalation of $Fe(acac)_3$ into lamellar vanadyl n-hexylphosphate

Figure 1 shows XRD patterns of untreated VHexP and the compounds treated with $Fe(acac)_3$. The VHexP gave strong diffraction line attributed to the (001) of lamellar structure at $2\theta = 4.70°$, indicating 1.88 nm of the $d(001)$ value [25,26]. High order diffraction lines at $2\theta = 9.16°$ and 13.62° attributed to the (002) and (003) were also observed [25,26]. After the treatment with $Fe(acac)_3$, Fe(0.1)-VHexP and Fe(0.5)-VHexP gave the XRD patterns of lamellar structure as VHexP, while the (001) diffraction lines were shifted to higher angle at $2\theta = 5.40°$ for Fe(0.1)-VHexP and 5.32° for Fe(0.5)-VHexP, which indicate decrease in the $d(001)$ value to 1.63 nm and 1.66 nm, respectively.

Table 1 lists the P/V and Fe/V ratios of VHexP and the compounds treated with $Fe(acac)_3$. The bulk P/V ratios of these compounds were nearly unity. The bulk Fe/V ratios were 0.04 for Fe(0.1)-VHexP and 0.08 for Fe(0.5)-VHexP, respectively. The bulk Fe/V ratio increased as the loading ratio increased, but that was significantly small in comparison with the loading ratio. The surface Fe/V ratio was the same as the bulk one within an experimental error.

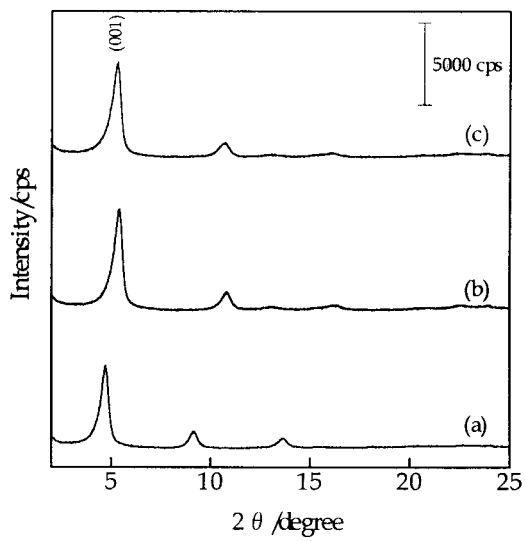

Fig. 1 XRD patterns of precursors. (a) VHexP, (b) Fe(0.1)-VHexP and (c) Fe(0.5)-VHexP.

Table 1 Bulk and surface composition of the precursors.

Precursor	P/V ratio	Fe/V ratio	
	Bulk[a]	Bulk[a]	Surface[b]
VHexP	1.02	0.00	0.00
Fe(0.1)-VHexP	1.03	0.04	0.05
Fe(0.5)-VHexP	1.02	0.08	0.08

[a] Determined by ICP-AES.
[b] Determined by XPS.

Microstructure of catalyst

Table 2 lists compositions and surface area of the catalysts. The bulk P/V ratios were about unity. The bulk Fe/V ratios of the catalysts were almost the same as the Fe/V ratios of the precursors listed in Table 1. The surface Fe/V ratio was the same as the bulk one. The surface areas of the catalysts were determined to be 2.9, 1.7, and 0.8 $m^2 g^{-1}$ for VHexP-VPO, Fe(0.1)-VPO, and Fe(0.5)-VPO, respectively.

Table 2 Composition and surface area of the catalysts.

Catalyst	P/V ratio	Fe/V ratio		Surface area[c]
	Bulk[a]	Bulk[a]	Surface[b]	($m^2 g^{-1}$)
VHexP-VPO	1.01	0.00	0.00	2.9
Fe(0.1)-VPO	1.05	0.05	0.05	1.7
Fe(0.5)-VPO	1.04	0.08	0.08	0.8

[a] Determined by ICP-AES.
[b] Determined by XPS.
[c] Surface area after the selective oxidation of *n*-butane.

The XRD patterns of the catalysts after the calcination are shown in Fig. 2. The XRD patterns of these catalysts basically showed that of $(VO)_2P_2O_7$ [2] and other diffraction lines were not observed. The three catalysts gave almost the same relative intensities of the diffraction lines. VHexP-VPO (Fig. 2a) gave almost the same angles of diffraction lines observed in a pure $(VO)_2P_2O_7$ reported in the literature [2]. The 2θ angles were sifted to low-angle direction with increasing of the Fe/V ratio, indicating some changes of lattice spacing. To estimate the lattice spacing precisely, the 2θ angles of the (200), (024) and (032) diffraction lines were measured with a step scan mode using Si powder as a internal standard. The results are listed in Table 3. The lattice spacing of the (200) for VHexP-VPO was 0.3867 nm. Those for the Fe-doped catalysts were larger by ca. 0.0010 nm than that for VHexP-VPO, being 0.3877 nm for Fe(0.1)-VPO and 0.3879 nm for Fe(0.5)-VPO, respectively. The

lattice spacings of the (024) and (032) for the Fe-doped catalysts were also larger than those for VHexP-VPO.

Figure 3 presents infrared spectra of the catalysts. These catalysts gave bands approximately at 634 cm^{-1} ($\delta(PO_3)$), 745 cm^{-1} (ν(P-O-P)), 797 cm^{-1} (ν(V-O=V)), 940 cm^{-1} (ν(P-OH)) 1002 cm^{-1} (ν(V=O)), 1070 cm^{-1} ($\nu(PO_3)$), and 1110 – 1280 cm^{-1} ($\nu(PO_3)$) [29]. In the case of Fe(0.1)-VPO and Fe(0.5)-VPO, the band at 1002 cm^{-1} for ν(V=O) was weakened.

Table 3 The 2θ angles of the (200), (024) and (032) diffraction lines of the Fe-doped $(VO)_2P_2O_7$ catalysts[a].

Catalyst	2θ angle (deg.)			Lattice spacing (nm)		
	(200)	(024)	(032)	(200)	(024)	(032)
VHexP-VPO	23.00	28.51	30.01	0.3867	0.3131	0.2978
Fe(0.1)-VPO	22.94	28.48	29.95	0.3877	0.3134	0.2984
Fe(0.5)-VPO	22.93	28.46	29.94	0.3879	0.3137	0.2985

[a] The 2θ angles of diffraction lines were measured with Cu Kα radiation (λ=0.1542 nm) by a step scan mode using Si powder as a internal standard.

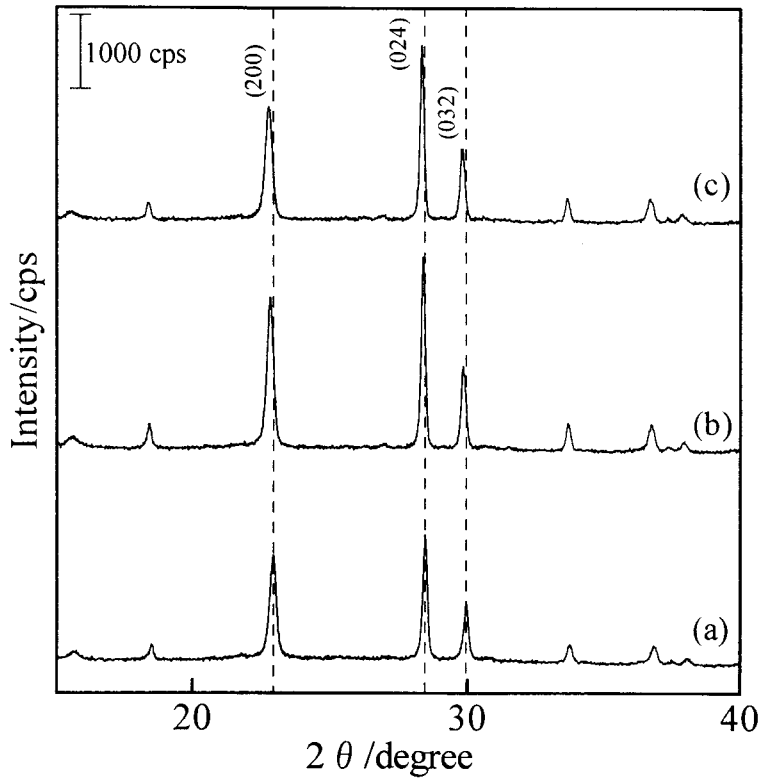

Fig. 2 XRD patterns of catalysts after the calcination at 823 K under 5 % *n*-butane and 20 % O_2 in N_2 balance for 12 h. (a) VHexP-VPO, (b) Fe(0.1)-VPO and (c) Fe(0.5)-VPO.

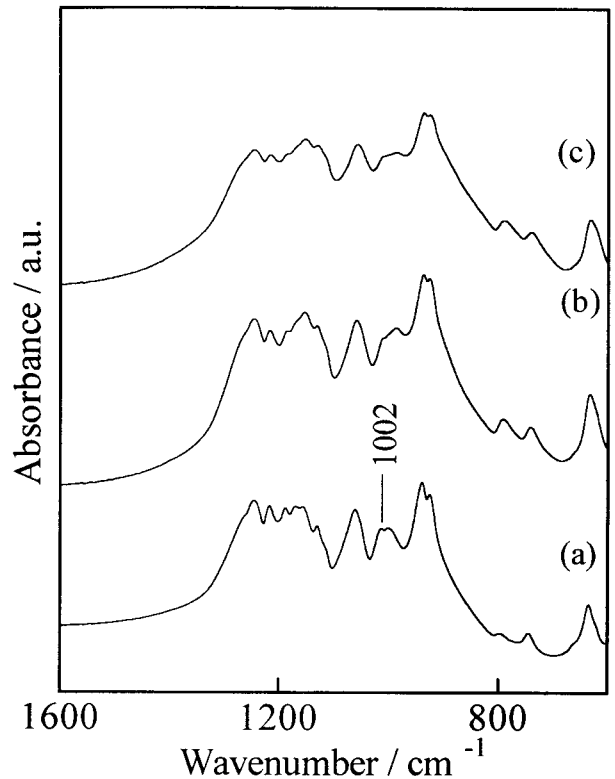

Fig. 3 IR spectra of catalysts after the calcination. (a) VHexP-VPO, (b) Fe(0.1)-VPO and (c) Fe(0.5)-VPO.

Figure 4 provides the XPS spectra of the catalyst, where $V(2p_{1/2})$, $V(2p_{3/2})$, $Fe(2p_{1/2})$, and $Fe(2p_{3/2})$ peaks are observed. For VHexP-VPO, the peak of $V(2p_{3/2})$ was observed at 517.5 eV, while the peaks of Fe(0.1)-VPO and Fe(0.5)-VPO were shifted to 517.9 eV which was as 0.4 eV high as that of VHexP-VPO. The $Fe(2p_{3/2})$ peaks are observed at 713.1 eV for the Fe-doped catalysts and the peak intensity increased in proportion to the Fe/V ratio.

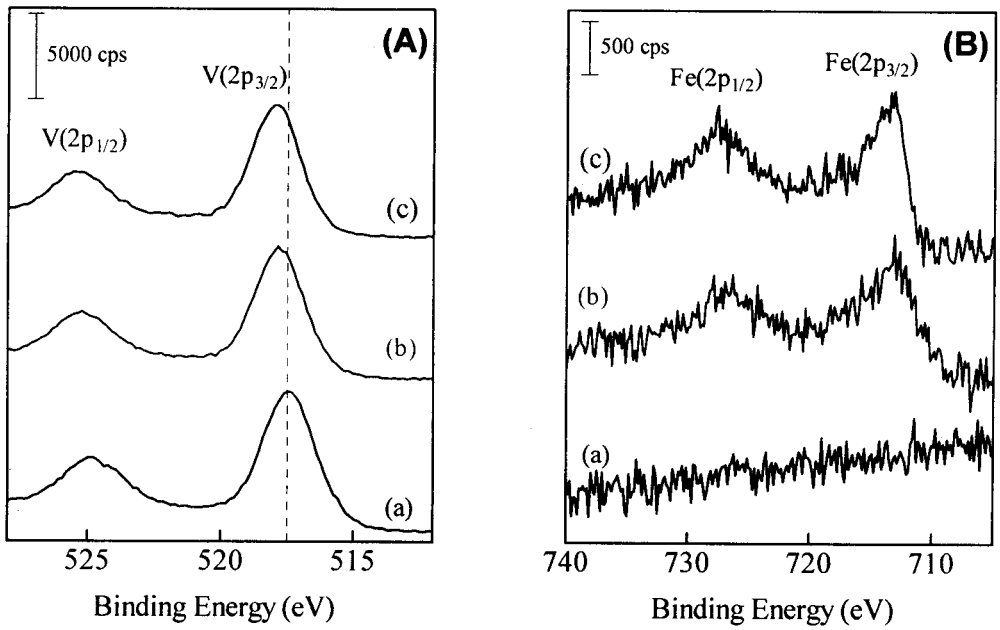

Fig. 4 X-ray photoelectron spectra of catalysts after the reaction. Part A (left), vanadium; Part B (right), iron. Before measurements, the catalysts were pretreated under 5.0 % *n*-butane and 20 % O_2 in N_2 balance at 723 K for 2 h. (a) VHexP-VPO, (b) Fe(0.1)-VPO and (c) Fe(0.5)-VPO.

Rates of reduction and re-oxidation

Fig. 5 provides the time-profile of reduction with *n*-butane and re-oxidation with air at 723 K. In the time profile of reduction (Fig. 5A), level of the reduction was expressed as an amount of oxygen abstracted from the catalyst. Amounts of abstracted oxygen ($Amount_{abstract}$) and oxygen uptake ($Amount_{uptake}$) were estimated from Eq. (1), in which these amounts were expressed per surface area.

$$Amount_{abstract} \text{ or } Amount_{uptake} = \frac{W_t - W_0}{16 \times W_0 \times SA} \qquad (1)$$

Where W_0 (g) and W_t (g) represent the catalyst weight at first and a certain time, respectively, and SA ($m^2\ g^{-1}$) is a surface area.

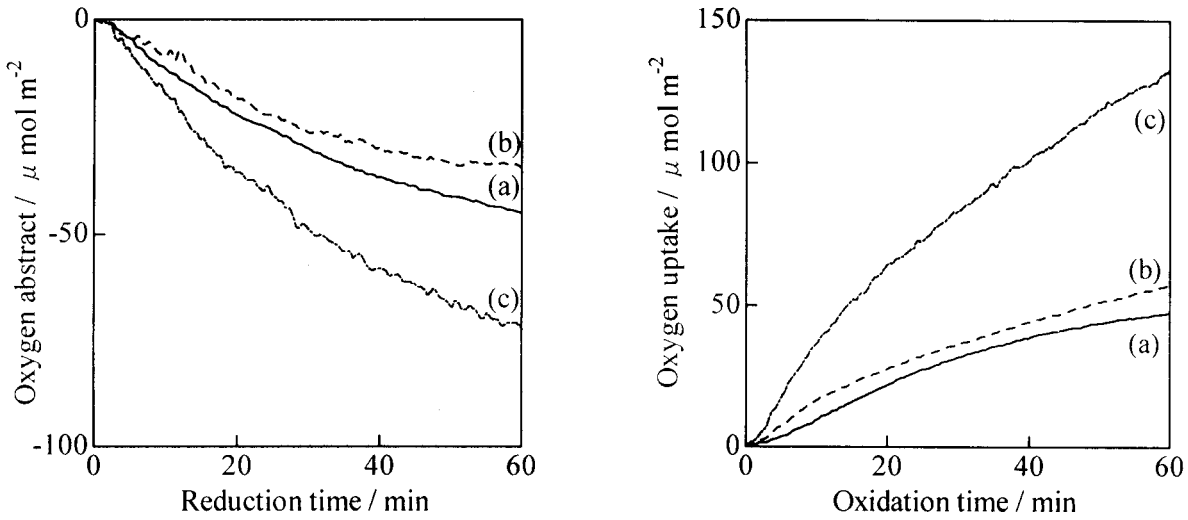

Fig. 5 Time-profile of reduction with 5.0 % *n*-butane (A) and re-oxidation with air (B) at 723 K. Prior to the measurements, the catalysts were pretreated under 5.0 % *n*-butane and 20 % O_2 in N_2 balance at 723 K for 2 h. The amount of abstracted oxygen or oxygen uptake were calculated from the weight decrease or increase monitored by TG/DTA apparatus. (a) VHexP-VPO, (b) Fe(0.1)-VPO and (c) Fe(0.5)-VPO.

It is generally accepted that the selective oxidation of *n*-butane over $(VO)_2P_2O_7$ catalyst proceeds via a redox cycle between V^{4+} and V^{5+} [30,31]. Pepera et al. reported that the number of surface layers involved in the redox processes during the oxidation of *n*-butane is about unity [30]. In addition, Okuhara et al. showed that the diffusion of oxygen atoms is limited to a few layers of $(VO)_2P_2O_7$ during the reaction [32]. Therefore, it can be considered that Fig. 5 shows the

time-profiles of reduction and re-oxidation at a top few surface layers of the catalyst.

As shown in Fig. 5A, VHexP-VPO and Fe(0.1)-VPO gave nearly same reduction profiles, while it was observed that Fe(0.5)-VPO was reduced faster and deeper than VHexP-VPO and Fe(0.1)-VPO. The initial reduction rates of the catalysts estimated from the slope of the curve within 10 min are summarized in Table 4. The order of the initial reduction rates was Fe(0.1)-VPO (59 μmol m^{-2} h^{-1}) < VHexP-VPO (68 μmol m^{-2} h^{-1}) < Fe(0.5)-VPO (100 μmol m^{-2} h^{-1}). The reduction rate of Fe(0.5)-VPO was about 1.5 times faster than that of VHexP-VPO.

The re-oxidation rate increased with increasing of the Fe/V ratio as shown in Fig 5B. The initial re-oxidation rates estimated from the slope of the curve within 10 min are summarized in Table 4. The initial re-oxidation rates were 62, 92, and 269 μmol·m^{-2}·h^{-1} for VhexP-VPO, Fe(0.1)-VPO, and Fe(0.5)-VPO, respectively. The ratio of initial re-oxidation rate to reduction rate listed in Table 4 was in the order: VHexP-VPO (0.9) < Fe(0.1)-VPO (1.6) < Fe(0.5)-VPO (2.7).

Table 4 Initial rates of reduction and re-oxidation of the catalysts[a].

Catalyst	Rate (μmol m^2 h^{-1})		Ratio of re-oxidation/reduction
	reduction	re-oxidation	
VHexP-VPO	68	62	0.9
Fe(0.1)-VPO	59	92	1.6
Fe(0.5)-VPO	100	269	2.7

[a] The rate were estimated from the slop of the curve within 10 min on the re-oxidation or reduction profile.

Catalytic oxidation of n-butane

Time courses of the conversion and selectivity over Fe(0.5)-VPO are given in Fig. 6. At the initial stage of the reaction, the conversion gradually decreased with time for 5.0 % *n*-butane and was nearly constant for 1.5 % *n*-butane. The selectivity increased with time for both 1.5 % and 5.0 % *n*-butane. After 5 h, both the conversion and selectivity reached nearly stationary values for both reaction conditions. Since the other catalysts gave similar time courses, the reaction rate and selectivity were estimated from the data collected after 5 h.

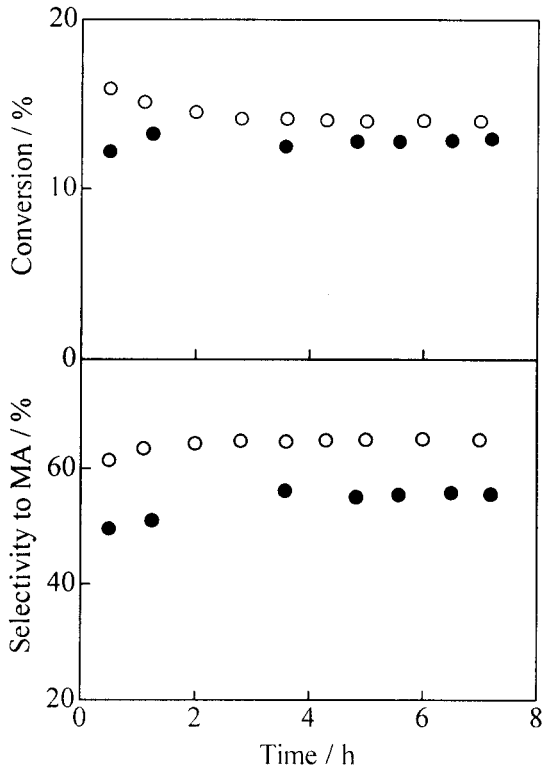

Fig. 6 Changes of the conversion and selectivity to maleic anhydride in the oxidation of *n*-butane over Fe(0.5)-VPO at 723 K with 20 % O_2. Concentrations of *n*-butane were (●) 1.5 % and (○) 5.0 %, respectively.

The dependencies for the rates of MA or CO_x ($CO+CO_2$) formation on the concentration of *n*-butane are given Fig. 7, where the concentration of O_2 is 20 %. The rates are expressed per unit surface area. Since the rate was estimated from the data that the conversion of *n*-butane was in the range of 10 – 15 %, consecutive oxidation of MA would be negligible [33,34]. The rates of MA and CO_x formations for Fe(0.1)-VPO and Fe(0.5)-VPO were larger than that of VHexP-VPO, and these rates increased with increasing of the Fe/V ratio. The reaction orders for MA and CO_x formation estimated from the slopes in Fig 7B are listed in Table 5. The reaction orders for MA formation (*n* of $P^{n}_{n\text{-butane}}$ = 0.4) was unchanged by the addition of Fe. On the other hand, the addition caused the decrease of the reaction order for CO_x formation on the concentrations of *n*-butane from (*p* of $P^{p}_{n\text{-butane}}$ =) 0.3 to 0.1.

Table 5 Reaction orders for MA and CO_x formation on the catalysts[a].

Catalyst	$r_{MA}=kP^{n}_{n\text{-butane}}P^{m}_{O2}$			$r_{COx}=k'P^{p}_{n\text{-butane}}P^{q}_{O2}$		
	k[a]	n	m	k'[a]	p	q
VHexP-VPO	550	0.4	0.2	297	0.3	0.3
Fe(0.1)-VPO	612	0.4	0.1	227	0.1	0.5
Fe(0.5)-VPO	725	0.4	0.1	463	0.1	0.6

[a] $\mu mol \cdot m^{-2} \cdot h^{-1}$

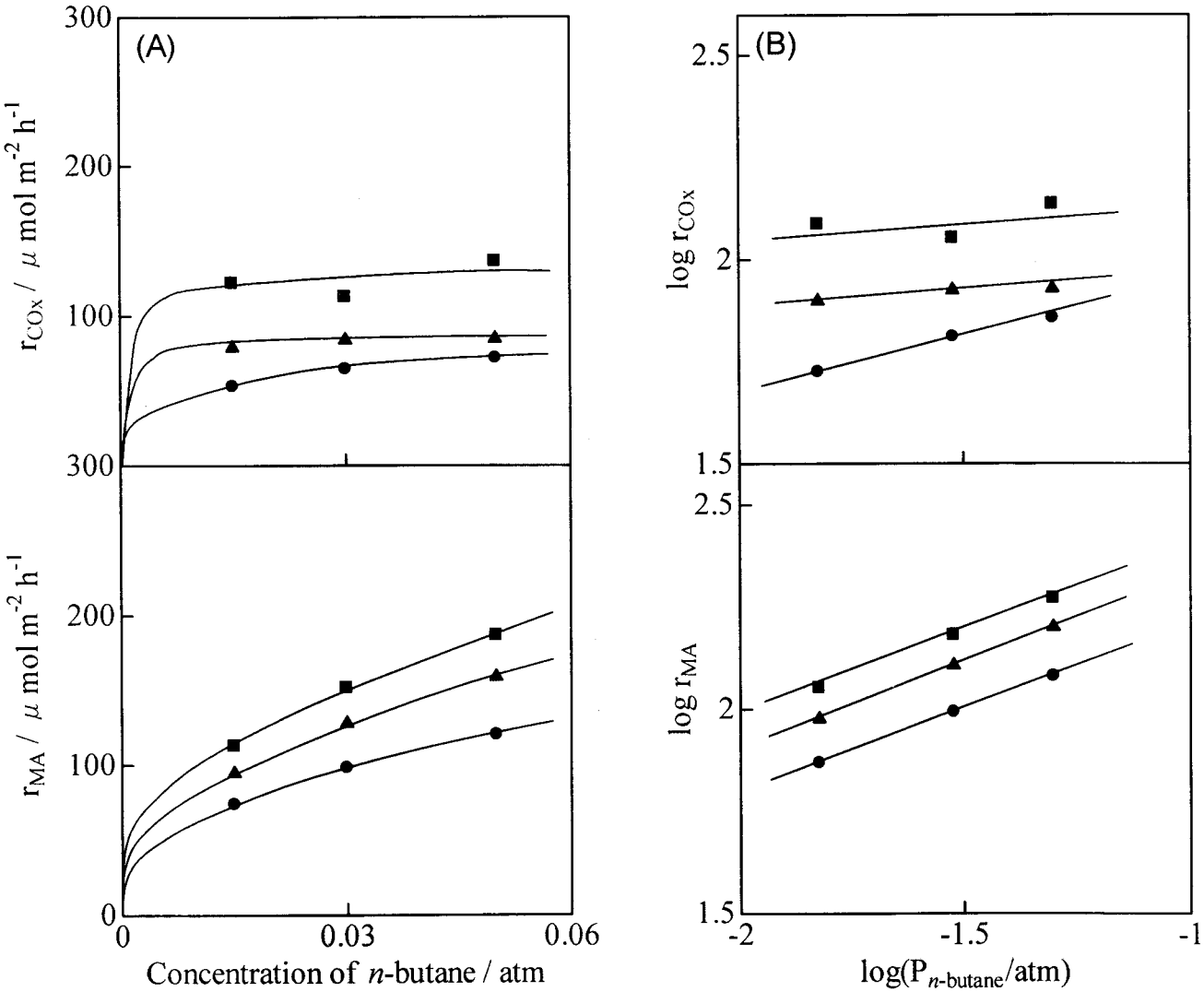

Fig. 7 Dependencies of rates for maleic anhydride and CO_x formation on concentration of *n*-butane. The concentration of O_2 is 20 % and the reaction temperature is 723 K. r_{MA} and r_{COx} represent rate for maleic anhydride and CO_x formation, respectively: (●) VHexP-VPO, (▲) Fe(0.1)-VPO and (■) Fe(0.5)-VPO.

Fig. 8 shows the dependence of the rates on the concentration of O_2, where the concentration of *n*-butane was 1.5 %. The rates of MA formation for Fe(0.1)-VPO and Fe(0.5)-VPO were larger than that for VHexP-VPO. The reaction order for MA formation listed in Table 5 was decreased with the addition of Fe, being (*m* of P^m_{O2} =) 0.3, 0.1 and 0.1 on VHexP-VPO, Fe(0.1)-VPO and Fe(0.5)-VPO, respectively. On the other hand, the reaction order for CO_x formation greatly increased with the addition of Fe as (*q* of P^q_{O2} =) 0.3, 0.5 and 0.6 on VHexP-VPO, Fe(0.1)-VPO and Fe(0.5)-VPO, respectively.

Figure 9 gives the dependence of the selectivity to MA on the concentrations of *n*-butane and O_2. The selectivity on VHexP-VPO scarcely varied with changes of *n*-butane and O_2 concentrations. On the contrary, the selectivity on the Fe-doped catalyst showed great dependence on these concentrations. The selectivity at 1.5 % *n*-butane was in the order: Fe(0.5)-VPO < Fe(0.1)-VPO < VHexP-VPO. The selectivity increased greatly on the Fe-doped catalyst as concentration of *n*-butane increased, because the rates for CO_x formation on the catalysts was almost independent of *n*-butane concentration, while those for MA formation increased (Fig. 7). Consequently, the order of the selectivity with 5.0 % *n*-butane was counterchanged to Fe(0.5)-VPO < VHexP-VPO < Fe(0.1)-VPO. At low O_2 concentration (10 %), Fe(0.1)-VPO showed highest selectivity among these catalysts. Fe(0.5)-VPO gave lowest selectivity to MA under the all experimental concentrations.

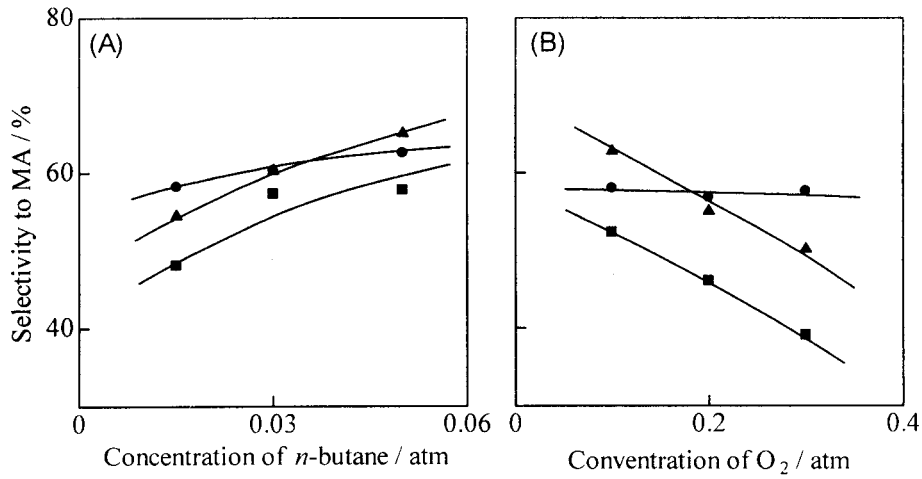

Fig. 9 Influences of selectivity to maleic anhydride on concentrations of (A) *n*-butane and (B) O_2. The reaction temperature is 723 K. The concentration of O_2 and *n*-butane are 20 % for dependence on *n*-butane (left) and 1.5 % for dependence on O_2 (right), respectively. (●) VHexP-VPO, (▲) Fe(0.1)-VPO and (■) Fe(0.5)-VPO.

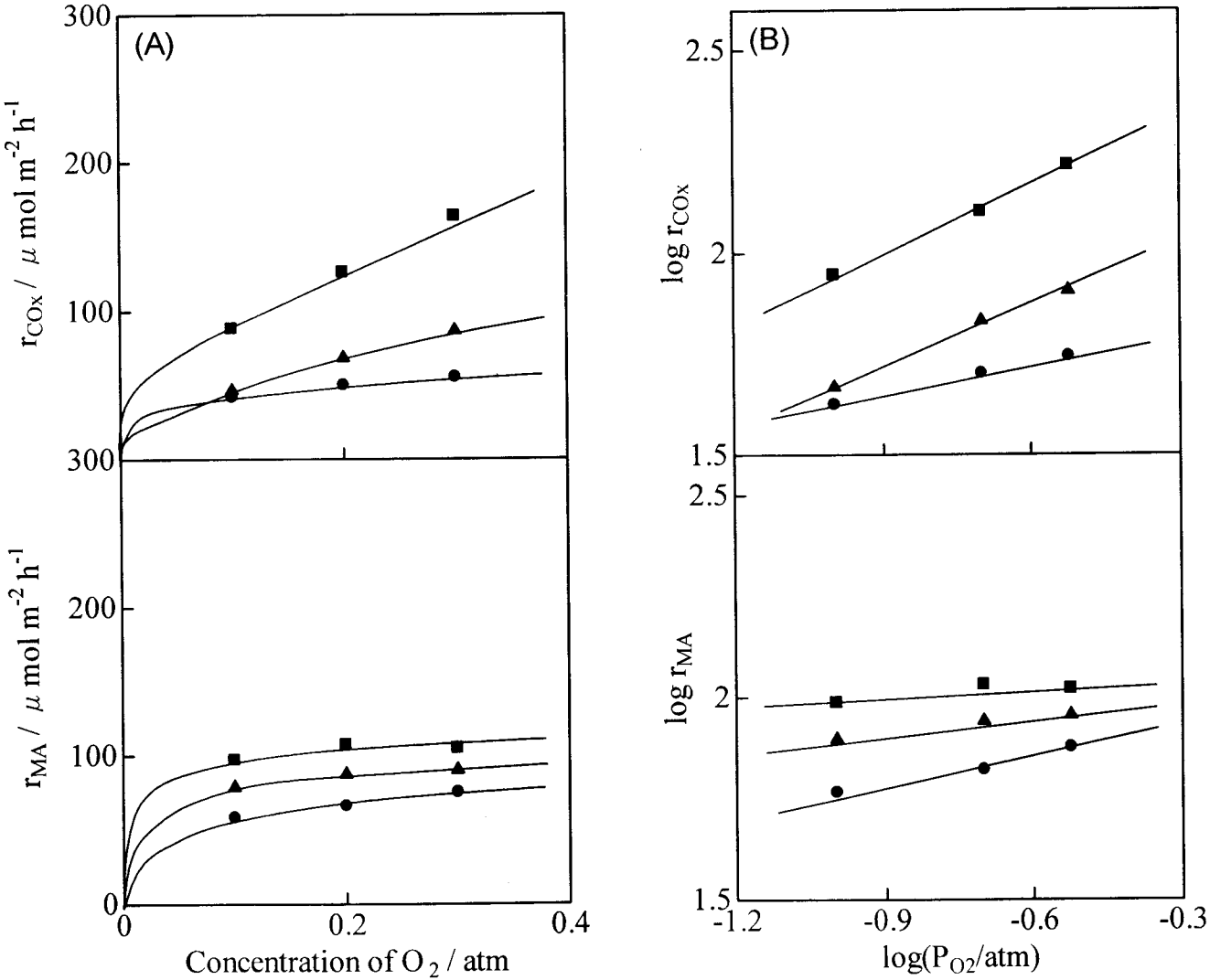

Fig. 8 Dependencies of rates for maleic anhydride and CO_x formation on concentration of O_2. The concentration of *n*-butane is 5.0 % and the reaction temperature is 723 K. r_{MA} and r_{COx} represent rate for maleic anhydride and CO_x formation, respectively: (●) VHexP-VPO, (▲) Fe(0.1)-VPO and (■) Fe(0.5)-VPO.

Discussion

Intercalation of $Fe(acac)_3$ into lamellar vanadyl n-hexylphosphate

As listed in Table 1, the bulk Fe/V ratios were almost the same as those of the surface Fe/V ratios for both Fe(0.1)-VHexP and Fe(0.5)-VHexP. The XRD of VHexP showed a typical pattern for lamellar compound [26]. After the treatments of $Fe(acac)_3$, Fe(0.1)-VHexP and Fe(0.5)-VHexP also kept the lamellar structure, even though the $d(001)$ values slightly decreased. Considering from the consistency with the bulk and surface Fe/V ratio, $Fe(acac)_3$ was uniformly dispersed in the crystallites. These results indicate that $Fe(acac)_3$ was successfully intercalated into the interlayer of VHexP.

As shown in Chapter 4.2, $Fe(acac)_3$ can be intercalated into lamellar vanadyl benzylphosphate (abbreviated as VBzP), $VO((C_6H_5CH_2)_{0.7}/H_{0.3})\cdot(C_6H_5CH_2OH)_{0.5}$, by the same conditions of the treatment. In the case of VBzP, benzyl alcohols existed in the interlayer were replaced by $Fe(acac)_3$ with causing little decrease of the $d(001)$ value [28]. VHexP is shown to be $VO\{(n\text{-}C_6H_{13})_{0.6}/H_{0.4}\}PO_4\cdot(n\text{-}C_6H_{13}OH)_{0.5}$ and has
alcohols in their interlayer space as well as VBzP [26]. Therefore, it can be expected that the intercalation of $Fe(acac)_3$ into VHexP occurred in accordance with the same mechanism for that into VBzP.

It is considered that an interaction between host (lamellar compounds) and guest (metal-complexes) is greatly dependent on their properties, *e.g.*, shape, size and kind of organic group, charge density and interlayer distance for lamellar compounds, and size and kind of ligand for metal-complexes. VHexP and VBzP have nearly the same basal spacing (1.78 nm for VBzP and VHexP for 1.90 nm, respectively), but the character of interlayer space is different; i.e. benzyl or *n*-hexyl group. In the case of VBzP [28], since the surface Fe/V ratio (0.18) was about twice as in the bulk (0.08), it is considered that some part of $Fe(acac)_3$ aggregates on the surface. On the other hand, in the case of VHexP, the surface Fe/V ratio was almost the same as the bulk ratio as listed in Table 1. These results clearly demonstrate that VHexP is a suitable host material for the intercalation of $Fe(acac)_3$.

Structure of Fe-doped catalysts

The structure of the Fe-doped catalysts is basically $(VO)_2P_2O_7$ as confirmed from XRD patterns (Fig. 2), although lattice spacings of the Fe-doped catalysts spread in comparison with the Fe-free $(VO)_2P_2O_7$ as listed in Table 3. Since the surface Fe/V ratio of the Fe-doped catalysts was almost the

same as the bulk one, Fe is considered to uniformly disperse in the bulk.

A question is where the Fe ions exist in $(VO)_2P_2O_7$. Two possible cases should be considered; the first is that the Fe ions are substituted for V^{4+}, namely substitutional solid solution. The second is that the Fe ions are located at interstitial positions, that is, interstitial solid solution. It is generally known that interstitial compounds are formed, only when penetrating ions are significantly small in comparison with lattice ions. Since the van der Waals radius of Fe^{3+} (0.079 nm) is rather larger than that of V^{4+} (0.072 nm), it is quite unlikely that the Fe ions are located at interstitial positions of $(VO)_2P_2O_7$ crystal.

As listed in Table 2, the lattice spacing increases linearly with the Fe/V ratio. In addition, the vibration of ν(V=O) was weakened by the addition of Fe as shown in Fig. 3, suggesting that the number of V^{4+} ions decreased. As mentioned above, Fe^{3+} has rather larger van der Waals radius than V^{4+}. It is known that substitutional solid solution often takes place when the radius of penetrating ions are close to that of lattice ions. Therefore, it is concluded that the Fe ions are substituted for V^{4+} in $(VO)_2P_2O_7$.

Kinetics and role of Fe

From Figs. 7 and 8, the kinetics for MA formation are given in Eqs. 2-4, where r_{MA}, r'_{MA} and r''_{MA} are the rates for MA formation. $P_{n\text{-butane}}$ and P_{O2} are partial pressures of *n*-butane and O_2, respectively, and k_{VHexP}, $k'_{Fe(0.1)}$ and $k''_{Fe(0.5)}$ represent the rate constants.

$$r_{MA} = k_{VHexP} P^{0.4}_{n\text{-butane}} P^{0.2}_{O2} \qquad \text{(VHexP-VPO)} \qquad (2)$$

$$r'_{MA} = k'_{Fe(0.1)} P^{0.4}_{n\text{-butane}} P^{0.1}_{O2} \qquad \text{(Fe(0.1)-VPO)} \qquad (3)$$

$$r''_{MA} = k''_{Fe(0.5)} P^{0.4}_{n\text{-butane}} P^{0.1}_{O2} \qquad \text{(Fe(0.5)-VPO)} \qquad (4)$$

The rate constants are in the order: $k_{VHexP} < k'_{Fe(0.1)} < k''_{Fe(0.5)}$ (Table 5). The dope of Fe causes the increase of the rate constant and the decrease of the reaction order on the partial pressure of O_2, indicating that the property of the active sites for MA formation is changed.

The overall reaction rate is considered to be a result of specific reaction rate (per active site) and the number of the active sites. Okuhara et al. [35] demonstrated that MA is formed selectively on the basal (200) plane of $(VO)_2P_2O_7$, on the other hand, side planes are non-selective for this reaction. Considering from that, the number of the active site can be greatly dependent on the proportion of

exposure of the crystal plane, that is, morphology of the catalyst. VHexP-VPO was transformed from VHexP by the calcination. The Fe-doped catalysts were also obtained from the intercalation compounds that VHexP incorporates $Fe(acac)_3$ in the interlayer space. As shown in Fig. 3, the relative intensities in the XRD of these catalysts were almost the same. This result indicates that the morphologies of these catalysts are resemble each other, that is, the ratio of the (200) planes having the active sites for MA formation is almost the same. Therefore, it is considered that a role of the Fe is mainly to enhance the specific reaction rate for MA formation.

The selective oxidation of *n*-butane over $(VO)_2P_2O_7$ has been accepted to proceed via a redox mechanism at a few surface layers [30-32]. On the basis of this mechanism, the MA formation can be simplified to following two steps [30], where [ ] and [O] represent a vacant site and a oxidized site of the catalyst surface, respectively. O_2, Bu and MA represent oxygen, *n*-butane and maleic anhydride in a gas phase, and k_{ox} and k_{re} are rate constants of re-oxidation and reduction, respectively.

$$[\ ] + O_2 \xrightarrow{k_{ox}} [O] \qquad (5)$$

$$[O] + Bu \xrightarrow{k_{re}} MA + [\ ] \qquad (6)$$

When the reaction reached the stationary state, the rate of re-oxidation (eq. 5) is equal to that of reduction (eq. 6), and the stationary oxidation state of the surface is proportional to k_{ox}/k_{re}. A general expression of the rate for MA formation is expressed in Eq. (7) from this process [30].

$$r_{MA} = \frac{1}{(1/k_{re}P_{n\text{-}butane}) + (\alpha/\ k_{ox}P_{O2})} \qquad (7)$$

Here α indicates the stoichiometric number of O_2 required for this reaction (α=3.5).

In this expression, if k_{re} is much lower than k_{ox} ($k_{re} << k_{ox}$), the expression will be reduced to $k_{re}P^{1.0}{}_{n\text{-butane}}P^{0.0}{}_{O2}$. On the contrary, if k_{re} is much higher than k_{ox} ($k_{re} >> k_{ox}$), the expression becomes $k_{ox}\alpha^{-1}P^{0.0}{}_{n\text{-butane}}P^{1.0}{}_{O2}$. Thus, the ratio of the reaction order on *n*-butane concentration (n) to that of O_2 concentration (m) is related to the ratio of k_{ox} to k_{re}. As k_{ox}/k_{re} becomes higher, n/m will become larger. In addition, if both k_{ox} and k_{re} become larger, the rate constant (k_{VHexP}, $k'_{Fe(0.1)}$ and $k''_{Fe(0.5)}$) of MA formation in Eqs. 2-4 will become large.

The dope of Fe raises the rate constant for MA formation as listed in Table 5. As mentioned above, that is due to the enhanced specific reaction rate by that dope. This result suggests that the

dope of Fe can raise the rates of both reduction and re-oxidation. In addition, the dope of Fe also causes the drop of the *n/m* ratio from 4.0 to 2.0, suggesting that the rate of re-oxidation becomes much faster that that of reduction. As shown in Fig. 5, the Fe-doped catalysts, in fact, gave higher rate of both reduction and re-oxidation. Furthermore, the ratio of re-oxidation to reduction rates increase with increasing of the Fe/V ratio (Table 4), indicating that the rate of re-oxidation becomes much faster than that of reduction.

The Fe ions exist not only in the bulk but also on the surface. The peak of $V(2p_{3/2})$ was observed at 517.5 eV on VHexP-VPO in XPS (Fig. 4a). On the other hand, Fe(0.1)-VPO and Fe(0.5)-VPO gave the peak at 517.9 eV (Figs. 4b,c). According to the past reports about XPS for vanadium phosphorus oxides [36-38], the binding energy of $V^{5+}(2p_{3/2})$ in $VOPO_4$ and $V^{4+}(2p_{3/2})$ in $(VO)_2P_2O_7$ are observed in the range of
518.0-518.4 eV and 516.9-517.1 eV, respectively. In the present study, since the catalysts were quenched at a stationary state of the selective oxidation of *n*-butane, the XPS spectra would reflect the oxidation state of V ions at this state. The binding energies of these catalysts indicate that the surface of the Fe-doped catalysts is in a higher oxidation state in comparison with the Fe-free catalyst. That is consistent with the kinetics and the rates of reduction and re-oxidation. Therefore, it is concluded that the Fe enhances the redox ability, especially re-oxidation of the active sites for MA formation. This retains the catalyst surface at an appropriate oxidation state during the reaction, resulting in the higher rate of MA formation.

The kinetics for CO_x formation are shown in Eqs. (8-10) from Figs. 7 and 8, where r_{COx}, r'_{COx} and r''_{COx} are the rates of CO_x formation.

$$r_{COx} = q_{VHexP} P^{0.3}_{n\text{-butane}} P^{0.3}_{O2} \qquad \text{(VHexP-VPO)} \qquad (8)$$

$$r'_{COx} = q'_{Fe(0.1)} P^{0.1}_{n\text{-butane}} P^{0.4}_{O2} \qquad \text{(Fe(0.1)-VPO)} \qquad (9)$$

$$r''_{Cox} = q''_{Fe(0.5)} P^{0.1}_{n\text{-butane}} P^{0.6}_{O2} \qquad \text{(Fe(0.5)-VPO)} \qquad (10)$$

The dope of Fe causes increase of the rate constant, decreases of the reaction order on partial pressure of *n*-butane, and increases of the reaction order on partial pressure of O_2. CO_x formation has been considered to take place on the different sites from those for MA formation [40]; for example, this concerns with adsorbed oxygen species [40,41]. We deduce that the Fe^{3+} ions on the surface form another active sites for CO_x formation, which reveal different dependencies on partial pressures

of *n*-butane and O_2.

Application of Fe-doped catalyst under high partial pressure of n-butane

From an industrial viewpoint, the operation under high concentrations of *n*-butane can achieve a higher space-time yield of MA. To realize such operation, a catalyst having high activity and selectivity under the high concentrations of *n*-butane is required. In addition to that, concentration of O_2 falls to very low at a high conversion of *n*-butane under the reaction condition of high *n*-butane concentration, because usually the feed of *n*-butane in air is industrially used as a reaction mixture. Therefore, the catalyst is also desired to have a high activity and selectivity under the low concentrations of O_2.

As shown in Fig. 7, the rate for MA formation is high on the whole partial pressure of *n*-butane. Furthermore, the rate scarcely falls even at the low partial pressure of O_2 on the Fe-doped catalysts (Fig. 8). Consequently, the Fe-doped catalyst gave high selectivity to MA under both the high partial pressure of *n*-butane and low partial pressure of O_2 as shown in Fig. 9. These results demonstrated that the dope of Fe by using of intercalation of $Fe(acac)_3$ is promising technique for preparation of efficient catalysts that is suitable for operation under the high partial pressure of *n*-butane.

Conclusion

$Fe(acac)_3$ was successfully intercalated into vanadyl *n*-hexylphosphate by heating in toluene. The obtained intercalation compound was transformed to $(VO)_2P_2O_7$ by calcination under the reaction condition of *n*-butane oxidation. The Fe ions uniformly spread in $(VO)_2P_2O_7$. The Fe-doped catalyst exhibited the high catalytic performance for MA formation. It was revealed that the Fe-doped catalyst possessed high redox ability, especially re-oxidation. The high redox ability on a surface layers of the Fe-doped catalyst results in the high catalytic performance for the selective oxidation of *n*-butane.

References

[1] B.K. Hodnett, *Catal. Rev. -Sci. Eng.*, **17** (1985) 373.

[2] E. Bordes, *Catal. Today*, **1** (1987) 499.

[3] G. Centi, F. Trifirò, J.R. Ebner, V.M. Franchetti, *Chem. Rev.*, **88** (1988) 55.

[4] F. Cavani, F. Trifirò, *Chemtech*, **24** (1994) 18.

[5] G.J. Hutchings, *Appl. Catal.*, **72** (1991) 1.

[6] M.T. Sananes-Schultz, F. Ben Abdelouahab, G.J. Hutchings, J.C. Volta, *J. Catal.*, **163** (1996) 346.

[7] D. Ye, A. Satsuma, A. Hattori, T. Hattori, Y. Murakami, *Catal. Today*, **16** (1993) 113.

[8] F.B. Abdelouahab, R. Olier, M. Ziyad, J.C. Volta, *J. Catal.*, **157** (1995) 687.

[9] D. Ye, A. Satsuma, T. Hattori, Y. Murakami, *J. Chem. Soc., Chem. Commun.*, (1990) 1337.

[10] G. Bagnasco, L. Benes, P. Galli, M.A. Massucci, P. Patrono, G. Russo, M. Turco, *Stud. Surf. Sci. Catal.*, **119** (1998) 653.

[11] M. Hatano, M. Masayoshi, K. Shima, M. Ito, *US Patent* 5128299 (1992).

[12] M.J. Mummey, *EP Patent* 326536 A1 (1989).

[13] J.W. Johnson, D.C. Johnston, A.J. Jacobson, J.F. Brody, *J. Am. Chem. Soc.*, **100** (1984) 8123.

[14] T. Shimoda, T. Okuhara, M. Misono, *Bull. Chem. Soc. Jpn.*, **58** (1985) 2163.

[15] K. Beneke, G. Lagaly, *Inorg. Chem.*, **22** (1983) 1503.

[16] T. Nakato, Y. Furumi, N. Terao, T. Okuhara, *J. Mater. Chem.*, **10** (2000) 737.

[17] V.V. Guriants, J.B. Benziger, S. Sundaresan, I.E. Wachs, J.-M. Jehng, *Chem. Mater.*, 7 (1995) 1493.

[18] J.W. Johnson, A.J. Jacobson, J.F. Brody, J.T. Lewandowski, *Inorg. Chem.*, **23** (1984) 3842.

[19] G. Huan, J.W. Johnson, J.F. Brody, D.P. Goshorn, A.J. Jacobson, *Mater. Chem. Phys.*, **35** (4993) 199.

[20] E.M. Sabbar, M.E. de Roy, A. Ennaqadi, G. Gueho, J.P. Besse, *Chem. Mater.*, **10** (1998) 3856.

[21] N, Mizuno, H. Hatayama, S. Uchida, A. Taguchi, *Chem. Mater.*, **13** (2001) 179.

[22] M. Roca, J.E. Haskouri, S. Cabrera, A.B. Porter, J. Alamo, D.B. Porter, M.D. Marcos, P. Amorós, *Chem. Commun.*, (1998) 1883.

[23] T. Nakato, Y. Furumi, T. Okuhara, *Chem. Lett.*, (1998) 611.

[24] N. Hiyoshi, N. Yamamoto, Y. Okuhara, *Chem. Lett.*, (2001) 484.

[25] Y. Kamiya, E. Nishikawa, A. Satsuma, N. Mizuno, T. Okuhara, *J. Jpn. Petro. Inst.*, **44** (2001) 265.

[26] Y. Kamiya, E. Nishikawa, A. Satsuma, T. Okuhara, *Bull. Chem. Soc. Jpn.*, (in press).

[27] N. Hiyoshi, N. Yamamoto, Y. Kamiya, E. Nishikawa, T. Okuhara, *Catal. Today*, **71** (2001) 129.

[28] A. Satsuma, Y. Kijima, S. Komai, Y. Kamiya, E. Nishikawa, T. Hattori, *Catal. Today*, **71** (2001) 161.

[29] G. Busca, F. Cavani, G. Centi, F. Trifirò, *J. Catal.*, **99** (1986) 400.

[30] M. Pepera, J.L. Callaham, M.J. Desmond, E.C. Milberger, P.R. Blum, N.J. Bremer, *J. Am. Chem. Soc.*, **107** (1985) 4883.

[31] G. Koyano, T. Okuhara, M. Misono, *J. Am. Chem. Soc.*, **120** (1998) 767.

[32] T. Okuhara, M. Misono, *Catal. Today*, **16** (1993) 61.

[33] H. Igarashi, K. Tsuji, T. Okuhara, M. Misono, *J. Phys. Chem.*, **97** (1993) 7065.

[34] G. Centi, G. Fornasari, F. Trifirò, *Ind. Eng. Chem. Prod. Res. Dev.*, **24** (1985) 32.

[35] K. Inumaru, T. Okuhara, M. Misono, *Chem. Lett.*, (1995) 1992.

[36] N.B. Harrouch, H. Batis, A. Ghorbel, J.C. Vedrine, J.C. Volta, *J. Catal.*, **128** (1991) 248.

[37] L.M. Cornaglia, C. Caspani, E.A. Lomgardo, *Appl. Catal.*, **74** (1991) 15.

[38] T.P. Moser, G.L. Schrader, *J. Catal,*. **104** (1987) 99.

[40] U. Rodemerck, B. Kubis, H.-W. Zanthoff, M. Baerns, *Appl. Catal. A,* **153** (1997) 203.

[41] J.T. Gleaves, J.R. Ebner, T.C. Kuechler, *Catal. Rev. –Sci. Eng.* **30** (1988) 49.

Chapter 5

Vanadyl Pyrophosphate Catalysts with Thin Film Morphology Prepared by Intercalation, Exfoliation and Reduction of $VOPO_4 \cdot 2H_2O$ in Alcohol

Abstract

A new method through intercalation and exfoliation of $VOPO_4 \cdot 2H_2O$ crystallites in primary alcohol (1-propanol or 1-butanol), followed by reduction with the alcohol, have been investigated for the preparation of catalyst precursor. Lamellar compounds, consisting of V^{4+}, P^{5+} and alkyl group with thin film-like morphology, were formed and was characterized by means of XRD, IR, TG/DTA, and elemental analysis. The chemical formula of the precursor obtained by exfoliation-reduction in 1-butanol was shown to be $VO\{(n\text{-}C_4H_9)_{0.16}H_{0.84}\}PO_4 \cdot 0.8H_2O$. On the other hand, a direct reduction of $VOPO_4 \cdot 2H_2O$ in the alcohol gave a mixed phase shown by $(VOHPO_4 \cdot 0.5H_2O)_{0.3}(VO\{(n\text{-}C_4H_9)_{0.3}H_{0.7}\}PO_4 \cdot 3H_2O)_{0.7}$ comprising plate-like microcrystallites. These precursors transformed to $(VO)_2P_2O_7$ phase during an activation process at 703 K in the presence of a mixture of *n*-butane 1.5 % and O_2 17 % in He balance. The obtained $(VO)_2P_2O_7$ through the exfoliation-reduction was well-crystallized and consisted of thin flaky crystallites. It was found that $(VO)_2P_2O_7$ thus prepared through the exfoliation-reduction was highly active and selective for oxidation of *n*-butane.

Introduction

Selective oxidation of *n*-butane to maleic anhydride (abbreviated as MA) is one of commercialized applications in the gas-phase oxidation of lower alkanes with oxygen [1]. Vanadyl pyrophosphate, $(VO)_2P_2O_7$, is a main component of a commercial catalyst for this reaction [2-5]. One of major problems in the commercial plant is the insufficient yield of MA. It is thus desirable to improve the yield by development of the catalytic performance.

Since the catalytic activity and selectivity of $(VO)_2P_2O_7$ are greatly dependent on the microstructure of the crystallites [6-8], control of the microstructure is critical for improvement of the catalytic performance. It is well known that vanadyl hydrogen phosphate hemihydrate, $(VOHPO_4 \cdot 0.5H_2O)$ a precursor for $(VO)_2P_2O_7$, can be also obtained by reduction of $VOPO_4 \cdot 2H_2O$ with alcohol [9]. Hutchings et al. [10,11] reported that the morphology of the precursor could be controlled by a choice of alcohol used as reducing agent.

Exfoliation technique has been developed from intercalation of various layered materials like clay [12], zirconium phosphate [13], niobates [14], and titanates [15], in which exfoliation is a method delaminating stacked inorganic sheets in solvent by infinite swelling of their interlayer space. $VOPO_4 \cdot 2H_2O$ is one of layered compounds and possesses a high intercalating capability [16].

The aim of this Chapter is preparing the precursor and catalyst through intercalation, exfoliation and reduction of $VOPO_4 \cdot 2H_2O$ in primary alcohol in order to preferentially expose the (100) plane. The obtained crystallites have been systematically characterized in order to elucidate the features of this preparation method. Furthermore, the catalytic property for the selective oxidation of *n*-butane has been examined, comparing with that of conventional catalyst.

Experimental

Preparation of precursors

$VOPO_4 \cdot 2H_2O$ was prepared according to the literature [16]. A mixture of V_2O_5 (24 g, Wako Pure Chemical Ind. Ltd.) and 85%H_3PO_4 (133 cm^3, Wako Pure Chemical Ind. Ltd.) and H_2O (577 cm^3) was refluxed at 388 K for 16 h to form precipitates. The obtained solid was filtered, washed with acetone, and dried at room temperature for 16 h. The solid was confirmed to be $VOPO_4 \cdot 2H_2O$ by XRD and IR. $VOPO_4 \cdot 2H_2O$ (0.5 g) was added to 1-propanol or 1-butanol (50 cm^3, Wako Pure Chemical Ind. Ltd.) at room temperature. The suspension was stepwise heated at room temperature, 303, 323, or 343 K for 1 h at each temperature. Then the solution was further refluxed at 363 K (1-propanol) or 383 K (1-butanol) for 24 h to obtain light-blue precipitates. The obtained solids from 1-propanol and 1-butanol are denoted to EP(1-Pr) and EP(1-Bu), respectively.

As a reference, the precursors were separately prepared by the conventional methods, e.g., the direct reduction of $VOPO_4 \cdot 2H_2O$ with alcohol [11] and the organic solvent method [8]. For the direct reduction, $VOPO_4 \cdot 2H_2O$ (5.0 g) was added to 1-propanol, 1-butanol or 2-butanol (50 cm^3, Wako Pure Chemical Ind. Ltd.) at room temperature, followed by refluxed at 363 K (1-propanol) or 383 K (1-butanol and 2-butanol) for 18 h. The solids obtained from 1-propanol, 1-butanol and 2-butanol are denoted to P(1-Pr), P(1-Bu) and P(2-Bu), respectively. For the organic solvent method, the precursor $VOHPO_4 \cdot 0.5H_2O$ (denoted as P-3) was prepared using isobutyl alcohol and benzyl alcohol [8], and the corresponding $(VO)_2P_2O_7$ (denoted as C-3) was obtained by the calcination at 773 K in 9.1 % O_2 (He balance).

Characterization

Powder XRD patterns were obtained on an X-ray diffractometer (Rigaku Miniflex) with CuK_α radiation (λ=0.154 nm). Infrared spectra were recorded with an IR spectrometer (Bio-rad FTS-7) by a KBr method. SEM images were taken by using a Hitachi S-2100A scanning electron microscope.

Thermogravimetric analysis (TG/DTA) was performed in a flow of dry air (100 cm^3 min^{-1}) by using a Seiko Instruments TG/DTA-6300. The sample was heated from 303 K to 853 K at a rate of 10 K min^{-1}.

Elemental analysis of the samples for C and H were carried out at the Center for Instrumental analysis, Hokkaido University. The contents of V and P were determined by an inductively coupled plasma atomic emission spectrometer (ICP-AES, Shimadzu ICPS-8000), in which the sample powder was dissolved into hot H_2SO_4, and the solution was diluted with water to about 30 ppm of V and P. The content of oxygen in the sample was calculated by subtracting the sum of weights of V, P, C, and H.

The average oxidation number of V was determined by a redox titration method according to the literature [18]. The surface area was measured by a BET method with automatic adsorption system (BELSORP 28SA, BEL Japan Inc.).

Catalytic oxidation of n-butane

Catalytic oxidation of *n*-butane was performed in a flow reactor (Pyrex tube, inside diameter of 10 mm) under an atmospheric pressure at 703 K using a mixture consisting of *n*-butane 1.5 vol%, O_2 17 vol%, and He (balance). The precursor was activated in the reactant mixture by heating from room temperature to 703 K at a rate of 10 K min^{-1}. The products were analyzed with gas chromatographs, an FID-GC (Shimadzu 8A) equipped with Porapak QS column for *n*-butane and MA, and a high speed GC (TCD, Area Japan M-200) with Porapak Q and Molecular Sieves 5A columns for O_2, CO, and CO_2. The catalysts derived from EP(1-Bu) and P(1-Bu) are denoted to EC(1-Bu) and C(1-Bu), respectively.

Results and discussion

Catalyst precursors obtained through exfoliation of $VOPO_4 \cdot 2H_2O$

When the powder of $VOPO_4 \cdot 2H_2O$ (lemon yellow) was stepwise heated in 1-butanol at room temperature, 303 K, 323 K, and 343 K for 1 h at each temperature, the alcohol suspension became homogeneous yellow solution. By evaporating the resulting homogeneous solution at 333 K, a yellow-green powder was formed. XRD pattern and IR spectrum of the solid were the same as those of the starting $VOPO_4 \cdot 2H_2O$ (the data were not shown). As will be discussed elsewhere [17,19,20], $VOPO_4$ sheets were delaminated in 1-butanol solution (exfoliation). Subsequent refluxing the

exfoliation solution for 24 h produced light-blue precipitates. Also in the case of 1-propanol, a homogeneous alcoholic solution was obtained and light-blue precipitate was formed by further refluxing.

SEM images are shown in Fig. 1. The starting $VOPO_4 \cdot 2H_2O$ consisted of square platelets with the lateral dimensions of about 10 μm and thickness of about 1 μm (Fig. 1a). As Figs. 1b and c show, the precursor obtained by intercalation, exfoliation, and reduction (EP(1-Pr) and EP(1-Bu)) consists of thin films (thickness; less than 0.1 μm) randomly gathered. On the other hand, P(1-Bu) was aggregates of plate-like microcrystallites (Fig. 1d).

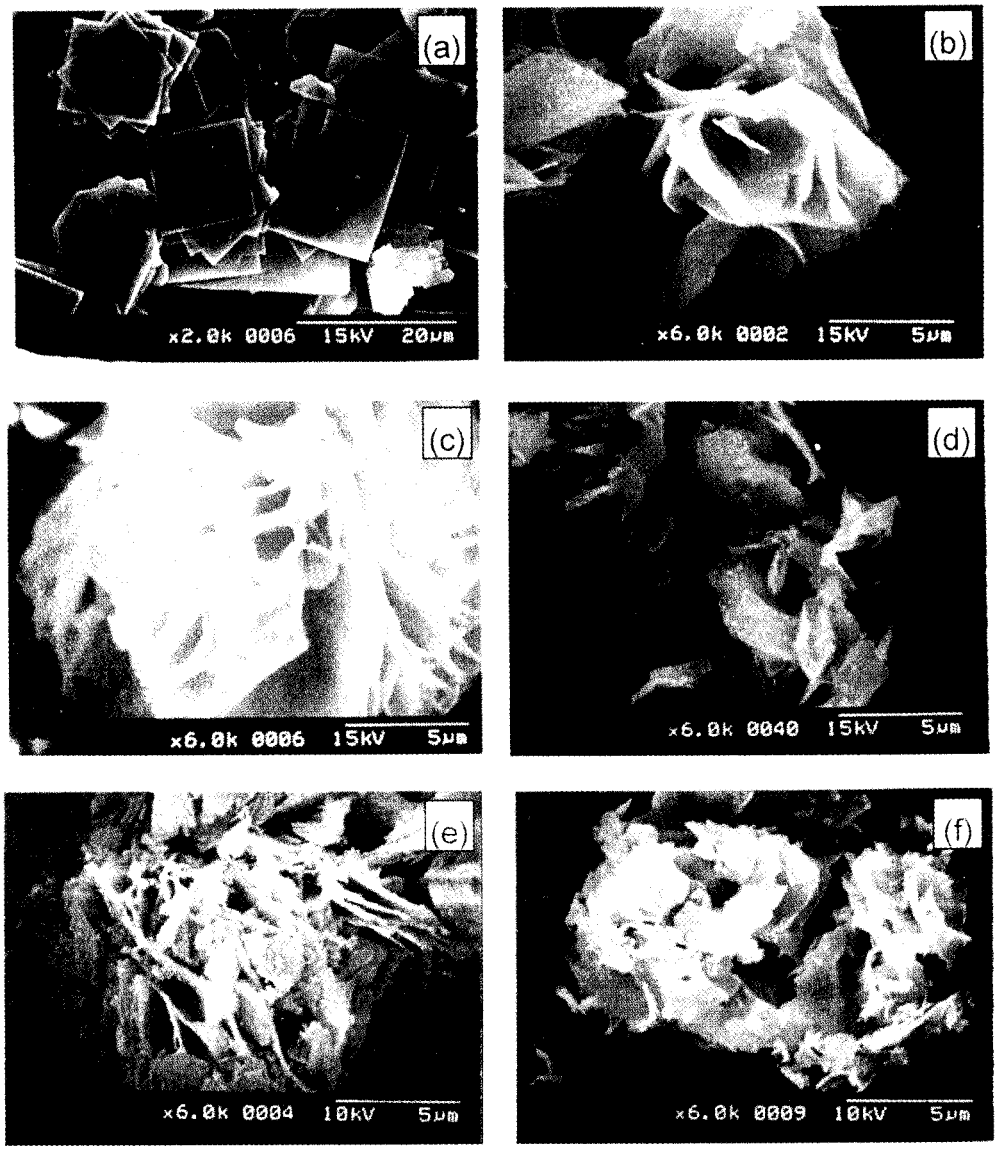

Fig. 1 SEM micrographs of vanadium phosphorus oxides. (a) $VOPO_4 \cdot 2H_2O$, (b) EP(1-Pr), (c) EP(1-Bu), (d) P(1-Bu), (e) EC(1-Bu), and (f) C(1-Bu).

Table 1 summarizes the results of the elemental chemical analysis of EP(1-Bu) and P(1-Bu), together with average oxidation numbers of V. The P/V ratios of both precursors were nearly unity and the average oxidation numbers were about +4.0. The R/P ratio of EP(1-Bu) estimated from the C/P ratio was 0.16 (R = *n*-C_4H_9), indicating *n*-butyl group is incorporated in EP(1-Bu). The R/P ratio of P(1-Bu) was 0.08, which was less than that of EP(1-Bu).

Figure 2 shows the XRD patterns of starting $VOPO_4 \cdot 2H_2O$ and the obtained precursors. The XRD pattern of P(2-Bu) corresponds to that of $VOHPO_4 \cdot 0.5H_2O$ with characteristic XRD lines (Fig. 1f) [21]. As shown in Figs 2b and c, the XRD patterns of the precursors obtained by the exfoliation-reduction process differ from that of P(2-Bu). EP(1-Pr) and EP(1-Bu) gave intense peaks at less than 10° of 2θ, suggesting a lamellar compound with intercalated alcohol molecules. Assuming that these intense peaks correspond to a diffraction from the (001) plane, the basal spacings (d_{001}) are estimated to be 0.98 nm and 1.07 nm for EP(1-Pr) and EP(1-Bu), respectively, and these values are larger than that of $VOPO_4 \cdot 2H_2O$ (0.74 nm) (Fig. 2a). The XRD patterns show peaks assignable to the (002) lines at 18.2° (0.49 nm) for EP(1-Pr) and 16.6° (0.53 nm) for EP(1-Bu), respectively. Molecular lengths of 1-propanol and 1-butanol are 0.464 nm and 0.596 nm, respectively, where the molecular length as the distance between O and H of $-CH_3$ is estimated on the basis of the covalent bond length with MOPAC (FUJITSU, WinMOPAC Ver. 3.0). Since the d_{001} value of EP(1-Bu) is larger than that of EP(1-Pr), it is considered that the alkyl groups play an essential role in constructing the lamellar structure.

The precursors obtained by direct reduction in 1-propanol and 1-butanol also gave typical patterns due to lamellar compound (Figs. 2d and e). The d_{001} values for P(1-Pr) and P(1-Bu) were 1.59 nm and 1.57 nm, respectively, which were larger than those of EP(1-Pr) and EP(1-Bu). Since d_{001} value changed scarcely when 1-butanol was used instead of 1-propanol, the size of alkyl group dose not influence the basal spacing. For P(1-Pr) and P(1-Bu), a strong sharp line at 30.52° of 2θ was observed, which agrees with a diffraction of the (220) plane for $VOHPO_4 \cdot 0.5H_2O$. Furthermore, an XRD line at 15.64° assigned to the (001) line for $VOHPO_4 \cdot 0.5H_2O$ was observed. Hutchings et al. [11] reported that similar process produced $VOHPO_4 \cdot 0.5H_2O$ with a specific VPD ($VOPO_4 \cdot 2H_2O$ route) morphology which favor thin platelets in the [001] direction. Therefore, it is deduced that P(1-Pr) and P(1-Bu) is a mixture of $VOHPO_4 \cdot 0.5H_2O$ and the lamellar compound.

Table 1 Elemental analysis and average oxidation number of vanadium for the precursors obtained from $VOPO_4 \cdot 2H_2O$ in 1-butanol.

Precursor[a]	Weight percentage[b]					Average oxidation number of V	Formula
	V	P	C	H	O[c]		
EP(1-Bu)	24.79 (1.00)	15.83 (1.05)	3.76 (0.64)	2.95 (6.01)	52.67 (6.76)	3.95	$VO\{(C_4H_9)_{0.2}H_{0.8}\}PO_4 \cdot 0.8H_2O$
P(1-Bu)	25.12 (1.00)	15.95 (1.04)	1.93 (0.33)	2.23 (4.49)	54.77 (6.94)	4.05	$(VOHPO_4 \cdot 0.5H_2O)_{0.3}(VO\{(C_4H_9)_{0.3}H_{0.7}\}PO_4 \cdot 2H_2O)_{0.7}$

[a] EP(1-Bu) and P(1-Bu) were obtained by exfoliation-reduction and direct reduction of $VOPO_4 \cdot 2H_2O$ in 1-butanol, respectively.

[b] The figures in parentheses are relative atomic ratios.

[c] Oxygen content was estimated by subtracting the sum of weights of V, P, C, and H.

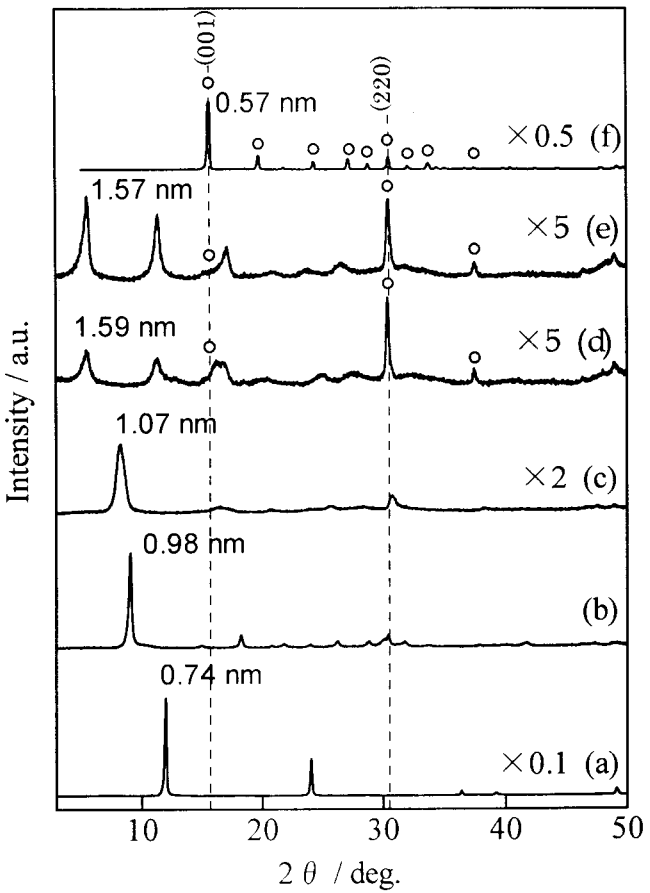

Fig. 2 XRD patterns of vanadium phosphorus oxides. (a) $VOPO_4 \cdot 2H_2O$, (b) EP(1-Pr), (c) EP(1-Bu), (d) P(1-Pr), (e) P(1-Bu), and (f) P(2-Bu). (○) $VOHPO_4 \cdot 0.5H_2O$.

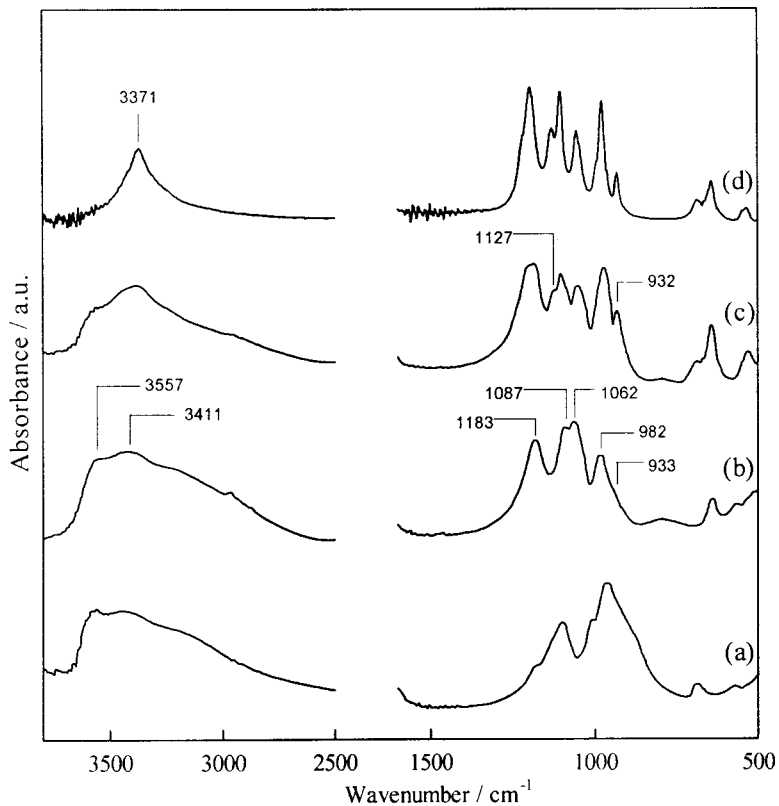

Fig. 3 Infrared spectra of vanadium phosphorus oxides. (a) $VOPO_4 \cdot 2H_2O$, (b) EP(1-Bu), (c) P(1-Bu), and (d) P(2-Bu).

Infrared spectra of $VOPO_4 \cdot 2H_2O$ and the precursors are given in Fig. 3. The spectrum of P(2-Bu) are consistent with that of $VOHPO_4 \cdot 0.5H_2O$ (Fig. 3d) [7]. The bands for P(2-Bu) were assigned to $\nu(PO_3)$ for 1197, 1103, and 1055 cm^{-1}, δ(P-OH) for 1131 cm^{-1}, ν(V=O) for 977 cm^{-1}, and ν(P-OH) for 932 cm^{-1} [7]. All precursors gave similar spectra to that of $VOHPO_4 \cdot 0.5H_2O$ in lattice vibration region (less that 1500 cm^{-1}), indicating that a structure of V-P-O layer for the precursors is analogous to that of $VOHPO_4 \cdot 0.5H_2O$. For EP(1-Bu), the bands at 1183, 1087, and 1062 cm^{-1} are assigned to $\nu(PO_3)$ and 982 cm^{-1} to ν(V=O) (Fig. 3b). In addition, the band at 933 cm^{-1} (shoulder) is assignable to ν(P-OH). The P(1-Bu) displayed similar bands to P(2-Bu) in lattice vibration region, although the bands were broadened. EP(1-Bu) and P(1-Bu) gave a broad band over 3000 cm^{-1}, which is similar to $VOPO_4 \cdot 2H_2O$ (Fig. 3a), due to water weakly held in interlayer space.

TG/DTA profiles of EP(1-Bu), P(1-Bu) and P(2-Bu) are illustrated in Fig. 4. As shown in Fig. 4a, the sharp weight loss with endothermic below 450 K and loose weight loss with exothermic above 500 K were observed for EP(1-Bu). The initial weight loss may be attributed to loss of intercalated water molecules. Considering the exothermic and relatively high temperatures, the weight loss above 500 K is probably due to combustion of *n*-butyl group connected by a covalent bond. From these results, the chemical formula of EP(1-Bu) was estimated to be $VO\{(n\text{-}C_4H_9)_{0.16}H_{0.84}\}PO_4 \cdot 0.8H_2O$. For P(1-Bu), the weight decreased in three steps at temperature range of (1) below 400 K, (2) 400 – 570 K, and (3) above 570 K (Fig. 4b). Endothermic valley observed at 650 K is attributed to transformation from $VOHPO_4 \cdot 0.5H_2O$ to $(VO)_2P_2O_7$ as shown for P(2-Bu) (Fig. 4c). Since P(1-Bu) is a mixture of $VOHPO_4 \cdot 0.5H_2O$ and the lamellar compound, the chemical formula of P(1-Bu) is described as $(VOHPO_4 \cdot 0.5H_2O)_x \cdot (VO((C_4H_9)_y/H_{1-y})PO_4 \cdot nH_2O)_{1-x}$.

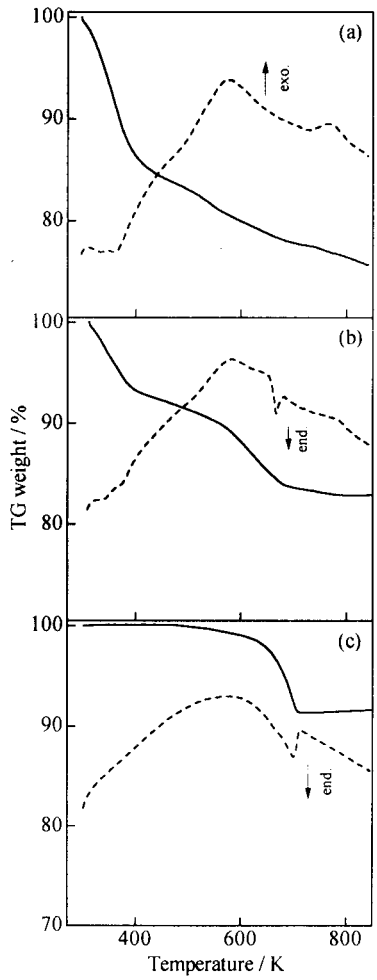

Fig. 4 TG/DTA profile of vanadium phosphorus oxides in air. (a) EP(1-Bu), (b) P(1-Bu), and (c) P(2-Bu).

We estimated x=0.3, y=0.3, and n=3 to satisfy the elemental analysis and TG result as listed in Table 1.

Based on these results, the schematic structures of EP(1-Bu) and P(1-Bu) are depicted in Fig. 5. The structure of V-P-O layer for both precursors is similar to $VOHPO_4 \cdot 0.5H_2O$. For EP(1-Bu), the alkyl group plays an essential role in constructing the lamellar structure. P(1-Bu) is a mixture of $VOHPO_4 \cdot 0.5H_2O$ and lamellar compound. The interlayer space of the lamellar compound is fulfilled with intercalated water molecules to form the lamellar structure. That may be a reason that the basal spacing of these compounds is not affected by the size of the alkyl groups.

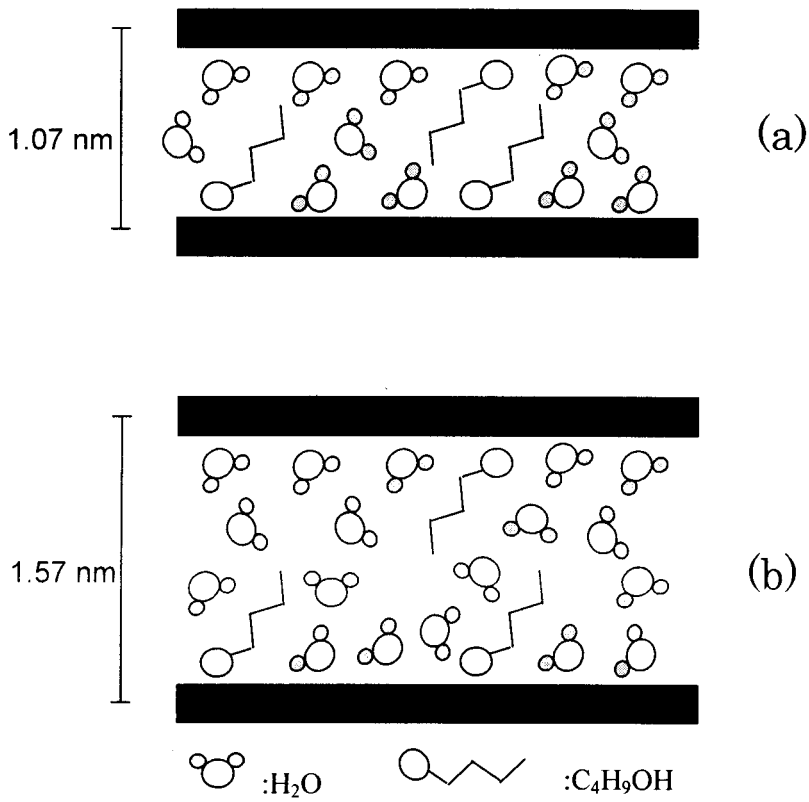

Fig. 5 Schematic structure of (a) EP(1-Bu) and (b) P(1-Bu).

Catalytic oxidation of n-butane

Figure 6 shows the time course of the oxidation of *n*-butane over EC(1-Bu) and C(1-Bu). In order to adjust the conversion, the reactions were performed in the different reaction conditions, that is, W/F = 120 $g \cdot h \cdot mol^{-1}$ for EC(1-Bu), and 163 $g \cdot h \cdot mol^{-1}$ for C(1-Bu), respectively (W = catalyst weight (g), and F = flow rate of n-butane ($mol \cdot h^{-1}$)). As shown in Fig 6, the conversion and selectivity to MA increased at the initial stage of the reaction over both C(1-Bu) and EC(1-Bu). The stationary values were obtained after about 80 h of the reaction, indicating that these catalysts were equilibrated. Thus the reaction rate and selectivity were determined from the data collected around 100 h.

Figure 7 presents W/F dependence of the conversion of *n*-butane. The activity of EC(1-Bu) is high compared with that of C(1-Bu).

Figure 8 gives the change in the selectivity to MA as a function of the conversion of *n*-butane. Fig. 8 demonstrates that EC(1-Bu) is more selective that C(1-Bu). In addition, it is noted that the selectivity to MA was higher than 70 % at low conversions over EC(1-Bu).

In Table 2, the catalytic data are summarized. From the slope of the curve at low W/F region (less than 80 $g \cdot h \cdot mol^{-1}$) in Fig. 7, the reaction rate was determined. The great difference in the catalytic activity for EC(1-Bu) and C(1-Bu) is attributed to the difference in the surface area, since the specific activity defined as the rate per surface area was comparable with each other. It should be noted that EC(1-Bu) was more active than C-3, which is known to be effective for the n-butane oxidation [1,4,8]. The selectivity of EC(1-Bu) was comparable to that of C-3.

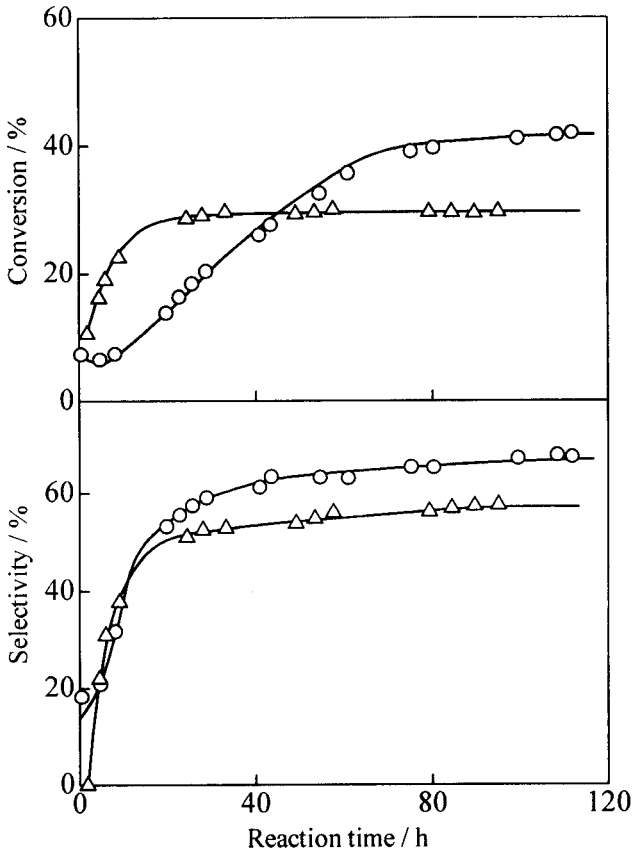

Fig. 6 Changes of the conversion and selectivity to maleic anhydride in the oxidation of *n*-butane over various V-P oxide catalysts: (○) EC(1-Bu); and (△) C(1-Bu). The reaction was performed at 703 K with *n*-butane (1.5 %), O_2 (17 %), and He (balance). W/F = 120 g·h·mol^{-1} for EC(1-Bu), and 163 g·h·mol^{-1} for C(1-Bu), respectively.

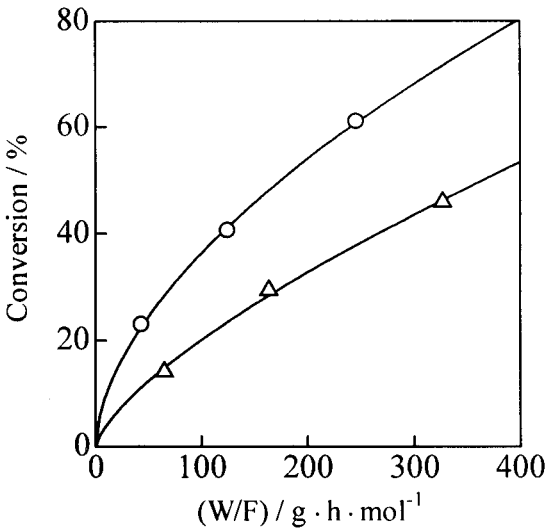

Fig. 7 Dependence of the conversion of *n*-butane on the contact time: (○) EC(1-Bu) and (△) C(1-Bu). The reaction was performed at 703 K with *n*-butane (1.5 %), O_2 (17 %), and He (balance).

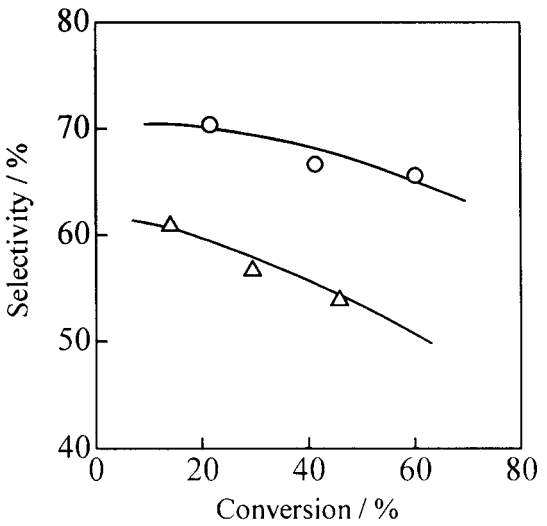

Fig. 8 Selectivity to MA as a function of the conversion of *n*-butane: (○) EC(1-Bu) and (△) C(1-Bu). The reaction was performed at 703 K with *n*-butane (1.5 %), O_2 (17 %), and He (balance).

Table 2 Surface area, size of crystallites and catalytic performance of V-P oxides for oxidation of *n*-butane[a]

Catalyst[b]	Surface area[c] ($m^2\ g^{-1}$)	Size of crystallites (nm)			Rate (10^{-4} mol $g^{-1}\ h^{-1}$)	Selectivity to MA[g] (%)	
		length	D_{SA}[d]	D_{XRD}[e]		20 %[h]	50%[h]
EC(1-Bu)	41	1000	15	20	60 (1.5)[f]	71	67
C(1-Bu)	22	3000	29	7	26 (1.2)[f]	59	53
C-3	36	-----	----	----	24 (0.7)[f]	----	72[i]

[a] The reaction was performed with a mixture of *n*-butane (1.5 %), O_2 (17 %), and He (balance) at 703 K.

[b] EC(1-Bu) and C(1-Bu) were obtained from EP(1-Bu) and P(1-Bu), respectively, and C-3 is $(VO)_2P_2O_7$ prepared by organic solvent method.

[c] Surface area after the reaction.

[d] Thickness estimated from surface area and density of $(VO)_2P_2O_7$.

[e] Thickness estimated with Scherrer's equation [23].

[f] Rate per surface area (10^{-4} mol $m^{-2}\ h^{-1}$)

[g] Selectivity based on *n*-butane.

[h] Conversion of *n*-butane.

[i] Selectivity at 56 % of the conversion

As shown in Fig. 1, the crystallites of EP(1-Bu) were fractured to small flaky crystallites by the calcination under the reaction condition (Fig. 1e) . On the other hand, the plate-like morphology of C(1-Bu) (Fig. 1f) was basically kept to that of the precursor (Fig. 1d).

Powder XRD patterns and IR spectra of the catalysts after the reaction are shown in Fig. 9. Both EC(1-Bu) and C(1-Bu) gave XRD diffraction lines only due to $(VO)_2P_2O_7$ (Fig. 9A). However, the difference in the line-width was detected between these catalysts; EC(1-Bu) gave more sharp lines. As shows in Fig. 9B, EC(1-Bu) gave IR bands at 632 cm^{-1} ($\delta(PO_3)$), 744 cm^{-1} (ν(P-O-P)), 796 cm^{-1} (ν(V-O=V)), 970 cm^{-1} (ν(V=O)), and 1092, 1143, 1220, and 1239 cm^{-1} ($\nu(PO_3)$) [7]. Contrary to EC(1-Bu), the bands at 1099 cm^{-1} and 1220 cm^{-1} (($\nu(PO_3)$) were weak for C(1-Bu). XRD and IR data suggest that the crystallinity of EC(1-Bu) is higher than that for C(1-Bu).

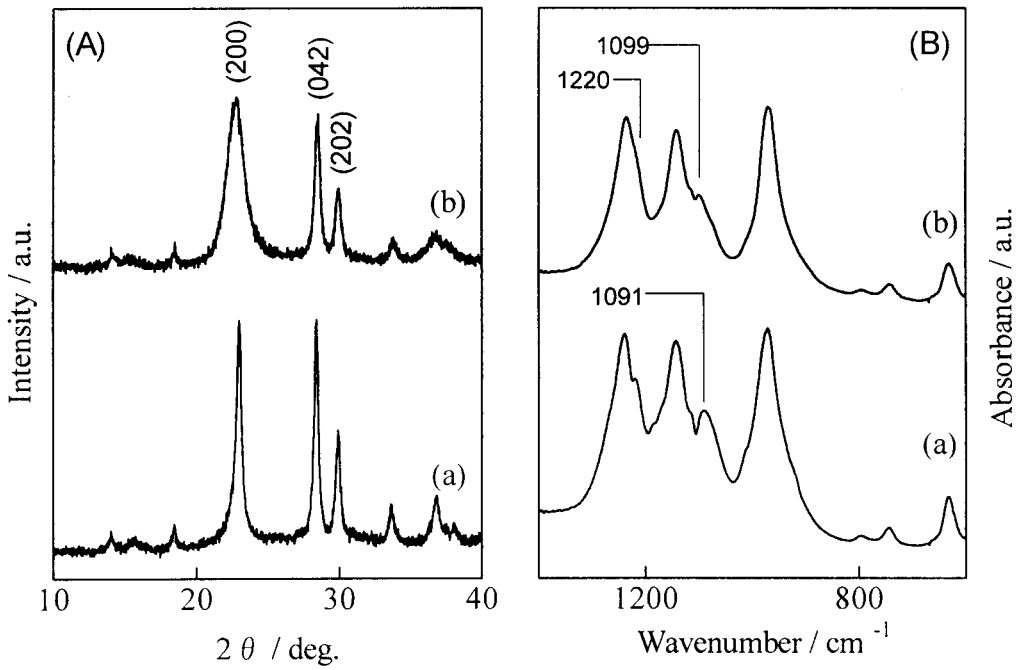

Fig. 9 XRD patterns (A, left) and IR spectra (B, right) of V-P oxide catalysts after the reaction: (a) EC(1-Bu) and (b) C(1-Bu).

The size of crystallites and surface area are summarized in Table 2. The surface area of EC(1-Bu) was about two times higher than that of C(1-Bu). As will be discussed below, the thinner microcrystallites are formed by the exfoliation-reduction metho. Thus the resulting crystallites have high surface area._ The thickness of the crystallites was estimated from surface area using the

following equation 1 or from the XRD line-width of the (200) line using Scherrer's equation 2 [23].

$$2/D_{SA} + 4/L = S \cdot \rho \qquad (1)$$

$$D_{XRD} = (\alpha \cdot \lambda)/(\Delta 2\theta \cdot \cos\theta_0) \qquad (2)$$

In eq. 1, D_{SA} is a thickness of crystallite, L is length of the crystallite, S is surface area, and ρ is the density (3.34×10^{-12} g μm^{-3}) of $(VO)_2P_2O_7$ [24]. In eq. 2, D_{XRD} is a thickness of crystallite, α is a constant (1.0), $\Delta 2\theta$ is a line-width of the (200) line, and θ_0 is an angle of the (200) line.

D_{SA} of EC(1-Bu) was estimated to be 15 nm which is approximately the same as D_{XRD} (20 nm). On the other hand, D_{SA} (29 nm) of C(1-Bu) was greatly different from D_{XRD} (7 nm). When XRD lines are broadened by a structural disorder in the sample solid, the Scherrer's equation is considered to underestimates a size of crystallites. C(1-Bu) gave broad lines in XRD, although D_{SA} of C(1-Bu) is larger than that of EC(1-Bu). P(1-Bu) contains larger quantities of alkyl groups and water molecules and larger d_{001} value compared with EP(1-Bu), which may induce the structural disorder in C(1-Bu) in the transformation of P(1-Bu) to C(1-Bu). This is the reason for the broader XRD lines for C(1-Bu). Therefore, we chose D_{SA} to estimate the thickness. The thickness of EC(1-Bu) was about half of that of C(1-Bu), resulting in the higher surface area of EC(1-Bu).

Okuhara et al. [6] reported that the basal plane of $(VO)_2P_2O_7$, on which characteristic pair sites (V^{4+}-O-V^{4+}) are located, is selective for MA formation, but the side planes are non-selective for the selective oxidation of *n*-butane. Since EC(1-Bu) consisted of thin flaky crystallites, the basal plane was more exposed on EC(1-Bu) as compared with C(1-Bu). Therefore, one of the reason for the high selectivity of EC(1-Bu) is the influence of the greater extent of the fraction of the basal plane. In addition, the nature of the basal plane of EC(1-Bu) would be preferable for the selective formation of MA. These results demonstrate that the present method utilizing intercalation, exfoliation and reduction of $VOPO_4 \cdot 2H_2O$ in primary alcohol is useful for development of efficient catalyst.

Conclusion

Powder of $VOPO_4 \cdot 2H_2O$ was exfoliated by stepwise heating in 1-butanol. The obtained precursor was a lamellar compound and the chemical formula was $VO\{(n\text{-}C_4H_9)_{0.16}H_{0.84}\}PO_4 \cdot 0.8H_2O$ with randomly gathered thin film. The precursor was transformed to $(VO)_2P_2O_7$ consisting of thin

flaky crystallites during an activation process at 703 K in the presence of a reaction mixture. The catalyst showed high activity and selectivity for the selective oxidation of *n*-butane in comparison with the catalyst obtained by the direct reduction of $VOPO_4 \cdot 2H_2O$.

References

[1] S. Albonetti, F. Cavani, F. Trifirò, *Catal. Rev. -Sci. Eng.*, **38** (1996) 413.

[2] E. Bordes, *Catal. Today*, **1** (1987) 499.

[3] G. J. Hutchings, *Appl. Catal.*, **72** (1991) 1.

[4] G. Centi, F. Trifirò, J. R. Ebner, V. M. Franchetti, *Chem. Rev.*, **88** (1988) 55.

[5] B. K. Hodnett, *Catal. Rev. -Sci. Eng.*, **27** (1985) 373.

[6] K. Inumaru, T. Okuhara, M. Misono, *Chem. Lett*,. (1992) 947.

[7] G. Busca, F. Cavani, G. Centi, F. Trifirò, *J. Catal.*, **99** (1986) 400.

[8] Y. Kamiya, E. Nishikawa, T. Okuhara, T. Hattori, *Appl. Catal. A*, **206** (2001) 103.

[9] J. W. Johnson, D. C. Johnston, A. J. Jacobson, J. F. Brody, *J. Am. Chem. Soc.*, **106** (1984) 8123.

[10] I. J. Ellison, G. J. Hutchings, M. T. Sananes, J. C. Volta, *J. Chem. Soc., Chem. Commun.*, (1994) 1093.

[11] M. T. Sananes, I. J. Ellison, S. Sajip, A. Burrows, C. J. Kiely, J. C. Volta, G. J. Hutchings, *J. Chem. Soc., Faraday Trans.* **92** (1996) 137.

[12] E. R. Kleinfeld, G. S. Furgson, *Science*, **265** (1994) 370.

[13] S. W. Kelle, H. -N. Kim, T. E. Mallouk, *J. Am. Chem. Soc.*, **116** (1994) 8817.

[14] R. Abe, K. Shinohara, A. Tanaka, M. Hara, J. N. Kondo, K. Domen, *Chem. Mater.*, **9** (1997) 2179.

[15] T. Sakaki, S. Nakano, S. Yamauchi, M. Watanabe, *Chem. Mater.*, **9** (1997) 602.

[16] G. Ladwig, *Z. Anorg. Allg. Chem.*, **338** (1965) 266.

[17] N. Hiyoshi, N. Yamamoto, T. Okuhara, *Chem. Lett.*, (2001) 484.

[18] B. K. Hodnett, P. Permanne, B. Delmon, *Appl. Catal.*, **6** (1983) 231.

[19] T. Nakato, Y. Furumi, T. Okuhara, *Chem. Lett.*, (1998) 611.

[20] N. Yamamoto, N. Hiyoshi, T. Okuhara, *Chem. Mater.*, (in press).

[21] H. Igarashi, K. Tsuji, T. Okuhara, M. Misono, *J. Phys. Chem.*, **97** (1993) 7065.

[22] J. W. Johnson, A. J. Jacobson, J. F. Brody, S. M. Rich, *Inorg. Chem.*, **21** (1982) 3820.

[23] P. Scherrer, *Göttinger Nachrichem*, **2** (1918) 98.

[24] P. T. Nguyen, R. D. Hoffman, A. W. Sleight, *Mater. Res. Bull.*, 30 (1995) 1055.

Chapter 6

Highly Porous Vanadium Phosphorus Oxides from Vanadyl Alkylphosphates

Abstract

Highly porous vanadium phosphorus oxides of high specific surface area were synthesized by thermal treatment of layered vanadyl *n*-butylphosphate in N_2. The surface area of vanadium phosphorus oxides was greatly increased by thermal treatment within a temperature range of 500–550 K, and reached 225 m^2 g^{-1} after treatment at 568 K. The N_2 adsorption-desorption isotherm of vanadium phosphorus oxide is a Type IV isotherm, indicating that this material is mesoporous. Micropore and mesopore size distributions were determined from Saito-Foley analysis using an Ar adsorption isotherm and Dollimore-Heal analysis using an N_2 desorption isotherm, respectively. The pores show a bimodal distribution in the micropore and mesopore region, and the micropores show a broad distribution with small volume (0.004 cm^3 g^{-1}). The mesopores, which have a size of 4.4 nm and a volume of 0.272 cm^3 g^{-1}, were probably formed from fractures of microcrystallites along layers of vanadyl *n*-butylphosphate.

Introduction

Vanadium phosphorus oxides (V-P oxides) are highly functional materials in magnetism, catalysis, electrodes, and other fields. Many reports address V-P oxides of various nanostructures; that is, intercalation compounds [1-4], lamellar compounds [5-11], large crystallites [12], mesostructured materials [13-16], and thin layered compounds [17,18]. Among these oxides, vanadyl pyrophosphate ($(VO)_2P_2O_7$) is the main component of a commercial catalyst for selective oxidation of *n*-butane to maleic anhydride [19,20].

Porous V-P oxides of high specific surface area are desirable for use as catalysts, catalyst carriers, and adsorbents. Although an intercalation compound of vanadyl phosphate with Ni acetate was reported to be microporous [23], most V-P oxides reported thus far, including $(VO)_2P_2O_7$, $VOPO_4$, and $VO(PO_4)_2$, are non-porous or macroporous [21,22]. Various mesostructured V-P oxides have been synthesized by surfactant templating methods [12-16]. However, removing the templates to form mesoporous V-P oxides has proven difficult [12,15].

As reported in the Chapter 4, the author have synthesized a layered vanadyl *n*-butylphosphate, $VO\{(n\text{-}C_4H_9)_x/H_{1-x}\}PO_4\cdot(n\text{-}C_4H_9OH)_y$ ($x + y = 0.96$). In the Chapter 7, a highly porous V-P oxide was synthesized by thermal treatment of the vanadyl *n*-butylphosphate.

Experimental

Materials

Vanadyl *n*-butylphosphate was prepared as described in the Chapter 4. V_2O_5 (29.2 g, Koso Chemical Co., Ltd.) was reduced with a mixture of isobutyl alcohol (180 cm^3, Koso Chemical Co., Ltd.) and benzyl alcohol (120 cm^3, Koso Chemical Co., Ltd.) at the refluxing temperature (387 K) for 3 h. The obtained black solid was separated by filtration. The solid (about 20 g) was added to 300 cm^3 of 1-butanol, and then a mixture of P_2O_5 (29.6 g, Koso Chemical Co., Ltd.) and toluene (70 cm^3, Koso Chemical Co., Ltd.) was slowly added to the suspension with stirring at room temperature. The mixture was then refluxed for 3 h. The resultant solid was separated by filtration, washed with acetone, and dried at room temperature for 16 h. Elemental analysis and infrared spectroscopy reveal that the obtained solid is $VO\{(n\text{-}C_4H_9)_x/H_{1-x}\}PO_4\cdot(n\text{-}C_4H_9OH)_y$ ($x + y = 0.96$, abbreviated as VBuP) [24]. VBuP (0.5 g) was placed in a Pyrex tubing reactor (inside diameter of 8 mm), and heated in a flow of N_2 (20 $cm^3\ min^{-1}$) at a rate of 5 K min^{-1}. The sample was maintained at constant temperature for 1 h, and cooled to room temperature in the N_2 flow. Hereafter, the V-P oxide obtained at a given temperature will be denoted as V-P(*treatment temperature*).

Characterization

Both N_2 adsorption-desorption and Ar adsorption isotherms were obtained by use of an automatic adsorption-desorption system (BELSORP 28SA, BEL Japan Inc.), at liquid N_2 temperature (77 K) and liquid Ar temperature (87 K), respectively. Specific surface area of the V-P oxides was determined from an N_2 adsorption isotherm by the BET method. Mesopore and micropore size distributions were obtained on the basis of N_2 desorption isotherms obtained by the Dollimore-Heal (DH) method [26] and Ar adsorption isotherms obtained by the Saito-Foley method [27], respectively.

Powder X-ray diffraction (XRD) was recorded on an X-ray diffractometer (Rigaku RINT-1400) with Cu K_α radiation ($\lambda = 0.154$ nm). Infrared spectra were obtained with an IR spectrometer (JASCO FTIR-470/Plus) using a pressed disk made from a mixture of the sample powder and KBr. SEM images were taken by a Hitachi S-2100 B scanning electron microscope. Transmission electron micrographs (TEM) were measured by a Hitachi H-7000 operated at 100 kV.

Elemental analysis of the compounds was performed with a Mikroanalytisches Labor Pascher (Germany) for V, P, C, and H. The content of oxygen in the sample was calculated by subtracting the

sum of the weights of V, P, C, and H. The average oxidation number of V was determined by a redox titration method using $KMnO_4$ and $FeSO_4(NH4)_2SO_4 \cdot 6H_2O$ in accordance with the literature [28].

Results and discussion

Surface area and pore size distribution

Figure 1 shows BET surface area as a function of treatment temperature. Fresh VBuP and V-P(508) have surface areas of 8 and 6 $m^2\ g^{-1}$, respectively. As seen in the figure, surface area increased greatly after thermal treatment within the temperature range of 510 K-550 K, and maximum surface area (225 $m^2\ g^{-1}$) was obtained at 568 K. Treatment above 700 K decreased the high surface area. When VBuP was treated at 773 K, the produced V-P-oxide had a surface area of only 36 $m^2\ g^{-1}$.

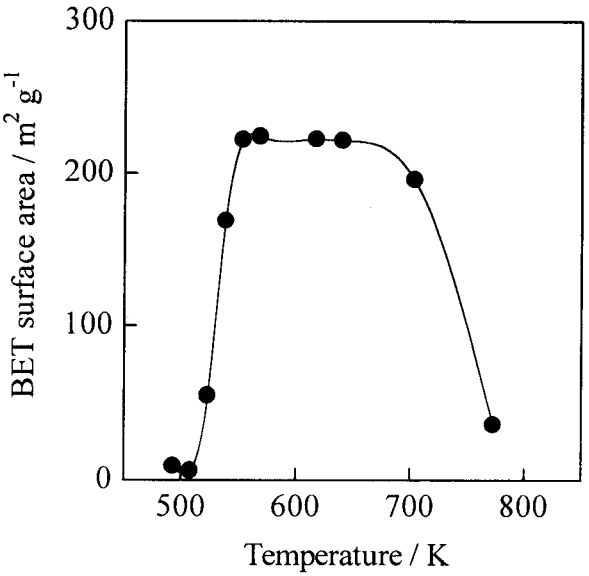

Fig. 1 Change in specific surface area as a function of temperature of thermal treatment in N_2.

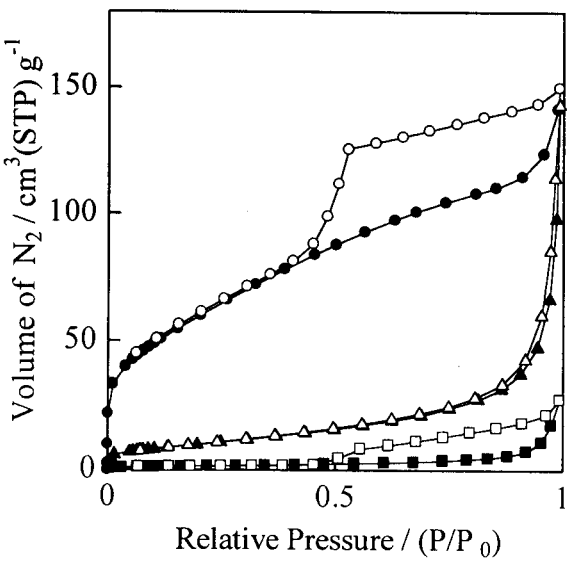

Fig. 2 Nitrogen adsorption-desorption isotherm at 77 K for vanadium phosphorus oxide obtained by thermal treatment of the vanadyl *n*-butylphosphate in N_2 at 508 K (■, □), 568 K (●, ○), and 773 K (▲, △). Solid and open symbols correspond to adsorption and desorption branches, respectively.

Figure 2 shows N_2 adsorption-desorption isotherms for V-P(508), V-P(568), and V-P(773). V-P(508) shows a Type V isotherm, indicating that V-P(508) is mesoporous [29], and the hysteresis loop is not clear. V-P(568) shows a Type IV isotherm, indicating that V-P(568) is a mesoporous material [29], and the hysteresis loop of V-P(568) is much larger than that of V-P(508). The shape of the hysteresis loop at $P/P_0 > 0.5$ can be classified as a typical B type under de Boer classification [29], suggesting the existence of slit-shaped pores. In addition, a steep increase in adsorption at very low pressures suggests the presence of micropores. In contrast, V-P(773) shows a Type III isotherm, which is usually observed for non-porous or macroporous materials [29].

In order to determine the micropore size distribution of V-P(568), an adsorption isotherm of Ar was measured. Figure 3 shows the adsorption isotherm of Ar for V-P(568) within a low pressure range (P/P_0 = 10^{-5} - 10^{-1}), in the form of a semi-log plot. A gentle transition of adsorption is observed at a relative pressure of about 10^{-4} – 10^{-3}. Above 10^{-3}, a nearly linear increase in the adsorption is observed. V-P(568) shows low adsorption of Ar as compared with H-ZSM-5 and NaY reported previously by Okuhara et al. [30].

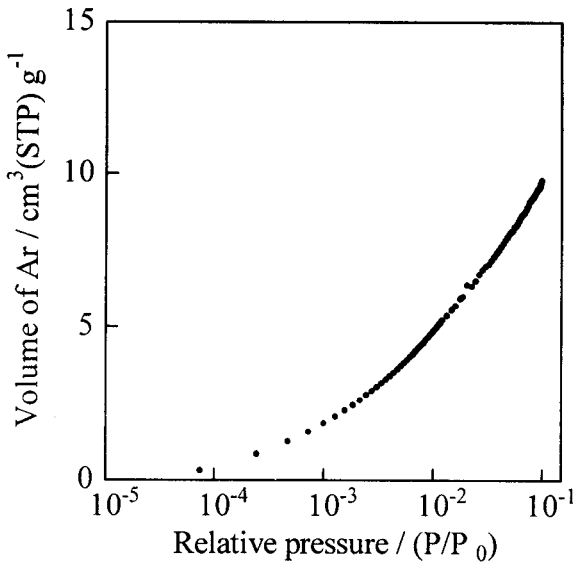

Fig. 3 Argon adsorption isotherm within low pressure range for vanadium phosphorus oxide obtained by thermal treatment of the vanadyl *n*-butylphosphate in N_2 at 568 K.

Figure 4 shows mesopore size distributions of V-P(508), V-P(568), and V-P(773) and micropore size distribution of V-P(568), the mesopore and micropore size distributions having been obtained from the desorption branch of an N_2 isotherm and the adsorption branch of an Ar isotherm, respectively. V-P(508) shows a very small peak at 3.5–5.0 nm, and V-P(773) has few mesopores. V-P(568) has bimodal pores, in the micropore and mesopore regions, with a narrow distribution and a large peak at 4.4 nm being observed in the mesopore region. In contrast, a broad, weak peak is detected in the micropore region. Okuhara et al. reported that non-porous materials such as SiO_2 show no peak in the micropore region when subjected to the same analysis of Ar adsorption isotherm [30]. Thus, micropores are actually present in V-P(568). Pore volumes of mesopore and micropore for V-P(568) were estimated to 0.272 $cm^3\ g^{-1}$ and 0.004 $cm^3\ g^{-1}$, respectively. The surface areas of the walls of the mesopores and micropores were estimated to be 312 $m^2\ g^{-1}$ and 19 $m^2\ g^{-1}$ from Eq. (1), respectively, indicating that the mesopores contribute greatly to total surface area.

$$S = \Sigma 2V_i/R_i \qquad (1)$$

In Eq. (1), S is a surface area derived from the mesopores or micropores; R_i is pore radius, and V_i is pore volume for pores of size R_i.

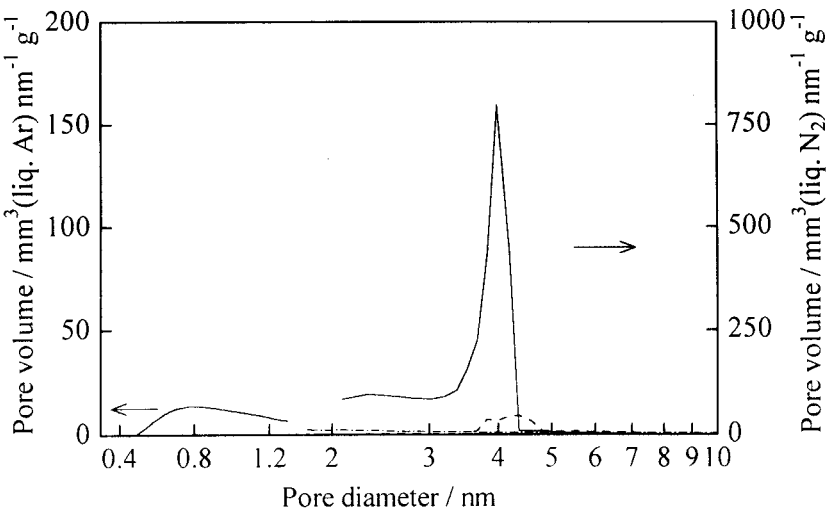

Fig. 4. Mesopore and micropore size distributions for vanadium phosphorus oxide obtained by thermal treatment of vanadyl *n*-butylphosphate in N_2 at 508 K (----), 568 K (——), and 773 K (-·-·-). Mesopore size distribution was derived from the Dollimore-Heal method using the desorption branch of the N_2 isotherm. Micropore size distribution was obtained from the Saito-Foley method using the Ar adsorption isotherm.

Figure 5 shows a *t*-plot for V-P(568), which was obtained from the N_2 adsorption isotherm. The total surface area estimated from the *t*-plot is 196 m^2 g^{-1}, which is consistent with the BET surface area (225 m^2 g^{-1}). The *t*-plot shows an upward deviation from the straight line, which is attributable to capillary condensation for mesopores [29]. In contrast, a downward deviation expected to result from the presence of micropores is not observed clearly.

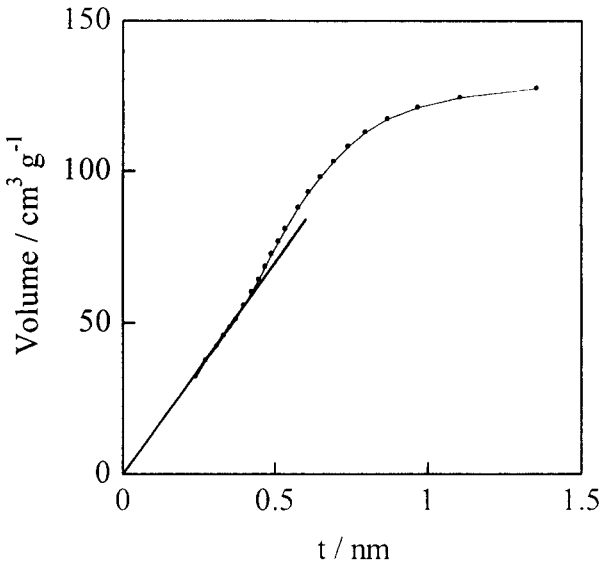

Fig. 5 The *t*-plot of vanadium phosphorus oxide obtained by thermal treatment of vanadyl *n*-butylphosphate in N_2 at 568 K

3.2 Formation of pores

Figure 6 shows the XRD patterns of VBuP, V-P(508), V-P(568), and V-P(773). The XRD pattern of VBuP (Fig. 6a) suggests a layered compound with a basal spacing of 1.54 nm [24]. The layered structure is maintained up to 508 K (Fig. 6b), but the oxide becomes amorphous after treatment at 568 K (Fig. 6c). The great increase in surface area with treatment at 568 K suggests that the formation of pores in the V-P oxides is probably related to destruction of the layered structure of VBuP. No crystalline phases were detected, even for V-P(773) (Fig. 6d).

Figure 7 shows the IR spectra of VBuP, V-P(508), V-P(568), and V-P(773). The IR bands of VBuP (Fig.7a) were assigned to $\nu(PO_3)$ for 1057, 1093, and 1198 cm^{-1}, $\nu(V{=}O)$ for 981 cm^{-1}, and vibration of a P-O-C bond for 1151 cm^{-1} (shoulder) [25]. The IR pattern is retained up to 508 K (Fig. 7b), but changes greatly with treatment at 568 K (Fig. 7c). These findings are consistent with the results of XRD. Since C-H vibrations of *n*-butyl group at 2850–3000 cm^{-1} [25] for VBuP (Fig. 6a) were not detected in V-P(568), the layered structure of VBuP is thought to have been destructed with elimination of the *n*-butyl groups.

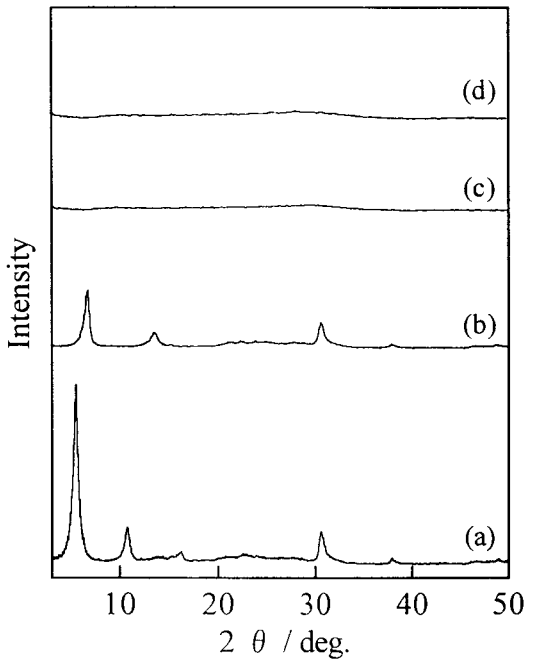

Fig. 6 Powder XRD patterns for (a) vanadyl *n*-butylphosphate and vanadium phosphorus oxide obtained by thermal treatment of vanadyl *n*-butylphosphate in N_2 at (b) 508 K, (c) 568 K, and (d) 773 K.

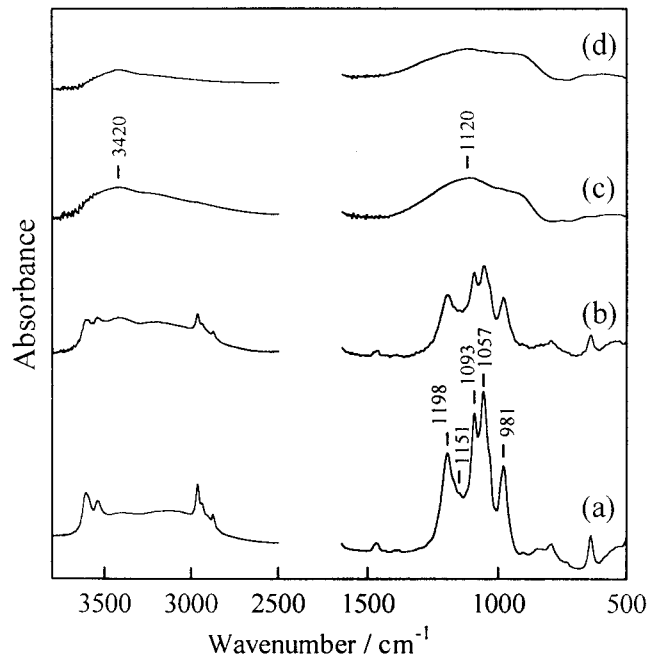

Fig. 7 IR spectra for (a) vanadyl *n*-butylphosphate and vanadium phosphorus oxide obtained by thermal treatment of vanadyl *n*-butylphosphate in N_2 at (b) 508 K, (c) 568 K, and (d) 773 K.

Table 1 lists the results of elemental analysis for fresh VBuP and V-P(568), together with the average oxidation number of V. Since the C/V ratio for VBuP (3.58) decreases to 0.58 for V-P(568), the *n*-butyl groups that exist between V-P-O layers in VBuP are removed by thermal treatment. The amounts of V, P, C, H, and O in V-P(568) were found to be 29.8, 18.2, 4.1, 0.8, and 47.1 wt%, respectively. The P/V atomic ratio of V-P(568) is almost unity, and the average oxidation number of V for V-P(568) is +3.75. On the basis of these data, the chemical formula of V-P(568) is deduced to be $VP_{1.00}O_{4.38} \cdot 0.69(H_2O) \cdot 0.58C$, V and P having oxidation numbers of +3.75 and +5.00 respectively. The carbon content of V-P(568) is 4.1 wt%. When V-P(568) was treated in a mixture of O_2 5 vol% and N_2 95 vol% at 598 K for 4 h, the carbon content decreased to only 0.5 wt%, and surface area maintained a high value (182 $m^2\ g^{-1}$). Therefore, we can reasonably consider the pores and high surface area of V-P(568) to have originated not from the carbonaceous materials, but from the V-P oxide itself. With thermal treatment, the average oxidation number of the compound decreased from +4.01 for VBuP to +3.75 for V-P(568) (Table 1). In other words, the treatment had an effect of drawing out oxygen from the V-P-O layers, and this is a probable reason for the structure of the walls in V-P(568) being amorphous.

Figure 8, shows SEM images of fresh VBuP and V-P(568). VBuP resembles bunches of grapes (Fig. 8a). V-P(568) shows essentially the same morphology as VBuP (Fig. 8b), with large numbers of cracks present at the boundaries of the grape-bunches.

Table 1 Elemental analysis data and average oxidation number of vanadium for vanadyl *n*-butylphosphate and vanadium phosphorus oxide obtained by thermal treatment of vanadyl *n*-butylphosphate at 568 K in N_2.

Treatment temperature (K)	Elemental analysis (wt%)					Atomic ratio of P/V	Atomic ratio of C/V	Oxidation number of V
	V	P	C	H	O[a]			
untreated	23.3	14.3	21.1	4.2	37.2	1.01	3.85	+4.01
568 K	29.8	18.2	4.1	0.8	47.1	1.00	0.58	+3.75

[a] Oxygen content was estimated by subtracting the sum of weights of V, P, C, and H.

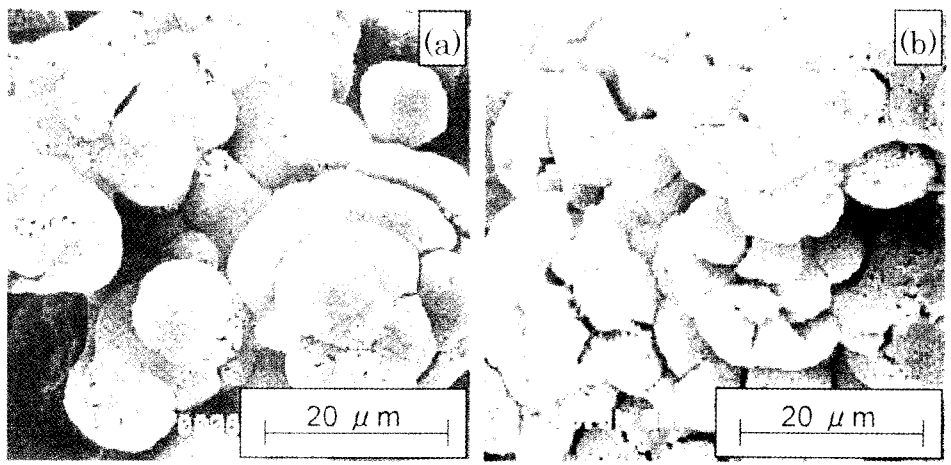

Fig 8 Scanning electron micrographs of (a) vanadyl *n*-butylphosphate and (b) vanadium phosphorus oxide obtained by thermal treatment of vanadyl *n*-butylphosphate in N_2 at 568 K

Figure 9 shows a typical TEM image of V-P(568). Numerous streaky gaps are observed as white lines in microcrystallites. The gaps have an estimated width of about 5 nm, which is close to the size of mesopores (4.4 nm) estimated from N_2 isotherms. Thus, the mesopores are presumed to correspond to the streaky gaps. VBuP is a layered compound consisting of alternating layers of V-P-O (0.40 nm) and *n*-butyl (1.14 nm) [24]. When the *n*-butyl layers are removed from VBuP by thermal treatment, the microcrystallites of VBuP shrink in the direction of layer stacking. At this time, the microcrystallites are partially fractured, due not to withstand stress acting on the microcrystallites. From the TEM image (Fig. 9), the height of the one fragment in the microcrystallites is estimated to be about 8 nm. In view of the height of the V-P-O layer (0.40 nm), we would expect that one layer among about 20 might be fractured.

Fig. 9 TEM image of vanadium phosphorus oxide obtained by thermal treatment of vanadyl *n*-butylphosphate in N_2 at 568 K.

Conclusions

Highly porous V-P oxides of high surface area were synthesized by the thermal treatment of vanadyl *n*-butylphosphate in N_2 with treatment temperature ranging from 525 K to 705 K. Micropores and mesopores were characterized from N_2 adsorption-desorption isotherms and Ar adsorption isotherms, respectively. These porous V-P oxides were found to possess mainly mesopores having a

width of about 4.4 nm.

References

[1] K. Beneke, G. Lagaly, *Inorg. Chem.*, **22** (1983) 1503.

[2] L. Beneš, R. Hyklová, J. Kalousová, J. Votinský, *Inorg. Chim. Acta*, **177** (1990) 71.

[3] A. De Stefanis, A. A. G. Tomlinson, *J. Mater. Chem.*, **5** (1994) 319.

[4] T. Nakato, Y. Furumi, N. Terao, T. Okuhara, *J. Mater. Chem.*, **10** (2000) 737.

[5] S. H. Horowitz, *WO Patent* (1998) 98/15353.

[6] V. V. Guliants, J. B. Benziger, S. Sundaresan, I. E. Wachs, J.-M. Jehng, *Chem. Mater.*, **7** (1995) 1493.

[7] J. W. Johnson, A. J. Jacobson, J. F. Brody, J. T. Lewandowski, *Inorg. Chem.*, **23** (1984) 3842.

[8] G. Huan, J. W. Johnson, J. F. Brody, D. P. Goshorn, A. J. Jacobson, *Mater. Chem. Phys.*, **35** (1993) 199.

[9] G. Huan, A. J. Jacobson, J. W. Johnson, D. P. Goshorn, *Chem. Mater.*, **4** (1992) 661.

[10] E. M. Sabbar, M. E. de Roy, A. Ennaqadi, C. Gueho, J. P. Besse, *Chem. Mater.*, **10** (1998) 3856.

[11] J. W. Johnson, J. F. Brody, R. M. Alexander, *Chem. Mater.*, **2** (1990) 198.

[12] N. Mizuno, H. Hatayama, S. Uchida, A. Taguchi, *Chem. Mater.*, **13** (2001) 179.

[13] T. Doi, T. Miyake, *Chem. Commun*,. (1996) 1635.

[14] T. Abe, A. Taguchi, M. Iwamoto, *Chem. Mater.*, **7** (1995) 1429.

[15] J. E. Haskouri, M. Roca, S. Cabrera, J. Alamo, A. B. Porter, D. B. Porter, M. D. Marcos, P. Amorós, *Chem. Mater.*, **11** (1999) 1446.

[16] H. Hatayama, M. Misono, A. Taguchi, N. Mizuno, *Chem. Lett.*, (2000) 884.

[17] N. Hiyoshi, N. Yamamoto, N. Terao, T. Nakato, T. Okuhara, *Stud. Surf. Sci. Catal.*, **130** (2000) 1715.

[18] T. Nakato, Y. Furumi, T. Okuhara, *Chem. Lett.*, (1998) 611.

[19] G. Centi, F. Trifirò, J. R. Ebner, V. M. Franchetti, *Chem. Rev.*, **88** (1988) 55.

[20] B. K. Hodnett, *Catal. Rev. Sci. Eng.*, **27** (1985) 373.

[21] M. T. Sananes, I. J. Ellison, S. Sajip, A. Burrows, C. J. Kiely, J. C. Volta, G. J. Hutchings, *J. Chem. Soc., Faraday Trans*,. **92** (1996) 137.

[22] T. Shimoda, T. Okuhara, M. Misono, *Bull. Chem. Soc. Jpn.*, **58** (1985) 2163.

[23] B. G. Shpeizer, X. Ouyang, J. M. Heising, A. Clearfield, *Chem. Mater.*, **13** (2001) 2288.

[24] Y. Kamiya, E. Nishikawa, A. Satsuma, N. Mizuno, T. Okuhara, *J. Jpn. Petro. Inst.*, **44** (2001) 193.

[25] N. Hiyoshi, N. Yamamoto, Y. Kamiya, E. Nishikawa, T. Okuhara, *Catal. Today* (in press).

[26] D. Dollimore, G. R. Heal, *J. Colloid Interface Sci.*, **33** (1970) 508.

[27] A. Saito, H. Foley, *AIChE J.*, **37** (1991) 429.

[28] B. K. Hodnett, P. Permanne, B. Delmon, *Appl. Catal.*, **6** (1983) 231.

[29] S. J. Gregg, K. S. W. Sing, Adsorption, "*Surface Area and Porosity, 2nd edn.*" Academic Press, London, (1982).

[30] T. Yamada, K. Johkan, T. Okuhara, *Microporous Mesoporous Mater.*, **26** (1998) 109.

Chapter 7

Summary and General Conclusion

7.1 Summary of each Chapter

As mentioned in Chapter 1, the author proposed for developing the catalyst of high performance that adequate design of the structure/composition makes the properties of the active sites improved, consequently, the catalytic performance must be improved. The first subject of this thesis (Part I) is to establish the concepts that how the reduction and re-oxidation properties, and acidic property should be controlled to improve the catalytic performance. The second subject of this thesis (Part II) is to develop the vanadium phosphorus oxide catalysts with novel structure on the basis of controlling the structure and composition. The main results obtained are summarized as follows.

Part I. Property of the Active Sites Controlling Catalytic Performance in the Selective Oxidation of n-Butane.

Part I established the concepts that how the reduction and re-oxidation properties, and acidic property should be controlled to improve the catalytic performance.

In Chapter 2, relationship between the reduction and re-oxidation properties, and catalytic performances was investigated by using three types of the $(VO)_2P_2O_7$ catalysts with different microstructures. The catalysts were prepared in organic solvent (VPO-org), by reduction of $VOPO_4 \cdot 2H_2O$ (VPO-redu), and in aqueous medium (VPO-aq). The rates of MA formation per surface area greatly depended on the catalysts; VPO-org was much active, especially at the high partial pressure of *n*-butane. Reaction kinetics suggested that VPO-org had higher re-oxidation ability, by which the surface of VPO-org was retained as a higher oxidation state during the reaction. Actually, it was confirmed that the V^{5+} density of VPO-org during the reaction was about twice those of the other catalysts, and VPO-org showed higher rates of re-oxidation estimated by measurement of re-oxidation with air. It was concluded that the high catalytic activity of VPO-org is due to this high ability of re-oxidation. This would be caused from enhancement of the migration of the oxygen ions near the surface induced by the structural disorder of the catalyst. These results established the concept that the re-oxidation ability should be improved for improving the catalytic activity.

In Chapter 3, the relationship between acidic property and catalytic performance was investigated. First (in Chapter 3.1), a new characterization method for quantitative determination of amount as well as

strength of Brønsted and Lewis acid sites separately was established. This method was a temperature programmed desorption (TPD) using 3,5- and 2,6-dimethylpyridine (3,5-DMP and 2,6-DMP, respectively) as probes. 2,6-DMP was confirmed to be adsorbed on Brønsted acid sites selectively with the purging at 523 K, when catalyst had no very strong Lewis acid sites, whereas 3,5-DMP was adsorbed on both Brønsted and Lewis acid sites in this temperature. In addition, it was experimentally demonstrated that the desorption temperatures of 2,6-DMP and 3,5-DMP adsorbed on one acid site were almost the same. From these results, it was elucidated that 3,5-DMP-TPD, 2,6-DMP-TPD, and the differential spectra indicate the total, Brønsted, and Lewis acid sites, respectively.

Second (in Chapter 3.2), acidic properties of $(VO)_2P_2O_7$ catalysts were evaluated by the DMP-TPD method, and then, the effects of the acidic properties on MA formation were elucidated. The $(VO)_2P_2O_7$ catalysts had four types of acid sites: weak and strong Brønsted acid sites, and weak and strong Lewis acid sites. The acidic properties greatly depended on the catalysts. VPO-org had a higher density of the strong Brønsted acid sites, but these acid sites were relatively weak compared to the other catalysts. VPO-redu had a higher density of the strong Lewis acid sites. VPO-aq had fewer acid sites except for the weak Brønsted acid sites. The selectivity to MA at low conversion increased with the density of the strong Lewis acid sites, indicating the importance of these acid sites for MA formation. The strong Brønsted acid sites may promote the consecutive oxidation of MA. From the information obtained in Chapter 3, it can be claimed that increase in the density of the strong Lewis acid sites, and contrary decrease in that of the strong Brønsted acid sites are effective for improving the selectivity to MA.

Part II. Vanadium Phosphorus Oxide Catalysts with Novel Structures

Part II developed three types of vanadium phosphorus oxide catalysts with novel structures derived from lamellar compounds on the basis of controlling the structure and composition.

In Chapter 4, iron-doped $(VO)_2P_2O_7$ catalyst was developed by intercalation of iron-complex into lamellar vanadyl alkylphosphate. First (in Chapter 4.1), novel lamellar vanadyl alkylphosphates were synthesized and characterized systematically. The vanadyl alkylphosphates were synthesized by reaction of a solid mixture of V_2O_5 and V_4O_5 with P_2O_5 in primary aliphatic, secondary aliphatic, alicyclic, and aliphatic alcohols. These vanadyl alkylphosphates had primal characteristics of the bulk structure, that is, V-O-V pair sites, valence state of V^{4+} and P/V ratio of 1.0. Since the vanadyl alkylphosphates possessed weakly held alcohol in their interlayer spaces, these materials were expected to accommodate guest molecules. The

catalysts obtained from the vanadyl alkylphosphates showed high catalytic performance for the *n*-butane oxidation to MA.

Second (in Chapter 4.2), intercalations of iron-complex such as $Fe(acac)_3$ and ferrocene were investigated by using vanadyl benzylphosphate as host. The vanadyl benzylphosphate and iron-complex was heated at 358 K in toluene. From characterization of the compounds obtained, it was confirmed that these iorn-complexs were successfully intercalated uniformly without significant distraction of the layer structure.

Third (in Chapter 4.3), the method investigated in Chapter 4.2 was applied to modification of vanadyl *n*-hexylphosphate and the catalytic properties in the selective oxidation of *n*-butane were investigated. $Fe(acac)_3$ was successfully intercalated uniformly in the case of the vanadyl *n*-hexylphosphate as well. The obtained material was transformed to single phase of $(VO)_2P_2O_7$ by a calcination. The doped Fe ions uniformly dispersed in the bulk and were mainly substituted for V^{4+} ions. The catalytic activity for MA formation per unit surface area on the Fe-doped catalyst was higher than that on Fe-free catalyst. The reaction kinetics suggested that the Fe-doped catalyst had higher reduction and especially re-oxidation ability. The Fe-doped catalyst gave higher rate of both the reduction and especially re-oxidation than the Fe-free catalyst, and the surface of the Fe-doped catalyst under the reaction was in a higher oxidation state. It was concluded that the doped Fe ions can enhance the reduction and especially re-oxidation ability of the catalyst, resulting in the higher catalytic performance in the *n*-butane oxidation.

Chapter 5 presented a new preparation method of the catalyst preferential expose of the (100) plane by intercalation, exfoliation, and reduction of $VOPO_4 \cdot 2H_2O$ in alcohols. The exfoliated sheets of $VOPO_4 \cdot 2H_2O$ were obtained by stepwise heating of $VOPO_4 \cdot 2H_2O$ crystallites in 1-butanol or 1-propanol. Subsequent reduction of these sheets produced the precursor. This precursor consisted of thin films-like microcrystallites randomly gathered. On the contrary, the precursor obtained by direct reduction of $VOPO_4 \cdot 2H_2O$ was aggregates of plate-like microcrystallites. The catalyst obtained through the exfoliation (VPO-exf) was highly active and selective compared to the catalyst by the conventional method (VPO-conv). It was confirmed that the thickness of VPO-exf was about half of that of VPO-conv, suggesting preferential expose of the (100) plane. That is one of the reasons for the high selectivity on VPO-exf. In addition, VPO-exf gave higher surface area, and showed high crystalline $(VO)_2P_2O_7$. These would also contribute to the high activity and selectivity of VPO-exf.

In Chapter 6, highly porous vanadium phosphorus oxides of high surface area were synthesized by

thermal treatment of the vanadyl *n*-butylphosphate in N_2. The surface area of vanadium phosphorus oxides was greatly increased by thermal treatment within a temperature range of 500–550 K, and reached 225 $m^2 g^{-1}$ after treatment at 568 K. The pores of the vanadium phosphorus oxides showed a bimodal distribution in the micropore and mesopore region, and mainly consist of mesopores. The mesopores, which have a size of 4.4 nm and a volume of 0.272 $cm^3 g^{-1}$, were probably formed from fractures of microcrystallites along layers of vanadyl *n*-butylphosphate by the thermal treatment in N_2.

7.2 General Conclusion

Almost all developments of the $(VO)_2P_2O_7$ catalyst have been performed by the trial-and-error method, however, now this method must be at the edge of its capabilities for improving their catalytic performances. In this thesis, the author presented the relationships between the catalyst preparation and catalytic performance as Scheme 2 in Chapter 1, and proposed the concept for developing the catalyst of high performance that the adequate design of the structures and composition of the $(VO)_2P_2O_7$ catalyst makes the properties of the active sites improved, consequently, the catalytic performance must be improved. However, there were the following critical two problems before the present thesis: (1) It could not be imaged that what-like structure and composition were suitable to improve the chemical property of the active sites, because understanding of the relationship between the chemical properties of the active sites and catalytic performance was insufficient to understand how these properties should be controlled. (2) The level of catalyst preparation of $(VO)_2P_2O_7$ was far from "designing" the structure and composition, even if one could know what-like structure and composition of $(VO)_2P_2O_7$ were required.

The following conclusions can be drawn from the summary of each chapter mentioned above.

1. The re-oxidation ability should be improved to improve the catalytic performance per active sites. Concerning the acidic property, increase in the density of the strong Lewis acid sites, and contrary decrease in that of the strong Brønsted acid sites are effective for improving the selectivity to MA.

2. The catalysts of novel structures with high catalytic performances in the selective oxidation of *n*-butane can be developed on the basis of the adequately designing their structure and composition. (1) First, the new precursors, vanadyl alkylphosphates, were developed. The Fe ions uniformly dispersing in the $(VO)_2P_2O_7$ catalyst was synthesized by intercalation of iron-complex into lamellar vanadyl alkylphosphates, followed by calcination. This catalyst had high reduction and especially re-oxidation ability. (2) The catalyst with thin films-like microcrystallites, which had preferential expose of the (100) plane, was synthesized by intercalation, exfoliation, and reduction of $VOPO_4 \cdot 2H_2O$ in alcohol. (3) Highly porous vanadium phosphorus oxides of high surface area (225 $m^2\ g^{-1}$) can be synthesized by thermal treatment of lamellar vanadyl *n*-butylphosphate in N_2. The pores mainly consist of mesopores,

which are formed from fractures of microcrystallites along layers of the vanadyl *n*-butylphosphate.

3. Method for quantitative determination of amount and strength of Brønsted and Lewis acid sites separately was established. This method will be available for investigations involving functions of acid sites on solid acid catalysts as well as the $(VO)_2P_2O_7$ catalyst.

7.3 Future Prospects

The present thesis developed three types of the V-P oxide catalysts with the novel structures, that is, the catalysts synthesized by (1) intercalation of iron-complex into lamellar vanadyl alkylphosphate, (2) intercalation, exfoliation, and reduction of $VOPO_4 \cdot 2H_2O$ in alcohol, and (3) thermal treatment of vanadyl alkylphosphate in N_2. Although each catalyst has a potential performance, the catalyst combined with these three preparation methods will achieve the promising performances for the selective oxidation of *n*-butane. For example, $VOPO_4 \cdot 2H_2O$ is exfoliated in alcohol followed by addition of promoter and then, the exfoliated sheets are reduced to form precursor. Besides that, thermal treatment of the vanadyl alkylphosphate intercalating iron-complex will give the catalyst with both high surface area and reduction and re-oxidation abilities. These are prospects for the catalyst with further high performance in the selective oxidation of *n*-butane.

The present thesis demonstrated that the re-oxidation property, crystal plane and surface area can be controlled by the three preparation methods. Acidic property is another factor controlling the catalytic performance. Chapter 3 established the method for quantitative determination of Brønsted and Lewis acid sites separately, and clarified the relationship between the acidic property and catalytic performance. However, controlling the acidic property has been unachievable. The cause of this is lack of the information on the structure of these acid sites at molecular level. Further quantitative estimation of acidic property on well-characterized $(VO)_2P_2O_7$ catalyst by the DMP-TPD method will clarify their structures. Consequently, this information will open up adequately designing the acidic property for MA formation on the basis of controlling the structure and composition of the $(VO)_2P_2O_7$ catalyst.

So far, almost all commercial heterogeneous-catalysts have been developed by the conventional trial-and-error method. In their initial studies, this method may be effective in seeking good catalyst and/or improving the catalytic performance. Some of them were industrialized at a stretch. However, this method must have a fate of reaching the end of the improvement eventually, because variable factors in the preparation of the catalysts are not so much. Difficulties of latest target-reaction with which heterogeneous catalysts are dealing are apt to increase. One of the ways to overcome this includes the multicomponent catalyst. It can be expected that the multcomponent catalyst is highly structure sensitive. Recently, the technique of combinatorial chemistry is applied in some developments of heterogeneous catalysts. This technique is helpful for minimizing time for developing the multicomponent catalysts. However, the author

conceives that it is also difficult to apply this technique in mature catalytic systems of structure sensitive reaction systems, because this technique can performed no more than combination of many elements. The present thesis demonstrated that adequate control of the structure and composition can improved the catalytic performance of even mature catalytic system. This new strategy established in the present thesis proved that mature catalytic system had a possibility of further improving its catalytic performance. The author hopes to apply this strategy to the developments of other heterogeneous catalysts presumed to reach the limit of improving their catalytic performances.

List of publications

I .Original papers corresponding to this thesis.

Chapter 2.

1. Catalytic property of vanadyl pyrophosphates for selective oxidation of *n*-butane at high *n*-butane concentrations.
   Yuichi Kamiya, Eiichiro Nishikawa, Toshio Okuhara, Tadashi Hattori.
   Appl. Catal. A, **206**, 103-112 (2001)

Chapter 3.

3.1

2. Dimethylpyridine-temperature programmed desorption (DMP-TPD) for measurement of strength of Brønsted and Lewis acid sites on metal oxide catalysts.
   Atsushi Satsuma, Yuichi Kamiya, Yenni Westi, Tadashi Hattori.
   Appl. Catal. A, **194/195**, 253-263 (2000).

3.2

3. The role of Brønsted and Lewis acid sites of vanadyl pyrophosphate measured by dimethylpyridine-temperature programmed desorption in the selective oxidation of butane.
   Yuichi Kamiya, Hiroyuki Nishiyama, Miki Yashiro, Atsushi Satsuma, Tadashi Hattori.
   J. Jpn. Petro. Inst. (in press)

Chapter 4.

4.1.

4. Synthesis of novel layered vanadyl alkylphosphates as catalyst precursors for selective oxidation of *n*-butane.
   Yuichi Kamiya, Eiichiro Nishikawa, Atsushi Satsuma, Noritaka Mizuno, Toshio Okuhara.
   Sekiyu Gakkaishi (Letter), **44**, 265-266 (2001).

5. Preparation and characterization of lamellar vanadyl alkylphosphates as catalyst precursors for selective oxidation of *n*-butane.
   Yuichi Kamiya, Eiichiro Nishikawa, Atsushi Satsuma, Toshio Okuhara.
   Bull. Chem. Soc. Jpn. (in press)

6. Oxidation of *n*-butane over vanadyl pyrophosphates prepared from lamellar vanadyl alkylphosphates
   Norihito Hiyoshi, Naoki Yamamoto, Yuichi Kamiya, Eiichiro Nishikawa, Toshio Okuhara.
   Catal. Today, **71,** 129-135 (2001).

4.2

7. Insertion of iron-complex to lamellar vanadyl benzylphosphate for preparation of well-defined catalyst.
   Atsushi Satsuma, Yuki Kijima, Shin-ichi Komai, Yuichi Kamiya, Eiichiro Nishikawa, Tadashi Hattori.
   Catal. Today, **71**, 161-167 (2001).

4.3

8. Selective oxidation of *n*-butane over iron doped vanadyl pyrophosphate prepared from lamellar vanadyl *n*-hexylphosphate.
   Yuichi Kamiya, Yuki Kijima, Takuya Ohkura, Atsushi Satsuma, Tadashi Hattori.
   Appl. Catal. A, (submitted).

Chapter 5.

9. Preparation of catalyst precursor for selective oxidation of *n*-butane by exfoliation-reduction of $VOPO_4 \cdot 2H_2O$ in primary alcohol.
   Yuichi Kamiya, Satoshi Ueki, Norihito Hiyoshi, Naoki Yamamoto, Toshio Okuhara.
   Catal. Today, (in press).

Chapter 6.

10. Highly porous vanadium phosphorus oxides derived from vanadyl *n*-butylphosphate.
    Yuichi Kamiya, Eiichiro Nishikawa, Atsushi Satsuma, Miki Yoshimune, Toshio Okuhara.
    Microporous and Mesoporous Mater., **54**, 277-283 (2002).

II. Other publications.

11. Determination of the acid strength of binary oxide catalysts using temperature programmed desorption of pyridine.
    Atsushi Satsuma, Yenni Westi, Yuichi Kamiya, Tadashi Hattori, Yuichi Murakami.
    Bull. Chem. Soc. Jpn., **70**, 1311-1317 (1997).

12. Radical type catalytic oxidation of butane at low temperatures over *in-situ* prepared silica species.
    Atsushi Satsuma, Naruaki Sugiyama, Yuichi Kamiya, Tadashi Hattori.
    Chem. Lett., 1051-1052 (1997).

13. Low temperature radical oxidation of butane over *in-situ* prepared silica species.
    Atsushi Satsuma, Naruaki Sugiyama, Yuichi Kamiya, T. Kamatani, Tadashi Hattori.
    Stud. Surf. Sci. Catal., **130,** 1799-1804 (2000).